Well-defined polymeric architectures by Reversible Addition-Fragmentation chain Transfer polymerisation: Synthesis, characterisation and application as oil and lubricant additives

Guillaume Moriceau

A thesis submitted in partial fulfilment of the requirements for the degree of

Doctor of Philosophy in Chemistry

Department of Chemistry

University of Warwick

September 2018

Table of contents

Declaration

Experimental work contained in this thesis is original research carried out by the author, unless otherwise stated, in the Department of Chemistry at the University of Warwick or at Lubrizol's Chemical Synthesis department, Hazelwood, Derbyshire between October 2014 and September 2018. No material contained herein has been submitted for any other degree, or at any other institution.

Results from other authors are referenced in the usual manner throughout the text.

Signed: _____ Date: _____

Guillaume Moriceau

Acknowledgements

I would like to thank first my supervisor Professor Sébastien Perrier who gave me the great opportunity to undertake this PhD at the University of Warwick. I am very grateful for all the support and encouragement he provided me. Thanks for being always optimistic, enthusiastic, and helpful throughout this PhD experience.

Then, I want thanks the people who helped me through my long student career. Thank you Sophie Guillaume for your great advices and for all the help and support you dedicated to me during my master project and beyond. Thank you also Sandrine Cammas-Marion, Gilles Ponchel, Christine Vauthier, and René Gree, for your help and support.

Next, I would like to thank Antonio Mastrangelo, HyungSoo Kim, Paul O'Hora, Joby Winn, Timothy Smith, David Moreton, and the company Lubrizol for their contributions and guidance throughout my research.

Now, I would like to acknowledge all the Perrier group, starting with the Postdocs who helped me during this great experience (Guillaume Gody, Johannes Brendel, Matthias Hartlieb, Sylvain Catrouillet, Carlos Sanchez-Cano, Raoul Peltier, Edward Mansfield, Joaquin Sanchis-Martinez (Ximo), and all the others. I would like to continue with all my colleagues sharing with me offices, labs or corridor: Caroline B., Andrew K., Liam M., Junliang Z., Joji T., Agnès K., Alex C., Majda A., Sophie L., Tammie B., Julia R., Sean E., Andy L., Pratik G., Tom F., Robert R., Fannie B., Jie Y., Qiao S., Satu H., Maria K., Clement D., Philip D., Ming L.K., Daniel L., Rachel H., Sam L., Nikolaos E., Glen J., Patrick de J., Paul W., and all the other people forgotten across the Perrier, Wilson, and Haddleton groups. Thanks to Polymer Characterisation RTP (Daniel Lester) and the Warwick Chemistry NMR facility (Ivan Prokes) for providing such great support.

Special thanks to my friends, colleagues, lawyers, housemate, pub mates, pubs, PolySynApps, who helped me through all kind of situations and made my life better during my time at Warwick (Joji Tanaka, George Pappas, Dan and Rachel Lester, Cookie, Marie the innocent, Benoit and Maria, Sam, Philip, Raoul, Carlos, Pratik, Agnès, the Broomfield Tavern, The Duck, The Terrace Bar, The Inspire, The Clarence, The Chestnut,…).

Finally, I'd like to thank my family for all their support and especially my parents for everything they have done for me. I am also very grateful to my partner, Nathalie Ségaud, for her constant support and love through the completion of this PhD. Thanks for your patience and passion during these 4 years of distance relationship.

Thanks to all of you guys! That was fantastic time!

Abbreviations

4xCTA	Tetrafunctional CTA-Ester
AgTFA	Silver trifluoroacetate
ATRP	Atom transfer radical polymerisation
ChainExt	Chain extension
CRP	Controlled radical polymerisation
CSIRO	Commonwealth scientific and industrial research organisation
CTA	Chain transfer agent
CTA-Acid	S-1-dodecyl-S'-(α,α'-dimethyl-α'-acetic acid)trithiocarbonate
CTA-Ester	Butyl-2-methyl-2-[(dodecylsulfanylthiocarbonyl)sulfanyl] propionate
C_{tr}	Chain transfer constant
C_{tr}^{app}	Apparent chain transfer constant
$Đ$	Molar mass distribution (dispersity)
DCTB	Trans-2-[3-(4-tert-Butylphenyl)-2-methyl-2-propenylidene]malononitrile
dn/dc	Refractive index increment
DP	Degree of polymerisation
DRI	Differential refractometer
DSC	Differential scanning calorimetry
dTG	Differential thermogravimetric curves
ESI-MS	Electrospray ionisation mass spectroscopy
ESI-ToF-MS	Electrospray ionisation time of flight mass spectrometry
IV	Intrinsic viscosity
KV	Kinematic viscosity
L	Livingness
LAc	Lauryl acrylate
LAM	Less activated monomers
LMA	Lauryl methacrylate
LRP	living radical polymerisation
LS	Light-scattering

MALDI-ToF	Matrix assisted laser desorption ionisation – time of flight
MAM	More activated monomers
MMA	Methyl methacrylates
M_n	Number average molar mass
$M_{n,theo}$	Theoretical molar mass (NMR)
MOFs	Metal organic frameworks
M_p	Peak molar mass
MSA	Methane sulfonic acid
M_w	Weight average molar mass
NMP	Nitroxide-mediated polymerisation
NOE	Nuclear overhauser effect
OLED	Organic light-emitting diode
PABTC	(Propanoic acid)yl butyl trithiocarbonate
PET-RAFT	Photo-induced electron transfer RAFT polymerisation
PISA	Polymerisation-induced self-assembly
PMMA	Poly(methyl methacrylate)
PPD	Pour point depressant
PPT	Pour point
PSMA	Poly(Styrene-*co*-Maleic Anhydride)
RAFT	Reversible addition-fragmentation chain transfer (polymerisation)
RDRP	Reversible deactivation radical polymerisation
R_g	Radius of gyration
R_h	Hydrodynamic radius
RI	Refractive index
R_p	Rate of polymerisation/propagation
SEC	Size exclusion chromatography
SET-LRP	Single-electron transfer living radical polymerisation
SMUI	Single monomer unit insertion
T_c	Crystallisation temperature

TE	Thickening efficiency
T_g	Glass transition temperature
TGA	Thermogravimetric analysis
T_i	Maximum rate of degradation temperature
T_m	Melting temperature
UHMW	Ultra-high molecular weight
UV	Ultraviolet
V-40	1,1′-Azobis(cyclohexane-1-carbonitrile)
V601	Dimethyl 2,2'-azobis(2-methylpropionate)
VI	Viscosity index
α	Mark-Houwink parameter

List of Figures

List of Tables

List of Schemes

List of Publications

The following publications have been produced from the work detailed in this thesis.

From the work presented in Chapter 3:

Functional multisite copolymer by one-pot sequential RAFT copolymerization of styrene and maleic anhydride

Moriceau, G.; Gody, G.; Hartlieb, M.; Winn, J.; Kim, H.; Mastrangelo, A.; Smith, T.; Perrier, S. *Polym. Chem.* 2017.

From the work presented in Chapter 4:

Influence of grafting density and distribution on material properties using well-defined alkyl functional poly(styrene-*co*-maleic anhydride) architectures synthesised by RAFT

Moriceau, G.; Tanaka, J.; Lester, D.; Pappas, G.; Cook, A.; O'Hora, P.; Winn, J.; Smith, T.; and Perrier, S. - *To be submitted*

From the work presented in Chapter 5:

Well-defined alkyl functional poly(styrene-*co*-maleic Anhydride) architectures as pour point and viscosity modifiers for lubricating oil.

Moriceau, G.; Lester, D.; Pappas, G.; O'Hora, P.; Winn, J.; Smith, T.; and Perrier, S. - *To be submitted*

Abstract

Reversible addition-fragmentation chain transfer (RAFT) polymerisation was exploited to synthesise well-defined graft copolymers *via* a scalable route and study their potential as oil and lubricant additives (rheology modifiers).

The RAFT polymerisation process was adapted to industrial conditions (industrial grade CTA and one-pot process) and graft materials were synthesised using styrene and maleic anhydride as a comonomer system (polystyrene-*co*-maleic anhydride or PSMA).

Prior to synthesising well-defined materials, the purity of the industrial grade CTA-Ester from Lubrizol (*c.a.* 80 %) and its performances (C_{tr} and kinetics) for styrene and methacrylates (methyl and lauryl) monomers were determined. RAFT polymerisation conditions were optimised and a polystyrene macroCTA (DP = 10) with controlled molar mass, narrow dispersity and high livingness was obtained.

A one-pot sequential monomer addition strategy was developed to synthesise a multisite copolymer composed of a polystyrene backbone (DP = 50) with maleic anhydride units inserted locally (every 10 units in average). The subsequent functionalisation of maleic anhydride moieties with long aliphatic alcohols (stearyl/C18) yield to a graft material with low density of alkyl side chains.

A library of well-defined PSMA materials with various composition (alternating, block, multiblock, and multisite) and topology (linear, star, and graft) was also achieved. The subsequent functionalisation of the PSMA copolymers with various aliphatic alcohols (lauryl/C12 and behenyl/C22) allowed the preparation of graft materials with controlled density and distribution of side chains. The influence of copolymer composition and structure, and the effect of long alkyl chain addition on the physical and thermal properties of the materials, were demonstrated.

Finally, the well-defined graft PSMA materials were investigated as rheology modifiers in two mineral oils (group II and III) and the influence of polymer composition, grafting density and distribution, molar mass, and side chain length on pour point, viscosity index (VI) and thickening efficiency (TE) were investigated. The performances of graft PSMA materials as oil and lubricant additives were demonstrated.

Chapter 1 Industrial Challenges in RAFT technology

Abstract

The success of free radical polymerisation in industry arises from its numerous advantages such as, scalable process, compatible with a wide range of monomers and low cost. With the emergence of reversible deactivation radical polymerisation (RDRP) in the 90s, a new era began in materials science. The development of RDRP techniques have enabled the synthesis of highly complex polymeric architectures (for example blocks, stars and brushes) with controlled molar mass, narrow dispersity, and tailored functionality. Access to well-defined functional materials with original properties is beneficial to improve current technologies and offers the possibility for the creation of new markets. Among the RDRP techniques, reversible addition-fragmentation chain transfer (RAFT) technology has been described as one of the most promising. With the recent expiration of the original RAFT patents, RAFT technology is now considered as a method of choice for the large scale production of well-defined complex polymeric materials and is expected to play an increasing role in the development of future materials and their associated markets.

This chapter provides an overview of RAFT technology and discusses its strength and challenges. The basic principles of RAFT polymerisation are introduced and the key points for an optimised RAFT process summarised. Current industrial applications are presented and the future industrial developments are put into perspective. A brief introduction of Lubrizol interests is provided to establish the context and understand the work presented in this thesis.

1.1 Radical Polymerisation: Evolution and Current Market

Since the discovery of synthetic rubber in the early 1910s (F. Hofmann) and it subsequent industrial production (Bayer AG), the plastic industry has continuously grown (9% a year on average between 1950-2012) where the total volume of plastic materials generated per year reached 335 million tonnes in 2016.[1-3] Among these plastics, approximately 50% are made by radical chemistry, ranking the radical polymerisation industry at the top of plastic producers.[4] The main reason for this industrial success is found in the numerous advantages of the radical process compared to other polymerisation techniques (easy to process and implement in large scale, compatible with a wide range of monomers, tolerance towards many functional groups and impurities, compatible with protic solvent including water, batch-to-batch reproducibility and low cost). Free radical polymerisation (FRP) is now considered as a mature technology and is perfectly suited for the production of the large volumes of commodity plastics which enrich the lives of millions of people on a daily basis. However, the FRP process is inefficient for the synthesis of well-defined polymers with controlled molecular structure, and predetermined and narrow molar mass distributions. These limitations were overcome in the 90s with the emergence of reversible-deactivation radical polymerisation (RDRP) techniques, also known as controlled/living radical polymerisation (LRP). RDRP techniques were developed after much effort to understand and integrate previous developments from the field of organic chemistry, conventional radical polymerisation and living ionic polymerisation (Figure 1.1).[5]

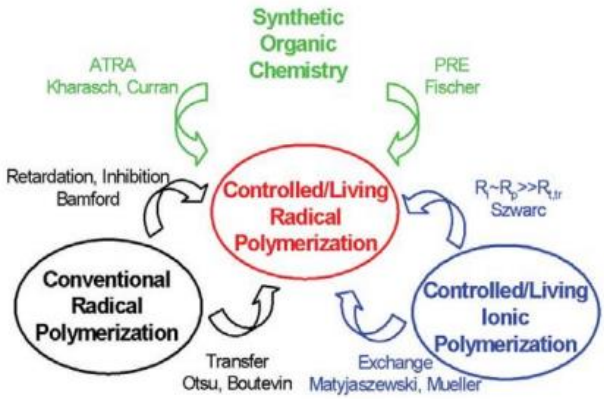

Figure 1.1. Development of CRP by integration of advances in several field of chemistry. Figure reprinted from Matyjaszewski *et al.*, 2005).

The main RDRP techniques including, nitroxide-mediated polymerisation (NMP),[6, 7] metal-mediated radical polymerisation (including atom transfer radical polymerisation, ATRP and SET-LRP),[8-12] and reversible addition-fragmentation chain transfer (RAFT) polymerisation,[13-15] have been used for the last twenty years at both academic and industrial level. RDRP participated greatly in the improvement of existing material and device performances, and led to new applications in a wide range of fields including macromolecular engineering, materials science, electronics, energy, healthcare and biotechnology. Besides the ability to synthesise materials with controlled molar mass and narrow dispersity, these techniques have provided a versatile route to prepare well-defined materials with specific monomer composition and distribution (alternating, block/multiblock, multisite and gradient copolymers), complex architectures (star, comb, brushes and hyperbranched), and with tuneable functionality (telechelic and miktoarm) (Figure 1.2). This allows for the design of materials with specific features and properties (amphiphilic materials, self-assembly or responsive) with applications in many relevant fields including: drug delivery (prodrugs, nanoparticles or bioconjugates), biomedical (hydrogels), advanced materials (composites), surface modification (coatings), energy (polyelectrolytes).

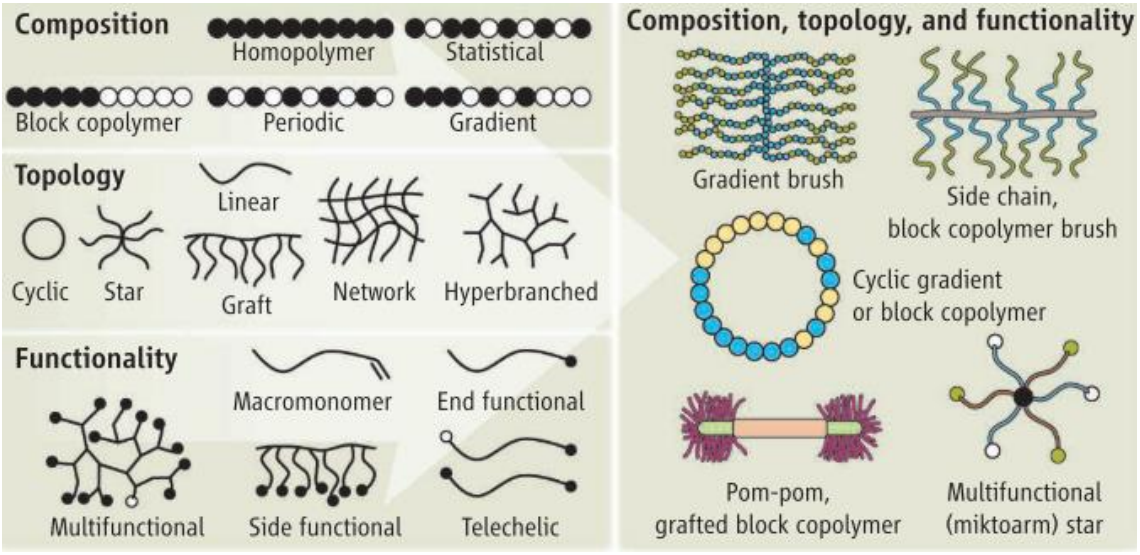

Figure 1.2. Summary of polymer designs achievable using RDRP techniques. (Figure reprinted from Matyjaszewski, 2011).[16]

RDRP techniques have already played an important role in the development of many applications and participated in the emergence of new markets of speciality polymers including adhesives, compatibilizers, cross-linkers, dispersants, emulsifiers, surface modifiers, rheology modifiers, antiscale agents and foam control agents. The main associated industries are nanotechnology, aerospace, aircraft, automobile, energy, electronics, paint and coatings, water treatment, metal treatment, agriculture, pharmaceutical and biomedical technologies, home and personal care and cosmetic. However, despite a 20 billion dollar per year market predicted in 2000, limited commercial examples of large-scale RDRP products have emerged.[17] Besides a wide range of intellectual property covering these technologies, the main limitation to the rapid industrial development of all modern RDRP techniques is the lack of large scale availability of control agents and inherent complications linked to their nature (cost-performance balance, stability, toxicity and ecological viability).[18] Nonetheless, it is predicted that the intensive research to implement RDRP control agents and the recent expiration of the original RAFT patents will lead to new industrial developments. The industrial developments using RDRP techniques were described in a recent review by Destarac.[19]

1.2 The RAFT Technology

Since its discovery in 1998, independently by two research teams working in close collaboration with industry (Zard *et al*. at Rhodia/Solvay and Rizzardo *et al.* at CSIRO in collaboration with Dupont), the RAFT technology has been described as the most versatile and powerful radical polymerisation technique for the synthesis of well-defined polymers with complex chemical architectures (diblock, multiblock, hyperbranched and star).[20-23] The RAFT technology combines features from "living" polymerisation (control of M_w and $Đ$) and the versatility of conventional free radical process as only the RAFT agent is added to the conventional polymerisation setup.[23] RAFT is applicable to a wide range of monomer types including styrenics, (meth)acrylates and (meth)acrylamides, vinyl esters (*e.g.* vinyl acetate) and vinyl amides (*e.g.* N-vinylpyrrolidone). The process is compatible with a broad variety of reaction conditions, such as polymerisation in bulk, solution or heterogeneous media (emulsion, inverse emulsion). Moreover, it is tolerant to

a variety of solvents including most organic solvents, protic solvents such as methanol or water, supercritical CO_2 and ionic liquids.[14] For these reasons, RAFT polymerisation has been adopted as a powerful tool by the scientific community to generate materials with a broad range of applications from materials science to medicine. Since its first report, a growing interest from both academia and industry was observed, as shown by the numerous scientific publications (>300 reviews and >8000 publications) and the number of patents filled (>1000 patent applications from over 100 companies).[23] With the recent expiration of the original RAFT patents (CSIRO, Dupont, and Rhodia/Solvay), an increase of commercial exploitation and the creation of new markets based on the RAFT technology is thus expected. Recent industrial developments using RAFT technology are discussed below and more details on the practical aspects of RAFT polymerisation can be found in a recent perspective by Perrier.[23]

1.2.1 RAFT mechanism and process optimisation

The general mechanism of RDRP techniques is based on a rapid equilibrium between active and dormant chains, which can be achieved by either reversible deactivation/termination (NMP, ATRP) or degenerative transfer (RAFT) (Figure 1.3).

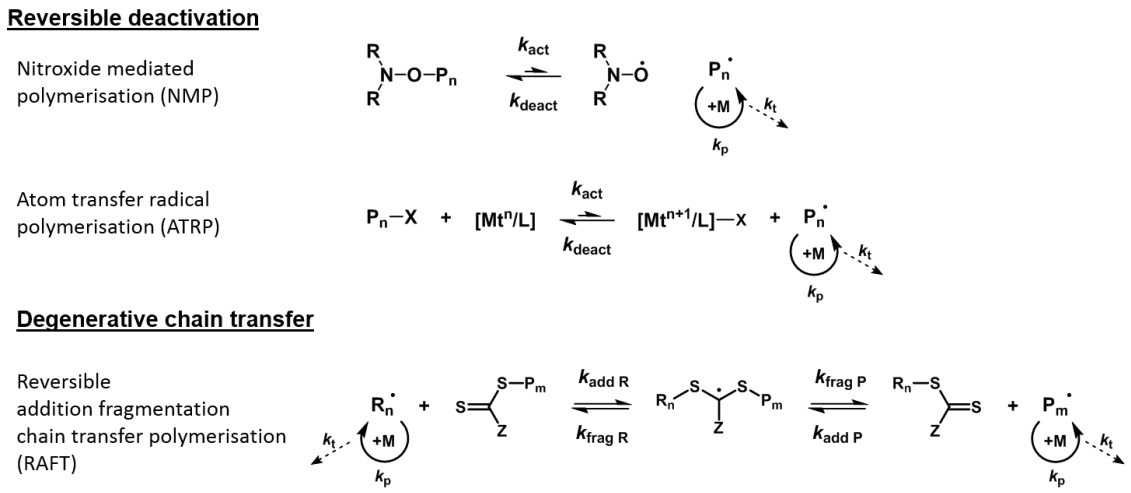

Figure 1.3. Different RDRP mechanisms.

In a degenerative transfer system, there is no change in the overall radicals during the activation-deactivation process, as the chain transfer reaction generates a new propagating radical and a new chain transfer agent with the same reactivity as the original chain carrier and chain-transfer agent.[24] In contrast with the reversible deactivation systems (based on persistent radical effect), an external source of radicals is required for the degenerative process (*e.g.* decomposition of azo/peroxide compounds).[25] This is a key requirement in RAFT process, which, in combination with appropriate polymerisation conditions, allows the control of the polymerisation rate (R_p) and the number fraction of living chains (L, "livingness"). This is illustrated in equation 1.1 and 1.2 where the initiator concentration is shown as an important parameter.

$$R_p(t) = k_p.[M].\sqrt{\frac{f.k_d.[I]_0.e^{-k_d.t}}{k_t}} \qquad 1.1$$

where R_p is polymerisation rate, k_p is the propagation rate coefficient, [M] the monomer concentration, f the initiator efficiency, k_d the decomposition rate coefficient of the initiator, $[I]_0$ the initial initiator concentration, and k_t the termination rate coefficient.

$$L\ (\%) = \frac{[CTA]_0}{[CTA]_0 + 2.f.[I]_0.(1 - e^{-k_d.t}).\left(1 - \frac{f_c}{2}\right)} \qquad 1.2$$

where L is the number fraction of living chains (assuming negligible irreversible chain transfer events), $[CTA]_0$ and $[I]_0$ are the initial concentration of chain transfer agent and initiator, respectively. The term '2' is included as one molecule of azo-initiator generates two radicals with a certain efficiency f (typically 0.5 for diazo-initiators). The term $1\text{-}f_c/2$ represents the number of chains produced by bimolecular terminations with a coupling factor f_c ($f_c = 1$ means 100% bimolecular termination by combination; $f_c = 0$ means 100% bimolecular termination by disproportionation).

Similarly to the free radical polymerisation process, the RAFT mechanism begins with an initiation step and the generation of radicals (Figure 1.4). The active radical species formed (I_n•) will then react with the RAFT agent (chain transfer agent, CTA), typically a

thiocarbonylthio moiety (*e.g.* dithioesters, trithiocarbonates or xanthates), through the C=S bond (k_{add}) to give a radical intermediate (active-dormant chain pre-equilibrium). During the pre-equilibrium step, the intermediate radical reversibly fragments towards either the initial radical species ($k_{-add\ I}$) or the re-initiating R• group ($k_{frag\ R}$), depending on the efficiency of the CTA with the respect to the monomer used (see next section). The R• group can then add back onto the radical intermediate ($k_{-frag\ R}$) or reinitiates polymerisation by adding to the monomer ($k_{re\text{-}in}$), starting a new propagating polymer chain (k_p). Once the CTA has been entirely consumed and macroCTAs are the sole transferring species, the RAFT process enters chain equilibration (main equilibrium). Ideally, the rate of activation/deactivation (addition/fragmentation) is higher than the rate of propagation (less than one monomer unit added per cycle) and therefore all chains have equal opportunity to grow (growing at the same rate), ultimately yielding control over molar mass distribution.

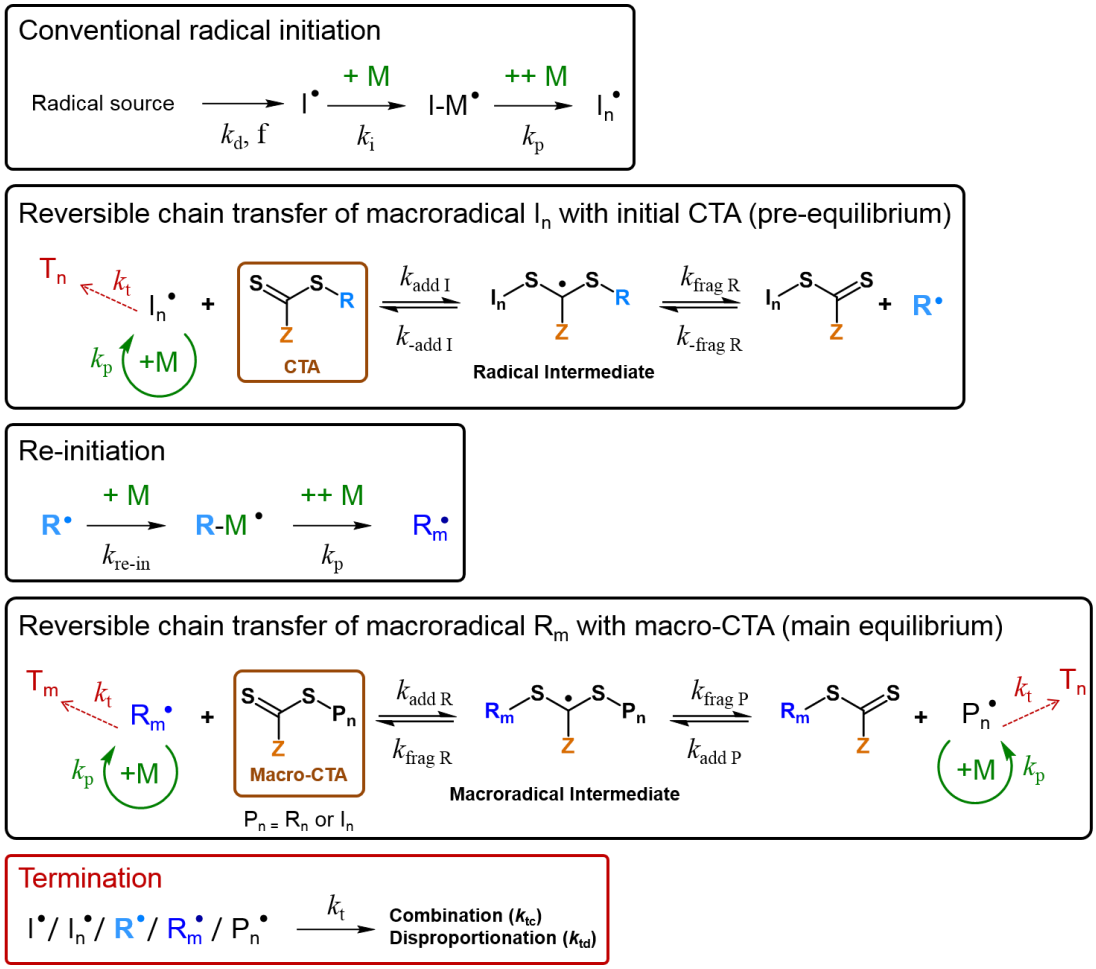

Figure 1.4. Representation of RAFT mechanism.

At any given time during the main equilibrium, most of the chains are in a dormant state and, when released, they are free to propagate, undergo chain transfer or terminate as in conventional free radical polymerisation. Termination reactions (k_t) occur either through combination (k_{tc}) or disproportionation (k_{td}). In contrast with reversible deactivation systems (*e.g.* NMP and ATRP), termination events do not lead to a loss of transfer moieties ("livingness"), but the number of chains with the thiocarbonylthio end-group (ω end-group) remain constant over the reaction time regardless of the amount of termination events. It is important to note that RAFT polymerisation produces chains with and without a thiocarbonylthio ω end-chains (living and dead respectively), and chains with different α end-chains depending on the nature of the initiation (chains with RAFT agent R group and initiator derived chains). Remarkably, the relative number of these chains can be predicted from the number of radicals generated and the number of CTA used during the reaction time.[23] In the case of thermally initiated systems (diazo/peroxide), the amount of radicals produced (dead chains) is accessible *via* the initiator rate of decomposition expressed by its half-life ($t_{1/2}$). The concentration of radicals produced over time is obtained from kinetic and Arrhenius equations:

$$[Init]_t = [Init]_0 \times e^{-kd.t} \qquad 1.3$$

$$k_d = A \times e^{-E_a/RT} \; and \; t_{1/2} = \ln 2 \, / k_d \qquad 1.4$$

where $[Init]_t$ and $[Init]_0$ are the initiator concentration at time t (s) and t_0, k_d is the rate coefficient of the initiator decomposition at considered temperature, A is the Arrhenius frequency factor, E_a is the activation energy for initiator decomposition, R = 8.3142 J/mol.K, T is the temperature (K), and $t_{1/2}$ is the half-life (s).

Considering the number of radical species generated is generally low compared to CTA in an optimised RAFT reaction, a high fraction of α, ω-functionalised chains is maintained, giving defined polymers with high chain-end fidelity. Importantly, these end-groups can be used for post-polymerisation modifications yielding functional polymers.

Besides the initiator concentration, other parameters can be tuned to optimise the polymerisation process. For instance, it is possible to maintain a high rate of polymerisation by using monomers with a high propagation rate (k_p) at high concentration

(*e.g.* acrylamides), and initiators with high efficiency (*f*) or high decomposition rate (k_d).[26, 27] Tuning these parameters can allow a fast polymerisation rate while using a lower initiator concentration, and maintaining a low number fraction of dead chains (equation 1.2). The optimisation of the RAFT process is of great importance for the synthesis of complex copolymers such as multiblock structures requiring sequential chain extension. By exploiting the degenerative process and optimising the conditions, the synthesis of multiblock copolymers at full conversion and a number of blocks as high as 20 was achieved recently.[28] This methodology has been used in this project for the synthesis of well-defined polymeric architectures (multisite, alternating, block and multiblock, and star copolymers) and the results are presented in chapter 3 and 4.

1.2.2 RAFT agents: features and availability

The RAFT process relies on the addition of a RAFT agent which is essential to obtain controlled polymerisation. A wide range of efficient RAFT agents is now available allowing the controlled polymerisation of a variety of vinyl monomers including "More Activated Monomers" (MAMs), such as butadiene, isoprene, styrene, (meth)acrylates and (meth)acrylamides, and maleic anhydride, and "Less Activated Monomers" (LAMs) such as vinyl acetate, N-vinylpyrrolidone, vinyl chloride, and 1-alkenes.[15, 29, 30] The classification of a monomer as a MAM or LAM reflects its ability to react in a free radical process. It depends on the stability of the macroradical formed and is influenced by electronic stabilisation and steric factors. The selection of the RAFT agent is a key aspect to obtain optimal control over RAFT polymerisation and is achieved by an appropriate selection of the Z and R group depending on the type of monomer polymerised. Fortunately, the influence of the R- and Z- group has been extensively reviewed and general guidelines are available (Figure 1.5).[30-33] The Z group modifies the reactivity of the thiocarbonylthio group (C=S) towards radical addition and governs the stability of the intermediate radical (Figure 1.4). For optimised RAFT, it is important to favour the formation of the intermediate by ensuring a higher reactivity of the C=S bond towards radical addition than the C=C bond of the monomer. The R group also influences the reactivity of the thiocarbonylthio group (C=S) towards radical addition and plays a crucial role in the reinitiation process. The R group must be a good leaving group to promote fragmentation (high $k_{\text{frag R}}$) and must be able to rapidly reinitiate propagation (high $k_{\text{re-in}}$)

to ensure the reactivation of all chains in same the time frame to obtain narrow molar mass distribution.

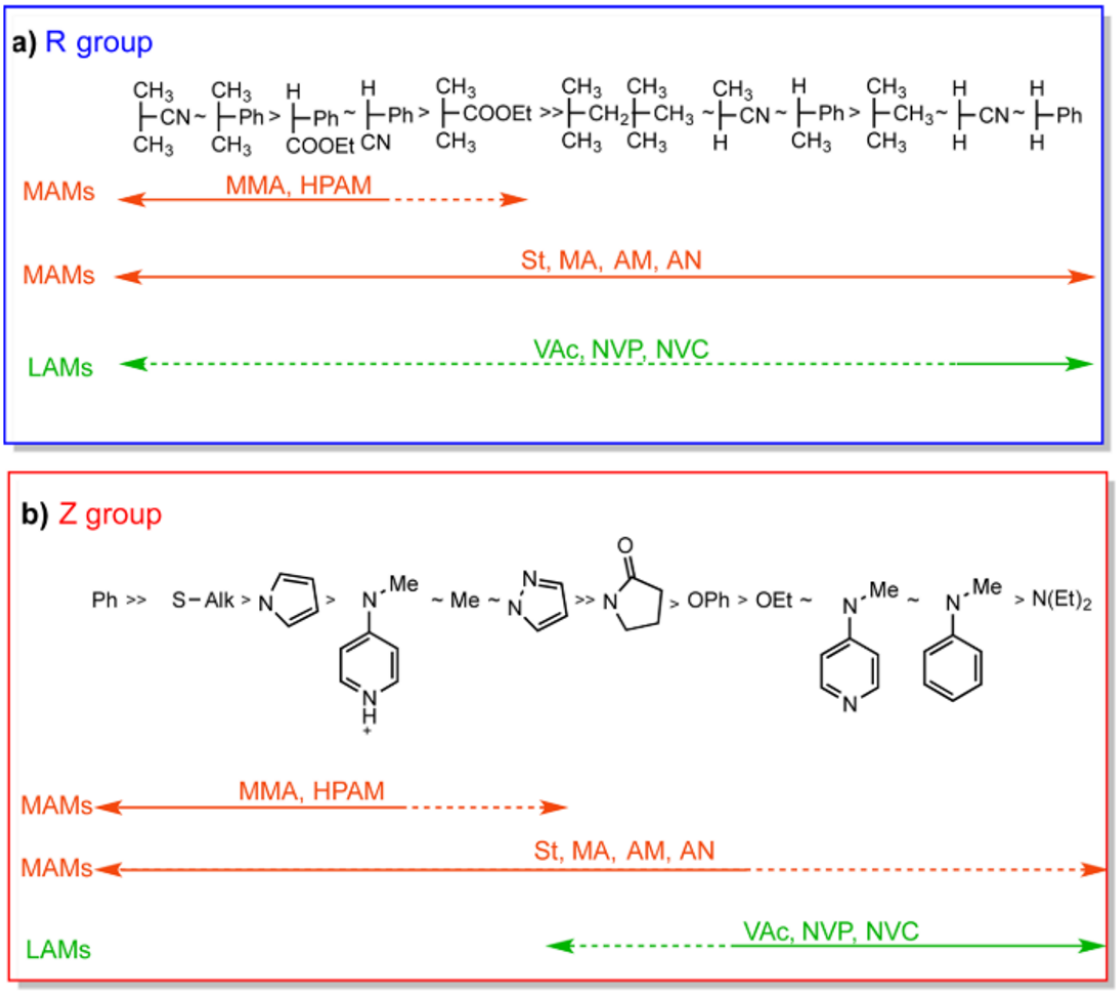

Figure 1.5. Guidelines for the selection of appropriate CTA depending on monomer polymerised. a) Selection of R group. b) Selection of Z group. Plain line indicates good control whereas dashed line indicates partial control (*i.e.* control of molar mass but poor control over dispersity or substantial retardation in case of LAMs). Figure reprinted from Perrier, 2017 and adapted from Keddie *et al.*, 2012.

These factors impact directly the efficiency of the RAFT agents, defined in terms of a chain transfer coefficient (C_{tr}), and the partition coefficient (ϕ), as expressed in the following equations:

$$C_{tr} = \frac{k_{tr}}{k_p} \quad 1.5$$

$$k_{tr} = k_{add}\phi = k_{add}\frac{k_{frag}}{k_{-add} + k_{frag}} \quad 1.6$$

$$\phi = \frac{k_{frag}}{k_{-add} + k_{frag}} \quad 1.7$$

The chain transfer constant, C_{tr} describes the reactivity/affinity of the propagating radical (I_n•) towards the thiocarbonylthio moieties, and the partition coefficient ϕ indicates the preference for the radical intermediate (or macroradical intermediate) to fragment either towards the re-initiating radical or towards the starting material. For a RAFT agent with a high chain transfer constant, the radical is rapidly exchanged among the chains (one or less monomer unit added per activating-deactivating cycle), leading to a higher probability for the chains to grow at similar rate.[34, 35] A number of methods have been used for the determination of chain transfer constants of RAFT agents and the conventional approaches include the Mayo plot method and the Walling & Moad method.[31, 33, 36-38] In these methods, the chain transfer constant is obtained from experimental data and derived from approximated mathematical equations thus, it is usually reported as the apparent chain transfer constant (C_{tr}^{app}). The determination of C_{tr}^{app} allows for direct evaluation of RAFT agents activity, however, the comparison must be made for one type of monomer polymerised in similar conditions, especially temperature.

These methods have been used for the evaluation of the industrial CTA-Ester provided by Lubrizol for this project and are presented in more detail in Chapter 2.

The different classes of accessible RAFT agents (Figure 1.6) including dithioesters (Z = C-alkyl or aryl), trithiocarbonates (Z = S-alkyl), xanthates (Z = O-alkyl), and dithiocarbamates (Z = N-alkyl) allow the controlled polymerisation of monomers with various reactivity (MAMs and LAMs), however, their efficiency is generally limited to a specific monomer category.[39] Generally, the more active RAFT agents such as dithiobenzoates, or trithiocarbonates are more adapted for polymerisation of MAMs (relatively good leaving groups), as they help with the stabilisation of the intermediate radical and provide a high rate of chain transfer with respect to propagation. In contrast, less active RAFT agents such as xanthates and dithiocarbamates are typically used for LAMs (poor leaving group), requiring less stable intermediate radicals to favour fragmentation of the propagating radical.

	Dithioesters 	**Trithiocarbonates** 	**Xanthates** 	**Dithiocarbamates** 
Advantages	✓ High control on MAMs including methacrylates and methacrylamides	✓ High control on MAMs ✓ Simple Synthesis ✓ Produced in Large scale ✓ Good Stability	✓ Versatile CTAs ✓ Relative control on MAMs (acrylamides and acrylates) ✓ Control LAMs (vinyl esters , vinyl amides, vinyldiene fluoride) ✓ Produced in Large scale	✓ Versatile CTAs ✓ Control MAMs (acrylates, Acyamides) ✓ Control LAMs (vinyl Esters, vinyl Chloride,..) ✓ "Switchable" RAFT agents (poly(MAMs-*b*-polyLAMs)
Limitations	X Unstable (hydrolysis) X Inhibition of LAMs X Retardation at high [CTA]	X Retardation or Inhibition of LAMs X Require feeding to control methacrylates	X Available under licence	X Activity depends on substituent on N
Popular RAFT Agents	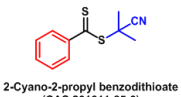 2-Cyano-2-propyl benzodithioate (CAS 201611-85-0) 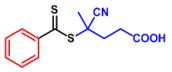 4-Cyano-4-(thiobenzoylthio) pentanoic acid (CAS 201611-92-9)	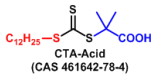 CTA-Acid (CAS 461642-78-4)  CTA-Ester (Lubrizol)  Blockbuilder DB (Arkema) 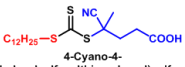 4-Cyano-4-[(dodecylsulfanylthiocarbonyl)sulfanyl] pentanoic acid (CAS 870196-80-8)	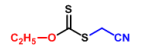 O-ethyl cyanomethylsulfanylmethanethioate (59463-54-6) 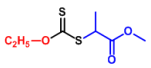 Rhodixan A1 (Solvay)	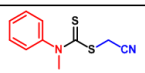 Cyanomethyl methyl(phenyl) carbamodithioate (CAS 76926-16-4) 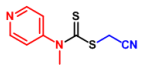 Cyanomethyl methyl(4-pyridyl)carbamodithioate "switchable" (CAS 1158958-89-4)  2-Cyanopropan-2-yl N-methyl-N-(pyridin-4-yl)carbamodithioate "switchable" (CAS 1158958-96-3)
Suppliers	▪ Sigma-Aldrich ▪ Strem Chemicals ▪ TCI Chemicals	▪ Sigma-Aldrich ▪ Strem Chemicals ▪ TCI Chemicals ▪ Boron Molecular	▪ ChemTik ▪ Solvay (Rhodia)	▪ Sigma-Aldrich ▪ Strem Chemicals ▪ TCI Chemicals ▪ Boron Molecular

Figure 1.6. General classes/structures and features of popular RAFT agents.[15, 23]

Among the different classes of RAFT agents, dithiobenzoates(Z = C-aryl) offer the best control over polymerisation of MAMs including good control of methacrylates and methacrylamides, however, their instability (hydrolysis), retardation for certain MAMs, and inhibition over LAMs polymerisation limits their applications (Figure 1.6). Trithiocarbonates exhibit good overall activity for the polymerisation of MAMs, are relatively stable, and are accessible by simple synthetic procedures. Xanthates and dithiocarbamates are versatile CTAs providing great overall control over LAMs and relative control over MAMs. This was used to synthesise block copolymers of MAMs (*e.g.* acrylamides and acrylates) and LAMs (*e.g.* vinyldiene fluoride,[40] vinyl acetate,[41, 42] and N-vinylpyrrolidone[43]).[23] The recent developments on "switchable" RAFT agents (Figure 1.6) have also allowed the synthesis of poly(MAMs-*b*-LAMs) from monomers with very different reactivity (*e.g.* styrene and vinyl acetate).[42, 44-46] Generally, the controlled synthesis of block copolymers through sequential monomer addition requires the selection of an appropriate type of RAFT agent and a specific order of monomer addition. The RAFT agent's R group must be a good leaving group with respect to the first monomer polymerised, and the Z group must be compatible with following monomers. After the first block synthesis, the R group becomes a polymer chain containing the first monomer (macroCTA), thus, the choice of the following monomer must be made accordingly. As in most RDRP systems, the more active monomers (better leaving group) must be polymerised first to ensure the good fragmentation of the R group from the macro CTA. Moreover, several alternating methods have been recently reported to either activate the RAFT agent or artificially increase its efficiency (C_{tr}), leading to better control of polymerisation of LAMs and synthesis of poly(MAMs-*b*-LAMs).[47, 48] For instance, monomer feeding (semi-batch) has been used for the synthesis of copolymers beginning with a less activated monomer.[48] The feeding process allows to artificially increase the CTA efficiency (C_{tr}) by encouraging the fragmentation-propagation of the R group from the initial CTA or macroCTA. This strategy was recently explored to increase the reactivity of Lubrizol's CTA-Ester for the controlled synthesis of methacrylate monomers.[49]

To control (co)polymerisation of both MAMs and LAMs, and achieve complex copolymers, a wide range of RAFT agents are now commercially available. Several companies such as Strem Chemicals,[50] Sigma-Aldrich,[51] and TCI[52] can provide small

quantities of various RAFT agents for research purposes (under CSIRO licence). Boron Molecular,[53] a spin-off company from CSIRO, has been recently licenced to manufacture and supply both research and commercial quantities of RAFT agents.[53] Moreover, a few other examples of industrial scale-up of specific RAFT agents have been reported (Rhodixan A1,[18] Blockbuilder DB[54] and CTA-Ester[55]), however, they are not commercial yet, and can be obtained on demand only (Figure 1.6). In the 2000s, the availability of RAFT agents was presented as a major limitation for the industrial development of RAFT technology, however, a range of RAFT agents are now accessible (from grams to metric tons) removing limitations to the development and commercialisation of new polymers, and promoting the creation of new markets based on RAFT technology.

In this project we have studied the performance of the non-commercial CTA-Ester produced in large scale by Lubrizol. The features and performance of industrial grade CTA-Ester on methacrylates and styrene RAFT polymerisation are presented in Chapter 2.

1.2.3 Industrial applications

1.2.3.1 Strengths and limitations of RAFT

With a process similar in many aspects to the well-established free radical polymerisation, RAFT technology has distinct advantages over competing technologies, providing solid bases for an industrial development. Scaling-up RAFT polymerisation is purely implemental and requires minimal adaptation of traditional reactor setups.[18, 23, 56] As discussed above, RAFT allows the controlled polymerisation of a broad range of monomers including vinyl esters (*e.g.* vinyl acetate), vinylamides (*e.g.* N-vinylpyrrolidone), providing an advantage compared to other techniques, such as NMP and ATRP, typically providing minimal control.[29] Furthermore, RAFT offers some advantages with respect to free radical polymerisation as it allows preparation of ethylene polymer with reduced branching (backbiting), and enables the introduction of functional groups within polyethylene by copolymerisation with vinyl acetates.[57] In addition, while conventional polymerisation of dienes (*e.g.* butadiene, isoprene and chloroprene) typically leads to cross-linking relatively early in the reaction, RAFT enables much higher conversions before gelation of the system.[58] Moreover, RAFT is compatible with a range

of solvents (including aqueous) and can be performed in bulk, homogeneous solution and heterogeneous systems such as emulsion or dispersion.[59-62] Recently, RAFT polymerisation was performed in continuous flow reactors, a processing system which has recently grown in interest for the large scale production of complex polymeric architectures, demonstrating again the versatility of the RAFT technique.[63-67]

The initial limitations linked to the RAFT agents (availability and end group removal) seems to be overcome today, as a wide range of RAFT agents are commercially available, and a number of methods have been developed to remove or take advantage (functionalisation) of RAFT agent end-groups.[68-70] Moreover, with the expiration of the original RAFT patents by the end of 2018 (CSIRO, Dupont, Rhodia/Solvay), the major limitation due to the extensive intellectual property will disappear, allowing more scope for commercial uses and the creation of new markets. The current developments in RAFT technology involve major international companies including Dupont, Solvay, Arkema, Lubrizol, Agfa Graphics, DSM, L'Oréal, Baush&Lomb, Syngenta, and Unilever.[19, 23] Their interest in RAFT technology lies in the design of complex polymeric architectures inaccessible by conventional technologies and which exhibit original properties for the development of high performance materials. The major fields of application include paint and coating (pigment dispersants), energy (oil, fuels, batteries, and solar cells), adhesives, cosmetics, dispersants, electronics, lubricants, biomedical, drug delivery, and agrochemicals.

1.2.3.2 Applications:

Over time, RAFT technology has been exploited through different aspects almost exclusively by the CSIRO with Dupont and Solvay/Rhodia. Several companies have now shown their interest and a few examples of industrial developments were recently given in a perspective by Perrier and a review by Destarac.[19, 23]

CSIRO has been harnessing its invention through a technology alliance with Dupont, and one of the first commercial applications of RAFT technology was developed in collaboration with Orica (Dulux) as an environmentally-friendly paint with enhanced flow, adhesion, abrasion resistance and durability.[71, 72] More recently, CSIRO have shown interest in several fields of application such as optoelectronics (photovoltaics, OLEDs and sensors),[73, 74] metal organic frameworks (MOFs),[75] personal care,[76] biomedical (RNAi and drug delivery, and antimicrobials),[77-80] and processing development for the

synthesis of highly defined polymers (light-induced RAFT, high-throughput and continuous flow).[81-83]

In the 2000s Solvay (Rhodia) reported their first commercial product based on xanthate-mediated RAFT technology (so-called MADIX), as non-ionic amphiphilic block copolymers for emulsion stabilisation (Rhodibloc® RS).[18, 84] In the 2010's, Solvay extended their portfolio of diblock technologies by developing a new series of block copolymers as cementing additives (fluid loss and gas migration control) for oilfield application (Rhodibloc® FL and Rhodibloc® GC).[85-88] Solvay has continued to be active with block polymers for the oilfield, and has developed micellar RAFT/MADIX polymerisation process, a direct aqueous route to synthesise amphiphilic block copolymers.[89, 90] Solvay also recently showed their interest in RAFT polymerisation-induced self-assembly (PISA) in emulsion for the synthesis of surfactant-free latexes of vinyldiene chloride polymers with application in the packaging industry.[91, 92]

Lubrizol has been also exploring RAFT technology and developed their first commercial product in 2011, under licence from CSIRO.[93] Lubrizol developed the large scale production of CTA-Ester (Figure 1.6) and exploited the RAFT process for the production of star-shaped methacrylate polymers (Asteric™) for commercial application in lubricant technology.[55] Recently, Lubrizol have shown particular interest in RAFT technology for the development of complex polymeric architectures such as well-defined graft copolymers, copolymer brushes, and multiblock star copolymers for application in biomedical, lubricants, oilfield, and paint industries.[94-96] The work presented in this thesis was supported by Lubrizol and had for objective of developing materials with potential application in lubricants and oilfields.

DSM also exploited RAFT technology for the preparation of a series of latexes with controlled surface functionalisation for application in coatings with improved surface properties. Functional amphiphilic copolymers were used for surfactant free emulsion polymerisation resulting in latexes with tailored functionality. For instance, films with improved properties were developed through the use of latexes containing cationic charged chains (*e.g.* anti-microbial activity, anti-static properties),[97] crosslinkable moieties (*e.g.* improved mechanical properties, solvent or strains resistance, and improved adhesion),[98] crystalline side chains (*e.g.* improved physical properties for packaging) and metal binding moieties (*e.g.* anticorrosion).[99] Recently DSM and BASF

have shown a similar interest in PISA for the preparation of diblock copolymer nano-assembly/nano-objects.[100-103] BASF has been also exploring RAFT technology for the development of textile surface modifiers using amphiphilic triblock copolymers.[104]
Other example of applications of RAFT technology can be found in biomedical and pharmaceutical companies (*e.g.* Phase RX and Nexgenia) with the development of drug delivery systems using stimuli-responsive polymers and polymer-drug conjugates.[105-107]

1.2.4 Future directions of RAFT

The RAFT process is now established as a versatile and robust synthetic tool for the development of materials with original properties and has demonstrated its industrial potential. Among the various polymeric architectures achievable by RAFT, diblock, stars and branched copolymers have been extensively studied and exploited by industries for typical applications such as, dispersants, emulsifiers, compatibilizers and rheology modifiers. Recently, considerable attention has been focused on implementing the RAFT process for efficient production of complex materials and facilitating their industrial developments. For instance, promising advances have been made in continuous flow processing, light-induced/photocontrolled RAFT polymerisation (direct photolysis, PET-RAFT), microwave-assisted RAFT and heterogeneous polymerisation systems (dispersion and emulsion PISA).[19, 23, 108, 109]
The continuous flow reactor processing offers excellent control over exothermic reaction, simplicity of operation, high throughput rates, uniform product quality, relatively low operating costs, and is a promising alternative process for the large scale production of complex organic molecules and polymer materials.[64-66, 108, 110-114] Photocontrolled RAFT polymerisation (direct Photolysis-RAFT and PET-RAFT) has been intensively studied recently and provides advantages such as room temperature processing and temporal control on polymerisation reaction (switch on and off).[115-118] Recent advances have shown the combination of photocontrolled RAFT polymerisation with continuous flow processing and emulsion polymerisation.[66] Recently, photocontrolled RAFT was exploited for the synthesis of well-defined copolymers (block and multiblock), sequence controlled copolymers, and ultra-high molecular weight (UHMW) polymers.[81, 119, 120] The microwave assisted RAFT polymerisation was also considered to improve polymerisation reaction rates and achieve higher monomer conversions, however, scale-up of microwave processes remains challenging.[121-123] Furthermore, polymerisation-induced self-assembly

(PISA) in emulsion or dispersion using RAFT has recently emerged as an efficient and robust approach to produce block copolymer nano-objects with controlled size, morphology, and surface chemistry. Because of its advantages, including versatility, efficiency, cost-effectiveness, and potential scalability, the PISA process is now considered as a promising route to synthesise amphiphilic diblock copolymers for commercial applications.[91, 92, 124-128]

Moreover, significant efforts have been directed toward the preparation of advanced polymers with tunable monomer sequences (multisite, multiblock and gradient copolymers).[28, 81, 108, 129-131] The importance of controlling monomer distribution to tune the physicochemical and biological properties of copolymers has been demonstrated in several recent studies.[132-140] Gradient copolymers have already attracted much attention from academia and industry as they exhibit original properties (broad glass transition and improved interfacial stabilisation) useful for applications including shock and noise absorbing materials, emulsifiers and dispersants.[139, 141-144] Multiblock copolymers have also gained interest and were used in recent studies to investigate the effect of polymer microstructures on diverse properties such as thermal behaviours or antimicrobial activity.[132, 135] In this thesis, significant efforts were dedicated to the synthesis of copolymers with controlled comonomer distribution (multisite, block, multiblock and alternating) and various architectures (linear, star and grafted copolymers) to study the relation between structure and properties for application in lubricants (pour point depressants and viscosity modifiers).

Another challenge is the controlled synthesis of ultra-high molar mass copolymers giving access to materials with high mechanical strength and, at the same time, reducing the cost associated with the CTA.[120, 145, 146] Furthermore, with the recent progress in the polymerisation of challenging monomers such as ethylene, diene, vinyl chloride, fluorinated monomers and cyclic ketene acetals, the development of new materials is likely.[40, 57, 58, 147-150] Cyclic ketene acetals are particularly interesting as their copolymerisation with traditional vinyl polymers allows the incorporation of degradable ester linkages into vinyl polymers backbones. This is a very promising advance towards the development of new degradable/environmental-friendly materials. Beyond these considerations, RAFT polymerisation has also gained a lot of attention for the synthesis of polymer conjugates for biomedical application (peptide, protein, drug and

RNA/DNA),[151-153] the synthesis of advanced architectures (star, cyclic polymers and single chain nanoparticles),[154-157] and material surface and interface engineering.[158]

1.3 PSMA Materials by RAFT

Poly(styrene-*alt*-maleic anhydride) (PSMA) are interesting materials combining sequence controlled monomer distribution (alternating) and facile access to highly functional materials.[159-163] PSMAs are popular materials in industry where they are commonly used as intermediates of specialty polymers, polymeric surfactants, compatibilizers and high functionality cross-linking agents. PSMA materials and their derivatives have been used for diverse applications including paper sizing, coatings, pigment dispersions, inks and over print varnishes formulations, leather retanning, microelectronics fabrication and processing, plasticisers and as rheology modifiers to name few.[164-167]

Lubrizol is one among the numerous companies using the great properties of PSMA materials and develops polymeric additive technologies for paint, coatings, lubricants, and fuels.[168, 169] Lubrizol has been using PSMA as viscosity modifiers for various applications including performance improvers for automatic transmission fluids and hydraulic fluids (shear stability, low temperature fluidity, and dispersing activity). Alkyl functionalised PSMA have been particularly useful in improving low temperature performance of oil derivatives. Their performance as pour point depressants has also been demonstrated in literature.[170-174] However, because PSMAs are produced industrially using a free radical polymerisation process, their study is restricted to PSMA materials with limited control of molecular composition and structure. With the recent development in controlled radical polymerisation techniques, it is now possible to synthesise PSMA with complex architectures allowing the development of materials with new properties. The RAFT polymerisation of well-defined PSMA copolymers is already established.[159, 175-178] Therefore the RAFT process appears as a method of choice to develop advanced PSMA materials with potential interest for Lubrizol activities.

1.4 Scope of the thesis

The overall aim of this project is to exploit RAFT polymerisation to synthesise graft copolymers with potential application in oil industry.

This project was conducted in collaboration with Lubrizol, one of the few industrial companies which have developed large scale production of RAFT agents (CTA-Ester) and scaled up the RAFT polymerisation process. To anticipate industrial production of the materials synthesised in this study, the RAFT polymerisation process was optimised using industrial grade CTA-Ester from Lubrizol. In order to develop materials with original properties, the synthesis of well-defined PSMA materials by RAFT was investigated. The synthesis of PSMA by free radical polymerisation is limited to alternating PSMA with poor structural control and yielding highly grafted materials after functionalisation. In this project, RAFT polymerisation was exploited to synthesise well-defined PSMA with control of density and distribution of side chain functionality, and study the effect on rheology properties.

- In chapter 2, we investigated the purity of the CTA-Ester provided by Lubrizol and evaluate its performance for RAFT polymerisation of styrene and methyl methacrylate, two monomers of Lubrizol interest.
- In Chapter 3, we develop a one-pot sequential monomer addition strategy for the gram scale synthesis of a multisite PSMA allowing the preparation of graft materials with low density of side chains.
- In chapter 4, we extended the synthetic strategy to prepare a library of PSMA materials with various density of side chains. The effect of side chain distribution on solution behaviour and thermal properties was also studied.
- In chapter 5, we evaluate the performance of the PSMA materials as pour point depressants and viscosity modifiers in two mineral oils to determine their potential as lubricant additives.

1.5 References

(1) Franz, H. German Patents 250 691; 235 423; 250 335. **1909**.
(2) Hofmann, F. Synthetic caoutchouc from technical standpoint. *Angew. Chem.* **1912**, 25, 1462-67.
(3) PlasticEurope. Plastics-the Facts 2017. https://www.plasticseurope.org/en/resources/market-data
(4) Matyjaszewski, K.; Davis, T. P., *Handbook of radical polymerization*. John Wiley & Sons, **2003**.
(5) Matyjaszewski, K.; Spanswick, J. Controlled/living radical polymerization. *Mater. Today* **2005**, 8 (3), 26-33.
(6) Georges, M. K.; Veregin, R. P. N.; Kazmaier, P. M.; Hamer, G. K. Narrow molecular weight resins by a free-radical polymerization process. *Macromolecules* **1993**, 26 (11), 2987-2988.
(7) Nicolas, J.; Guillaneuf, Y.; Lefay, C.; Bertin, D.; Gigmes, D.; Charleux, B. Nitroxide-mediated polymerization. *Prog. Polym. Sci.* **2013**, 38 (1), 63-235.
(8) Kato, M.; Kamigaito, M.; Sawamoto, M.; Higashimura, T. Polymerization of Methyl Methacrylate with the Carbon Tetrachloride/Dichlorotris- (triphenylphosphine)ruthenium(II)/Methylaluminum Bis(2,6-di-tert-butylphenoxide) Initiating System: Possibility of Living Radical Polymerization. *Macromolecules* **1995**, 28 (5), 1721-1723.
(9) Wang, J.-S.; Matyjaszewski, K. Controlled/"living" radical polymerization. atom transfer radical polymerization in the presence of transition-metal complexes. *J. Am. Chem. Soc.* **1995**, 117 (20), 5614-5615.
(10) Matyjaszewski, K.; Tsarevsky, N. V. Macromolecular Engineering by Atom Transfer Radical Polymerization. *J. Am. Chem. Soc.* **2014**, 136 (18), 6513-6533.
(11) Matyjaszewski, K. Atom Transfer Radical Polymerization (ATRP): Current Status and Future Perspectives. *Macromolecules* **2012**, 45 (10), 4015-4039.
(12) Anastasaki, A.; Nikolaou, V.; Nurumbetov, G.; Wilson, P.; Kempe, K.; Quinn, J. F.; Davis, T. P.; Whittaker, M. R.; Haddleton, D. M. Cu(0)-Mediated Living Radical Polymerization: A Versatile Tool for Materials Synthesis. *Chem. Rev.* **2016**, 116 (3), 835-877.
(13) Chiefari, J.; Chong, Y. K.; Ercole, F.; Krstina, J.; Jeffery, J.; Le, T. P. T.; Mayadunne, R. T. A.; Meijs, G. F.; Moad, C. L.; Moad, G.; Rizzardo, E.; Thang, S. H. Living Free-Radical Polymerization by Reversible Addition−Fragmentation Chain Transfer: The RAFT Process. *Macromolecules* **1998**, 31 (16), 5559-5562.
(14) Perrier, S.; Takolpuckdee, P. Macromolecular design via reversible addition–fragmentation chain transfer (RAFT)/xanthates (MADIX) polymerization. *J. Polym. Sci., Part A: Polym. Chem.* **2005**, 43 (22), 5347-5393.
(15) Moad, G.; Rizzardo, E.; Thang, S. H. Living Radical Polymerization by the RAFT Process – A Third Update. *Aust. J. Chem.* **2012**, 65 (8), 985-1076.
(16) Matyjaszewski, K. Architecturally Complex Polymers with Controlled Heterogeneity. *Science* **2011**, 333 (6046), 1104-1105.
(17) Matheson, R. The commercialization of controlled polymer synthesis. *The Knowledge Foundation, Cambridge, MA, USA* **2000**.
(18) Destarac, M. Controlled Radical Polymerization: Industrial Stakes, Obstacles and Achievements. *Macromol. React. Eng.* **2010**, 4 (3-4), 165-179.
(19) Destarac, M. Industrial developments of reversible-deactivation radical polymerizations: is the induction period over? *Polym. Chem.* **2018**, 9 (40), 4947-4967.
(20) Corpart, P.; Charmot, D.; Zard, S. Z.; Biadatti, T.; Michelet, D. Method for block polymer synthesis by controlled radical polymerisation. Patent WO1998058974A1, **1998**.
(21) Le, T.; Moad, G.; Rizzardo, E.; Thang, S. Polymerization with living characteristics. Patent WO1998001478A1, **1998**.
(22) Barner-Kowollik, C., *Handbook of RAFT Polymerization*. John Wiley & Sons, **2008**.
(23) Perrier, S. 50th Anniversary Perspective: RAFT Polymerization—A User Guide. *Macromolecules* **2017**, 50 (19), 7433-7447.
(24) Jenkins Aubrey, D.; Jones Richard, G.; Moad, G. Terminology for reversible-deactivation radical polymerization previously called "controlled" radical or "living" radical polymerization (IUPAC Recommendations 2010). *Pure Appl. Chem.* **2009**, 82 (2), 483.
(25) Fischer, H. The Persistent Radical Effect: A Principle for Selective Radical Reactions and Living Radical Polymerizations. *Chem. Rev.* **2001**, 101 (12), 3581-3610.

(26) Gody, G.; Maschmeyer, T.; Zetterlund, P. B.; Perrier, S. Exploitation of the Degenerative Transfer Mechanism in RAFT Polymerization for Synthesis of Polymer of High Livingness at Full Monomer Conversion. *Macromolecules* **2014**, 47 (2), 639-649.
(27) Gody, G.; Maschmeyer, T.; Zetterlund, P. B.; Perrier, S. Pushing the Limit of the RAFT Process: Multiblock Copolymers by One-Pot Rapid Multiple Chain Extensions at Full Monomer Conversion. *Macromolecules* **2014**, 47 (10), 3451-3460.
(28) Gody, G.; Maschmeyer, T.; Zetterlund, P. B.; Perrier, S. Rapid and quantitative one-pot synthesis of sequence-controlled polymers by radical polymerization. *Nat. Commun.* **2013**, 4, 2505.
(29) Keddie, D. J. A guide to the synthesis of block copolymers using reversible-addition fragmentation chain transfer (RAFT) polymerization. *Chem. Soc. Rev.* **2014**, 43 (2), 496-505.
(30) Keddie, D. J.; Moad, G.; Rizzardo, E.; Thang, S. H. RAFT Agent Design and Synthesis. *Macromolecules* **2012**, 45 (13), 5321-5342.
(31) Chiefari, J.; Mayadunne, R. T. A.; Moad, C. L.; Moad, G.; Rizzardo, E.; Postma, A.; Thang, S. H. Thiocarbonylthio Compounds (SC(Z)S−R) in Free Radical Polymerization with Reversible Addition-Fragmentation Chain Transfer (RAFT Polymerization). Effect of the Activating Group Z. *Macromolecules* **2003**, 36 (7), 2273-2283.
(32) Moad, G.; Rizzardo, E.; Thang, S. H. Living Radical Polymerization by the RAFT Process. *Aust. J. Chem.* **2005**, 58 (6), 379-410.
(33) Chong, Y. K.; Krstina, J.; Le, T. P. T.; Moad, G.; Postma, A.; Rizzardo, E.; Thang, S. H. Thiocarbonylthio Compounds [SC(Ph)S−R] in Free Radical Polymerization with Reversible Addition-Fragmentation Chain Transfer (RAFT Polymerization). Role of the Free-Radical Leaving Group (R). *Macromolecules* **2003**, 36 (7), 2256-2272.
(34) Destarac, M. On the Critical Role of RAFT Agent Design in Reversible Addition-Fragmentation Chain Transfer (RAFT) Polymerization. *Poly. Rev.* **2011**, 51 (2), 163-187.
(35) Adamy, M.; van Herk, A. M.; Destarac, M.; Monteiro, M. J. Influence of the Chemical Structure of MADIX Agents on the RAFT Polymerization of Styrene. *Macromolecules* **2003**, 36 (7), 2293-2301.
(36) Mayo, F. R. Chain Transfer in the Polymerization of Styrene: The Reaction of Solvents with Free Radicals1. *J. Am. Chem. Soc.* **1943**, 65 (12), 2324-2329.
(37) Walling, C. The Use of S35 in the Measurement of Transfer Constants. *J. Am. Chem. Soc.* **1948**, 70 (7), 2561-2564.
(38) Moad, C. L.; Moad, G.; Rizzardo, E.; Thang, S. H. Chain Transfer Activity of ω-Unsaturated Methyl Methacrylate Oligomers. *Macromolecules* **1996**, 29 (24), 7717-7726.
(39) Moad, G. Mechanism and Kinetics of Dithiobenzoate-Mediated RAFT Polymerization – Status of the Dilemma. *Macromol. Chem. Phys.* **2014**, 215 (1), 9-26.
(40) Girard, E.; Marty, J.-D.; Ameduri, B.; Destarac, M. Direct Synthesis of Vinylidene Fluoride-Based Amphiphilic Diblock Copolymers by RAFT/MADIX Polymerization. *ACS Macro Lett.* **2012**, 1 (2), 270-274.
(41) Girard, E.; Tassaing, T.; Marty, J.-D.; Destarac, M. Influence of macromolecular characteristics of RAFT/MADIX poly(vinyl acetate)-based (co)polymers on their solubility in supercritical carbon dioxide. *Polym. Chem.* **2011**, 2 (10), 2222-2230.
(42) Destarac, M.; Charmot, D.; Franck, X.; Zard, S. Dithiocarbamates as universal reversible addition ‐ fragmentation chain transfer agents. *Macromol. Rapid Commun.* **2000**, 21 (15), 1035-1039.
(43) Guinaudeau, A.; Coutelier, O.; Sandeau, A.; Mazières, S.; Nguyen Thi, H. D.; Le Drogo, V.; Wilson, D. J.; Destarac, M. Facile Access to Poly(N-vinylpyrrolidone)-Based Double Hydrophilic Block Copolymers by Aqueous Ambient RAFT/MADIX Polymerization. *Macromolecules* **2014**, 47 (1), 41-50.
(44) Benaglia, M.; Chen, M.; Chong, Y. K.; Moad, G.; Rizzardo, E.; Thang, S. H. Polystyrene-block-poly(vinyl acetate) through the Use of a Switchable RAFT Agent. *Macromolecules* **2009**, 42 (24), 9384-9386.
(45) Dayter, L. A.; Murphy, K. A.; Shipp, D. A. RAFT Polymerization of Monomers with Highly Disparate Reactivities: Use of a Single RAFT Agent and the Synthesis of Poly(styrene-block-vinyl acetate) *Aust. J. Chem.* **2013**, 66 (12), 1564-1569.
(46) Benaglia, M.; Chiefari, J.; Chong, Y. K.; Moad, G.; Rizzardo, E.; Thang, S. H. Universal (Switchable) RAFT Agents. *J. Am. Chem. Soc.* **2009**, 131 (20), 6914-6915.
(47) Aoshima, H.; Uchiyama, M.; Satoh, K.; Kamigaito, M. Interconvertible Living Radical and Cationic Polymerization through Reversible Activation of Dormant Species with Dual Activity. *Angew. Chem.* **2014**, 126 (41), 11112-11116.

(48) Ilchev, A.; Pfukwa, R.; Hlalele, L.; Smit, M.; Klumperman, B. Improved control through a semi-batch process in RAFT-mediated polymerization utilizing relatively poor leaving groups. *Polym. Chem.* **2015**, 6 (46), 7945-7948.
(49) Akrach, M., Carbon black dispersion using polymeric dispersants prepared via RAFT polymerisation, unpublished PhD thesis, University of Warwick, **2018**.
(50) Strem-Chemicals. https://www.strem.com/catalog/family/RAFT+Agent/
(51) Sigma-Aldrich. https://www.sigmaaldrich.com/materials-science/polymer-science.html
(52) TCI. https://www.tcichemicals.com/eshop/en/hk/category_index/13075/
(53) Boron-Molecular. http://www.boronmolecular.com/RaftAgents
(54) Couvreur, L.; Guerret, O.; Laffitte, J.-A.; Magnet, S. J. P. P. Dibenzyltrithiocarbonate (DBTTC) perfomances overview of a commercially available RAFT agent. *Polym. Prepr. (Am. Chem. Soc., Div. Polym. Chem.)* **2005**, 46, 219.
(55) Brzytwa, A. J.; Johnson, J. Scaled Production of RAFT CTA–a STAR Performer. *Polym. Prepr. (Am. Chem. Soc., Div. Polym. Chem.)* **2011**, 52 (2), 533-534.
(56) Barner-Kowollik, C.; Perrier, S. The future of reversible addition fragmentation chain transfer polymerization. *J. Polym. Sci., Part A: Polym. Chem.* **2008**, 46 (17), 5715-5723.
(57) Dommanget, C.; D'Agosto, F.; Monteil, V. Polymerization of Ethylene through Reversible Addition–Fragmentation Chain Transfer (RAFT). *Angew. Chem.* **2014**, 53 (26), 6683-6686.
(58) Moad, G. Reversible addition–fragmentation chain transfer (co)polymerization of conjugated diene monomers: butadiene, isoprene and chloroprene. *Polym. Int.* **2017**, 66 (1), 26-41.
(59) Ferguson, C. J.; Hughes, R. J.; Nguyen, D.; Pham, B. T. T.; Gilbert, R. G.; Serelis, A. K.; Such, C. H.; Hawkett, B. S. Ab Initio Emulsion Polymerization by RAFT-Controlled Self-Assembly. *Macromolecules* **2005**, 38 (6), 2191-2204.
(60) Lowe, A. B.; McCormick, C. L. Reversible addition–fragmentation chain transfer (RAFT) radical polymerization and the synthesis of water-soluble (co)polymers under homogeneous conditions in organic and aqueous media. *Prog. Polym. Sci.* **2007**, 32 (3), 283-351.
(61) Zetterlund, P. B.; Kagawa, Y.; Okubo, M. Controlled/Living Radical Polymerization in Dispersed Systems. *Chem. Rev.* **2008**, 108 (9), 3747-3794.
(62) Zetterlund, P. B.; Thickett, S. C.; Perrier, S.; Bourgeat-Lami, E.; Lansalot, M. Controlled/Living Radical Polymerization in Dispersed Systems: An Update. *Chem. Rev.* **2015**, 115 (18), 9745-9800.
(63) Hornung, C. H.; Nguyen, X.; Kyi, S.; Chiefari, J.; Saubern, S. Synthesis of RAFT Block Copolymers in a Multi-Stage Continuous Flow Process Inside a Tubular Reactor. *Aust. J. Chem.* **2013**, 66 (2), 192-198.
(64) Martinez-Botella, I. Continuous Flow Synthesis of RAFT Block Copolymers. *Aust. J. Chem.* **2015**, 68 (1), 170-171.
(65) Gardiner, J.; Hornung, C. H.; Tsanaktsidis, J.; Guthrie, D. Continuous flow photo-initiated RAFT polymerisation using a tubular photochemical reactor. *Eur. Polym. J.* **2016**, 80, 200-207.
(66) Zaquen, N.; Yeow, J.; Junkers, T.; Boyer, C.; Zetterlund, P. B. Visible Light-Mediated Polymerization-Induced Self-Assembly Using Continuous Flow Reactors. *Macromolecules* **2018**, 51 (14), 5165-5172.
(67) Tonhauser, C.; Natalello, A.; Löwe, H.; Frey, H. Microflow Technology in Polymer Synthesis. *Macromolecules* **2012**, 45 (24), 9551-9570.
(68) Perrier, S.; Takolpuckdee, P.; Mars, C. A. Reversible Addition−Fragmentation Chain Transfer Polymerization: End Group Modification for Functionalized Polymers and Chain Transfer Agent Recovery. *Macromolecules* **2005**, 38 (6), 2033-2036.
(69) Willcock, H.; O'Reilly, R. K. End group removal and modification of RAFT polymers. *Polym. Chem.* **2010**, 1 (2), 149-157.
(70) Moad, G.; Rizzardo, E.; Thang, S. H. End-functional polymers, thiocarbonylthio group removal/transformation and reversible addition–fragmentation–chain transfer (RAFT) polymerization. *Polym. Int.* **2011**, 60 (1), 9-25.
(71) CSIROpedia. https://csiropedia.csiro.au/raft-polymerisation/
(72) Moad, G.; Thang, S. H. RAFT Polymerization: Materials of The Future, Science of Today: Radical Polymerization The Next Stage. *Aust. J. Chem.* **2009**, 62 (11), 1379-1381.
(73) Moad, G.; Chen, M.; Häussler, M.; Postma, A.; Rizzardo, E.; Thang, S. H. Functional polymers for optoelectronic applications by RAFT polymerization. *Polym. Chem.* **2011**, 2 (3), 492-519.
(74) Chen, M.; Häussler, M.; Moad, G.; Rizzardo, E. Block copolymers containing organic semiconductor segments by RAFT polymerization. *Org. Biomol. Chem.* **2011**, 9 (17), 6111-6119.

(75) Rubio-Martinez, M.; Avci-Camur, C.; Thornton, A. W.; Imaz, I.; Maspoch, D.; Hill, M. R. New synthetic routes towards MOF production at scale. *Chem. Soc. Rev.* **2017**, 46 (11), 3453-3480.
(76) Haeussler, M.; Chiefari, J.; Moad, G.; Rizzardo, *Polymers for Personal Care Cosmetics*. ACS Symposium Series, **2013**, Vol. 1148.
(77) Hinton, T. M.; Guerrero-Sanchez, C.; Graham, J. E.; Le, T.; Muir, B. W.; Shi, S.; Tizard, M. L. V.; Gunatillake, P. A.; McLean, K. M.; Thang, S. H. The effect of RAFT-derived cationic block copolymer structure on gene silencing efficiency. *Biomaterials* **2012**, 33 (30), 7631-7642.
(78) Michl, T. D.; Locock, K. E. S.; Stevens, N. E.; Hayball, J. D.; Vasilev, K.; Postma, A.; Qu, Y.; Traven, A.; Haeussler, M.; Meagher, L.; Griesser, H. J. RAFT-derived antimicrobial polymethacrylates: elucidating the impact of end-groups on activity and cytotoxicity. *Polym. Chem.* **2014**, 5 (19), 5813-5822.
(79) Gunatillake, P. A.; Hinton, T. M.; Thang, S.; Tizard, M. L. Branched polymers. US 20150056158 A1, **2015**.
(80) Fairbanks, B. D.; Gunatillake, P. A.; Meagher, L. Biomedical applications of polymers derived by reversible addition – fragmentation chain-transfer (RAFT). *Adv. Drug Delivery Rev.* **2015**, 91, 141-152.
(81) Fu, C.; Huang, Z.; Hawker, C. J.; Moad, G.; Xu, J.; Boyer, C. RAFT-mediated, visible light-initiated single unit monomer insertion and its application in the synthesis of sequence-defined polymers. *Polym. Chem.* **2017**, 8 (32), 4637-4643.
(82) Haven, J. J.; Guerrero-Sanchez, C.; Keddie, D. J.; Moad, G.; Thang, S. H.; Schubert, U. S. One pot synthesis of higher order quasi-block copolymer libraries via sequential RAFT polymerization in an automated synthesizer. *Polym. Chem.* **2014**, 5 (18), 5236-5246.
(83) Chiefari, J.; Hornung, C.; Postma, A.; Saubern, S. RAFT polymers. US 9650450 B2, **2017**.
(84) Deroo, S.; Morvan, M.; Destarac, M. Method for preparing an emulsion by diluting an emulsifiable concentrate comprising an amphiphilic copolymer. WO 2003090916 A2, **2005**.
(85) Cadix, A.; Wilson, J.; Barthet, C.; Phan, C.; Poix, C.; Dupuis, P.; Harrisson, S., Diblock copolymers: a new class of fluid loss control additive for oilfield cementing, SPE International Symposium on Oilfield Chemistry, Society of Petroleum Engineers, **2015**.
(86) Cadix, A.; Wilson, D. J. Block polymers for fluid loss control. US 20160214896 A1, **2016**.
(87) Cadix, A.; Wilson, J.; Phan, C.; Villafane, L.; Gomez, J. R.; Bzducha, W.; Feuillette, A.; Poix-Davaine, C.; Thant, K.; Nelson, T., New Diblock Copolymers as Fluid Loss Additive for High Temperature Cementing, Society of Petroleum Engineers, **2016**.
(88) Cadix, A.; Wilson, D. J. Sequenced polymers for monitoring the filtrate. WO 2016162387 A1 **2018**.
(89) Barthet, C.; Wilson, J.; Cadix, A.; Destarac, M.; Chassenieux, C.; Harrisson, S. Micellar RAFT/MADIX Polymerization. *ACS Macro Lett.* **2017**, 1342-1346.
(90) Wilson, J.; Destarac, M.; Cadix, A. Preparation of amphiphilic block polymers by controlled radical micellar polymerisation. WO 2013060741 A1, **2017**.
(91) Velasquez, E.; Rieger, J.; Stoffelbach, F.; D'Agosto, F.; Lansalot, M.; Dufils, P.-E.; Vinas, J. Surfactant-free poly(vinylidene chloride) latexes via one-pot RAFT-mediated aqueous polymerization. *Polymer* **2016**, 106, 275-284.
(92) Vinas, J.; Velasquez, E.; Dufils, P.-E.; Rieger, J.; Stoffelbach, F.; Lansalot, M.; D'agosto, F.; Charleux, B.; Vanderveken, Y. Process for the preparation of a vinylidene chloride polymer. WO 2013092587 A1, **2014**.
(93) CSIRO. Highlights of 2011-12. https://www.csiro.au/en/About/Our-impact/Reporting-our-impact/Annual-reports/
(94) Moriceau, G.; Gody, G.; Hartlieb, M.; Winn, J.; Kim, H.; Mastrangelo, A.; Smith, T.; Perrier, S. Functional multisite copolymer by one-pot sequential RAFT copolymerization of styrene and maleic anhydride. *Polym. Chem.* **2017**, 8 (28), 4152-4161.
(95) Kerr, A.; Hartlieb, M.; Sanchis, J.; Smith, T.; Perrier, S. Complex multiblock bottle-brush architectures by RAFT polymerization. *Chem. Commun.* **2017**, 53 (87), 11901-11904
(96) Bray, C.; Peltier, R.; Kim, H.; Mastrangelo, A.; Perrier, S. Anionic Multiblock Core Cross-Linked Star Copolymers via RAFT Polymerization. *Polym. Chem.* **2017**, 8 (36), 5513-5524.
(97) Schellekens, M. A. J.; Geurts, J.; Nabuurs, T.; Overbeek, G. C. Aqueous oligomer/polymer emulsion with cationic functionality. US 20100136353 A1, **2012**.
(98) Schellekens, M. A. J.; Nabuurs, T.; Geurts, J.; Overbeek, G. C. Water borne crosslinkable block copolymers obtained using raft. US 20110021689 A1, **2011**.
(99) Schellekens, M. A. J.; Nabuurs, T.; Geurts, J.; Overbeek, G. C. Adhesion to metal surfaces with block copolymers obtained using raft. WO 2010000725 A1, **2014**.

(100) Gonzato, C.; Semsarilar, M.; Jones, E. R.; Li, F.; Krooshof, G. J. P.; Wyman, P.; Mykhaylyk, O. O.; Tuinier, R.; Armes, S. P. Rational Synthesis of Low-Polydispersity Block Copolymer Vesicles in Concentrated Solution via Polymerization-Induced Self-Assembly. *J. Am. Chem. Soc.* **2014**, 136 (31), 11100-11106.
(101) Jones, E. R.; Mykhaylyk, O. O.; Semsarilar, M.; Boerakker, M.; Wyman, P.; Armes, S. P. How Do Spherical Diblock Copolymer Nanoparticles Grow during RAFT Alcoholic Dispersion Polymerization? *Macromolecules* **2016**, 49 (1), 172-181.
(102) Jones, E. R.; Semsarilar, M.; Wyman, P.; Boerakker, M.; Armes, S. P. Addition of water to an alcoholic RAFT PISA formulation leads to faster kinetics but limits the evolution of copolymer morphology. *Polym. Chem.* **2016**, 7 (4), 851-859.
(103) Byard, S. J.; Williams, M.; McKenzie, B. E.; Blanazs, A.; Armes, S. P. Preparation and Cross-Linking of All-Acrylamide Diblock Copolymer Nano-Objects via Polymerization-Induced Self-Assembly in Aqueous Solution. *Macromolecules* **2017**, 50 (4), 1482-1493.
(104) Messerschmidt, M.; Komber, H.; Häußler, L.; Hanzelmann, C.; Stamm, M.; Raether, B.; da Costa e Silva, O.; Uhlmann, P. Amphiphilic ABC Triblock Copolymers Tailored via RAFT Polymerization as Textile Surface Modifiers with Dual-Action Properties. *Macromolecules* **2013**, 46 (7), 2616-2627.
(105) Stayton, P. S.; Hoffman, A. S.; Convertine, A. J.; Benoit, D.; Duvall, C. L.; Johnson, P. H.; Gall, A. S. Diblock copolymers and polynucleotide complexes thereof for delivery into cells. US 9476063 B2, **2016**.
(106) Stayton, P. S.; Hoffman, A. S.; Convertine, A. J.; Duvall, C. L.; Benoit, D.; Overell, R. W.; Johnson, P. H.; Gall, A. S.; Prieve, M. G.; Paschal, A. E. Polymeric carrier. US 9006193 B2, **2015**.
(107) Nehilla B.J., P. N. M., Manganiello M.J. , Cox T., Emde M. Cell-surface molecule binding stimuli-responsive polymer compositions and methods cross-reference to related applications. WO 2017161051 A1, **2017**.
(108) Grubbs, R. B.; Grubbs, R. H. 50th Anniversary Perspective: Living Polymerization—Emphasizing the Molecule in Macromolecules. *Macromolecules* **2017**, 50 (18), 6979-6997.
(109) Hill, M. R.; Carmean, R. N.; Sumerlin, B. S. Expanding the Scope of RAFT Polymerization: Recent Advances and New Horizons. *Macromolecules* **2015**, 48 (16), 5459-5469.
(110) Nesvadba, P., *Radical Polymerization in Industry*. Encyclopedia of Radicals in Chemistry, Biology and Materials, John Wiley & Sons, **2012**.
(111) Hornung, C. H.; Guerrero-Sanchez, C.; Brasholz, M.; Saubern, S.; Chiefari, J.; Moad, G.; Rizzardo, E.; Thang, S. H. Controlled RAFT Polymerization in a Continuous Flow Microreactor. *Org. Process Res. Dev.* **2011**, 15 (3), 593-601.
(112) Rubens, M.; Latsrisaeng, P.; Junkers, T. Visible light-induced iniferter polymerization of methacrylates enhanced by continuous flow. *Polym. Chem.* **2017**, 8 (42), 6496-6505.
(113) Kuroki, A.; Martinez-Botella, I.; Hornung, C.; Martin, L.; Williams, E. G. L.; Locock, K.; Hartlieb, M.; Perrier, S. Looped flow RAFT polymerization for multiblock copolymer synthesis. *Polym. Chem.* **2017**, 8 (21), 3249-3254.
(114) Cole, K. P.; Groh, J. M.; Johnson, M. D.; Burcham, C. L.; Campbell, B. M., et al. Kilogram-scale prexasertib monolactate monohydrate synthesis under continuous-flow CGMP conditions. *Science* **2017**, 356 (6343), 1144-1150.
(115) Pan, X.; Tasdelen, M. A.; Laun, J.; Junkers, T.; Yagci, Y.; Matyjaszewski, K. Photomediated controlled radical polymerization. *Prog. Polym. Sci.* **2016**, 62, 73-125.
(116) McKenzie, T. G.; Fu, Q.; Uchiyama, M.; Satoh, K.; Xu, J.; Boyer, C.; Kamigaito, M.; Qiao, G. G. Beyond Traditional RAFT: Alternative Activation of Thiocarbonylthio Compounds for Controlled Polymerization. *Adv. Sci.* **2016**, 3 (9), 1500394.
(117) Chen, M.; Zhong, M.; Johnson, J. A. Light-Controlled Radical Polymerization: Mechanisms, Methods, and Applications. *Chem. Rev.* **2016**, 116 (17), 10167-10211.
(118) Xu, J.; Shanmugam, S.; Duong, H. T.; Boyer, C. Organo-photocatalysts for photoinduced electron transfer-reversible addition–fragmentation chain transfer (PET-RAFT) polymerization. *Polym. Chem.* **2015**, 6 (31), 5615-5624.
(119) Xu, J.; Jung, K.; Atme, A.; Shanmugam, S.; Boyer, C. A Robust and Versatile Photoinduced Living Polymerization of Conjugated and Unconjugated Monomers and Its Oxygen Tolerance. *J. Am. Chem. Soc.* **2014**, 136 (14), 5508-5519.
(120) Carmean, R. N.; Becker, T. E.; Sims, M. B.; Sumerlin, B. S. Ultra-High Molecular Weights via Aqueous Reversible-Deactivation Radical Polymerization. *Chem* **2017**, 2 (1), 93-101.
(121) Roy, D.; Ullah, A.; Sumerlin, B. S. Rapid Block Copolymer Synthesis by Microwave-Assisted RAFT Polymerization. *Macromolecules* **2009**, 42 (20), 7701-7708.

(122) Garrett, E. T.; Pei, Y.; Lowe, A. B. Microwave-assisted synthesis of block copolymer nanoparticles via RAFT with polymerization-induced self-assembly in methanol. *Polym. Chem.* **2016**, 7 (2), 297-301.
(123) Zetterlund, P. B.; Perrier, S. RAFT Polymerization under Microwave Irradiation: Toward Mechanistic Understanding. *Macromolecules* **2011**, 44 (6), 1340-1346.
(124) Xiao, W.; Zesheng, A. New Insights into RAFT Dispersion Polymerization-Induced Self-Assembly: From Monomer Library, Morphological Control, and Stability to Driving Forces. *Macromol. Rapid Commun.* **2018**, 0 (0), 1800325.
(125) Charleux, B.; Delaittre, G.; Rieger, J.; D'Agosto, F. Polymerization-Induced Self-Assembly: From Soluble Macromolecules to Block Copolymer Nano-Objects in One Step. *Macromolecules* **2012**, 45 (17), 6753-6765.
(126) Warren, N. J.; Armes, S. P. Polymerization-Induced Self-Assembly of Block Copolymer Nano-objects via RAFT Aqueous Dispersion Polymerization. *J. Am. Chem. Soc.* **2014**, 136 (29), 10174-10185.
(127) Canning, S. L.; Smith, G. N.; Armes, S. P. A Critical Appraisal of RAFT-Mediated Polymerization-Induced Self-Assembly. *Macromolecules* **2016**, 49 (6), 1985-2001.
(128) Derry, M. J.; Fielding, L. A.; Armes, S. P. Polymerization-induced self-assembly of block copolymer nanoparticles via RAFT non-aqueous dispersion polymerization. *Prog. Polym. Sci.* **2016**, 52, 1-18.
(129) Engelis, N. G.; Anastasaki, A.; Whitfield, R.; Jones, G. R.; Liarou, E.; Nikolaou, V.; Nurumbetov, G.; Haddleton, D. M. Sequence-Controlled Methacrylic Multiblock Copolymers: Expanding the Scope of Sulfur-Free RAFT. *Macromolecules* **2018**, 51 (2), 336-342.
(130) Xu, J.; Fu, C.; Shanmugam, S.; Hawker, C. J.; Moad, G.; Boyer, C. Synthesis of Discrete Oligomers by Sequential PET-RAFT Single-Unit Monomer Insertion. *Angew. Chem. Int. Ed.* **2017**, 56, 1-8.
(131) Lutz, J.-F.; Ouchi, M.; Liu, D. R.; Sawamoto, M. Sequence-Controlled Polymers. *Science* **2013**, 341 (6146), 1238149.
(132) Zhang, J.; Deubler, R.; Hartlieb, M.; Martin, L.; Tanaka, J.; Patyukova, E.; Topham, P. D.; Schacher, F. H.; Perrier, S. Evolution of Microphase Separation with Variations of Segments of Sequence-Controlled Multiblock Copolymers. *Macromolecules* **2017**, 50 (18), 7380-7387.
(133) Srichan, S.; Kayunkid, N.; Oswald, L.; Lotz, B.; Lutz, J.-F. Synthesis and Characterization of Sequence-Controlled Semicrystalline Comb Copolymers: Influence of Primary Structure on Materials Properties. *Macromolecules* **2014**, 47 (5), 1570-1577.
(134) Martin, L.; Peltier, R.; Kuroki, A.; Town, J.; Perrier, S. Investigating the Cell-Uptake of Guanidinium-Rich RAFT Polymers: Impact of Comonomer and Monomer Distribution. *Biomacromolecules* **2018**, 19 (8), 3190-3200.
(135) Kuroki, A.; Sangwan, P.; Qu, Y.; Peltier, R.; Sanchez-Cano, C.; Moat, J.; Dowson, C. G.; Williams, E. G. L.; Locock, K. E. S.; Hartlieb, M.; Perrier, S. Sequence control as a powerful tool for improving the selectivity of antimicrobial polymers. *ACS Applied Materials & Interfaces* **2017**, 9 (46), 40117-40126.
(136) Judzewitsch, P. R.; Nguyen, T.-K.; Shanmugam, S.; Wong, E. H. H.; Boyer, C. Towards Sequence-Controlled Antimicrobial Polymers: Effect of Polymer Block Order on Antimicrobial Activity. *Angew. Chem.* **2018**, 130 (17), 4649-4654.
(137) Moskowitz, J. D.; Wiggins, J. S. Semibatch RAFT copolymerization of acrylonitrile and N-isopropylacrylamide: Effect of comonomer distribution on cyclization and thermal stability. *Polymer* **2016**, 84, 311-318.
(138) Moraes, J.; Peltier, R.; Gody, G.; Blum, M.; Recalcati, S.; Klok, H.-A.; Perrier, S. Influence of Block versus Random Monomer Distribution on the Cellular Uptake of Hydrophilic Copolymers. *ACS Macro Lett.* **2016**, 5 (12), 1416-1420.
(139) Yanez-Macias, R.; Kulai, I.; Ulbrich, J.; Yildirim, T.; Sungur, P.; Hoeppener, S.; Guerrero-Santos, R.; Schubert, U. S.; Destarac, M.; Guerrero-Sanchez, C.; Harrisson, S. Thermosensitive spontaneous gradient copolymers with block- and gradient-like features. *Polym. Chem.* **2017**, 8 (34), 5023-5032.
(140) Harrisson, S.; Ercole, F.; Muir, B. W. Living spontaneous gradient copolymers of acrylic acid and styrene: one-pot synthesis of pH-responsive amphiphiles. *Polym. Chem.* **2010**, 1 (3), 326-332.
(141) Beginn, U. Gradient copolymers. *Colloid. Polym. Sci.* **2008**, 286 (13), 1465-1474.
(142) Couvreur, L. Method for synthesizing amphiphilic gradient copolymers soluble in an alkaline medium. WO2010018344A1, **2010**.
(143) Magnet, S.; Guerret, O.; Lefay, C.; Charleux, B. Use of copolymers with a composition gradient as stabilizers in emulsion free-radical polymerization. WO2006066971A1, **2013**.
(144) Zhang, J.; Farias-Mancilla, B.; Destarac, M.; Schubert, U. S.; Keddie, D. J.; Guerrero-Sanchez, C.; Harrisson, S. Asymmetric Copolymers: Synthesis, Properties, and Applications of Gradient and Other Partially Segregated Copolymers. *Macromol. Rapid Commun.* **2018**, 0 (0), 1800357.

(145) Read, E.; Guinaudeau, A.; James Wilson, D.; Cadix, A.; Violleau, F.; Destarac, M. Low temperature RAFT/MADIX gel polymerisation: access to controlled ultra-high molar mass polyacrylamides. *Polym. Chem.* **2014**, 5 (7), 2202-2207.
(146) Despax, L.; Fitremann, J.; Destarac, M.; Harrisson, S. Low concentration thermoresponsive hydrogels from readily accessible triblock copolymers. *Polym. Chem.* **2016**, 7 (20), 3375-3377.
(147) Abreu, C. M. R.; Fonseca, A. C.; Rocha, N. M. P.; Guthrie, J. T.; Serra, A. C.; Coelho, J. F. J. Poly(Vinyl Chloride): Current Status and Future Perspectives via Reversible Deactivation Radical Polymerization Methods. *Prog. Polym. Sci.* **2018**, 87, 34-69.
(148) Guerre, M.; Rahaman, S. M. W.; Améduri, B.; Poli, R.; Ladmiral, V. Limits of Vinylidene Fluoride RAFT Polymerization. *Macromolecules* **2016**, 49 (15), 5386-5396.
(149) Hill, M. R.; Kubo, T.; Goodrich, S. L.; Figg, C. A.; Sumerlin, B. S. Alternating Radical Ring-Opening Polymerization of Cyclic Ketene Acetals: Access to Tunable and Functional Polyester Copolymers. *Macromolecules* **2018**, 51 (14), 5079-5084.
(150) Hill, M. R.; Guégain, E.; Tran, J.; Figg, A. C.; Turner, A. C.; Nicolas, J.; Sumerlin, B. S. Radical Ring-Opening Copolymerization of Cyclic Ketene Acetals and Maleimides Affords Homogeneous Incorporation of Degradable Units. *ACS Macro Lett.* **2017**, 5 (10), 1071-1077.
(151) Danial, M.; My-Nhi Tran, C.; Young, P. G.; Perrier, S.; Jolliffe, K. A. Janus cyclic peptide–polymer nanotubes. *Nat. Commun.* **2013**, 4, 2780.
(152) Cook, A. B.; Peltier, R.; Hartlieb, M.; Whitfield, R.; Moriceau, G.; Burns, J. A.; Haddleton, D. M.; Perrier, S. Cationic and hydrolysable branched polymers by RAFT for complexation and controlled release of dsRNA. *Polym. Chem.* **2018**, 9 (29), 4025-4035.
(153) Larnaudie, S. C.; Brendel, J. C.; Romero-Canelón, I.; Sanchez-Cano, C.; Catrouillet, S.; Sanchis, J.; Coverdale, J. P. C.; Song, J.-I.; Habtemariam, A.; Sadler, P. J.; Jolliffe, K. A.; Perrier, S. Cyclic Peptide–Polymer Nanotubes as Efficient and Highly Potent Drug Delivery Systems for Organometallic Anticancer Complexes. *Biomacromolecules* **2018**, 19 (1), 239-247.
(154) Gregory, A.; Stenzel, M. H. Complex polymer architectures via RAFT polymerization: From fundamental process to extending the scope using click chemistry and nature's building blocks. *Prog. Polym. Sci.* **2012**, 37 (1), 38-105.
(155) Zhao, J.; Zhou, Y.; Zhou, Y.; Zhou, N.; Pan, X.; Zhang, Z.; Zhu, X. A straightforward approach for the one-pot synthesis of cyclic polymers from RAFT polymers via thiol–Michael addition. *Polym. Chem.* **2016**, 7 (9), 1782-1791.
(156) Zhang, J.; Gody, G.; Hartlieb, M.; Catrouillet, S.; Moffat, J.; Perrier, S. Synthesis of Sequence-Controlled Multiblock Single Chain Nanoparticles by a Stepwise Folding–Chain Extension–Folding Process. *Macromolecules* **2016**, 49 (23), 8933-8942.
(157) Hanlon, A. M.; Lyon, C. K.; Berda, E. B. What Is Next in Single-Chain Nanoparticles? *Macromolecules* **2016**, 49 (1), 2-14.
(158) Zoppe, J. O.; Ataman, N. C.; Mocny, P.; Wang, J.; Moraes, J.; Klok, H.-A. Surface-Initiated Controlled Radical Polymerization: State-of-the-Art, Opportunities, and Challenges in Surface and Interface Engineering with Polymer Brushes. *Chem. Rev.* **2017**, 117 (3), 1105-1318.
(159) De Brouwer, H.; Schellekens, M. A. J.; Klumperman, B.; Monteiro, M. J.; German, A. L. Controlled radical copolymerization of styrene and maleic anhydride and the synthesis of novel polyolefin-based block copolymers by reversible addition–fragmentation chain-transfer (RAFT) polymerization. *J. Polym. Sci., Part A: Polym. Chem.* **2000**, 38 (19), 3596-3603.
(160) Alfrey, T.; Lavin, E. The Copolymerization of Styrene and Maleic Anhydride. *J. Am. Chem. Soc.* **1945**, 67 (11), 2044-2045.
(161) Jenkins, A. D. Alternating copolymers. *Brit. Polym. J.* **1987**, 19 (1), 91-91.
(162) Trivedi, B. C.; Culbertson, B. M., Alternating Addition Copolymerizations. In *Maleic Anhydride*, Springer US: Boston, MA, **1982**.
(163) Klumperman, B. Mechanistic considerations on styrene-maleic anhydride copolymerization reactions. *Polym. Chem.* **2010**, 1 (5), 558-562.
(164) Huang, J.; Turner, S. R. Recent advances in alternating copolymers: The synthesis, modification, and applications of precision polymers. *Polymer* **2017**, 116, 572-586.
(165) Polyscope. Polyscope promotes SMA as 'versatile' polymer modifier for amorphous thermoplastics. *Add. Polym.* **2010**, 2010 (4), 2-3.
(166) Cray Valley. SMA®. http://www.crayvalley.com/products/sma-styrene
(167) Solenis. SCRIPSET™ COPOLYMER RESINS. https://solenis.com/en/industries/specialties-wood-adhesives/innovations/scripset-copolymer-resins/

(168) Lubrizol. MSC (Maleic Anhydride Styrene Copolymer). https://www.lubrizol.com/Lubricant-and-Fuel-Additives/Viscosity-Modifiers/Technologies/MSC
(169) Richards, S. N. Styrene-maleic anhydride based dispersant in a coating or ink. US 9416280 B2, **2007**.
(170) Cao, K.; Zhu, Q.-j.; Wei, X.; Yu, Y.-f.; Yao, Z. Influences of the Molecular Weight and its Distribution of Poly(styrene-alt-octadecyl maleimide) as a Flow Improver for Crude Oils. *Energy Fuels* **2016**, 30 (4), 2721-2728.
(171) Binks, B. P.; Fletcher, P. D. I.; Roberts, N. A.; Dunkerley, J.; Greenfield, H.; Mastrangelo, A.; Trickett, K. How polymer additives reduce the pour point of hydrocarbon solvents containing wax crystals. *PCCP* **2015**, 17 (6), 4107-4117.
(172) Al-Sabagh, A. M.; Noor El-Din, M. R.; Morsi, R. E.; Elsabee, M. Z. Styrene-maleic anhydride copolymer esters as flow improvers of waxy crude oil. *J. Pet. Sci. Eng.* **2009**, 65 (3), 139-146.
(173) Xu, J.; Qian, H.; Xing, S.; Li, L.; Guo, X. Synthesis of Poly(maleic acid alkylamide-co-α-olefin-co-styrene) Co-polymers and Their Effect on the Yield Stress and Morphology of Waxy Gels with Asphaltenes. *Energy Fuels* **2011**, 25 (2), 573-579.
(174) Wu, Y.; Ni, G.; Yang, F.; Li, C.; Dong, G. Modified Maleic Anhydride Co-polymers as Pour-Point Depressants and Their Effects on Waxy Crude Oil Rheology. *Energy Fuels* **2012**, 26 (2), 995-1001.
(175) Smith, A. A. A.; Autzen, H. E.; Laursen, T.; Wu, V.; Yen, M.; Hall, A.; Hansen, S. D.; Cheng, Y.; Xu, T. Controlling Styrene Maleic Acid Lipid Particles through RAFT. *Biomacromolecules* **2017**, 18 (11), 3706-3713.
(176) Germack, D. S.; Harrisson, S.; Brown, G. O.; Wooley, K. L. Influence of the structure of nanoscopic building blocks on the assembly of micropatterned surfaces. *J. Polym. Sci., Part A: Polym. Chem.* **2006**, 44 (17), 5218-5228.
(177) Harrisson, S.; Wooley, K. L. Shell-crosslinked nanostructures from amphiphilic AB and ABA block copolymers of styrene-alt-(maleic anhydride) and styrene: polymerization, assembly and stabilization in one pot. *Chem. Commun.* **2005**, 0 (26), 3259-3261.
(178) Zhu, M.-Q.; Wei, L.-H.; Li, M.; Jiang, L.; Du, F.-S.; Li, Z.-C.; Li, F.-M. A unique synthesis of a well-defined block copolymer having alternating segments constituted by maleic anhydride and styrene and the self-assembly aggregating behavior thereof. *Chem. Commun.* **2001**, 0 (4), 365-366.

Chapter 2 Evaluation of Lubrizol CTA-Ester: butyl-2-methyl-2-[(dodecylsulfanylthiocarbonyl)sulfanyl] propionate

Abstract

Prior to synthesising copolymers by RAFT using industrial grade CTA-Ester, the purity of the CTA and its performance towards RAFT polymerisation for styrene and methacrylates were investigated. The purity of the CTA-Ester (*ca*. 80 %) was assessed using ^{1}H-NMR spectroscopy and the impurities were identified using electron spray ionisation-time of flight mass spectrometry (ESI-ToF-MS). The performances were probed by measuring the apparent chain transfer constant (C_{tr}^{app}) and by studying the kinetics of the polymerisation for styrene and methacrylate monomers. The apparent chain transfer constant was initially measured using the Mayo Plot method for both monomers ($C_{tr}^{app} = 0.6$ for methyl methacrylate and 6 for styrene), before being determined with more accuracy by the Walling & Moad method for styrene ($C_{tr}^{app} = 27$). Experimentally, CTA-Ester was shown to provide good control over molar mass and a narrow dispersity for styrene polymerisation, whereas limited control was obtained for methyl and lauryl methacrylates. Optimisation of the RAFT conditions for the preparation of a polystyrene macroCTA of DP = 10 ($PSty_{10}$) is also reported. High conversion (conv. > 90 %) and reasonable livingness (L > 95 %) were achieved by using high monomer concentration (5 M) and minimum initiator concentration ($[CTA]_0/[V\text{-}40]_0 = 11$) in toluene at 100 °C for 10 hrs.

Figure 2.1. Picture of industrial grade CTA-Ester (80 % pure) provided by Lubrizol.

2.1 Introduction

Despite the RAFT process being shown to be easily scalable, the large scale production of complex polymeric architectures remains limited and is still a major challenge.[1] Lubrizol is among the few industrial companies which have scaled up the RAFT polymerisation process for preparing a variety of architectures, such as star-shaped poly(alkyl)methacrylates for application in lubricants and viscosity modifiers (Figure 2.2 - A).[2] The transposition of conventional free radical polymerisation into RAFT polymerisation is simple and only requires the addition of a chain transfer agent (CTA), however, RAFT agents available in large scale are scarce. For the large scale production of star-shaped poly(alkyl)methacrylates by RAFT, Lubrizol requires large quantities of a chain transfer agent. As no CTA was commercially available in bulk at that time, Lubrizol developed and scaled-up the synthesis of butyl-2-methyl-2-[(dodecylsulfanylthiocarbonyl)sulfanyl] propionate (CTA-Ester). CTA-Ester is an oil soluble trithiocarbonate RAFT agent with (-S-$C_{12}H_{25}$) as a Z group and a tertiary R group containing two methyls and a butyl ester (Figure 2.2 - B). The synthesis of CTA-Ester was adapted from the previously developed and published procedure for the synthesis of S-1-dodecyl-S'-(α,α'-dimethyl-α'-acetic acid)trithiocarbonate (CTA-Acid).[3]

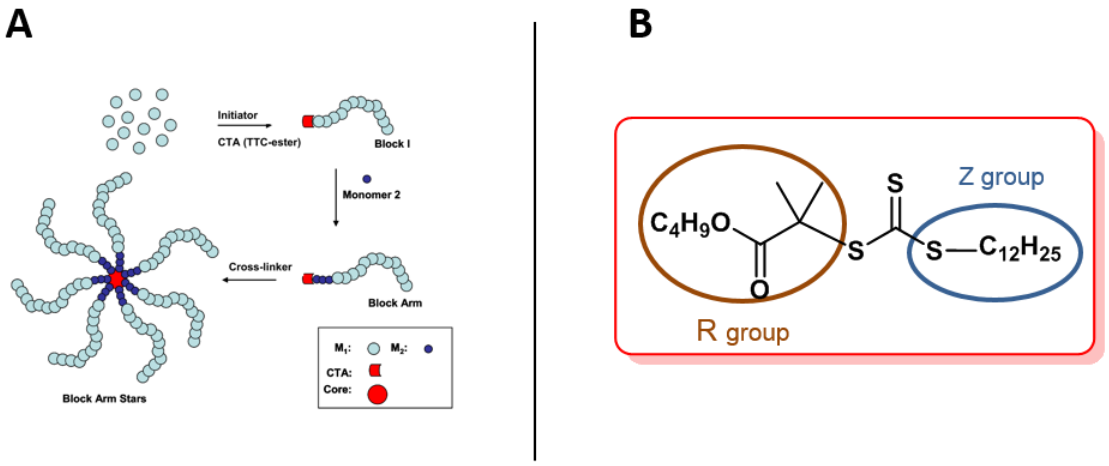

Figure 2.2 A) Schematic of RAFT polymerisation of Lubrizol's star-shape molecules.[2] B) Structure of CTA-Ester.

The original synthesis for CTA-Acid involved multiple steps and led to a high level of side products due to the use of a phase transfer catalyst producing non-soluble intermediates under these conditions. To overcome these issues, Lubrizol developed a new procedure in which 1-dodecanethiol, acetone (solvent and reagent), carbon disulfide and chloroform were combined in a one-pot process without the need of a phase transfer catalyst (Figure 2.3). The first synthetic step involves the reaction of dodecanethiol with a base (potassium hydroxide), forming a reactive nucleophilic thiolate species. Dodecyl trithiocarbonate potassium salt is then obtained by nucleophilic addition to carbon disulfide. At the same time, reactive dichloroepoxybutane is formed *via* reaction of chloroform with acetone in basic conditions. The subsequent ring opening SN2 reaction of dichloroepoxybutane with trithiocarbonate salt leads to the formation of an acyl chloride intermediate, which is hydrolysed *in situ* into a carboxylate group due to the presence of base. The intermediate carboxylate is then acidified with hydrochloric acid (HCl) to yield the desired CTA-Acid in high yield and purity. After a series of aqueous washes, phase separation and evaporation, a crude acid intermediate is obtained. CTA-Ester is then synthesised by subsequent acid catalysed esterification with butanol. This process leads to a technical grade product containing typically 80-90 % of pure CTA-Ester.

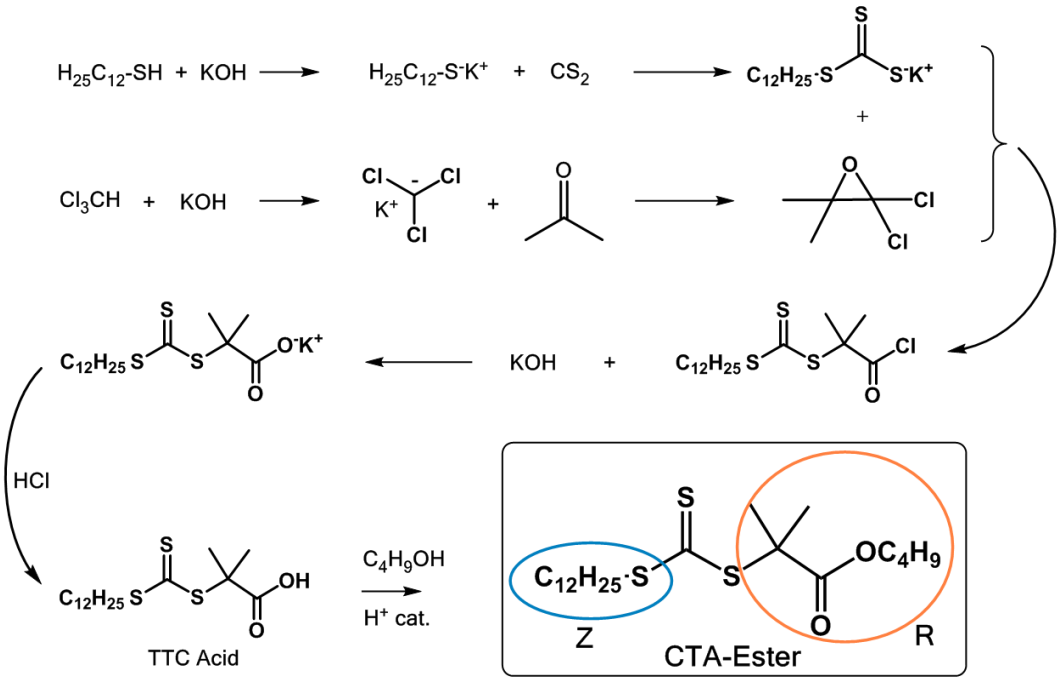

Figure 2.3 Synthetic route to synthesise CTA-Ester in large scale developed by Lubrizol.[2]

The most prevalent impurities were identified using electrospray ionisation time-of-flight mass spectrometry (ESI-ToF-MS) and NMR spectroscopy techniques. S,S'-bis(1-dodecyl)trithiocarbonate (Figure 2.4 - 1) was found to be the main impurity due to the reversibility of the trithiocarbonate formation in step one (Figure 2.3). Experiments on methacrylate monomers showed that it has no significant effect on molar mass control and that 10 % increase in concentration of technical grade CTA-Ester resulted in a polymer with M_n equivalent to a polymer prepared by using pure CTA-Ester.[2] A similar impurity (dibutyl trithiocarbonate), found in butyl-based RAFT agents, was also reported to have no influence on the polymerisation of styrene.[4]

CTA-Acid and CTA-Ester are among the rare RAFT agents produced in industrial scale and have already proven themselves to be efficient for the synthesis of complex architectures using common monomers such as methacrylates and styrene.[2, 3, 5-8] In this study, the purity of the industrial grade CTA-Ester provided by Lubrizol was assessed and its performance on RAFT polymerisation of styrene and methacrylate monomers in bulk and solution was investigated.

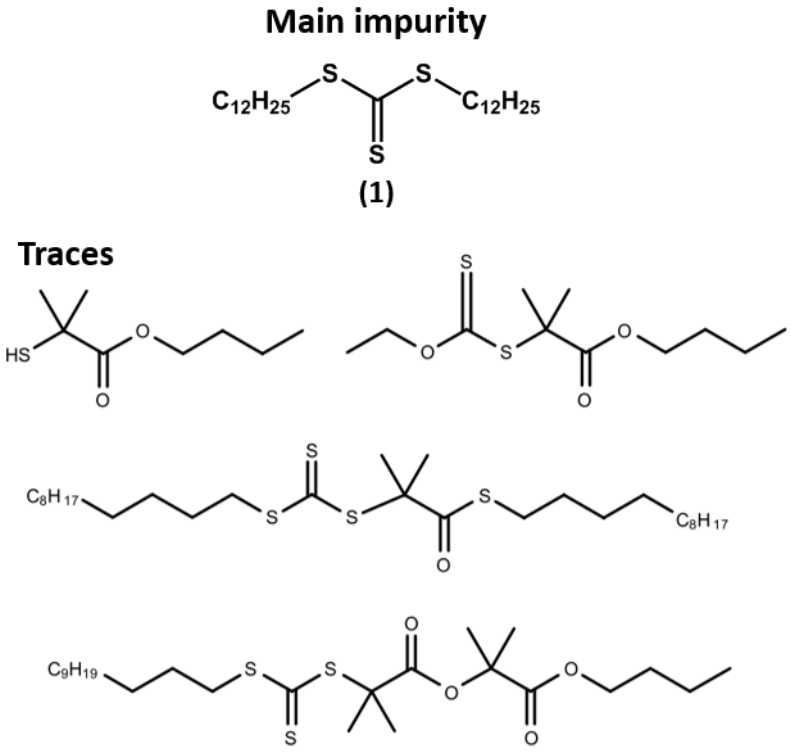

Figure 2.4 Byproducts generated during CTA-Ester synthetic process.[2]

2.2 CTA-Ester Purity

To study RAFT polymerisation using industrial grade CTA-Ester, a preliminary study on the batch purity was performed and a simple purification method was attempted. The ^{1}H-NMR spectroscopy analysis of two batches provided by Lubrizol revealed a purity between 70-90 %, varying from batch to batch. These differences can be explained by variation in the number of purification steps and storage conditions.[2] The purity was determined by comparing the peak assigned to the methylene protons next to the trithiocarbonate group (Figure 2.5 – peak 12 at 3.28 ppm) and the peak from the main impurity (3.36 ppm), using trioxane as a quantitative internal reference (peak 19 at 5.17 ppm), and using equation 2.3 and 2.4 shown in experimental section. The batch used for the synthesis of all the materials presented in this study was found to be approximately 80 % pure (Figure A2-1). An approximate purity of 80 % was considered to set-up RAFT polymerisation conditions and was shown to give good agreement between experimental and theoretical M_n values.

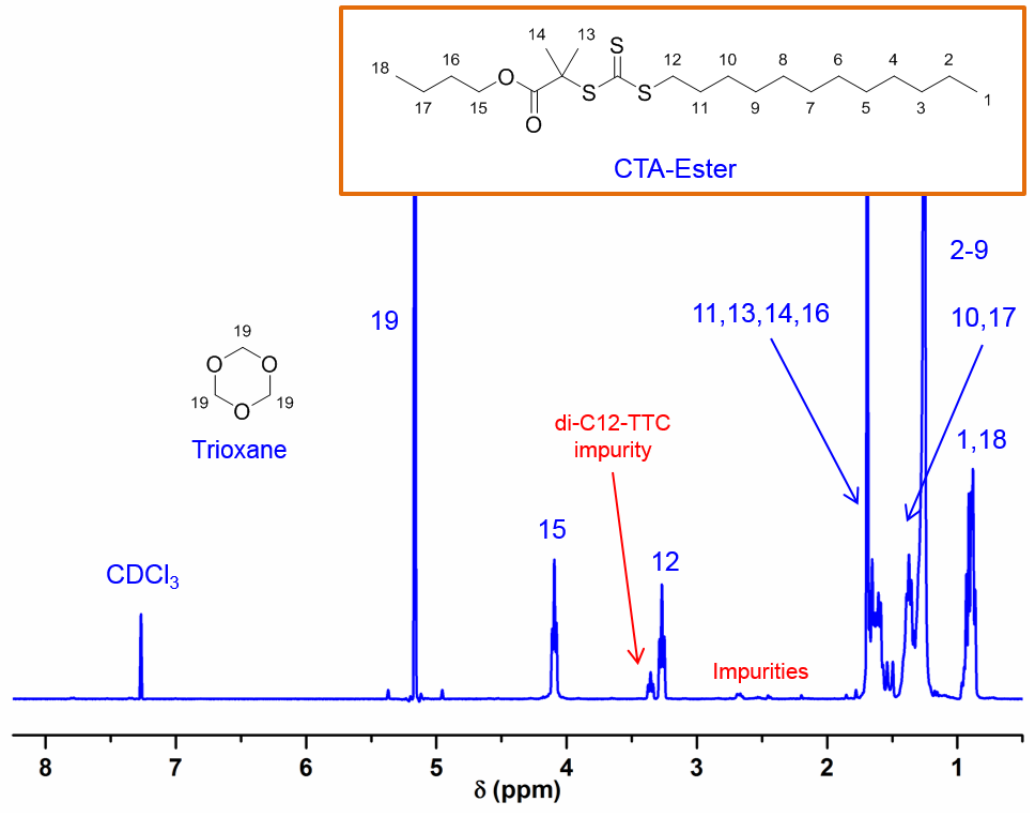

Figure 2.5 ^{1}H-NMR spectrum ($CDCl_3$) of industrial grade CTA-Ester.

Experimentally, it was observed that the main impurity recrystallises when the CTA mixture is dissolved in cold methanol or acetonitrile. Thus, a sample of technical grade CTA was purified by simple recrystallisation of impurities in cold acetonitrile, leading to almost full disappearance of the main impurity peak observed in the ^{1}H-NMR spectrum (Figure 2.6). However, the integration of the peak for $-CH_2$ next to the ester (4.10 ppm - 2.7 instead of 2) suggests that impurities containing an ester group possibly remain in the purified CTA. ESI-ToF-MS confirmed the presence of impurity traces, but no structure with ester groups were matched (Figure A2-2). ^{1}H-NMR spectroscopy analysis of the impurity mixture recovered showed a peak at 3.36 ppm and no ester peak at 4.10 ppm, as expected for the di-C12-TTC impurity (Figure A2-3). ESI-ToF-MS analysis of the impurity mixture further confirmed the presence of the di-C12-TTC (Figure A2-4).

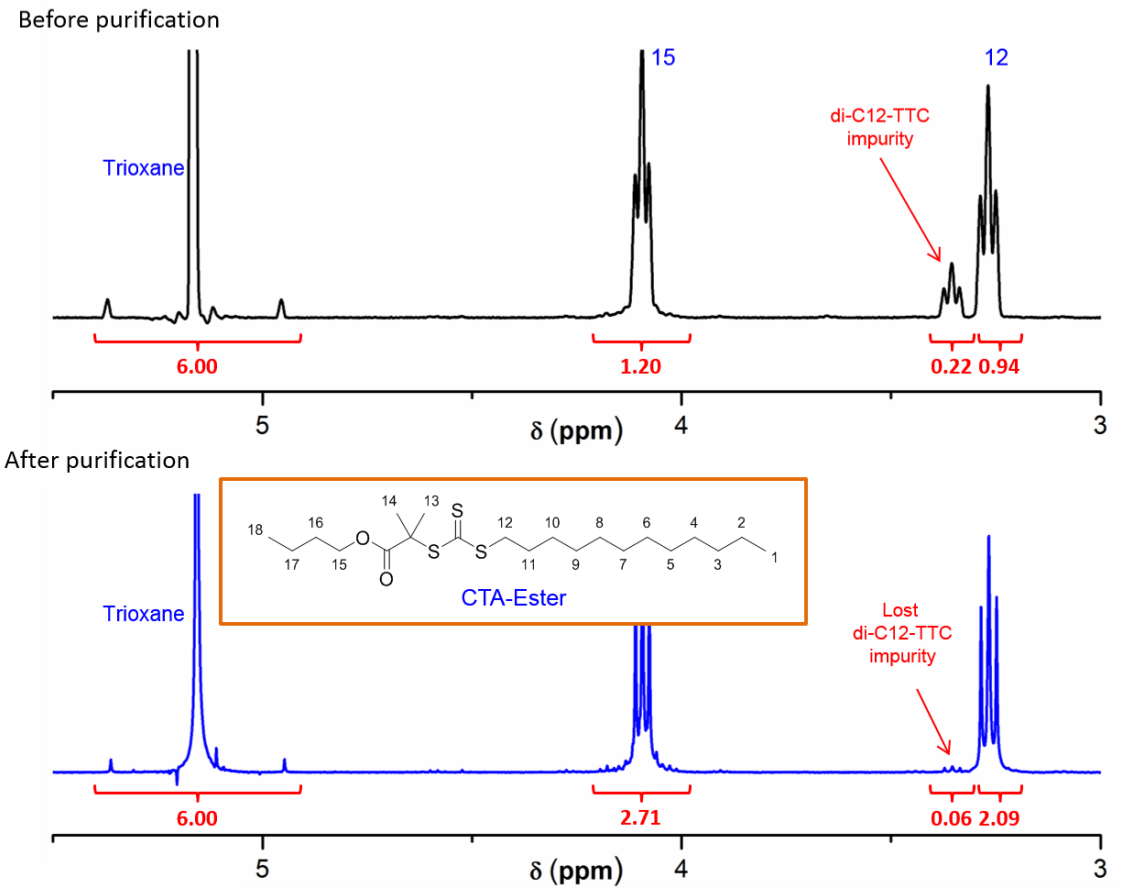

Figure 2.6 Magnified ^{1}H-NMR spectrum ($CDCl_3$) of industrial grade CTA-Ester (top) and CTA after purification (bottom).

A comparative study by size exclusion chromatography (SEC) between industrial grade CTA-Ester, purified CTA-Ester and the main impurity showed that the impurity is responsible for a peak around 600 g mol^{-1}, causing a high molar mass shoulder in the CTA mass distribution (Figure 2.7). The persistent shoulder, observed at low molar mass for the CTA-Ester before and after purification, suggests the presence of additional unknown impurities. Both high and low molar mass shoulders were detectable by UV-detector, suggesting the presence of trithiocarbonate groups in corresponding by-products. As the impurities are minor and not reactive, a small peak between 500-800 g mol^{-1} will be expected after polymerisation. Thus, the identification of impurities traces is important to better understand the kinetics of polymerisation and determine the efficiency of the RAFT agent.

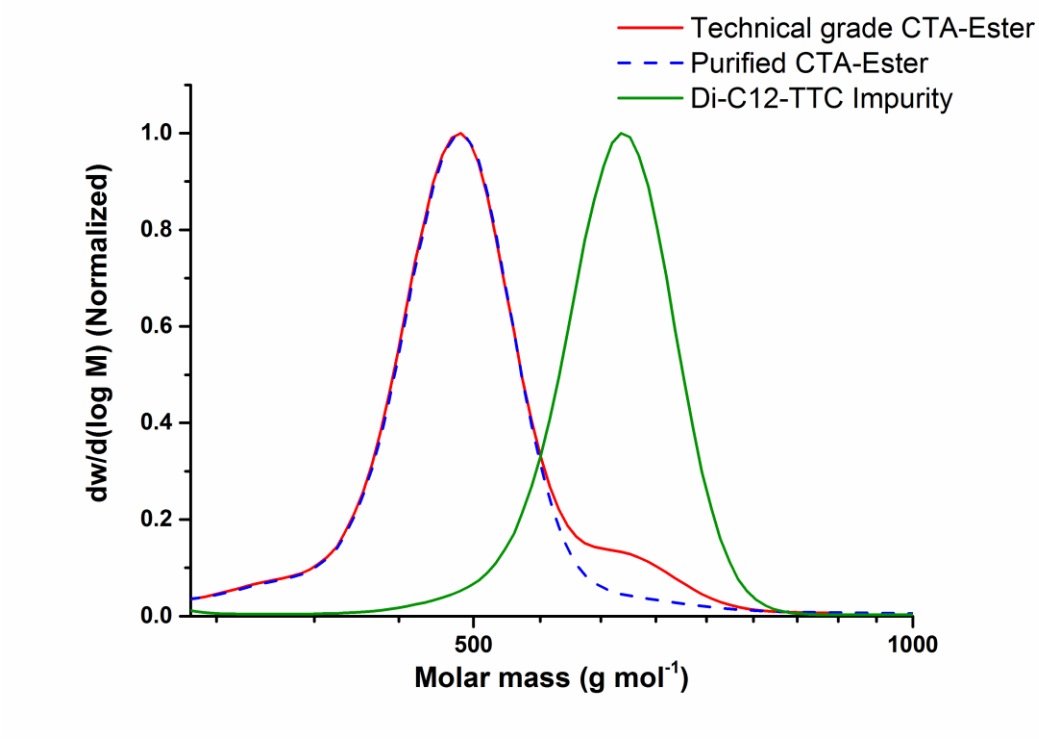

Figure 2.7 Molar mass distribution determined by SEC in THF using RI detector and polystyrene calibration for technical grade CTA-Ester (red), CTA-Ester after purification (blue) and di-C12-TTC impurity (green).

2.3 CTA-Ester Performance on RAFT Polymerisation

2.3.1 Chain transfer constant

The fundamentals of RAFT polymerisation have been reported in the introduction and the criteria of choice for CTAs were discussed. Rizzardo and co-workers have reported that the effectiveness of RAFT agents in radical polymerisation depends on the monomer used, the polymerisation conditions, and the nature of the CTA's Z and R groups.[9-12] Basic concepts about RAFT mechanism and the design of CTAs have also been reported in a number of useful reviews.[13, 14]

The chain transfer constant (C_{tr}) represents the affinity of the propagating radical toward the thiocarbonyl-thio moieties, and its determination allows for direct comparison of RAFT agent activity. However, the chain transfer constant is usually obtained from experimental data and derived from approximated mathematical equations thus, it is reported as the apparent chain transfer constant (C_{tr}^{app}).[9, 10] Furthermore, the C_{tr}^{app} values from different CTAs have to be compared for one type of monomer polymerised under similar conditions, especially temperature. The determination of apparent chain transfer constant by conventional approaches, such as the Mayo plot method, is relatively straightforward but is restricted to CTAs with low transfer activity.[10, 15] Nonetheless, it is recognised as an easy way to obtain preliminary data for any CTA and most of the values reported in polymer handbooks have been obtained *via* this method.[16-18] By measuring the number average degree of polymerisation (DP) as a function of CTA concentration (DP targeted), an approximate value of chain transfer can be calculated using the Mayo equation:

$$\frac{1}{\mathrm{DP}} = \frac{1}{\mathrm{DP}^0} + C_{tr}^{app}\frac{[\mathrm{CTA}]}{[\mathrm{M}]} \qquad 2.1$$

where DP^0 is the number average degree of polymerisation in absence of CTA. C_{tr}^{app} is then obtained by plotting the inverse of DP *versus* the ratio [CTA]/[M] (Mayo plot), giving a linear plot, where the slope is equal to the C_{tr}^{app}. Experimentally, this was achieved by targeting polymers with different DPs. The C_{tr}^{app} of CTA-Ester was measured at 90 °C in bulk polymerisation for two monomers of interest to Lubrizol: styrene and methyl methacrylate (MMA). Due to their low reactivity ratio, styrene and methacrylate monomers typically require processing at elevated temperature (≥ 90 °C), and the

generation of large amounts of radicals to obtain a high propagation rate coefficient.[19] While the measurement of the C_{tr}^{app} was achieved at high temperature, the initiator concentration was kept low to reduce bimolecular termination events. The polymerisations were stopped at low conversion (conv. < 15 %) to remain in the RAFT pre-equilibrium phase where transfer events are mostly due to the initial CTA. The C_{tr}^{app} values for styrene and methyl methacrylate, calculated by the Mayo plot (Figure A2-5), are shown in Table 2.1. The relatively high value for styrene polymerisation (*c.a.* 6) suggests that the transfer of propagating radical towards the RAFT agent is slightly favoured compared to monomer propagation ($C_{tr} = k_{tr}/k_p$), whereas for methyl methacrylate, the low value of chain transfer constant (*c.a.* 0.6) indicates preference to propagate in these conditions. This can be explained by the stability of the (tertiary) methacrylate propagating radical which is similar to the CTA-Ester's (tertiary) R group and therefore does not promote the addition-fragmentation. This observation is consistent with the theory discussed in the introduction about the design of CTAs. A more stable R group, such as a tertiary cyano-alkyl group, would be required to obtain a more efficient transfer and fragmentation in the case of methacrylates.[12]

Table 2.1. Apparent chain transfer constant determined by the Mayo method at 90 °C in bulk.

RAFT agents	Monomers	$[Init]_0$ ($mol.L^{-1}$)	% conv.	C_{tr}^{app} Mayo
CTA-Ester	Styrene	0.05	<10	5.7
	MMA	0.05	<20	0.6
PABTC	Styrene	0.05	<15	6.9

The chain transfer constant of another RAFT agent, (propanoic acid)yl butyl trithiocarbonate (PABTC), was also measured for styrene polymerisation at 90 °C for comparison. PABTC (Figure 2.8) is known to give relatively good control for styrene polymerisation.[20]

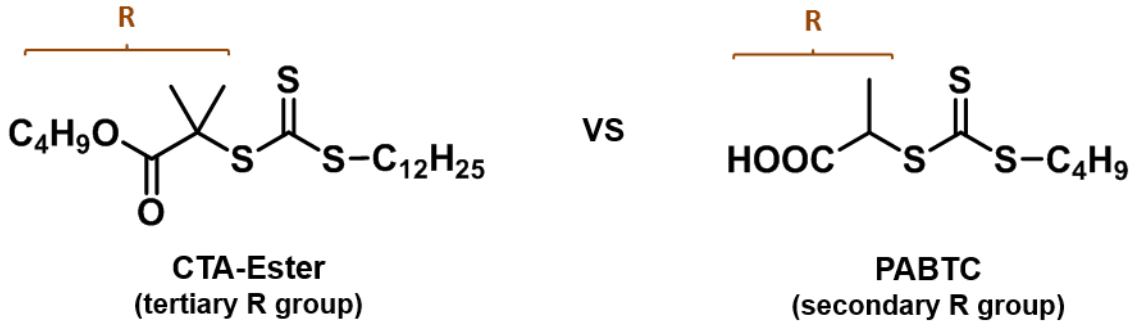

Figure 2.8 Structure of CTA-Ester and PABTC RAFT agents.

The chain transfer constant of PABTC measured by the Mayo plot (*c.a.* 7) was found to be similar to the CTA-Ester, suggesting that good control for styrene RAFT polymerisation can be expected using these two CTAs. As mentioned previously, the Mayo plot method is not adapted for CTAs with high chain transfer constants ($C_{tr} > 5$), thus, the value obtained for methyl methacrylate can be considered reliable whereas the value obtained for styrene is required to be measured by a more appropriate methodology. Therefore, the apparent chain transfer constant of CTA-Ester and PABTC were measured using the Walling & Moad method for styrene polymerisation at 90 °C in toluene (5 M), using equation 2.2.[9, 10, 21, 22]

$$C_{tr}^{app} \approx \frac{\mathrm{dln[CTA]}}{\mathrm{dln[M]}} \qquad 2.2$$

Briefly, the apparent chain transfer constant (C_{tr}^{app}) is determined by plotting ln[CTA] *versus* ln[M], where the slope of the linear regression corresponds to C_{tr}^{app} (Figure 2.9). The concentration of residual RAFT agent and monomer was determined by *in situ* ^{1}H-NMR spectroscopy, in toluene-d_8, by following the disappearance of the vinyl peak of styrene (5.25 ppm), and the methylene protons from the R group of the CTA-Ester (4.10 ppm), whereas the peak associated with the methine proton was used for PABTC (4.80 ppm).

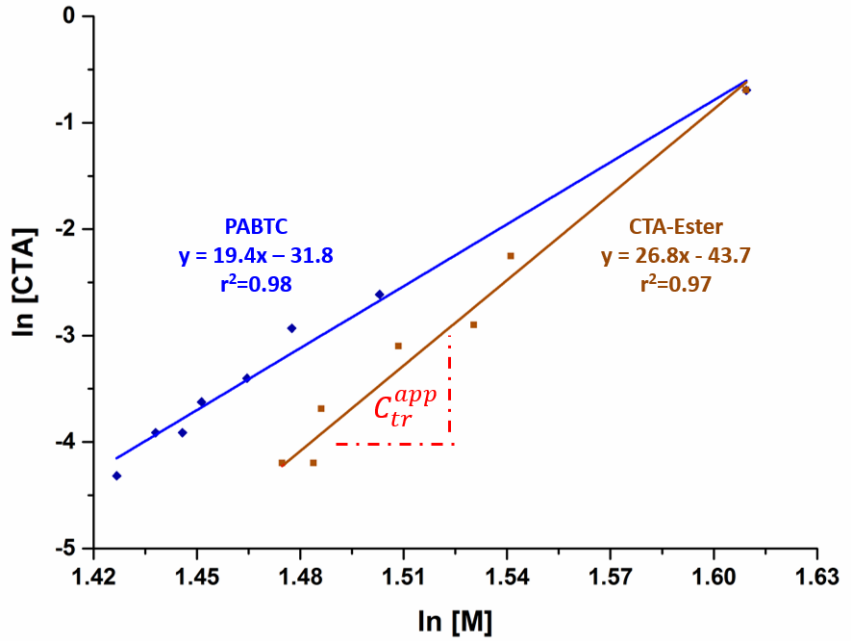

Figure 2.9 Apparent chain transfer constant for CTA-Ester and PABTC as determined by the Walling&Moad method for styrene polymerisation at 90 °C.

The C_{tr}^{app} values determined by this method (Table 2.2) were much higher than values obtained by the Mayo plot method. This was expected as the Mayo method typically underestimates C_{tr}^{app} values for efficient CTAs.[10] These results were also in good agreement with theory predicting an efficient transfer for CTAs with such R and Z groups, for styrene polymerisation.[12] The higher value of C_{tr}^{app} for CTA-Ester (*i.e.* 27) as compared to PABTC (*i.e.* 19) can be explained by the difference in R group. As the radical stability increases with the number of adjacent methyl groups (proton donor), CTA-Ester (tertiary R group) is expected to fragment more efficiently (forming a more stable radical) as compared to PABTC, which releases a secondary R group.

Table 2.2 Conditions and results for the determination of the apparent chain transfer constant by the Walling & Moad method for styrene [5 M] polymerisation at 90 °C in toluene-d_8.

RAFT agents	$[Init]_0$ ($mol.L^{-1}$)	% conv.	C_{tr}^{app} Walling & Moad
CTA-Ester	0.05	<13	27
PABTC	0.05	<17	19

By measuring the apparent chain transfer constant of CTA-Ester, good control over the batch polymerisation of styrenic monomers and poor control for methacrylates is to be expected in these conditions. To confirm these predictions and optimise polymerisation conditions, experimental kinetic studies were conducted.

2.3.2 Experimental kinetic study

The efficiency of CTA-Ester and PABTC for styrene and methacrylates polymerisation was assessed experimentally by following the evolution of the molar mass (M_n) and dispersity ($Đ$) with conversion. As mentioned previously, styrene and methacrylate monomers require processing at elevated temperature (≥ 90 °C), and the generation of large amounts of radicals to obtain a high propagation rate coefficient.[19] 1,1′-Azobis(cyclohexane-1-carbonitrile) (V-40) was used as radical initiator because of its suitable decomposition rate at 90 °C or 100 °C (10 hours half-life, decomposition temperature of 88 °C). Toluene and dioxane were selected as solvents as they are good solvents for both monomers, and they have high boiling points (110 °C and 102 °C respectively). The monomer and initiator were used at various concentrations, and the temperature was increased from 90 °C to 100 °C, in order to optimise reaction speed and control of molar mass.

Styrene

The polymerisations of styrene (DP =10) mediated by industrial grade CTA-Ester and pure PABTC were investigated at 90 °C and 100 °C in toluene and dioxane. The first experiment with CTA-Ester was performed in toluene at 90 °C using a moderate amount of initiator (0.025 M - Table 2.3 – Entry 1). These conditions did not lead to full conversion (conv. = 80 %), however, good control over molar mass and dispersity were achieved ($Đ$ = 1.10). PABTC was also tested in these conditions and, despite the polymerisation being more efficient (90 % conversion within 20 hours), the control over molar mass and dispersity was lower ($Đ$ = 1.20). This can be explained by the slower fragmentation of the R group of PABTC, causing more uncontrolled propagation at the beginning of the polymerisation process, while in the case of CTA-Ester, the rapid fragmentation enabled faster formation of controlled chains. Kinetic studies were then performed in dioxane at 90 °C (Table 2.3 – Entry 3) and 100 °C (Table 2.3 – Entry 4) using higher initiator concentration ($[CTA]_0/[Init]_0 < 10$) (Figure 2.10).

Table 2.3 Conditions and results for styrene polymerisation (DP_{10} – 5 M) using CTA-Ester and PABTC. SEC in THF with PS standards.

Entry	CTA	$[I]_0$ (mol.L^{-1})	$[CTA]_0$/ $[Init]_0$	Solv.	Temp. (°C)	Time (hrs)	% Conv.[a]	$M_{n,theo}$[a]	$M_{n,SEC}$[b]	$Đ$[b]	% L[c]
1	CTA-Ester	0.025	20	Toluene	90	20	80	1265	1250	1.10	98
2	PABTC	0.025	20	Toluene	90	20	91	1280	1000	1.20	98
3	CTA-Ester	0.070	7	Dioxane	90	18	98	1438	1350	1.18	95
4	CTA-Ester	0.070	7	Dioxane	100	10	97	1433	1250	1.06	94
5	CTA-Ester	0.045	11	Toluene	100	12	97	1430	1350	1.07	96

[a] Calculated by ^{1}H NMR using eq.2.5 and 2.6, [b] determined using SEC-THF with PS standards, [c] cumulative livingness using eq. 1.2

Dioxane was used to avoid overlapping peaks in ^{1}H-NMR and to obtain more accuracy in conversion data. Full conversion was obtained within 10 hours at 100 °C, whilst 18 hours were required at 90 °C (Figure 2.10 - A). The plot of molar mass *versus* conversion for the reaction at 90 °C revealed a linear evolution of M_n with conversion and low dispersity ($Đ < 1.2$) (Figure 2.10 - B). This indicates that the polymerisation occurs in a living-like manner and that good control can be obtained using industrial grade CTA-Ester. These experimental results were consistent with theory and chain transfer constant values. The livingness was calculated using equation 1.2 and was kept relatively high in these conditions.

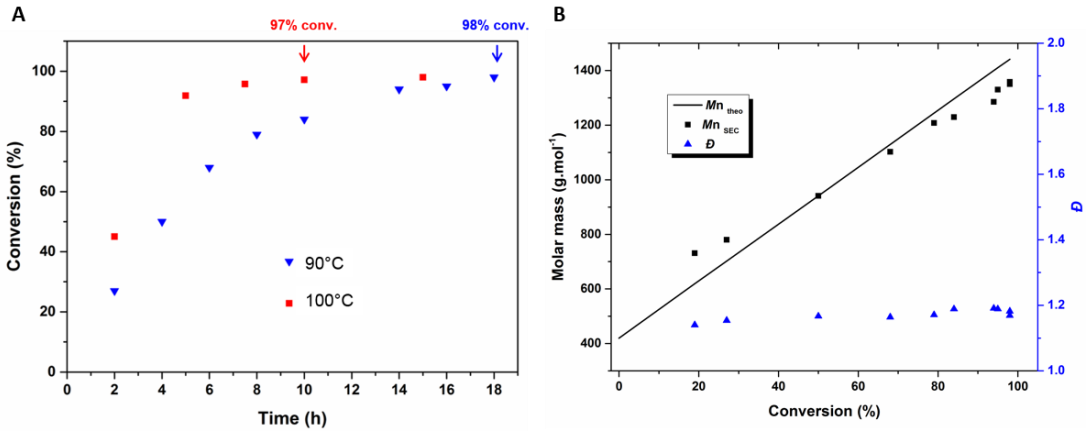

Figure 2.10 Kinetic data for styrene polymerisation in dioxane using CTA-Ester. A) Evolution of conversion *vs.* time at different temperatures and B) Evolution of the molar mass and dispersity with conversion at 90 °C.

Methyl and Lauryl Methacrylates

Despite the unoptimistic prevision for RAFT polymerisation of methacrylates using CTA-Ester in a batch process (*i.e.* low C_{tr}^{app}), Lubrizol succeeded in achieving large scale production of a variety of polyalkylmethacrylate architectures with relatively good control, by altering the procedure.[2] This unexpected control is due to the specific conditions used in the industrial process (*i.e.* semi-batch or feeding), compared to the batch process usually used for academic research. In fact, it is possible to artificially increase the C_{tr} of CTAs by using the semi-batch approach.[23] Feeding the monomer at the beginning of polymerisation decreases the ratio between monomer and CTA and increases the probability of the propagating radical to transfer to the CTA and undergo fragmentation of the R group.

For this study, methacrylate monomers were investigated in batch polymerisation, whereas the feeding process was investigated in a separate project.[24]

The polymerisation of two methacrylate monomers (methyl and lauryl – 1.25 M) using industrial grade CTA-Ester (DP = 100 targeted) was investigated at 90 °C in toluene using a moderate amount of initiator (0.004 M). Lauryl methacrylate and methyl methacrylate both reached near quantitative conversion within 20 hours (Figure 2.11).

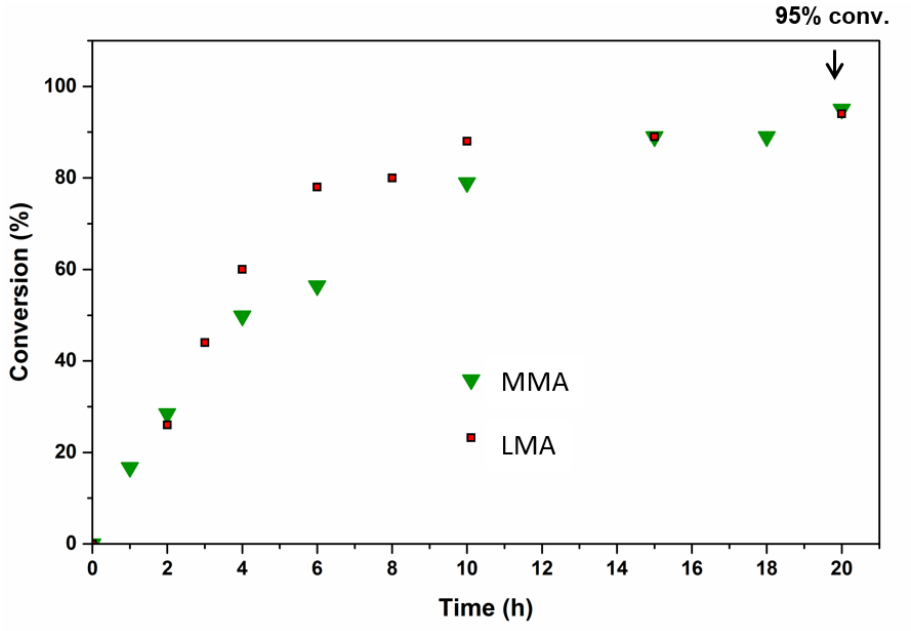

Figure 2.11 Evolution of conversion *vs.* time for methacrylate monomers (DP_{100} - 1.25 M) polymerisation in toluene using CTA-Ester at 90 °C and V-40 as initiator (0.004 M).

Despite both polymers showing final molar masses close to the theoretical values, the dispersities of the final materials were relatively broad (Table 2.4). The kinetic study revealed no linear evolution of molar mass with conversion, and dispersity values between 1.5 and 2.0 (Figure 2.12). This is a typical result for free radical polymerisation, indicating that CTA-Ester was poorly involved in the polymerisation process. These results were consistent with the theory and chain transfer constant values presented earlier. All these results showed the limitation of CTA-Ester for RAFT polymerisation of methacrylate monomers in the batch process, however, the use of optimised processes (semi-batch) was shown to improve the CTA-Ester efficiency leading to controlled polymers.[24] Thus, even if CTA-Ester does not appear as the optimal CTA for RAFT polymerisation of methacrylates in this study, it is still possible to produce poly(alkyl)methacrylates in a large scale using CTA-Ester by optimising the process.

Table 2.4 Conditions and results for methacrylates polymerisation (DP_{100} – 1.25 M) using CTA-Ester in toluene at 90 °C.

Entry	Mono	$[I]_0$ (mol.L^{-1})	$[CTA]_0$/ $[Ini]_0$	Time (hrs)	% Conv.[a]	$M_{n,theo}$[a]	$M_{n,SEC}$[b]	$Đ$ [b]
1	MMA	0.004	3	20	95	9,930	9,600	1.82
2	LMA	0.004	3	20	94	24,300	22,900	1.57

[a] Calculated by ^{1}H NMR using eq.2.5 and 2.6, [b] determined using SEC-THF with PS standards

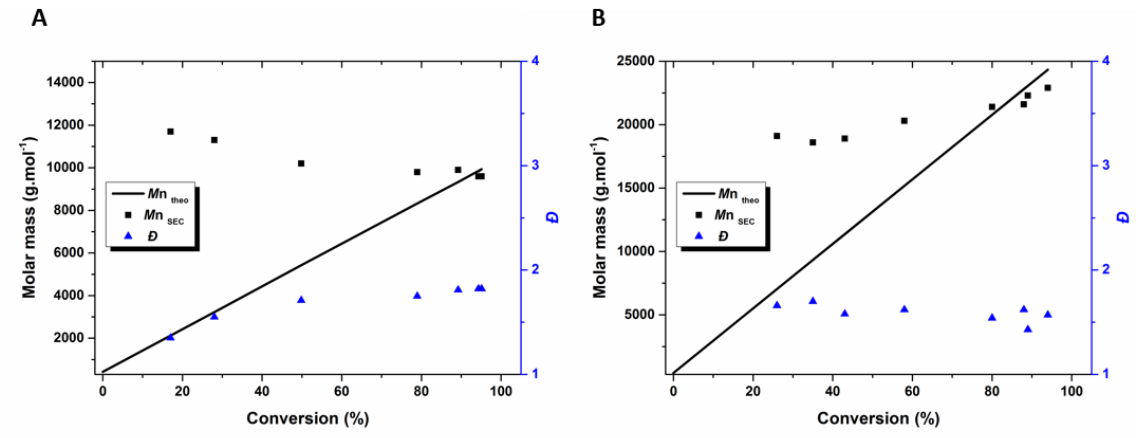

Figure 2.12. Kinetic data for methyl methacrylate (A) and laurylmethacrylate (B) polymerisation in toluene using CTA-Ester at 90 °C.

2.4 MacroCTA Synthesis Optimisation

Considering the excellent efficiency of industrial grade CTA-Ester for the RAFT polymerisation of styrene, the synthesis of well-defined architectures using this system was thus considered. Accessing controlled microstructures, such as block and multiblock, using RAFT process requires careful optimisation.[25-27] Ideally, each block should be synthesised with near-quantitative conversion (conv. ≥ 98 %) to avoid further purification, and with high degree of livingness to allow sequential chain extension ($L \geq$ 98 %). Here, the synthesis of a well-defined polystyrene macroCTA was optimised by varying several parameters such as monomer concentration, initiator concentration and temperature (Table 2.3).

A compromise of conversion and livingness was obtained using high monomer concentration ($[Sty]_0$ = 5 M) at 100 °C in toluene (Table 2.3 - Entry 5), a temperature and solvent allowing good rate of propagation for styrene (*i.e.* high k_p), while maintaining a low rate of monomer self-initiation compared to azo-initiator initiation.[28] In a degenerative process, it is important to use a controlled source of radicals in order to limit the fraction of dead chains.[27] V-40 was used as radical initiator for its 10 hour half-life decomposition temperature of 88 °C (2 hrs at 100 °C). Working at high monomer concentration has the advantage to allow for high polymerisation rates, however, the viscosity of the resulting polymer can be problematic for the following steps. This can also be an issue for industrial processes. The preliminary kinetic study (Table 2.3 - Figure 2.10) revealed that a ratio $[CTA]_0/[Initiator]_0$ = 7 gives full conversion (conv. = 97 %) within 10 hours, however, the large amount of initiator generated in these conditions limits the livingness (L = 94 %). A lower amount of initiator ($[CTA]_0/[I]_0$ = 11) was then considered in order to increase the livingness (L > 96 %) while retaining a relatively high conversion (conv. > 90 %).

The kinetic study performed under these conditions showed near quantitative conversion within 12 hours (conv. = 97 %) and a pseudo-first order kinetic (Figure 2.13, A). A linear evolution of M_n with conversion and low dispersities were also observed (Figure 2.13, B). By using these optimized conditions it was possible to obtain a polystyrene macroCTA (DP =10) with relatively high conversion (conv. > 95 %) and slightly improved livingness (L = 96 %).

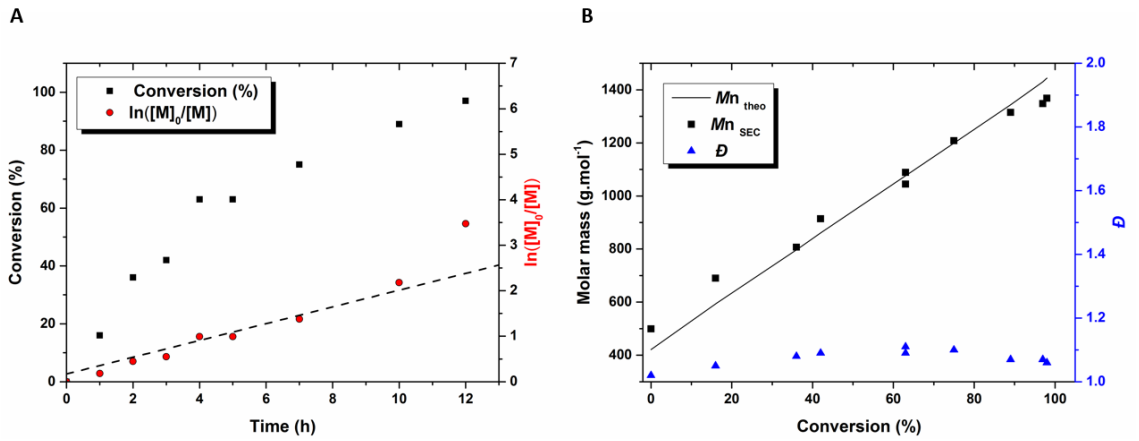

Figure 2.13 A) Kinetic investigation and evolution of conversion *vs.* time. B) Evolution of experimental molar mass ($M_{n,SEC}$) *vs.* theoretical molar mass ($M_{n,theo}$) and dispersity ($Đ$). Study performed using CTA-Ester at 100 °C with $[M]_0$ = 5 M and $[I]_0$ = 0.045 M ($[CTA]_0/[I]_0$ = 11).

2.5 Conclusion

The industrial grade CTA-Ester produced by Lubrizol was investigated, and its performance towards RAFT polymerisation was assessed. The purity of the industrial grade CTA provided by Lubrizol was established using NMR techniques and was found to be approximately 80 %. Performances of the CTA were evaluated experimentally for styrene and methacrylate monomers (methyl and lauryl) *via* the determination of chain transfer constants, and *via* kinetic investigation in typical conditions. Despite CTA-Ester being promising for styrene polymerisation ($C_{tr}^{app} = 27$), methyl methacrylate revealed poor transfer ability ($C_{tr}^{app} = 0.6$). This was confirmed by experimental kinetic studies using typical RAFT conditions in bulk. While the RAFT polymerisation gave polystyrene with narrow dispersity, no control (no linear evolution of M_n with conversion and broad dispersities) were observed for methacrylates (methyl and lauryl). The use of different CTAs (with cyano-alkyl R group) or process optimisation (feeding) was proposed as a good alternative to achieve RAFT polymerisation of methacrylates. Furthermore, the ability of CTA-Ester towards styrene was exploited to synthesise polystyrene macroCTA (DP = 10) in order to prepare copolymers with complex architecture.

2.6 Experimental

Materials

Styrene (Sty, ≥ 99 %), methyl methacrylate (MMA, 99 %), lauryl methacrylate (LMA, 96 %) were obtained from Sigma-Aldrich and passed through neutral alumina prior to use to remove inhibitor. Industrial grade CTA-Ester was provided by Lubrizol and used without purification (≈ 80 % pure).[2, 3] (propanoic acid)yl butyl trithiocarbonate (PABTC, 99 %) was synthesised following a procedure previously reported.[29] 1,1'-Azobis(cyclohexane-1-carbonitrile) (V-40, $T_{1/2\text{-}10h}$ = 88 °C, 98 %) was obtained from Sigma-Aldrich and used as received. 1, 4-dioxane and toluene were obtained from Fisher Scientific and used as received. Toluene-d_8 (99 % D atom), Chloroform-d ($CDCl_3$ - 99.9 % D atom) obtained from Sigma-Aldrich were used for ^{1}H NMR analysis.

Characterisation techniques

^{1}H NMR spectra were recorded on either a Bruker DPX-300 or DPX-400 spectrometer at 27 °C using deuterated solvents obtained from Sigma-Aldrich. For *in situ* chain transfer constant determination, kinetics of reaction were followed by ^{1}H NMR spectroscopy recorded on a 600 MHz Bruker Avance III instrument by real-time NMR at desired reaction temperature (90 °C) and using a delay time (d_1) of 25 s and a number of scans of 4. TMS contained in the solvent was used as the internal standard and chemical shift values (δ) are reported in ppm.

SEC was carried out using Agilent 390-LC MDS instrument equipped with differential refractive index (DRI) and dual wavelength UV detectors. The system was equipped with 2 x PLgel mixed D columns (300 x 7.5 mm) and a PLgel 5 μm guard column and autosampler. The eluent was THF with 2 v/v % TEA (triethylamine) and 0.01 wt. % BHT (butylated hydroxytoluene) additives. Samples were run at 1 ml min^{-1} at 30 °C. Polystyrene standards (Agilent EasiVials) were used for calibration. Analyte samples were filtered through a PVDF membrane with 0.22 μm pore size before injection. Experimental molar mass ($M_{n,SEC}$) and dispersity ($Đ$) values were determined by conventional calibration using Agilent GPC/SEC software.

Determination of CTA-Ester purity

The purity of CTA-Ester and the fraction of the main impurity were determined using ^{1}H-NMR spectroscopy (Figure A2-1) in the presence of an internal reference (trioxane). By knowing the exact amount of crude CTA-Ester and trioxane used for ^{1}H-NMR analysis, it is possible to calculate the fraction of pure CTA-Ester contained in the mixture. By setting the integration of methylene protons from trioxane (6H – 5.17 ppm), it is possible to associate a concentration to a proton integration (n_{triox} = 2.55.10^{-4} mole → Int_{2H} = 2). Then, it is possible to calculate the number of moles corresponding to CTA-Ester (Int_{2H} = 0.94→ $n_{CTA,real}$ = 1.20^{-4} mole) using methylene proton integration (2H -3.28 ppm), or main impurity (2H – 3.38 ppm - Int_{2H} = 0.22→ $n_{Imp,real}$ = 2.8.10^{-5} mole), and calculate the real mass present in the original preparation ($m_{CTA,real}$ = 50.5 mg - $m_{Imp,real}$ = 12.5 mg). The purity or fraction of impurity is then calculated by comparing these values with initial mass used of CTA-ester as follow:

$$\%\ Pure\ CTA\ = \frac{m_{real}CTA}{m_{ini}CTA} = \frac{50.5}{61} \approx 83\ \% \qquad 2.3$$

$$\%\ Impurity\ = \frac{12.5}{61} \approx 20\ \% \qquad 2.4$$

Typical RAFT procedure (PSty$_{10}$)

Industrial grade CTA-Ester (2.6 g, 5 mmol), styrene (5.3 g, 50 mmol), V-40 (0.11 g, 0.45 mmol) and toluene (1.3 mL) were introduced into a vial equipped with a magnetic stirrer bar and sealed with a rubber septum. The solution was degassed using nitrogen for *ca.*15 min before being placed in a thermostated oil bath set at 100 °C. After a desired time, a sample was taken from polymerisation medium *via* degassed syringe for kinetic study. After reaction completion (*ca.* 12 hours), the mixture was allowed to cool down at room temperature and then opened to the atmosphere. Final materials were characterised using ^{1}H-NMR spectroscopy and SEC (monomer conversion = 97 %, $M_{n,theo}$ = 1,430 g mol^{-1}, $M_{n,SEC\text{-}THF}$ = 1350 g mol^{-1} and $Đ$ = 1.07).

Determination of monomer conversion.

The conversion was determined using ^{1}H-NMR by comparing integrals before and after reaction using vinyl protons from monomers (5.74 ppm for styrene – 6.10 ppm for MMA and LMA). The peak corresponding to methyl protons from CTAs was used as an internal reference (0.88 ppm for CTA-Ester – 0.72 ppm for PABTC).
Monomer conversions (p) were calculated from ^{1}H NMR data using equation 2.5.

$$p = \frac{[M]_0 - [M]_t}{[M]_0} = 1 - \frac{[M]_t}{[M]_0} = 1 - \frac{\int vinyl\ proton_{tf}}{\int vinyl\ proton_{t0}} \quad 2.5$$

where $[M]_0$ and $[M]_t$ are the concentrations of the monomer at time 0 and at time t, respectively, $\int vinyl\ proton_{tf}$ is the integration of the vinyl proton from monomer at final time, $\int vinyl\ proton_{t0}$ is the integration of the vinyl proton from monomer at time 0.

Calculation of $M_{n,theo}$

The theoretical number-average molar mass ($M_{n,th}$) was calculated using equation 2.6.

$$M_{n,th} = DP_{targ} \times p \times M_{mono} + M_{CTA} \quad 2.6$$

where DP_{targ} is the targeted degree of polymerisation, p is the monomer conversion, M_{mono} and M_{CTA} are molar mass of monomer and CTA (or macroCTA) respectively.

Calculation of livingness

The fraction of living chain calculated using equation 1.2 presented in introduction chapter.[25] We use $fc = 1$ as styrene mainly terminates by combination, and this value leads to an under-estimation of livingness for polymerisation that also terminate by disproportionation.

2.7 References

(1) Perrier, S. 50th Anniversary Perspective: RAFT Polymerization—A User Guide. *Macromolecules* **2017**, 50 (19), 7433-7447.
(2) Brzytwa, A. J.; Johnson, J. Scaled Production of RAFT CTA–a STAR Performer. *Polym. Prepr. (Am. Chem. Soc., Div. Polym. Chem.)* **2011**, 52 (2), 533-534.
(3) Lai, J. T.; Filla, D.; Shea, R. Functional Polymers from Novel Carboxyl-Terminated Trithiocarbonates as Highly Efficient RAFT Agents. *Macromolecules* **2002**, 35 (18), 6754-6756.
(4) Postma, A.; Davis, T. P.; Evans, R. A.; Li, G.; Moad, G.; O'Shea, M. S. Synthesis of Well-Defined Polystyrene with Primary Amine End Groups through the Use of Phthalimido-Functional RAFT Agents. *Macromolecules* **2006**, 39 (16), 5293-5306.
(5) Kerr, A.; Hartlieb, M.; Sanchis, J.; Smith, T.; Perrier, S. Complex multiblock bottle-brush architectures by RAFT polymerization. *Chem. Commun.* **2017**, 53 (87), 11901-11904
(6) Bapat, A. P.; Ray, J. G.; Savin, D. A.; Hoff, E. A.; Patton, D. L.; Sumerlin, B. S. Dynamic-covalent nanostructures prepared by Diels-Alder reactions of styrene-maleic anhydride-derived copolymers obtained by one-step cascade block copolymerization. *Polym. Chem.* **2012**, 3 (11), 3112-3120.
(7) Li, M.; De, P.; Gondi, S. R.; Sumerlin, B. S. End group transformations of RAFT‐generated polymers with bismaleimides: Functional telechelics and modular block copolymers. *J. Polym. Sci., Part A: Polym. Chem.* **2008**, 46 (15), 5093-5100.
(8) Mahanthappa, M. K.; Bates, F. S.; Hillmyer, M. A. Synthesis of ABA Triblock Copolymers by a Tandem ROMP−RAFT Strategy. *Macromolecules* **2005**, 38 (19), 7890-7894.
(9) Chiefari, J.; Mayadunne, R. T. A.; Moad, C. L.; Moad, G.; Rizzardo, E.; Postma, A.; Thang, S. H. Thiocarbonylthio Compounds (SC(Z)S−R) in Free Radical Polymerization with Reversible Addition-Fragmentation Chain Transfer (RAFT Polymerization). Effect of the Activating Group Z. *Macromolecules* **2003**, 36 (7), 2273-2283.
(10) Chong, Y. K.; Krstina, J.; Le, T. P. T.; Moad, G.; Postma, A.; Rizzardo, E.; Thang, S. H. Thiocarbonylthio Compounds [SC(Ph)S−R] in Free Radical Polymerization with Reversible Addition-Fragmentation Chain Transfer (RAFT Polymerization). Role of the Free-Radical Leaving Group (R). *Macromolecules* **2003**, 36 (7), 2256-2272.
(11) Moad, G.; Rizzardo, E.; Thang, S. H. Radical addition–fragmentation chemistry in polymer synthesis. *Polymer* **2008**, 49 (5), 1079-1131.
(12) Moad, G.; Rizzardo, E.; Thang, S. H. Living Radical Polymerization by the RAFT Process. *Aust. J. Chem.* **2005**, 58 (6), 379-410.
(13) Destarac, M. On the Critical Role of RAFT Agent Design in Reversible Addition-Fragmentation Chain Transfer (RAFT) Polymerization. *Poly. Rev.* **2011**, 51 (2), 163-187.
(14) Keddie, D. J.; Moad, G.; Rizzardo, E.; Thang, S. H. RAFT Agent Design and Synthesis. *Macromolecules* **2012**, 45 (13), 5321-5342.
(15) Mayo, F. R. Chain Transfer in the Polymerization of Styrene: The Reaction of Solvents with Free Radicals1. *J. Am. Chem. Soc.* **1943**, 65 (12), 2324-2329.
(16) Kukulj, D.; Davis, T. P. Mechanism of catalytic chain transfer in the free-radical polymerisation of methyl methacrylate and styrene. *Macromol. Chem. Phys.* **1998**, 199 (8), 1697-1708.
(17) Heuts, J. P. A.; Davis, T. P.; Russell, G. T. Comparison of the Mayo and Chain Length Distribution Procedures for the Measurement of Chain Transfer Constants. *Macromolecules* **1999**, 32 (19), 6019-6030.
(18) Adamy, M.; van Herk, A. M.; Destarac, M.; Monteiro, M. J. Influence of the Chemical Structure of MADIX Agents on the RAFT Polymerization of Styrene. *Macromolecules* **2003**, 36 (7), 2293-2301.
(19) Meyer, V. E. Reactivity ratios of styrene and methyl methacrylate at 90°C. *J. Polym. Sci. A1* **1967**, 5 (6), 1289-1296.
(20) Danial, M.; My-Nhi Tran, C.; Young, P. G.; Perrier, S.; Jolliffe, K. A. Janus cyclic peptide–polymer nanotubes. *Nat. Commun.* **2013**, 4, 2780.
(21) Walling, C. The Use of S35 in the Measurement of Transfer Constants. *J. Am. Chem. Soc.* **1948**, 70 (7), 2561-2564.
(22) Moad, C. L.; Moad, G.; Rizzardo, E.; Thang, S. H. Chain Transfer Activity of ω-Unsaturated Methyl Methacrylate Oligomers. *Macromolecules* **1996**, 29 (24), 7717-7726.
(23) Ilchev, A.; Pfukwa, R.; Hlalele, L.; Smit, M.; Klumperman, B. Improved control through a semi-batch process in RAFT-mediated polymerization utilizing relatively poor leaving groups. *Polym. Chem.* **2015**, 6 (46), 7945-7948.

(24) Akrach, M., Carbon black dispersion using polymeric dispersants prepared via RAFT polymerisation, unpublished PhD thesis, University of Warwick, **2018**.
(25) Gody, G.; Maschmeyer, T.; Zetterlund, P. B.; Perrier, S. Rapid and quantitative one-pot synthesis of sequence-controlled polymers by radical polymerization. *Nat. Commun.* **2013**, 4, 2505.
(26) Gody, G.; Maschmeyer, T.; Zetterlund, P. B.; Perrier, S. Pushing the Limit of the RAFT Process: Multiblock Copolymers by One-Pot Rapid Multiple Chain Extensions at Full Monomer Conversion. *Macromolecules* **2014**, 47 (10), 3451-3460.
(27) Gody, G.; Maschmeyer, T.; Zetterlund, P. B.; Perrier, S. Exploitation of the Degenerative Transfer Mechanism in RAFT Polymerization for Synthesis of Polymer of High Livingness at Full Monomer Conversion. *Macromolecules* **2014**, 47 (2), 639-649.
(28) Khuong, K. S.; Jones, W. H.; Pryor, W. A.; Houk, K. N. The Mechanism of the Self-Initiated Thermal Polymerization of Styrene. Theoretical Solution of a Classic Problem. *J. Am. Chem. Soc.* **2005**, 127 (4), 1265-1277.
(29) Ferguson, C. J.; Hughes, R. J.; Nguyen, D.; Pham, B. T. T.; Gilbert, R. G.; Serelis, A. K.; Such, C. H.; Hawkett, B. S. Ab Initio Emulsion Polymerization by RAFT-Controlled Self-Assembly. *Macromolecules* **2005**, 38 (6), 2191-2204.

Chapter 3 Functional Multisite Copolymer by One-Pot Sequential RAFT Copolymerisation of Styrene and Maleic Anhydride

Abstract

A Multisite copolymer with functionalisable units inserted at specific locations was synthesised by a one-pot reversible addition-fragmentation chain-transfer (RAFT) polymerisation. A sequential single monomer unit insertion (SMUI) and chain extension (ChainExt) strategy was applied using styrene (Sty) and maleic anhydride (MAnh) as comonomers. The multisite copolymer was based on a polystyrene (PSty) backbone (*c.a.* 5,900 g mol^{-1}) with MAnh units inserted locally at four positions in the backbone. First, a well-defined polystyrene macroCTA (DP = 10 - 1,500 g mol^{-1} - $Đ$ = 1.07) was synthesised using CTA-Ester (industrial grade) by following optimised RAFT conditions from the previous chapter (high conversion, high livingness and low dispersity). Subsequently, the polystyrene macroCTA was used for a one-pot SMUI using a small excess of MAnh monomer (DP = 1.5). The copolymer was chain extended by styrene leading to a polystyrene backbone with MAnh units (1.5 on average) located in the middle of the chain. By repeating SMUI and ChainExt, several units of MAnh were inserted locally along the polystyrene backbone (every 10 units on average) to give a functionalisable multisite copolymer ($Đ$ = 1.35). Long alkyl chains (C18) were added by esterification of maleic anhydride moieties to obtain branched architecture.

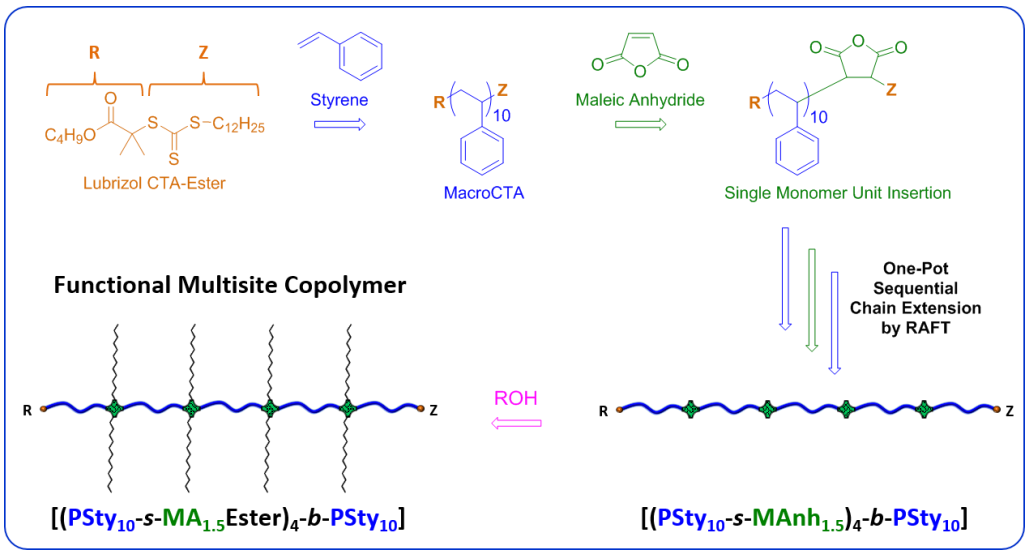

3.1 Introduction

With the emergence of controlled radical polymerisation (CRP) methods, advances have allowed the design of polymeric architectures with controlled microstructures and well-defined properties.[1-8] Nowadays, various structures such as alternating copolymers[9], multiblock copolymers[7, 10-15], graft copolymers, star-type[16], macro-cycles and macromolecular brushes[17, 18], are accessible *via* a variety of polymerisation techniques.[19-21] Among controlled radical polymerisation techniques, Reversible Addition-Fragmentation chain-Transfer (RAFT) polymerisation process appears to be the most versatile in terms of monomer choice, polymeric architectures and reaction conditions.[22-27] RAFT polymerisation is a free-radical polymerisation mediated by a chain transfer agent (CTA) allowing reversible activation/deactivation of the propagating radical and providing a "living" character. In this context, sequential RAFT copolymerisation of two or more monomers can allow the formation of block and multiblock copolymers.[28] Simultaneous copolymerisation involving two monomers can also lead to block-like structures, but generally leads to statistical, random, or alternating microstructures depending on monomer reactivity, polarity and steric hindrance. The radical copolymerisation of electron donating monomers (styrene) with electron accepting monomers such as unsaturated cyclic anhydrides (maleic anhydride or *N*-substituted maleimides) is particularly interesting. Due to their high rate coefficient of cross-propagation, conventional or controlled-radical polymerisations such as RAFT polymerisation of these comonomer pairs typically leads to almost perfect alternating copolymers.[29-33] This exceptional feature has been used to achieve sequence-controlled alternating copolymers,[34-37] polymer end-chain functionalisation[38-40] and single monomer unit insertion.[41-47]

Lutz and co-workers[41, 42, 48, 49] have used the donor/acceptor copolymerisation strategy to synthesise sequence-controlled macromolecules by NMP[4], ATRP[50] and SET-LRP.[51] They demonstrated incorporation of a large library of *N*-substituted maleimides into polystyrene (PSty) growing chains using one-pot sequential addition of various functional *N*-substituted maleimides at different times during the controlled-radical polymerisation process. This approach is very promising as it is rapid and versatile, however, it is limited in terms of sequence-control because of the statistical nature of chain-growth copolymerisation. One main drawback is the formation of chain-to-chain sequence

defects. Furthermore, statistical insertion of monomers results in the presence of chains without insertion, as well as chains with short alternating and/or statistical blocks.[52, 53]

To allow strict single monomer unit insertion (SMUI), an excess of acceptor monomer is required for the extension of the donor chains, however, this process requires tedious purification steps. Kallitsis *et al.* first described polystyrene chain end functionalisation with an excess of maleic anhydride (MAnh) using ATRP[38] followed by Harth *et al.* by NMP.[39] McLeary *et al.* were the first to observe SMUI during alternating copolymerisation of styrene (Sty) and maleic anhydride using RAFT.[54, 55] Feng and coworkers described the synthesis of miktoarm ABC star copolymers using SMUI of MAnh after a polystyrene block, followed by chain extension (ChainExt) with methyl acrylate and acrylamide monomers.[43] In another approach, Stayton *et al.* described SMUI of *N*-substituted maleimides using methacrylate and acrylamide polymers as macroCTA and showed their possible extension with styrene.[45] In their study, they also mentioned the possibility of obtaining multiple bioconjugation sites at defined intervals along a polymer backbone using sequential block copolymerisation, opening the way to unique architectures. This new copolymer structure has been mentioned in recent publications under the name of multisite copolymer.[53, 56, 57] As no official nomenclature exists for multisite-like structure, the letter "-*s*-" (site) was chosen here in the same way "-*b*-" is used for block copolymers. Recently, Fu *et al.* have used this concept to produce well-defined amphiphilic copolymer networks (co-networks) by RAFT.[46, 58] A linear polystyrene backbone with controlled number of functional groups (2, 4, and 6 maleimides), accurately inserted at certain positions, was achieved. Although the synthesis of a well-defined copolymer with a high level of sequence-control was shown, the process involved many undesired purification steps.

Recently, a RAFT-based one-pot sequential addition method has been reported by our group yielding well-defined multiblock copolymers containing complex sequences.[10] By tuning RAFT parameters (high monomer concentration, high temperature, minimum initiator concentration), full conversions were achieved and a high fraction of "living" chains was retained after each block extension, thus greatly simplifying the preparation of multiblock copolymers with a number of very short blocks as high as 20 and with relatively low molar mass distributions ($Đ < 1.4$).[59, 60]

In this chapter, we used optimised RAFT copolymerisation to produce a multisite

copolymer in a one-pot process by sequential SMUI and ChainExt using styrene and maleic anhydride as comonomers (Scheme 3.1). The optimised conditions presented in the previous chapter were used for the preparation of a well-defined polystyrene macroCTA (DP = 10). Maleic anhydride was then inserted by chain extension using a small excess of monomer (1.5 equiv.). The copolymer was chain extended by styrene leading to a polystyrene backbone with MAnh units in the middle. By repeating SMUI and ChainExt, several units of MAnh were inserted locally into the polystyrene backbone (every 10 units on average) to give a functionalisable multisite copolymer. The sequential SMUI/ChainExt process combined with high conversion of each block allows for good control of the copolymer sequence (accurate insertion), while the one-pot process decreases the number of purification steps usually needed to achieve such complex architectures. However, the process differ slightly from strict SMUI since 1.5 equiv. of MAnh is used, in a one-pot process, which leads to more than one unit, on average, inserted locally. Finally, esterification of each maleic anhydride unit with aliphatic alcohols (stearyl/C18) was performed in order to prepare a well-defined graft architecture with a controlled location and density of side chains. This graft-like copolymer structure with low density of long alkyl side chains is of interest for application as a rheology modifier in oil fields.

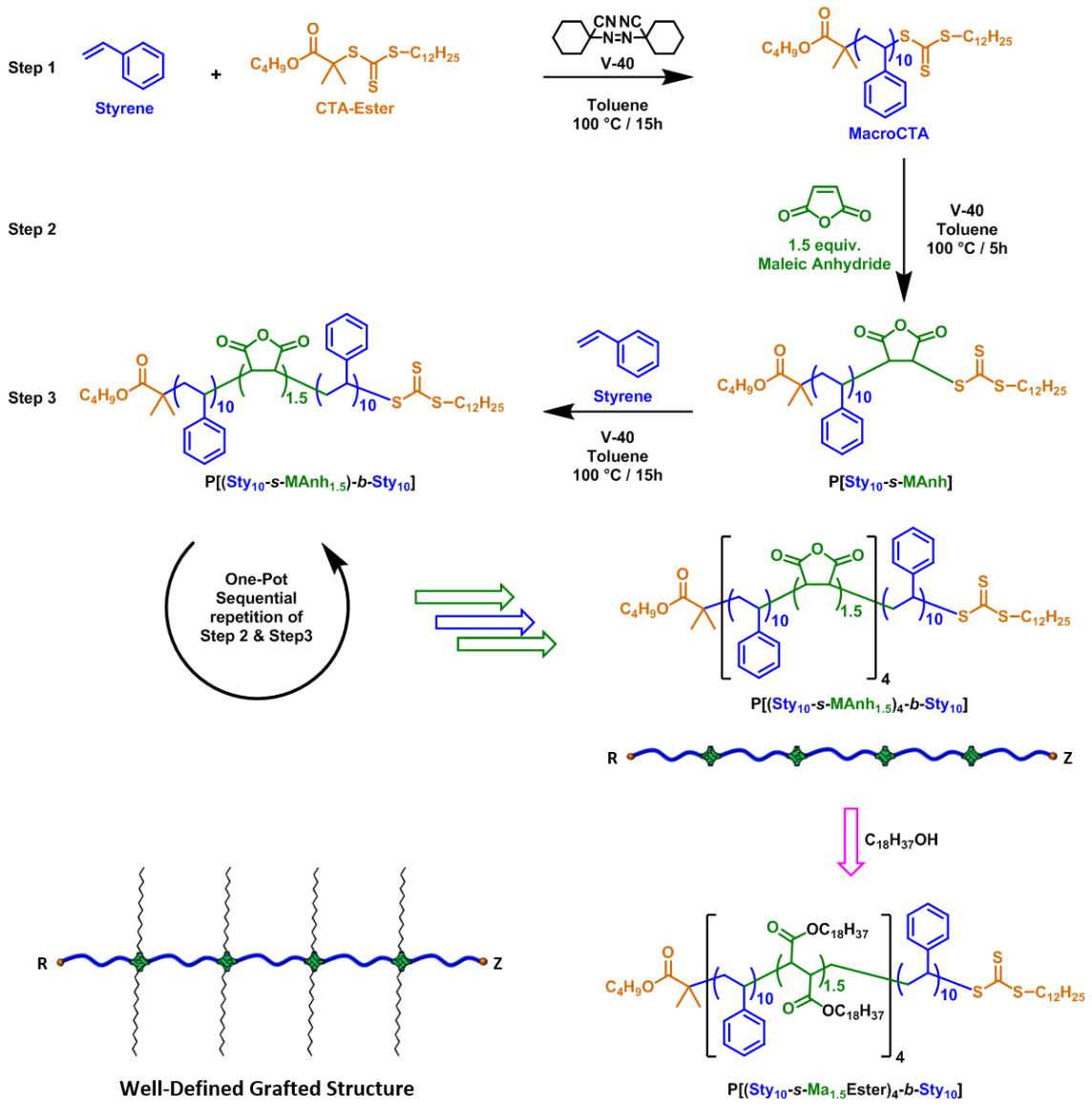

Scheme 3.1. Schematic representation of the one-pot synthesis of a multisite copolymer by sequential single monomer unit insertion and chain extension by RAFT and subsequent functionalisation by post-polymerisation esterification.

3.2 Results and Discussion

3.2.1 Polystyrene macroCTA

The polystyrene macroCTA was synthesised following the optimised conditions established in the previous chapter. The polymerisation of styrene (5 M) using industrial grade CTA-Ester (0.5 M) and V-40 as initiator (0.045 M) was performed in toluene at 100 °C (Table A3-1). The PSty macroCTA was achieved with reasonable conversion, low dispersity and high livingness (Table 3.1).

Table 3.1. Feature summary for polymer after each step

Entry	Monomer	DP_{targ}	$M_{n,targ}$ g mol^{-1}	% conv.$_{sty}$ [a]	$M_{n,theo}$ [a] g mol^{-1}	$M_{n,SEC}$ [b] g mol^{-1}	$Đ$ [b]	% $L_{cumul.}$ [c]
P[Sty]$_{10}$	Styrene	10	1500	93	1400	1400	1.07	96
P[Sty$_{10}$-*s*-MAnh$_{1.5}$]$_1$	MAnh	1.5	1600	-	-	1400	1.09	92
P[(Sty$_{10}$-*s*-MAnh$_{1.5}$)$_1$-*b*-PSty$_{10}$]	Styrene	10	2700	97	2500	2300	1.15	89
P[Sty$_{10}$-*s*-MAnh$_{1.5}$]$_2$	MAnh	1.5	2800	-	-	2300	1.15	86
P[(Sty$_{10}$-*s*-MAnh$_{1.5}$)$_2$-*b*-PSty$_{10}$]	Styrene	10	3800	92	3600	3200	1.17	82
P[Sty$_{10}$-*s*-MAnh$_{1.5}$]$_3$	MAnh	1.5	4000	-	-	3200	1.22	80
P[(Sty$_{10}$-*s*-MAnh$_{1.5}$)$_3$-*b*-PSty$_{10}$]	Styrene	10	5000	99	4800	4100	1.24	75
P[Sty$_{10}$-*s*-MAnh$_{1.5}$]$_4$	MAnh	1.5	5200	-	-	4000	1.28	73
P[(Sty$_{10}$-*s*-MAnh$_{1.5}$)$_4$-*b*-PSty$_{10}$]	Styrene	10	6200	89	5900	4700	1.35	68

[a] Calculated by ^{1}H NMR using equation 2.5, [b] determined using SEC-THF with polystyrene standards, [c] cumulative livingness using equation 1.2. MAnh conversion was not measurable by ^{1}H NMR as peak overlap with styrene.

3.2.2 Single monomer unit insertion by one-pot RAFT chain extension

The polystyrene macroCTA was used to perform SMUI of MAnh in a one-pot fashion (Scheme 3.1). Preliminary attempts (not shown) with 1 equivalent led to almost complete SMUI, however, residual PSty chains were observed (monitored by NMR spectroscopy as following). To ensure the complete reaction of the macroCTA with MAnh, a small excess of MAnh was used (1.5 unit per chain). While this strategy introduces defects in the copolymer structure (short alternating block), it should ensure the presence of grafting points locally inserted along the polymer backbone. Furthermore, the small excess of MAnh units introduced (0.5 MAnh for 10 Sty) leads to negligible structural defects. Toluene was used to dilute the reaction mixture and to maintain a processable viscosity, whereas a small amount of dioxane was used to solubilise the MAnh prior to addition. The initiator was mixed with the monomer and added at the same time to the reaction vessel, which was heated at 100 °C under a nitrogen atmosphere. In order to simplify the

process, the temperature and initiator were kept constant (V-40 at 100 °C). In fact, the chain extension with MAnh monomer could be achieved at the temperature typically used for the polymerisation of alternating poly(Sty-*alt*-MAnh) (60 °C),[34] however, changing the temperature would require the use of a different initiator and a purification step to remove left over previous initiator. Instead, the same conditions were used and the fraction of left over initiator was taken into consideration (Table A3-1). While a ratio $[CTA]_0/[Init]_0$ of 10 was necessary to polymerise styrene with high conversion, a ratio $[CTA]_0/[Init]_0$ of 20 was found to be sufficient for complete insertion of MAnh within 3 to 5 hours. The ^{1}H-NMR spectrum of the macroCTA (Figure 3.1, A and C) shows the typical styrene backbone peak between 1.3-2.5 ppm and aromatic protons between 6.4-7.3 ppm. The peak between 4.6-5.0 ppm is due to the methine proton of the styrene unit located next to the trithiocarbonate and is typical for polystyrene synthesised by RAFT. The peaks at 0.88, 1.26, 1.65, 3.25, and between 3.4-3.6 ppm are characteristic of CTA-Ester chain end. The peak from residual styrene monomer (5.25 and 5.75 ppm) and impurities from industrial grade CTA-Ester (4.10, 3.30 and 2.65 ppm) were also observed. After SMUI (Figure 3.1, B and D) the signal of the methine proton of the styrene unit next to the trithiocarbonate disappeared and a new peak between 4.0-4.5 ppm appeared, corresponding to the methine proton of the maleic anhydride unit, inserted next to trithiocarbonate.

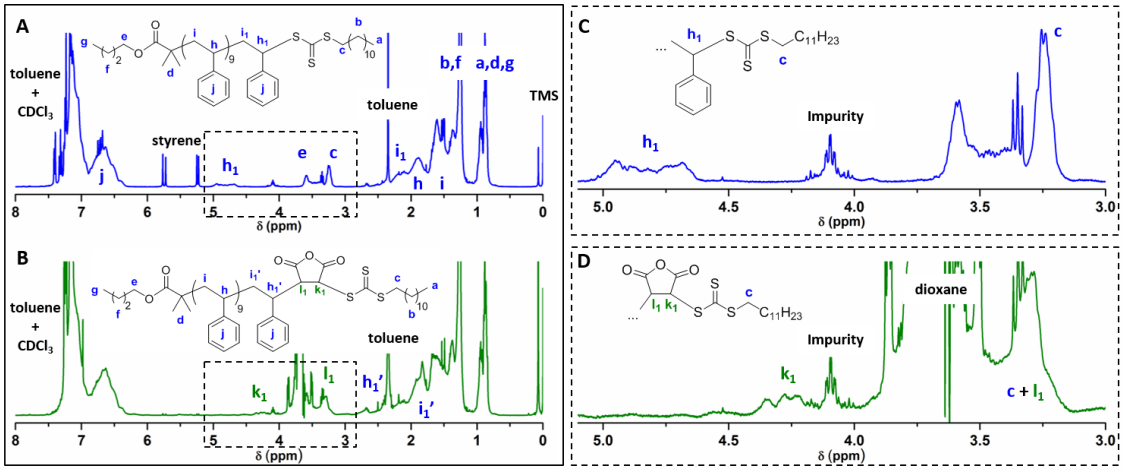

Figure 3.1. A and B are full ^{1}H-NMR spectra ($CDCl_3$) for polystyrene macroCTA ($P[Sty]_{10}$) after 15 h reaction and copolymer ($P[Sty_{10}$-*s*-$MAnh_{1.5}]_1$) after 5 h of SMUI reaction respectively. C and D are zoomed-in spectra for A and B respectively showing the position of methine proton next to trithiocarbonate for each monomer.

Feng *et al.* observed a similar peak shift after functionalising the polystyrene chain end using MAnh and dithiobenzoate RAFT agent.[43] Thus, it was possible to monitor the SMUI yield by following the appearance/disappearance of peaks between 4.0-5.0 ppm. Figure 3.1 - D shows that after 5 hrs, the styrene end group was fully replaced by maleic anhydride. Unfortunately, the conversion of MAnh was not accessible by ^{1}H-NMR spectroscopy as the vinyl peak of the cyclic anhydride (7.0 ppm) overlapped with the aromatic protons of styrene (6.4-7.3 ppm). It is also worth noting that after SMUI, the peaks corresponding to unreacted styrene (5.25 and 5.75 ppm) disappeared indicating that short alternating and / or random blocks were formed due to the presence of styrene from the previous step and excess of MAnh. Figure 3.2 shows the SEC molar mass distribution of macroCTA before and after SMUI, as well as the CTA-Ester impurities. After SMUI, a small shift towards higher molar mass was observed while no change of the molar mass distribution was detected. The residual peak at low molar mass was attributed to unreactive CTA-Ester impurities studied in the previous chapter.

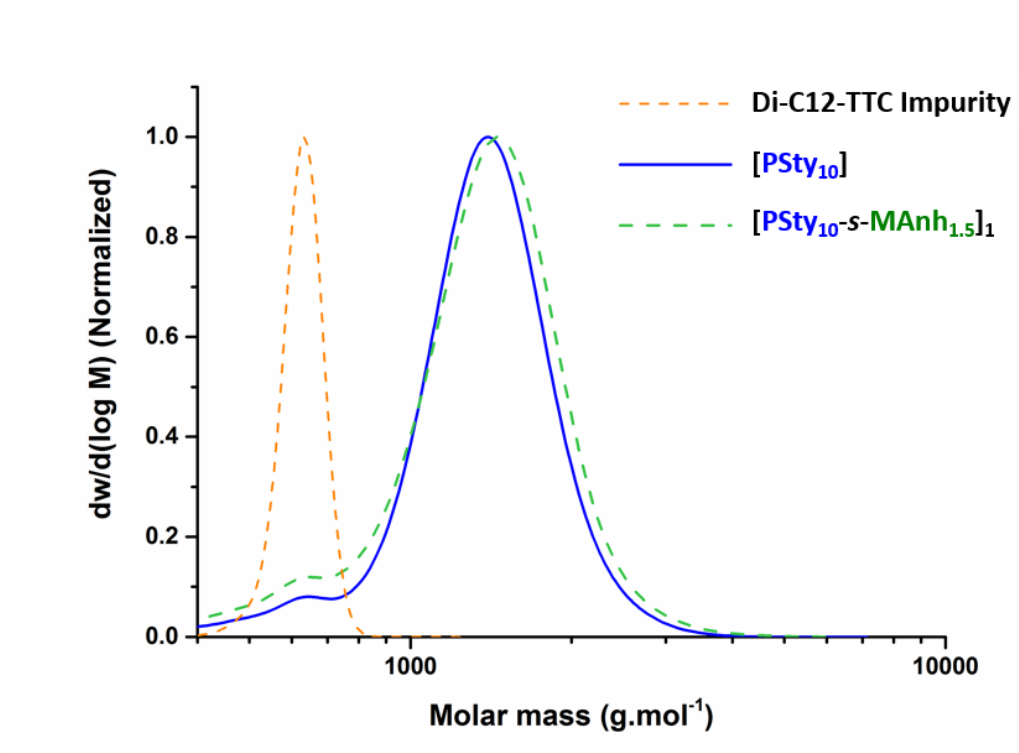

Figure 3.2. SEC molar mass distribution showing RI traces for di-C12-TTC impurity from CTA-Ester (dash orange), macroCTA before (blue) and after SMUI (dash green). SEC in THF using polystyrene calibration.

The diversity of populations obtained after SMUI was also investigated by MALDI-ToF mass spectrometry. Figure 3.3 shows spectra of polystyrene macroCTA before (blue) and after maleic anhydride insertion (green). The spectrum obtained for polystyrene macroCTA shows one narrow main population with m/z in agreement with the theoretical molar mass (1,400 g mol^{-1}). The proposed structure contains the R group from the CTA-Ester, a styrene block and a double bond at the ω-chain end (Figure 3.3 – structure A). The comparison between measured and calculated isotopic distribution was consistent with the proposed structures (Figure 3.3 - C). Fragmentation of the Z group into a stable conjugated double bond is commonly observed for polystyrene synthesised by RAFT and is mainly attributed to the presence of the silver salt, which can act as a catalyst to cleave the weak C-S bond between the polymer and chain transfer agent in the mass spectrometer.[61, 62]

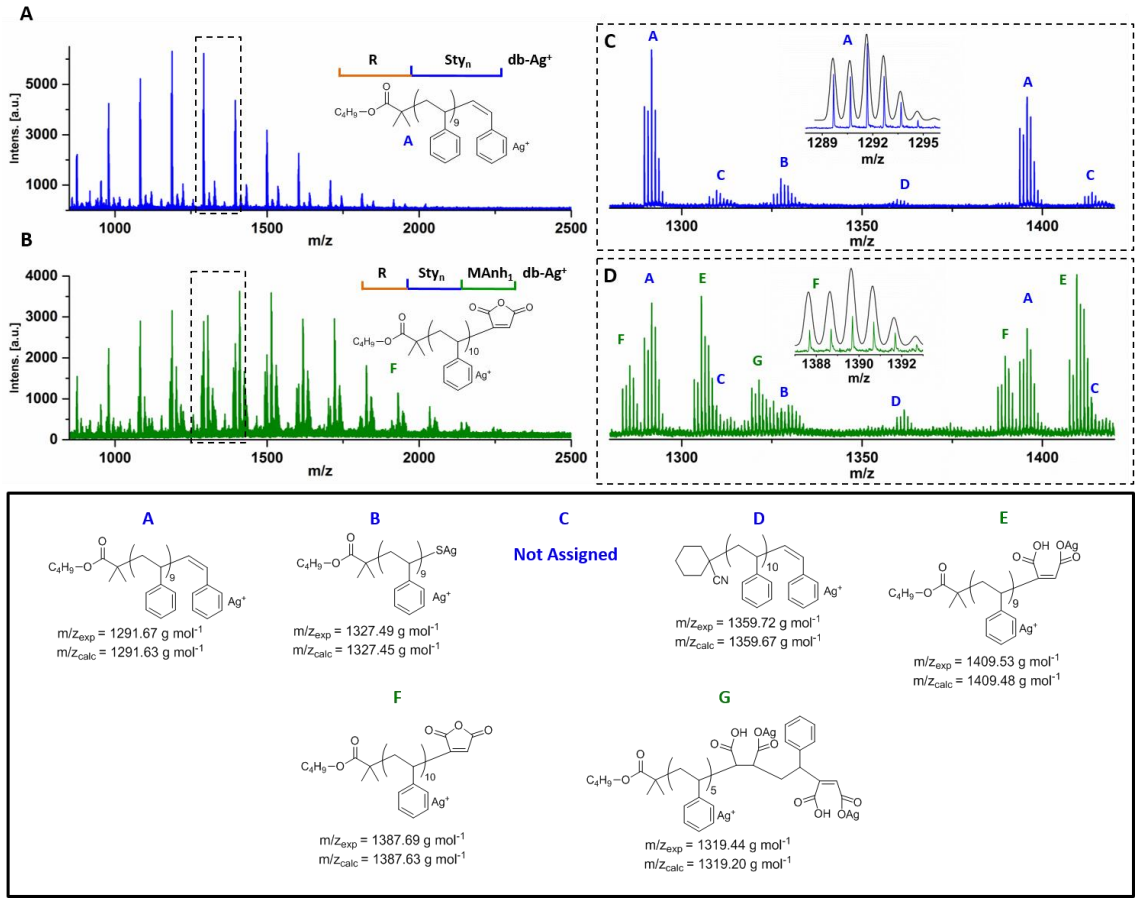

Figure 3.3. A and B are full MALDI-ToF mass spectra for polystyrene macroCTA (P[Sty]$_{10}$) after 15 h reaction and copolymer (P[Sty$_{10}$-*s*-MAnh$_{1.5}$]$_1$) after 5 h of SMUI reaction respectively. C and D are zoomed spectra for A and B respectively.

Minor populations with similar structures but with different end-group fragmentation types were also observed (structure B-D). The MALDI spectrum after SMUI was also recorded (Figure 3.3 – B-D). Surprisingly, higher laser intensity was required to obtain similar signal strength compared to styrene terminated fragments (*ca.* 5 % higher). The addition of maleic anhydride at the end of polystyrene chains appeared to make the polymer more difficult to ionise under these conditions and a more complex spectrum was obtained. The expected structure was observed (structure F), as well as structures corresponding to the copolymer with one and two ring-opened anhydride units (structure E and G). Structures with opened MAnh ring result in the reaction of cyclic anhydride with silver salt either during the sample preparation or ionisation process. The structure with two MAnh units was expected due to the incomplete conversion of the first block (conv. = 93 %). The residual styrene is consumed (as confirmed by NMR), forming alternating short blocks with excess of MAnh. The spectrum also reveals a peak with high intensity corresponding to residual macroCTA (structure A). If most of the macroCTA is reacted at this step (as shown by NMR), the high intensity of the peak can be explained by the differences in ionisation process, which appear to be more challenging for polymers with MAnh as a terminal unit. It should be noted that since MALDI is not a quantitative method, a residual amount of macroCTA can appear to be the main population due to its favourable ionisation process. This hypothesis was supported by the spectrum obtained after subsequent ChainExt with styrene (Figure 3.4), as a relatively clean spectrum at higher molar mass was obtained. The spectrum showed the expected copolymer structures with one and two MAnh units (Figure 3.4 - structures A-D), while a signal for homopolystyrene was barely observable (structures E). The very low intensity of chain extended homopolystyrene shows that the SMUI was achieved with high yield.

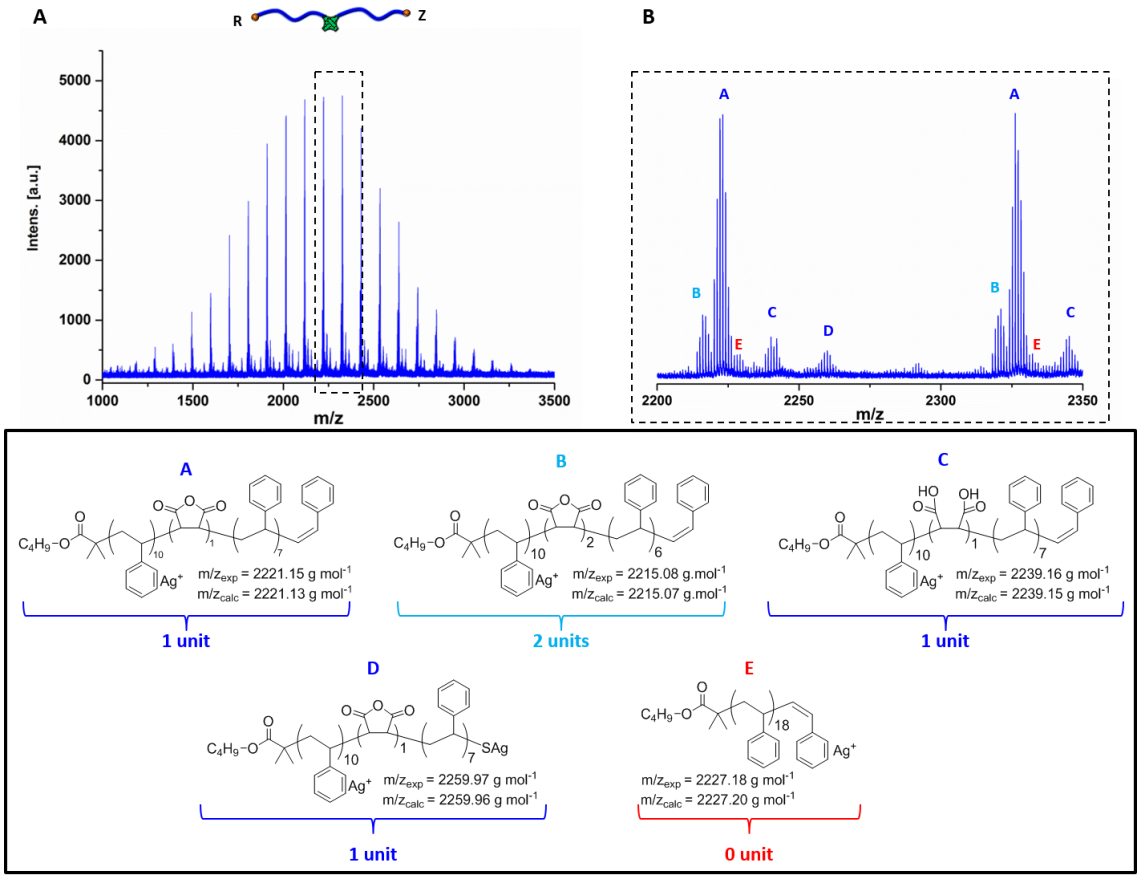

Figure 3.4. A) MALDI-ToF mass spectrum for [$PSty_{10}$-*s*-$MAnh_{1.5}$)$_1$-$PSty_{10}$] B) zoom corresponding to the region in the dashed square in A).

3.2.3 One-pot sequential SMUI and ChainExt by RAFT

The copolymer poly[Sty_{10}-*s*-$MAnh_{1.5}$] was used as a macroCTA and chain extended with styrene before performing sequential SMUI and ChainExt as described in Scheme 3.1. Four cycles were performed to achieve a multisite copolymer composed of a polystyrene backbone with MAnh monomers located every 10 units on average. Figure 3.5 shows the ^{1}H-NMR spectrum of the initial polystyrene macroCTA and a magnified area of the spectra after each SMUI and chain extension showing the alternation of styrene block and MAnh unit(s). The process can be followed by the appearance/disappearance of the characteristic peak of the methine proton of the last styrene unit (4.6-5.1 ppm). A similar behaviour was also observed for the last MAnh unit (4.0-4.5 ppm), however, it was less clear due to the overlap with CTA impurity peak (4.1 ppm). The conversion of styrene obtained after each chain extension was relatively high (conv. > 89 %) and was controlled by maintaining a low ratio between CTA and initiator concentrations after each step (Table A3-1).

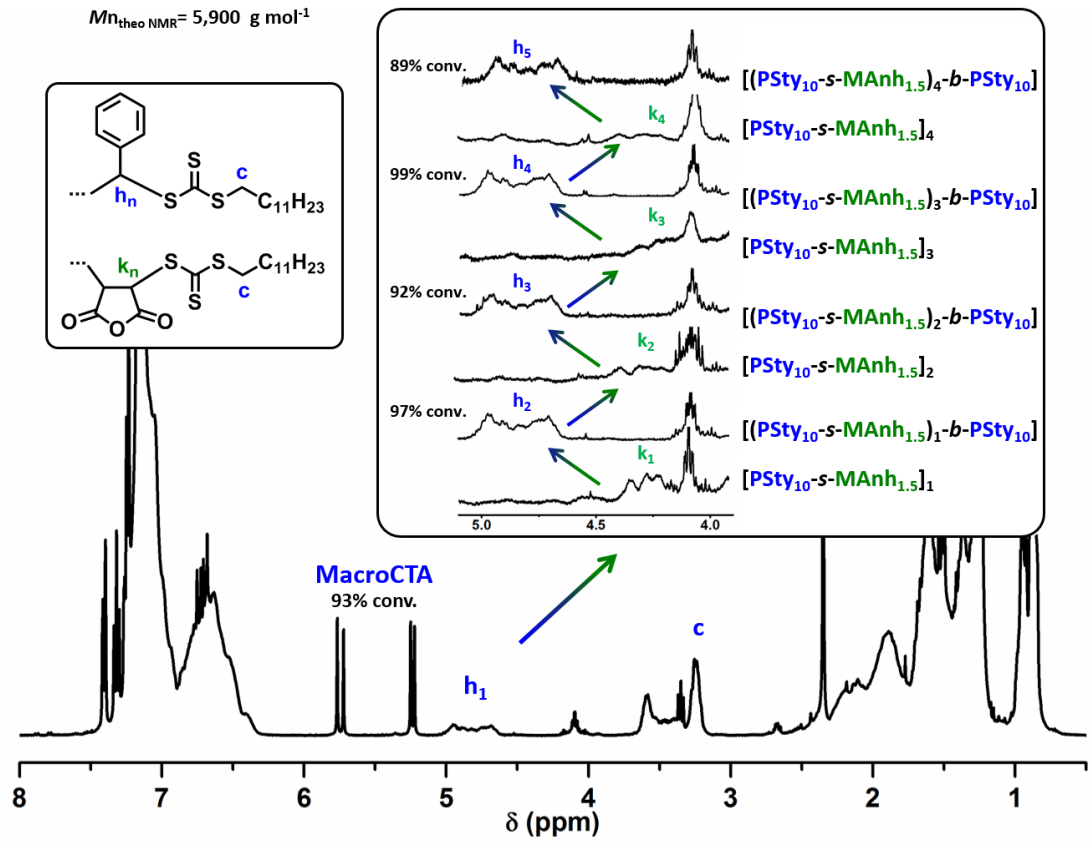

Figure 3.5. Sequential SMUI / ChainExt monitored by ^{1}H-NMR spectroscopy ($CDCl_3$).

Dilution after each chain extension was necessary to maintain low viscosity. As a result the monomer and initiator concentration after each step was restricted, leading to limitations in conversion and livingness. After four cycles of SMUI and ChainExt, the cumulative livingness had dropped to 68 % (Table 3.1). Thus, it became difficult to control the polymerisation after further chain extension as theoretically only two thirds of chains remaining were still bearing the CTA required for chain extension. This is the consequence of slowly propagating monomers such as styrene. The large amount of initiator required to reach high conversion by RAFT inherently increases the number of terminated chains. According to styrene conversion values, the theoretical molar mass of the final material was estimated at 5,900 g mol^{-1}. The polymer was purified by precipitation in hexane and 20 g of material was recovered (Figure A3-1). SEC analysis showed monomodal distributions and a clear shift to higher molar masses after each chain extension, confirming the synthesis of multiblock-like structure (Figure 3.6). A low molar mass tailing and a high molar mass shoulder were also observed after performing several cycles.

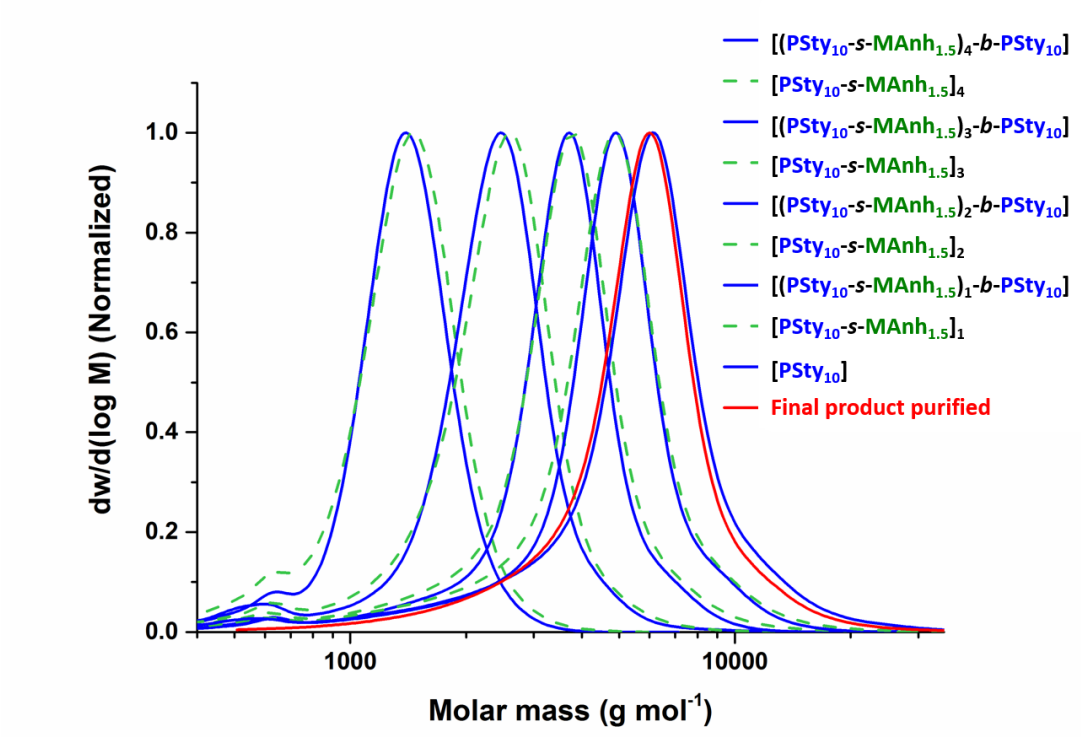

Figure 3.6. SEC molar mass distribution for polystyrene macroCTA followed by each step of SMUI (dashed green) and chain extension with styrene (blue). The final product after purification is shown in red. SEC in THF with polystyrene standards.

The low molar mass tailing was mainly attributed to the accumulation of dead chains ($L \approx 30$ % after 9 cycles) and initiator derived chains, as relatively high initiator concentrations were used in this system. The high molar mass shoulder was ascribed to bimolecular termination. The final material was recovered without CTA-Ester impurities (low molar mass peak) and with relatively narrow distribution for such complex architecture ($Đ = 1.35$). Moreover, the molar mass obtained by SEC ($M_{n,SEC}$ = 4,700 g mol^{-1}) was consistent with the theoretical value calculated from NMR results. A small deviation from the theoretical value was observed and can be explained by the increase of low molar mass chains after the third insertion which results in an underestimation of the overall molar mass of the final material ($M_{p,SEC}$ = 6,000 g mol^{-1}). Furthermore, a deviation was not surprising as the nature of the polystyrene backbone was affected by the presence of MAnh compared to the homopolystyrene standards used for SEC calibration. The presence of MAnh in the final material was also confirmed by IR as the peaks at 1,850 cm^{-1} and 1,770 cm^{-1}, characteristic of carbonyl stretching bands from cyclic anhydride, were observed (Figure 3.7).

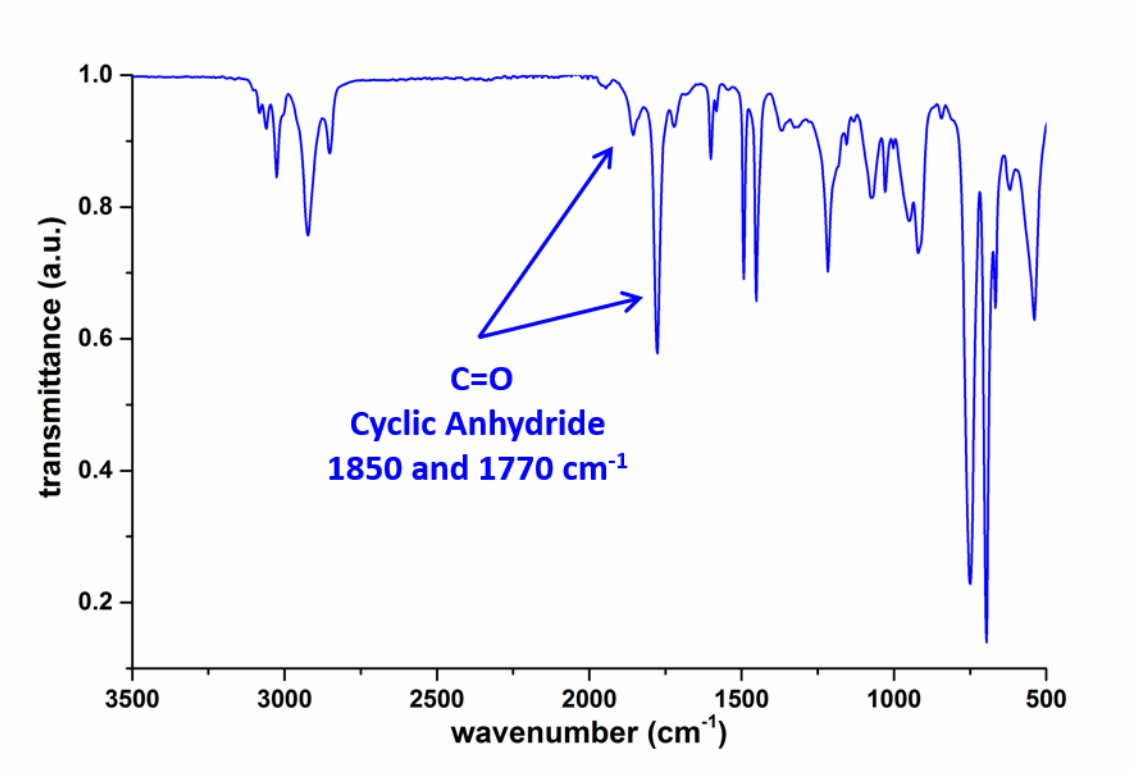

Figure 3.7. IR spectrum of the final multisite copolymer.

Figure 3.8 presents the MALDI-ToF mass spectrometry results after each polymerisation step. An increase in molar mass after each chain extension was observed, and the final spectrum shows clearly a peak between 4,000-7,000 g mol^{-1}, confirming the results previously obtained by NMR spectroscopy and size exclusion chromatography. The m/z values observed were assigned after each step (Figure A3-2 - Figure A3-7) and structures with 3, 4, 5 and 6 MAnh units were observed for the final material. As a small excess of MAnh (1.5 equiv.) was used for each SMUI, an average of 6 units was expected after 4 cycles of SMUI and ChainExt, thus, it was not surprising to observe structures with 4, 5 and 6 units inserted. The structure with 3 units was the result of an incomplete SMUI, however, as discussed previously these defects are marginal, indicating that the SMUI were successful in the majority of cases. After three cycles, strong signals corresponding to dead chains and initiator derived chains were observed at low molar mass, increasing the complexity of the MALDI-ToF mass spectra. The high intensity of these chains compared to the final material can be explained by the difference in length.

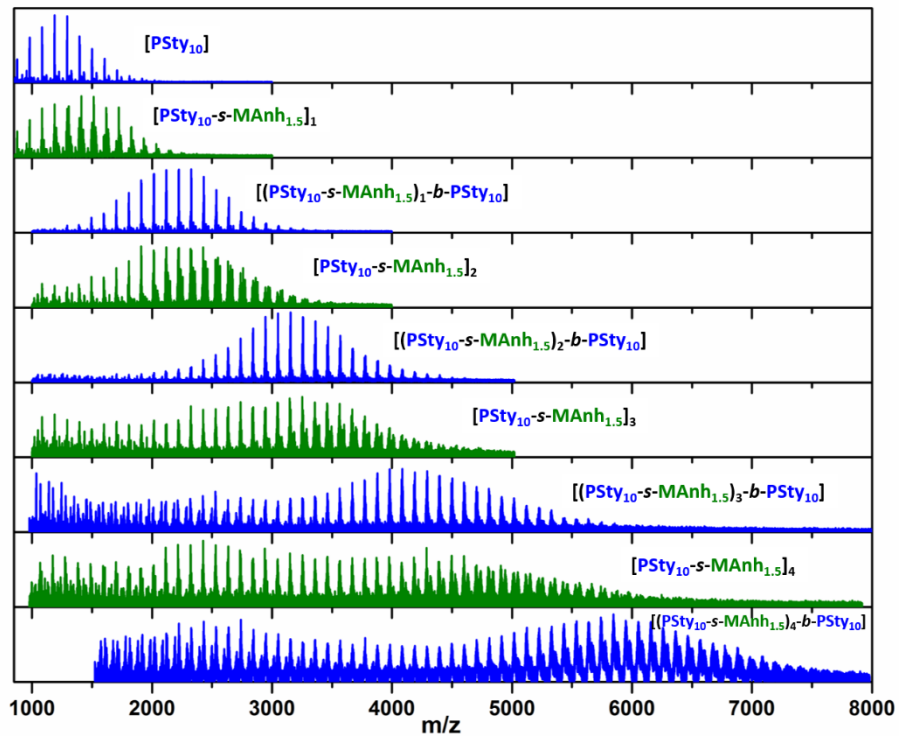

Figure 3.8. MALDI-ToF mass spectra measured after each polymerisation step from the polystyrene macroCTA at the top to multisite copolymers after four SMUI at the bottom. The spectrum were recorded using DCTB as a matrix and AgTFA as ionisation agent.

These low molar mass chains were clearly over-represented by MALDI-ToF-MS as only a low molar mass tail was observed by SEC (Figure 3.6). In addition, quantitative ^{13}C-NMR was attempted on the purified copolymer and revealed the presence of approximately 5 MAnh units (Figure A3-8 – peak at 171.7 ppm) incorporated as SMUI or short alternating blocks (Figure A3-8 – zoom 135-150 ppm).[63, 64]

3.2.4 Functionalisation of the multisite copolymer by esterification of maleic anhydride moieties.

To demonstrate the potential of the described well-defined functionalisable multisite copolymer, esterification of maleic anhydride units with a long alkyl alcohol (stearyl – $C_{18}H_{37}OH$) was attempted. The incorporation of long alkyl chains allows the formation of graft-like copolymers with potential applications as rheology modifiers. The esterification was performed using Dean-Stark apparatus under reflux of toluene and using methane sulfonic acid as a catalyst (MSA) (Figure 3.9). The reaction of cyclic anhydride with the alcohol is fast and irreversible for the mono-esterification process, whereas esterification of the free acid is relatively slow and requires a catalyst and the elimination of water. Figure 3.10 shows the ^{1}H-NMR spectrum of the copolymer before (top) and after (bottom) esterification. A peak corresponding to methylene protons next to an ester bond (3.3-4.2 ppm) clearly appeared after esterification, evidencing that functionalisation occurred. The number of alkyl chains inserted was determined by comparing the integral before and after esterification for the regions containing protons from alkyl chains (0.5-3.15ppm = 35H), and using aromatic protons from styrene as a reference.

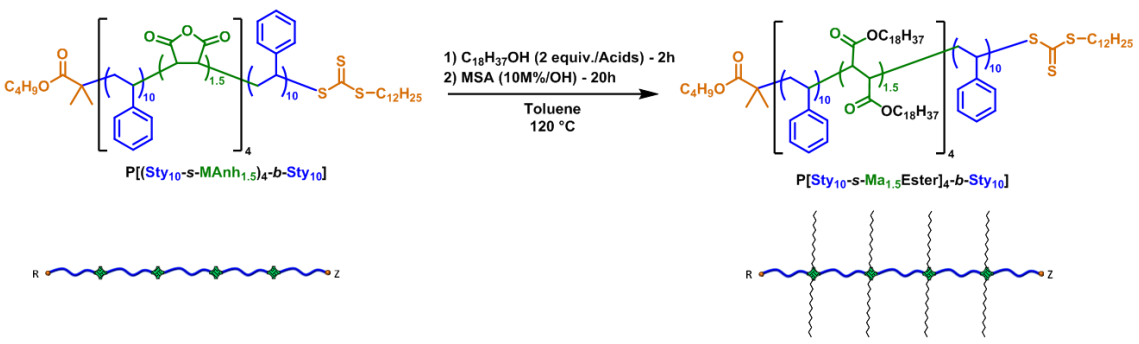

Figure 3.9. Scheme of esterification process for graft-like copolymer synthesis.

The calculated number of alkyl chains (12 per polymer chain) was consistent with a complete esterification, as an average of six maleic anhydride units was inserted in the multisite copolymer. The functionalisation of all maleic anhydride moieties was also confirmed by IR (Figure 3.11) as the peaks corresponding to cyclic anhydride disappeared (1,770 and 1,850 cm^{-1}) and a strong asymmetric ester peak appeared (1,730 cm^{-1}). SEC analysis showed an increase in molar mass after esterification while no change was observed for molar mass distribution (Figure 3.12). MALDI-ToF mass spectrometry was attempted, however, no results were obtained using previous conditions. A change in polymer properties was also observed, as its solubility in *n*-hexane increased.

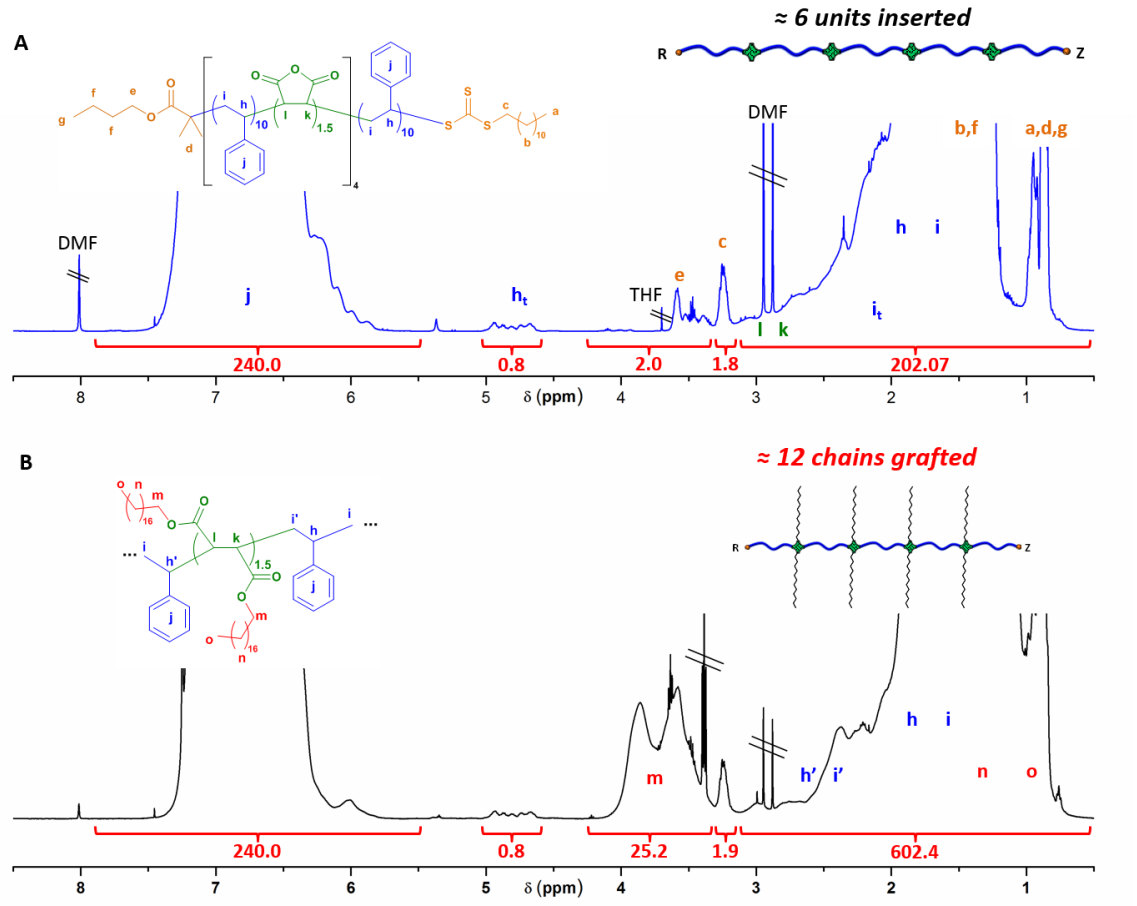

Figure 3.10. ^{1}H-NMR spectra ($CDCl_3$) for multisite copolymer before (A) and after (B) esterification.

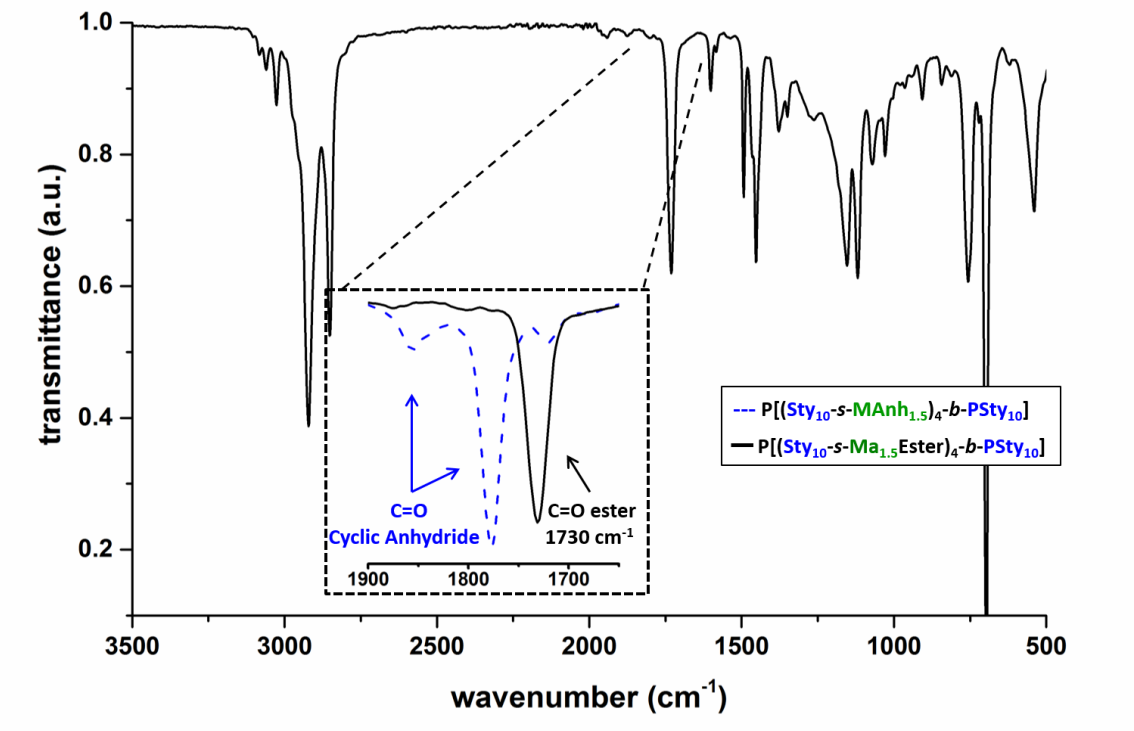

Figure 3.11. IR spectrum for the esterified multisite copolymer.

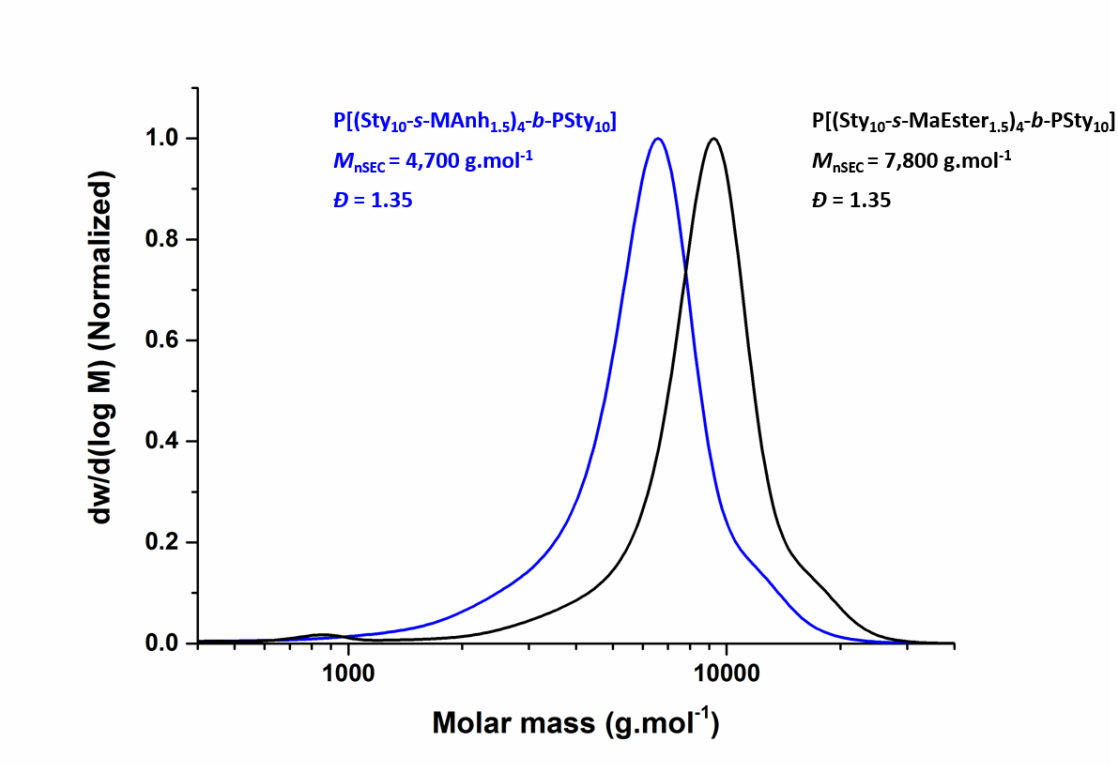

Figure 3.12. SEC molar mass distribution showing RI traces for multisite copolymer before (blue) and after (black) esterification with stearyl alcohol. SEC in THF using polystyrene calibration.

3.3 Conclusion

A multisite copolymer with pendent alkyl chains inserted locally was synthesised by a one-pot RAFT polymerisation process and post-polymerisation functionalisation. The preparation of the functionalisable multisite copolymer was achieved *via* sequential single monomer unit insertion and chain extension using styrene and maleic anhydride as comonomers and industrial grade CTA-Ester. After four cycles of SMUI and ChainExt, a polystyrene backbone with four functionalisable areas was achieved. An average of six MAnh units were inserted along the polystyrene backbone as either one local monomeric unit or as short alternating / random blocks with an overall dispersity of 1.35. By showing the possibility to synthesise a well-defined material with such complex architectures in gram scale (20 g) and, using industrial grade CTA, the great potential of RAFT polymerisation for industrial application was demonstrated. The quantitative functionalisation of each MAnh moiety was achieved by esterification with stearyl alcohol leading to a well-defined graft polymeric structure. By controlling the position and number of side chains, it is therefore possible to produce graft copolymers with a controllable density and distribution of side chain functionalities, allowing for new structure-property investigation.

3.4 Experimental

Materials

Styrene (Sty, ≥ 99 %) was obtained from Sigma-Aldrich and passed through neutral alumina prior to use to remove inhibitor. Industrial grade CTA-Ester was provided by Lubrizol and used without purification (≈ 80 % pure).[65, 66] Maleic anhydride (MAnh, ≥ 99 %), 1,1'-Azobis(cyclohexane-1-carbonitrile) (V-40, $T_{1/2\text{-}10h}$ = 88 °C, 98 %) and methane sulfonic acid (MSA, 70 wt. % in H_2O) were obtained from Sigma-Aldrich and used as received. 1, 4-dioxane and toluene were obtained from Fisher Scientific and used as received. Tetrahydrofuran (THF), diethyl ether and chloroform were obtained from Sigma-Aldrich and used as received. Hexane (99 %) was obtained from VWR chemical. Chloroform-d (99.9 % D atom) and acetone-d_6 (99.9 % D atom) obtained from Sigma-Aldrich were used for ^{1}H NMR analysis.

Characterisation techniques

^{1}H-NMR spectra were recorded on either a Bruker DPX-300 or DPX-400 spectrometer at 27 °C using deuterated solvents obtained from Sigma-Aldrich. Esterification yield was determined by ^{1}H-NMR measurements from a 600 MHz Bruker Avance instrument using a relaxation time of 25 s and 16 scans. ^{13}C-NMR measurements were performed on a 600 MHz Bruker Avance instrument (at 150 MHz) with a relaxation time of 10 s, high number of scans (>4k), and suppression of NOE (inverse gated decoupling).TMS contained in the solvent was used as the internal standard and chemical shift values (δ) are reported in ppm.

SEC was carried out using the same conditions and method as described in the previous chapter (SEC in THF).

Matrix-Assisted laser desorption/ionisation time of flight mass spectrometry (MALDI-ToF-MS) was performed on a Bruker Daltonics Ultraflex in the positive ion and reflection mode using external calibration (PEG1,500 and PEG5,000). *Trans*-2-[3-(4-*tert*-Butylphenyl)-2-methyl-2-propenylidene]malononitrile (DCTB), were used as matrix (300 mg mL^{-1} in THF) without further purification (Sigma-Aldrich). AgTFA salt was used as ionisation agents (10 mg mL^{-1} in THF). Matrix, salts and polymer solution (10 mg mL^{-1} in THF) were mixed in a 1:1:1 ratio and then, 2 μL of the mixture was deposited onto the MALDI target before insertion into the ion source chamber.

RAFT polymerisation of polystyrene macroCTA (DP = 10)

Industrial grade CTA-Ester (2.6 g, 5 mmol), styrene (5.3 g, 50 mmol), V-40 (0.11 g, 0.45 mmol) and toluene (1.3 mL) were charged into a two-neck round bottom flash equipped with a magnetic stirrer bar, a condenser on one neck and a rubber septum on the other neck (Table A3-1). The solution was degassed using nitrogen for *ca.*15 min before being placed in a thermostated oil bath set at 100 °C. After reaction completion (*ca.* 15 h) a sample was taken from the polymerisation medium for characterisation. Final materials were characterised using ^{1}H-NMR spectroscopy and SEC (monomer conversion = 93 %, $M_{n,theo}$ = 1,400 g mol^{-1}, $M_{n,SEC\text{-}THF}$ = 1400 g mol^{-1} and $Đ$ = 1.07).

Sequential single monomer unit insertion and chain extension procedure

The reactor vessel containing the macroCTA was flooded with a nitrogen stream and toluene (2 mL) was added for dilution. Both maleic anhydride (0.74 g, 7.5 mmol) and V-40 (0.062 g, 0.25 mmol) were added to the polymerisation medium *via* syringe (Table A3-1). The reaction mixture was degassed for *ca.*15 min and allowed to polymerise at 100 °C until reaction completion. A sample was taken from the polymerisation medium before and after each chain extension for characterisation. As MAnh is barely soluble in toluene, it was dissolved in a small amount of dioxane before addition. Importantly, the amount of initiator remaining after each cycle was taken into account for the following polymerisation step (calculated using equation 1.3). The final material was dissolved in minimum amount of chloroform and precipitated in hexane prior to characterisation and functionalisation.

Functionalisation of the multisite copolymer by esterification of MAnh moieties

The dried multisite copolymer (3 g, 0.5 mmol), stearyl alcohol (5 g, 18 mmol) and toluene (*ca.*17 mL) were added into a two-neck round bottom flask equipped with Dean-Stark apparatus. The flask was placed in a thermostated oil bath set at 120 °C and kept under nitrogen flux for 3 h. Then, the temperature was set at 90 °C and the methane sulfonic acid catalyst (0.25 g, 1 wt. %) was added by syringe through the septum. The temperature was set at 130 °C and the reaction was kept under nitrogen stream overnight. After evaporating the toluene, the mixture was dissolved using minimum amount of diethyl ether and precipitated three times in ethanol at room temperature. The precipitate

was dried overnight using a vacuum oven (40 °C) and recovered as a yellow solid.

Determination of monomer conversion.

The conversion after each extension with styrene was estimated by using the method as described in previous chapter (equation 2.5). Due to the overlap between vinyl peaks from the cyclic anhydride (7.0 ppm) and aromatic peaks of styrene (6.4-7.3 ppm), the conversion of MAnh was not estimated. Full MAnh conversion was assumed to calculate theoretical molar mass.

Calculation of $M_{n,theo}$

For the polystyrene macroCTA (homopolystyrene), the theoretical number-average molar mass ($M_{n,th}$) was calculated as described in previous chapter using equation 2.6.
After SMUI, the previous equation cannot be used as the MAnh conversion was not accessible by ^{1}H-NMR. Full MAnh conversion was assumed to calculate theoretical molar mass leading to equation 3.1.

$$M_{n,th,SMUI} = M_{n,th,macroCTA} + 1.5 \times M_{MAnh} \quad 3.1$$

where $M_{n,th,SMUI}$ is the theoretical number-average molar mass after SMUI, $M_{n,th,macroCTA}$ is the theoretical number-average molar mass of polystyrene macroCTA and M_{MAnh} the molar mass of maleic anhydride.

To determine the $M_{n,th}$ after further chain extension with styrene the following equation was used:

$$M_{n,th} = DP_{targ} \times p \times M_{mono} + M_{n,th,SMUI} \quad 3.2$$

Calculation of livingness

The fraction of living chain calculated using equation 1.2 presented in introduction chapter.[10] We use $fc = 1$ for styrene as it mainly terminates by combination (leads to an under-estimation), whereas, $fc = 0$ was used for MAnh as no information on termination are reported (leads to an over-estimation).

3.5 References

(1) Matyjaszewski, K. Macromolecular engineering: From rational design through precise macromolecular synthesis and processing to targeted macroscopic material properties. *Prog. Polym. Sci.* **2005**, 30 (8–9), 858-875.
(2) Matyjaszewski, K. Architecturally Complex Polymers with Controlled Heterogeneity. *Science* **2011**, 333 (6046), 1104-1105.
(3) Szwarc, M. Living polymers. Their discovery, characterization, and properties. *J. Polym. Sci., Part A: Polym. Chem.* **1998**, 36 (1), 9-15.
(4) Hawker, C. J.; Bosman, A. W.; Harth, E. New Polymer Synthesis by Nitroxide Mediated Living Radical Polymerizations. *Chem. Rev.* **2001**, 101 (12), 3661-3688.
(5) Kamigaito, M.; Ando, T.; Sawamoto, M. Metal-Catalyzed Living Radical Polymerization. *Chem. Rev.* **2001**, 101 (12), 3689-3746.
(6) Moad, G.; Rizzardo, E.; Thang, S. H. Radical addition–fragmentation chemistry in polymer synthesis. *Polymer* **2008**, 49 (5), 1079-1131.
(7) Bates, F. S.; Hillmyer, M. A.; Lodge, T. P.; Bates, C. M.; Delaney, K. T.; Fredrickson, G. H. Multiblock Polymers: Panacea or Pandora's Box? *Science* **2012**, 336 (6080), 434-440.
(8) Lutz, J.-F.; Ouchi, M.; Liu, D. R.; Sawamoto, M. Sequence-Controlled Polymers. *Science* **2013**, 341 (6146), 1238149.
(9) Cowie, J. M. G., *Alternating copolymers*. Springer Science & Business Media, **2013**.
(10) Gody, G.; Maschmeyer, T.; Zetterlund, P. B.; Perrier, S. Rapid and quantitative one-pot synthesis of sequence-controlled polymers by radical polymerization. *Nat. Commun.* **2013**, 4, 2505.
(11) Martin, L.; Gody, G.; Perrier, S. Preparation of complex multiblock copolymers via aqueous RAFT polymerization at room temperature. *Polym. Chem.* **2015**, 6 (27), 4875-4886.
(12) Zhang, J.; Gody, G.; Hartlieb, M.; Catrouillet, S.; Moffat, J.; Perrier, S. Synthesis of Sequence-Controlled Multiblock Single Chain Nanoparticles by a Stepwise Folding–Chain Extension–Folding Process. *Macromolecules* **2016**, 49 (23), 8933-8942.
(13) Engelis, N. G.; Anastasaki, A.; Nurumbetov, G.; Truong, N. P.; Nikolaou, V.; Shegiwal, A.; Whittaker, M. R.; Davis, T. P.; Haddleton, D. M. Sequence-controlled methacrylic multiblock copolymers via sulfur-free RAFT emulsion polymerization. *Nat. Chem.* **2017**, 9 (2), 171-178.
(14) Anastasaki, A.; Nikolaou, V.; Pappas, G. S.; Zhang, Q.; Wan, C.; Wilson, P.; Davis, T. P.; Whittaker, M. R.; Haddleton, D. M. Photoinduced sequence-control via one pot living radical polymerization of acrylates. *Chem. Sci.* **2014**, 5 (9), 3536-3542.
(15) Chuang, Y.-M.; Ethirajan, A.; Junkers, T. Photoinduced Sequence-Controlled Copper-Mediated Polymerization: Synthesis of Decablock Copolymers. *ACS Macro Lett.* **2014**, 3 (8), 732-737.
(16) Ren, J. M.; McKenzie, T. G.; Fu, Q.; Wong, E. H. H.; Xu, J.; An, Z.; Shanmugam, S.; Davis, T. P.; Boyer, C.; Qiao, G. G. Star Polymers. *Chem. Rev.* **2016**, 116 (12), 6743-6836.
(17) Sheiko, S. S.; Sumerlin, B. S.; Matyjaszewski, K. Cylindrical molecular brushes: Synthesis, characterization, and properties. *Prog. Polym. Sci.* **2008**, 33 (7), 759-785.
(18) Kerr, A.; Hartlieb, M.; Sanchis, J.; Smith, T.; Perrier, S. Complex multiblock bottle-brush architectures by RAFT polymerization. *Chem. Commun.* **2017**, 53 (87), 11901-11904
(19) Davis, K. A.; Matyjaszewski, K., *Statistical, Gradient, Block, and Graft Copolymers by Controlled/Living Radical Polymerizations*. Berlin, Springer Heidelberg, **2002**.
(20) Hadjichristidis, N.; Iatrou, H.; Pitsikalis, M.; Mays, J. Macromolecular architectures by living and controlled/living polymerizations. *Prog. Polym. Sci.* **2006**, 31 (12), 1068-1132.
(21) Gregory, A.; Stenzel, M. H. Complex polymer architectures via RAFT polymerization: From fundamental process to extending the scope using click chemistry and nature's building blocks. *Prog. Polym. Sci.* **2012**, 37 (1), 38-105.
(22) Goto, A.; Fukuda, T. Kinetics of living radical polymerization. *Prog. Polym. Sci.* **2004**, 29 (4), 329-385.
(23) Braunecker, W. A.; Matyjaszewski, K. Controlled/living radical polymerization: Features, developments, and perspectives. *Prog. Polym. Sci.* **2007**, 32 (1), 93-146.
(24) Chiefari, J.; Chong, Y. K.; Ercole, F.; Krstina, J.; Jeffery, J.; Le, T. P. T.; Mayadunne, R. T. A.; Meijs, G. F.; Moad, C. L.; Moad, G.; Rizzardo, E.; Thang, S. H. Living Free-Radical Polymerization by Reversible Addition−Fragmentation Chain Transfer: The RAFT Process. *Macromolecules* **1998**, 31 (16), 5559-5562.

(25) Le, T.; Moad, G.; Rizzardo, E.; Thang, S. Polymerization with living characteristics. Patent WO1998001478A1, **1998**.
(26) Perrier, S.; Takolpuckdee, P. Macromolecular design via reversible addition–fragmentation chain transfer (RAFT)/xanthates (MADIX) polymerization. *J. Polym. Sci., Part A: Polym. Chem.* **2005**, 43 (22), 5347-5393.
(27) Moad, G.; Rizzardo, E.; Thang, S. H. Living Radical Polymerization by the RAFT Process – A Second Update. *Aust. J. Chem.* **2009**, 62 (11), 1402-1472.
(28) Gody, G.; Barbey, R.; Danial, M.; Perrier, S. Ultrafast RAFT polymerization: multiblock copolymers within minutes. *Polym. Chem.* **2015**, 6 (9), 1502-1511.
(29) Alfrey, T.; Lavin, E. The Copolymerization of Styrene and Maleic Anhydride. *J. Am. Chem. Soc.* **1945**, 67 (11), 2044-2045.
(30) Tsuchida, E.; Tomono, T. Discussion on the mechanism of alternating copolymerization of styrene and maleic anhydride. *Makro. Ch.* **1971**, 141 (1), 265-298.
(31) Jenkins, A. D. Alternating copolymers. *Brit. Polym. J.* **1987**, 19 (1), 91-91.
(32) Matsumoto, A.; Kubota, T.; Otsu, T. Radical polymerization of N-(alkyl-substituted phenyl)maleimides: synthesis of thermally stable polymers soluble in nonpolar solvents. *Macromolecules* **1990**, 23 (21), 4508-4513.
(33) Rzaev, Z. M. O. Complex-radical alternating copolymerization. *Prog. Polym. Sci.* **2000**, 25 (2), 163-217.
(34) De Brouwer, H.; Schellekens, M. A. J.; Klumperman, B.; Monteiro, M. J.; German, A. L. Controlled radical copolymerization of styrene and maleic anhydride and the synthesis of novel polyolefin-based block copolymers by reversible addition–fragmentation chain-transfer (RAFT) polymerization. *J. Polym. Sci., Part A: Polym. Chem.* **2000**, 38 (19), 3596-3603.
(35) Chen, G.-Q.; Wu, Z.-Q.; Wu, J.-R.; Li, Z.-C.; Li, F.-M. Synthesis of Alternating Copolymers of N-Substituted Maleimides with Styrene via Atom Transfer Radical Polymerization. *Macromolecules* **1999**, 33 (2), 232-234.
(36) Lutz, J.-F.; Kirci, B.; Matyjaszewski, K. Synthesis of Well-Defined Alternating Copolymers by Controlled/Living Radical Polymerization in the Presence of Lewis Acids. *Macromolecules* **2003**, 36 (9), 3136-3145.
(37) Benoit, D.; Hawker, C. J.; Huang, E. E.; Lin, Z.; Russell, T. P. One-Step Formation of Functionalized Block Copolymers. *Macromolecules* **2000**, 33 (5), 1505-1507.
(38) Koulouri, E. G.; Kallitsis, J. K.; Hadziioannou, G. Terminal Anhydride Functionalized Polystyrene by Atom Transfer Radical Polymerization Used for the Compatibilization of Nylon 6/PS Blends. *Macromolecules* **1999**, 32 (19), 6242-6248.
(39) Harth, E.; Hawker, C. J.; Fan, W.; Waymouth, R. M. Chain End Functionalization in Nitroxide-Mediated "Living" Free Radical Polymerizations. *Macromolecules* **2001**, 34 (12), 3856-3862.
(40) Sasso, B.; Dobinson, M.; Hodge, P.; Wear, T. Synthesis of ω-End Group Functionalized Poly(methyl methacrylate)s via RAFT Polymerization. *Macromolecules* **2010**, 43 (18), 7453-7464.
(41) Pfeifer, S.; Lutz, J.-F. Development of a Library of N-Substituted Maleimides for the Local Functionalization of Linear Polymer Chains. *Chem. Eur. J.* **2008**, 14 (35), 10949-10957.
(42) Pfeifer, S.; Lutz, J.-F. A Facile Procedure for Controlling Monomer Sequence Distribution in Radical Chain Polymerizations. *J. Am. Chem. Soc.* **2007**, 129 (31), 9542-9543.
(43) Feng, X.-S.; Pan, C.-Y. Synthesis of Amphiphilic Miktoarm ABC Star Copolymers by RAFT Mechanism Using Maleic Anhydride as Linking Agent. *Macromolecules* **2002**, 35 (13), 4888-4893.
(44) Shi, G.-Y.; Tang, X.-Z.; Pan, C.-Y. Tadpole-shaped amphiphilic copolymers prepared via RAFT polymerization and click reaction. *J. Polym. Sci., Part A: Polym. Chem.* **2008**, 46 (7), 2390-2401.
(45) Henry, S. M.; Convertine, A. J.; Benoit, D. S. W.; Hoffman, A. S.; Stayton, P. S. End-Functionalized Polymers and Junction-Functionalized Diblock Copolymers Via RAFT Chain Extension with Maleimido Monomers. *Bioconjugate Chem.* **2009**, 20 (6), 1122-1128.
(46) Zhou, C.; Qian, S.; Zhang, A.; Xu, L.; Zhu, J.; Cheng, Z.; Kang, E.-T.; Yao, F.; Fu, G. D. A well-defined amphiphilic polymer co-network from precise control of the end-functional groups of linear RAFT polymers. *RSC Adv.* **2014**, 4 (16), 8144-8156.
(47) Xu, J.; Fu, C.; Shanmugam, S.; Hawker, C. J.; Moad, G.; Boyer, C. Synthesis of Discrete Oligomers by Sequential PET-RAFT Single-Unit Monomer Insertion. *Angew. Chem. Int. Ed.* **2017**, 56, 1-8.
(48) Zamfir, M.; Lutz, J.-F. Ultra-precise insertion of functional monomers in chain-growth polymerizations. *Nat. Commun.* **2012**, 3, 1138.

(49) Lutz, J.-F.; Schmidt, B. V. K. J.; Pfeifer, S. Tailored Polymer Microstructures Prepared by Atom Transfer Radical Copolymerization of Styrene and N-substituted Maleimides. *Macromol. Rapid Commun.* **2011**, 32 (2), 127-135.
(50) Jakubowski, W.; Min, K.; Matyjaszewski, K. Activators Regenerated by Electron Transfer for Atom Transfer Radical Polymerization of Styrene. *Macromolecules* **2006**, 39 (1), 39-45.
(51) Anastasaki, A.; Nikolaou, V.; Nurumbetov, G.; Wilson, P.; Kempe, K.; Quinn, J. F.; Davis, T. P.; Whittaker, M. R.; Haddleton, D. M. Cu(0)-Mediated Living Radical Polymerization: A Versatile Tool for Materials Synthesis. *Chem. Rev.* **2016**, 116 (3), 835-877.
(52) Lutz, J.-F. Writing on Polymer Chains. *Acc. Chem. Res.* **2013**, 46 (11), 2696-2705.
(53) Gody, G.; Zetterlund, P. B.; Perrier, S.; Harrisson, S. The limits of precision monomer placement in chain growth polymerization. *Nat. Commun.* **2016**, 7, 1-8.
(54) McLeary, J. B.; Calitz, F. M.; McKenzie, J. M.; Tonge, M. P.; Sanderson, R. D.; Klumperman, B. Beyond Inhibition: A ^{1}H NMR Investigation of the Early Kinetics of RAFT-Mediated Polymerization with the Same Initiating and Leaving Groups. *Macromolecules* **2004**, 37 (7), 2383-2394.
(55) van den Dungen, E. T. A.; Rinquest, J.; Pretorius, N. O.; McKenzie, J. M.; McLeary, J. B.; Sanderson, R. D.; Klumperman, B. Investigation into the Initialization Behaviour of RAFT-Mediated Styrene–Maleic Anhydride Copolymerizations. *Aust. J. Chem.* **2006**, 59 (10), 742-748.
(56) Lutz, J.-F. Aperiodic Copolymers. *ACS Macro Lett.* **2014**, 3 (10), 1020-1023.
(57) Rowan, S. J.; Barner-Kowollik, C.; Klumperman, B.; Gaspard, P.; Grubbs, R. B.; Hillmyer, M. A.; Hutchings, L. R.; Mahanthappa, M. K.; Moatsou, D.; O'Reilly, R. K.; Ouchi, M.; Sawamoto, M.; Lodge, T. P. Discussion on "Aperiodic Copolymers". *ACS Macro Lett.* **2016**, 5 (1), 1-3.
(58) Zhou, C.; Deng, L.; Yao, F.; Xu, L.; Zhou, J.; Fu, G. D. A Well-Defined Amphiphilic Polymer Conetwork from Sequence Control of the Cross-Linking in Polymer Chains. *Ind. Eng. Chem. Res.* **2014**, 53 (49), 19239-19248.
(59) Gody, G.; Maschmeyer, T.; Zetterlund, P. B.; Perrier, S. Pushing the Limit of the RAFT Process: Multiblock Copolymers by One-Pot Rapid Multiple Chain Extensions at Full Monomer Conversion. *Macromolecules* **2014**, 47 (10), 3451-3460.
(60) Gody, G.; Maschmeyer, T.; Zetterlund, P. B.; Perrier, S. Exploitation of the Degenerative Transfer Mechanism in RAFT Polymerization for Synthesis of Polymer of High Livingness at Full Monomer Conversion. *Macromolecules* **2014**, 47 (2), 639-649.
(61) Ladavière, C.; Lacroix-Desmazes, P.; Delolme, F. First Systematic MALDI/ESI Mass Spectrometry Comparison to Characterize Polystyrene Synthesized by Different Controlled Radical Polymerizations. *Macromolecules* **2009**, 42 (1), 70-84.
(62) Gruendling, T.; Hart-Smith, G.; Davis, T. P.; Stenzel, M. H.; Barner-Kowollik, C. Enhanced Ionization in Electrospray Ionization Mass Spectrometry of Labile End-Group-Containing Polystyrenes Using Silver(I) Tetrafluoroborate as Doping Salt. *Macromolecules* **2008**, 41 (6), 1966-1971.
(63) Ha, N. T. H. Determination of triad sequence distribution of copolymers of maleic anhydride and its derivates with donor monomers by ^{13}C n.m.r. spectroscopy. *Polymer* **1999**, 40 (4), 1081-1086.
(64) Barron, P. F.; Hill, D. J. T.; O'Donnell, J. H.; O'Sullivan, P. W. Applications of DEPT experiments to the carbon-13 NMR of copolymers: poly(styrene-co-maleic anhydride) and poly(styrene-co-acrylonitrile). *Macromolecules* **1984**, 17 (10), 1967-1972.
(65) Lai, J. T.; Filla, D.; Shea, R. Functional Polymers from Novel Carboxyl-Terminated Trithiocarbonates as Highly Efficient RAFT Agents. *Macromolecules* **2002**, 35 (18), 6754-6756.
(66) Brzytwa, A. J.; Johnson, J. Scaled Production of RAFT CTA–a STAR Performer. *Polym. Prepr. (Am. Chem. Soc., Div. Polym. Chem.)* **2011**, 52 (2), 533-534.

Chapter 4 Influence of Grafting Density and Distribution on Material Properties Using Well-Defined Alkyl Functional Poly(Styrene-*co*-Maleic Anhydride) Architectures Synthesised by RAFT

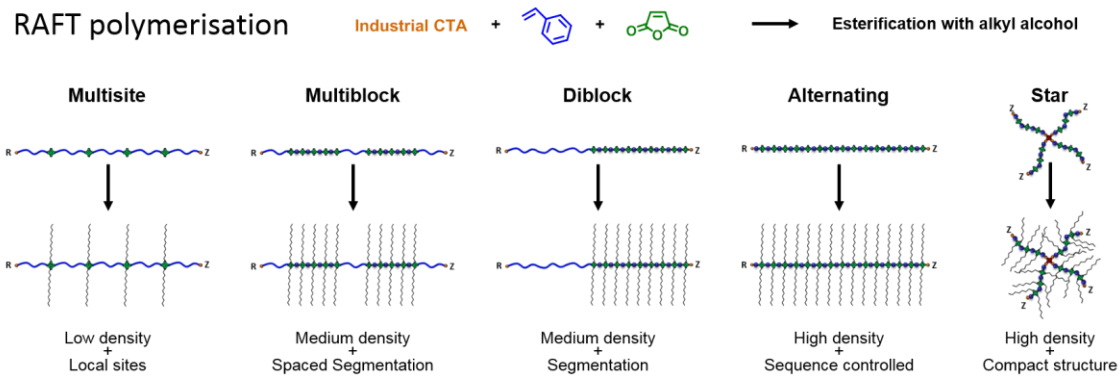

Influence of the molecular structure on the material behaviours in solution (R_g, R_h, α, IV) and thermal properties (TGA,DSC)

Abstract

Poly(styrene-*co*-maleic anhydride) copolymers (PSMA) with controlled number and distribution of maleic anhydride (MAnh) monomeric units were prepared by reversible addition-fragmentation chain transfer (RAFT) polymerisation. All polymers were synthesised with chain-transfer agents (CTA) suitable for an industrially scalable process (CTA-Ester and CTA-Acid). Linear and star architectures of alternating PSMA (alt-PSMA and 4xPSMA) were achieved in one-step synthesis, while a one-pot sequential chain-extension strategy was utilised to prepare diblock, multiblock and multisite copolymers. Furthermore, the MAnh units were subsequently functionalised with long alkyl alcohol chains (C22) to obtain graft-like copolymers. The features of the initial polymeric backbones, as well as the graft-copolymers, were characterised by a variety of analytical techniques. The polymer behaviour in solution was shown to be dependent on copolymer molar mass and grafting density. All the materials were shown to degrade close to 400 °C, varying slightly with MAnh content and molar mass. The rate of degradation was shown to be influenced by the MAnh content and polymeric architecture. A significant change of the T_g from 205 °C to 100 °C was observed for the alternating and multisite copolymers, respectively. Two T_g were observed for the diblock copolymer (99 °C and 168 °C), and only one T_g (120 °C) was observed for the multiblock, indicating differences in phase separation. Ultimately, the grafting of long aliphatic side chains (crystalline) onto the PSMA backbone, even at low density, was shown to drastically change the microphase ordering, as all the grafted copolymers became semi-crystalline. A difference of crystallisation temperature of about 30 °C was observed between low density material ($T_c \approx 7$ °C) and high density alternating material ($T_c \approx 40$ °C) illustrating the major impact of controlling the density and distribution of long aliphatic side chains on PSMA backbones.

4.1 Introduction

A significant challenge in modern macromolecular science is to mimic nature to achieve complex copolymers with controlled chemical composition and molecular structure.[1, 2] The rise of recent studies on advanced polymeric architectures, such as brushes, star polymers, cyclic polymers and other functional copolymers with controlled grafting density and distribution, suggests an increasing interest in this field.[3-9] Graft copolymers can adopt different conformations (such as coil, rodlike or wormlike) determined by their chemical composition, architecture, and their interaction with the solvent.[10-12] Moreover, the control over grafting density and distribution has also been found to be of fundamental importance when preparing tailored nanoscopic objects with interesting mechanical and physicochemical properties (*e.g.* self-assembling or stimuli-responsive materials).[13-16] Functional copolymers can also offer different properties depending on their grafting density and distribution of functional groups.[17, 18] The control of monomer sequence/distribution itself has been observed to be of interest to control some physical properties of copolymers such as solubility, amphiphilicity, assembly and thermal properties.[19, 20] Recently, the effect of block segregation (multiblock structure) on microphase separation and glass transition temperature (T_g) was demonstrated.[21] Another study on thermo-responsive, spontaneous gradient copolymers showed the effect of monomer sequence and distribution on glass transition and self-assembly behaviour.[22] These examples of non-grafted copolymers show the importance of controlling monomer distribution to tune the physicochemical properties of copolymers. As discussed in previous chapters, the radical copolymerisation of Sty and MAnh is a unique combination that offers functional materials of high sequence control with high density and distribution of the grafted functionalities.[23-25] Alternating poly(Sty-*alt*-MAnh) (PSMA) materials have been synthesised on an industrial scale by free radical polymerisation since the 1940s, and their derivatives are commonly used in applications such as rheology modifiers, plasticisers, polymeric surfactants and pigment dispersants.[26] Their advantageous mechanical and thermal properties, high chemical resistance and high degree of functionality are regularly described in scientific and technical reviews.[27-29] Moreover, with the recent developments in controlled radical polymerisation techniques (CRP) such as metal-mediated radical polymerisation (ATRP, SET-LRP, and metal catalysed),[30-32] nitroxide-mediated polymerisation (NMP),[33] and reversible addition-

fragmentation chain transfer (RAFT),[34] the exceptional features of this donor-acceptor system have been re-investigated to achieve well-defined alternating copolymers (controlled M_n, narrow dispersity),[35-37] polymer end-chain functionalisation[38] and single monomer unit insertion.[39-44] PSMA materials with various composition and controlled structure were also synthesised by exploiting the versatility of RAFT polymerisation.[45-48]

In the previous chapter, we showed the facile and scalable RAFT synthesis of a PSMA multisite copolymer with MAnh units inserted at specific locations along a polystyrene backbone.[39] The ability to synthesise functional materials with high degree of control on functional group distribution was demonstrated. In a recent study, Srichan *et al.* demonstrated the influence of monomer composition and sequence distribution of octadecyl styrene-*co*-N-substituted maleimide copolymers on the melting and crystallisation temperatures of semicrystalline materials, however, this is yet to be investigated for more advanced architectures.[17]

In this chapter, we exploited optimised RAFT polymerisation and the one-pot sequential chain-extension strategy for the preparation of a library of complex PSMA architectures (alternating, diblock, multiblock, multisite, and alternating star) (Scheme 4.1). The PSMA materials were subsequently functionalised with long aliphatic alcohols, leading to graft-like copolymers of controlled side-group density and distribution. The grafting density and distribution were evaluated, and their effects on the physical and thermal properties were studied.

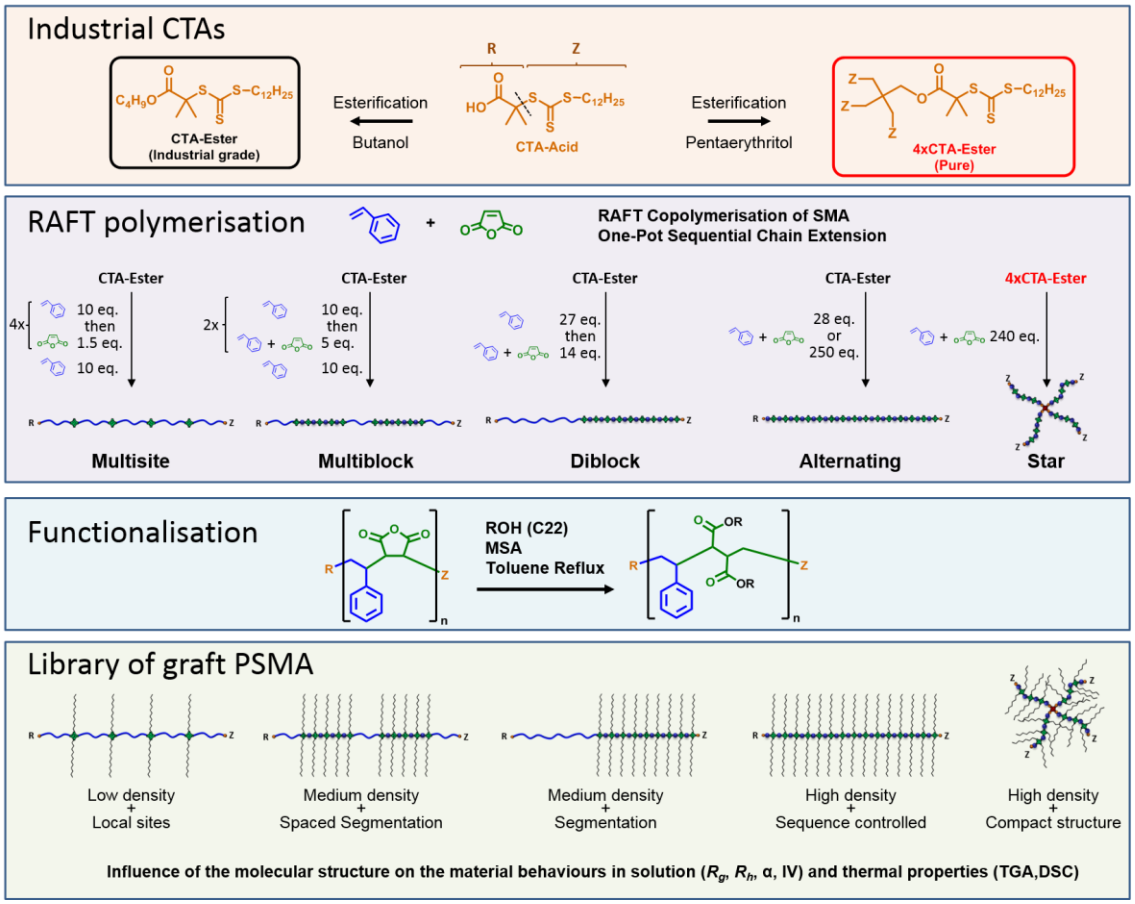

Scheme 4.1. Synthesis of well-defined grafted PSMA copolymers using optimised RAFT polymerisation with industrial CTAs and post-polymerisation esterification of MAnh units.

4.2 Results and Discussion

In this chapter we present the synthesis of a library of PSMA materials for the preparation of well-defined graft architectures, and the study of the influence of grafting density and distribution on material properties (Scheme 4.1). The PSMA backbones were synthesised by optimised RAFT polymerisation adapted from previous chapter and using industrial RAFT agents, anticipating industrial production.[49-51] The linear copolymers were synthesised using technical grade CTA-Ester without purification (80 % pure). Being able to obtain well-defined polymeric architectures using non-pure RAFT agents is essential for large scale development of the RAFT process and was shown in only a few recent studies.[39, 50] A tetrafunctional CTA-Ester (4xCTA) was also prepared from CTA-Acid (CTA-Ester precursor) giving access to a four arm PSMA star copolymer. The 4xCTA was synthesised by esterification of CTA-Acid and pentaerythritol in the presence of an acid catalyst (methane sulfonic acid), a process commonly used in industry (Dean-Stark) (Scheme 4.2). The synthesis of the 4xCTA was not optimised and approximately 1 gram of pure CTA was obtained after purification by column chromatography. The transformation of CTA-Acid into 4xCTA was confirmed by ^{1}H and ^{13}C-NMR spectroscopy (Figure A4-1 -Figure A4-2), and MALDI-ToF-MS (Figure A4-3).

Four linear PSMA copolymers with comparable molar mass (5,000-6,000 g mol^{-1}) but different monomer unit distributions were synthesised to study the influence of molecular structure on material properties, such as conformation in solution and thermal behaviour (Table 4.1).

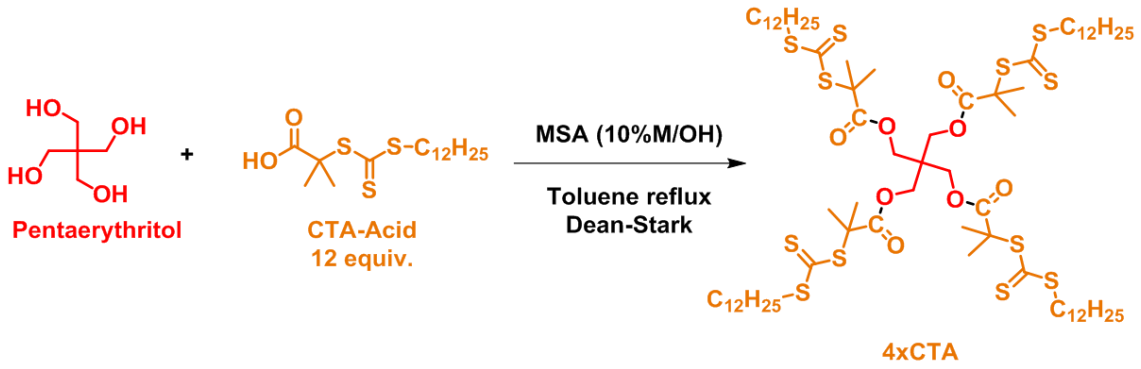

Scheme 4.2. Synthesis of the 4xCTA by Dean-Stark esterification.

Table 4.1. PSMA backbone features

Materials		$M_{n,theo}$[a] g mol^{-1}	$M_{n,RI}$[b] g mol^{-1}	$M_{n,3d\text{-}SEC}$[c] g mol^{-1}	$Đ_{RI}$[b]	MAnh [d]
P[SMA]$_{28}$	Alt-Linear	5,600	8,100 [f]	6,200 [f]	1.13 [f]	23
P[Sty$_{27}$-*b*-(SMA)$_{14}$]	Diblock	5,600	5,300 [f]	6,400 [e]	1.22 [f]	13
P[Sty$_{10}$-*b*-(SMA)$_5$]$_2$-*b*-PSty$_{10}$	Multiblock	5,100	4,100 [e]	5,100 [e]	1.20 [e]	10
P[(Sty$_{10}$-*s*-MAnh$_{1.5}$)$_4$-*b*-PSty$_{10}$]	Multisite	5,900	5,200 [e]	6,400 [e]	1.29 [e]	5
P[SMA]$_{250}$	Alt-Linear	50,600	54,500 [f]	48,200 [f]	1.19 [f]	225
4xP[SMA]$_{60}$	Alt-Star	47,600	47,200 [f]	44,900 [f]	1.15 [f]	200

[a] Calculated by ^{1}H-NMR using equation 2.5 and 2.6. [b] Obtained using conventional SEC with RI detector. [c] Obtained using triple-detection SEC. [d] Number of MAnh units calculated from ^{13}C-NMR using peak at 172 ppm. [e] SEC in Chloroform. [f] SEC in DMF

The maleic anhydride content (density) in each material (total DP = 50 - 56) was varied from 28 units for the alternating (highest density of side chains) to 6 units for the multisite copolymer (lowest density). Furthermore, the monomer distribution was tuned from perfectly alternating to a multiblock-like structure, varying the segmentation between the copolymers. A linear alternating PSMA (alt-PSMA-50k) with higher molar mass (DP = 250 - 50,000 g mol^{-1}), and its star analogue (4xPSMA – DP = 60 per arm- 50,000 g mol^{-1}), were also synthesised to compare the effects of the molar mass and architecture.

4.2.1 Synthesis of alternating PSMA materials

The synthesis of alternating PSMA by RAFT is relatively easy to accomplish and was achieved following a method adapted from previous studies.[35, 52] These experiments were performed at 60 °C using an equimolar feed ratio of Sty and MAnh monomers in the presence of either the industrial grade CTA-Ester or pure 4xCTA, while a minimum concentration of initiator (V601 - $T_{1/2\text{-}10h}$ = 66 °C) was added to obtain well-defined alternating PSMA materials within 24 hours (conv. > 90 %) (Table A4-1 and Table A4-2). Due to the nature of 4xCTA, linked to the core *via* the R group (Scheme 4.1), the RAFT polymerisation occurred *via* core-first strategy and using R group approach.[6, 53] This strategy allows the synthesis of star copolymers with a defined number of arms, growing from the core, however, it is also important to note that this strategy will produce linear species away from the core due to the initiator derived chains and the fragmentation of the Z group. The star copolymer was synthesised according to previous protocols, where

a minimum amount of initiator is added to limit these undesired events.[54] To our knowledge, this is the first reported example of a 4xPSMA star prepared by RAFT. The formation of well-defined alternating PSMA copolymers was confirmed by ^{1}H-NMR spectroscopy (Figure A4-4 - Figure A4-6), size exclusion chromatography (Figure A4-7), and MALDI-ToF-MS (Figure A4-8), all showing good agreement between theoretical and experimental molar mass values and narrow molar mass distribution (Table 4.1). The alternating nature of the copolymers was confirmed using ^{13}C-NMR spectroscopy. Briefly, the local neighbouring repeating unit (triad) can be categorically determined by following the relative chemical shift (δ_c) of the quaternary aromatic carbon (C_{arom}) of Sty residue at δ_c =135-150 ppm (Figure 4.1). It is known that an alternating sequence (M**S**M) shows a main peak at δ_c =135-141.5 ppm while for the random (S**S**M) and homopolystyrene (S**S**S), peaks between δ_c = 141.5-144.5 ppm and δ_c =144.5-148 ppm are observed, respectively.[55, 56] All alternating materials exhibited a main peak between δ_c =135-145 ppm confirming the main alternating nature of their monomer sequences (Figure 4.1 – D-F). The minor peaks in the random region were attributed to marginal Sty-Sty defects in the microstructures.

4.2.2 Synthesis of diblock PSty-*b*-PSMA

The synthesis of block copolymers of PSMA by RAFT in a one-step process (excess of styrene in monomer feed), was previously described in literature.[47, 48] Although this method seems quick and efficient to produce PSMA-*b*-PSty diblocks on a large scale, the excess of Sty in the monomer feed increases the probability of defects (Sty-Sty) in the monomer sequence of the PSMA block. Herein, the diblock was synthesised starting with a PSty block of DP = 27 and subsequent chain extension (one-pot) using an equimolar feed of Sty and MAnh to achieve an alternating PSMA block of DP = 14 (Table A4-3 - Table A4-4). While the first block (PSty macroCTA) was synthesised at 100 °C following a procedure optimised in previous chapters, the extension with SMA block was achieved following the conditions used above for alt-PSMA materials (60 °C using V601). Importantly, the complete consumption of the first initiator (V-40) during the first block synthesis allowed chain extension based on a different initiator system (V601) without taking into account the amount of previous initiator left. The synthesis of a well-defined diblock PSty$_{27}$-*b*-PSMA$_{14}$ with similar molar mass to the alternating material and narrow dispersity was confirmed by ^{1}H-NMR, SEC, and MALDI-ToF-MS (Table 4.1 – Figure

A4-9-Figure A4-11). Furthermore, the existence of two distinct peaks in the ^{13}C-NMR spectrum (Figure 4.1 - C) confirmed the presence of blocks with different nature (SSS *vs.* MSM) in the copolymer.

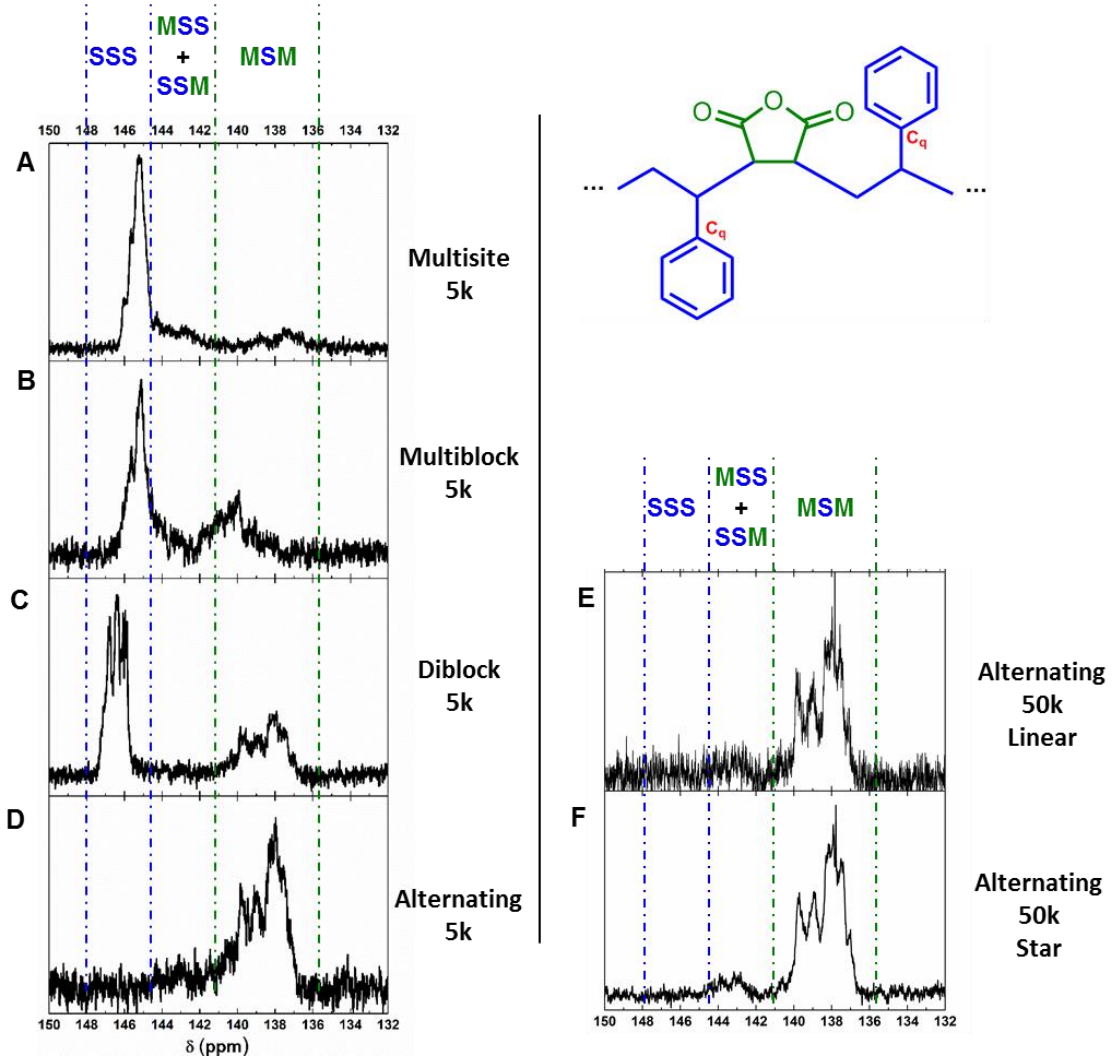

Figure 4.1. ^{13}C-NMR spectra showing quaternary carbon of styrene (C_q) for materials with different composition (S for styrene and M for maleic anhydride).

4.2.3 Synthesis of multiblock (PSty-*b*-PSMA)$_2$-*b*-PSty

A multiblock PSMA copolymer was designed to obtain two short blocks of alt-PSMA (DP = 5) in PSty backbone (every 10 units). In contrast to the diblock synthesis, a single initiator system (V-40) was used and the concentration of residual initiator after each step was taken into consideration. The PSty blocks were synthesised at 100 °C, however, a lower polymerisation temperature of 70 °C was applied for the PSMA block (Table A4-5). These conditions ensured a high propagation rate for the SMA comonomers, while limiting the homopolymerisation of styrene monomers (Sty-Sty defects). Following this method, a high conversion (conv. > 82 %) for each block was achieved (Table A4-6 - Figure A4-12), and the final material was obtained with a theoretical molar mass comparable to previous materials, and relatively good control over molar mass distribution (Table 4.1 – Figure A4-13). Similarly to the diblock copolymer, the presence of two distinct peaks in the ^{13}C-NMR spectrum confirmed the presence of blocks with different nature (SSS *vs.* MSM) (Figure 4.1 - B).

4.2.4 Synthesis of multisite (PSty-*s*-MAnh)$_4$-PSty

The synthesis and characterisation of the multisite PSMA are detailed in the previous chapter.[39] This original architecture was prepared in order to obtain a well-defined graft copolymer with low density and specific anchoring location of the side chains. The synthesis of the multisite copolymer was designed accordingly in order to distribute at least one MAnh unit (1.5 eq. used) on every 10 units of Sty, on average. The final copolymer was composed of 5 PSty blocks of DP = 10 each connected with 6 MAnh units on average, as 1.5 eq. of MAnh was added for each single monomer unit insertion (SMUI) step. The final multisite copolymer exhibited relatively narrow dispersity and molar mass comparable to previous materials (Table 4.1). The ^{13}C-NMR spectrum showed a major peak corresponding to homopolystyrene (144-148 ppm) and minor peaks corresponding to random and alternating sequences (Figure 4.1 – A). This was in good agreement with the expected structure as few MAnh units were dispersed locally in the PSty backbone, either as single monomer units (random triad) or, as short alternating blocks (alternating and random triads).

4.2.5 Synthesis of graft PSMA copolymers

All PSMA materials were functionalised by reacting the MAnh units with behenyl alcohol (C22) yielding graft-PSMA analogues (Scheme 4.1). Long alkyl chains were selected as functional side groups enabling graft-PSMA materials for use as potential rheology modifiers in the oil industry.[57-59] The full esterification of MAnh moieties was achieved in the presence of methane sulfonic acid (catalyst) under reflux of toluene in a Dean-Stark apparatus following a similar process used for 4xCTA preparation (Scheme 4.2). The esterification yield, average number of alkyl chains grafted, and molar mass of the final materials were determined by IR, quantitative ^{1}H and ^{13}C-NMR spectroscopy and triple-detection SEC (3d-SEC) (details in appendix). The IR spectrum showed a complete disappearance of the MAnh ester symmetric stretch at 1,850 cm^{-1} and the shift of the asymmetric ester peak from 1,770 cm^{-1} to 1,730 cm^{-1} (Figure A4-14 - Figure A 4-19). Additionally, the introduction of long alkyl chains greatly increased the intensity of the alkane C-H stretch peaks at 2,700-3,000 cm^{-1}. The number of alkyl chains grafted onto each backbone was determined from the ^{13}C NMR spectrum using the C_{arom} of Sty as the reference peak (δ_c = 126 ppm) and the peak from the methylene group adjacent to an ester linkage (64.5 ppm) (Figure A4-20 - Figure A4-31). Interestingly, the final number of alkyl chains grafted (N_{graft}) was consistent with the theoretical average number of MAnh inserted in the backbone, confirming the original backbone composition (Table 4.2).

Table 4.2. Evolution of PSMA features after grafting

	PSMA Backbones			Graft PSMAs				
Materials	$M_{n,3d\text{-}SEC}$[a] g mol^{-1}	$Đ_{RI}$[b]	MAnh[c]	N_{graft}[d]	% Yield[e]	$M_{n,calc}$[f] g mol^{-1}	$M_{n,3d\text{-}SEC}$[a] g mol^{-1}	$Đ_{RI}$[b]
Alt-Linear	6,200 [h]	1.13 [h]	23	40	87	18,700	21,900 [g]	1.16 [g]
Diblock	6,400 [g]	1.22 [h]	13	25	96	13,800	14,700 [g]	1.12 [g]
Multiblock	5,100 [g]	1.20 [g]	10	19	95	11,200	11,100 [g]	1.17 [g]
Multisite	6,400 [g]	1.29 [g]	5	10	99	9,200	9,300 [g]	1.20 [g]
Alt-Linear	48,200 [h]	1.19 [h]	225	394	87	179,800	174,200 [g]	1.26 [g]
Alt-Star	44,900 [h]	1.15 [h]	200	396	99	177,100	180,200 [g]	1.21 [g]

[a] Obtained using triple-detection SEC. [b] Obtained using conventional SEC with RI detector. [c] Number of MAnh units calculated from ^{13}C-NMR using peak at 172 ppm. [d] Calculated from ^{13}C-NMR using peak at 64.5 ppm. [e] Functionalisation yield calculated by comparing the number of alkyl chains grafted with number of MAnh units inserted. [f] Calculated from ^{13}C-NMR using $M_{n,theo}$ backbone + N_{graft} x $M_{w,Alkyl}$. [g] SEC in Chloroform. [h] SEC in DMF

The yield of esterification was calculated by comparing the number of alkyl chains grafted to the number of maleic anhydride units in each chain, determined previously. High yield of esterification (> 87 %) was confirmed for all materials. The alt-PSMA showed a slightly lower esterification yield as a result of limitations imposed by steric hindrance due to the higher MAnh density in the backbone. For this reason, the esterification of the alternating 4xPSMA star polymer was left to react longer (38 hours *vs.* 20 hours), which resulted in a higher esterification yield. These results indicate that the higher the MAnh density, the longer the reaction time needed to complete the esterification. Both materials with higher molar mass (linear and star 50k) showed comparable molar mass after grafting (≈ 180,000 g mol^{-1}). For all materials, a shift of the initial molar mass distribution towards higher molar mass and retention of narrow dispersity were observed after functionalisation (Table 4.2 – Figure A4-32 - Figure A4-37). The true molar mass values obtained by triple-detection were shown to be in good agreement with the calculated molar masses, confirming the complete esterification of the PSMA backbones, and the synthesis of functional materials with excellent control of side chain incorporation.

4.2.6 Comparison of PSMA materials features and properties

The synthesis of well-defined PSMA materials as well as their functionalisation with long alkyl chains was demonstrated. The different graft architectures (linear alternating, diblock, multiblock, and multisite) were prepared from PSMA backbones with comparable molar masses, as shown by triple-detection SEC and MALDI-ToF-MS (Figure 4.2).

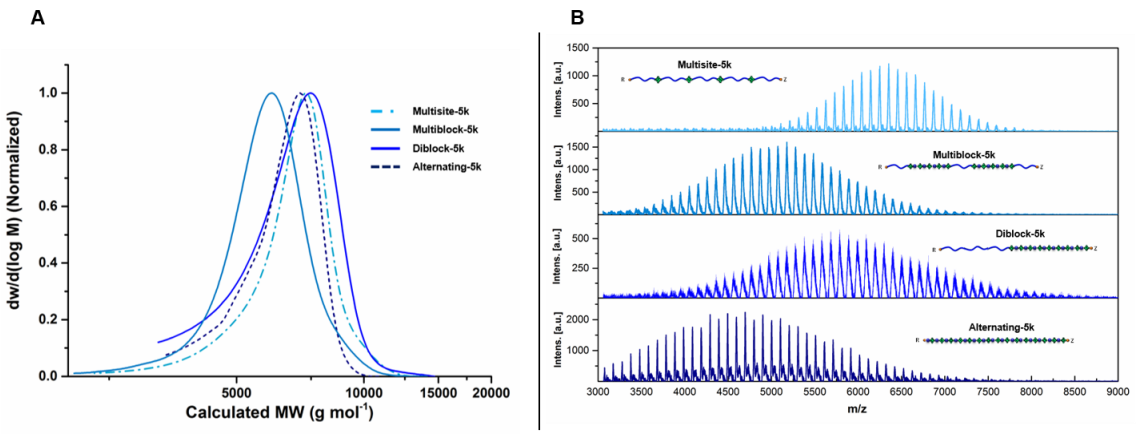

Figure 4.2. Comparison of molar mass distribution for short PSMA backbone measured by triple-detection SEC (A) and MALDI-ToF-MS (B).

While conventional SEC (DRI detection) provides rapid information on molar mass distribution and allows good comparison of polymers of similar nature, limited information can be obtained compared to more advanced detection methods. Here, triple-detection SEC (DRI, VS, and LS) was used to determine the true molar mass ($M_{n,3d\text{-}SEC}$) and gain complementary information, such as the radius of gyration (R_g) and hydrodynamic radius (R_h) (molecular size parameters), and the intrinsic viscosity (IV) and Mark-Houwink parameter (α).

4.2.7 Study of materials' behaviour in solution by 3d-SEC

The direct comparison of the materials' behaviour in solution was limited by their solubility as they were not all soluble in the same solvent. The alt-PSMAs with high content of MAnh exhibited poor solubility in $CHCl_3$ and therefore were analysed in DMF. On the other hand, all grafted materials showed good solubility in $CHCl_3$. All the non-grafted linear polymers (*ca.* 6,000 g mol^{-1}) had similar R_g (1.9-2.2 nm) and R_h (1.8-1.9 nm) parameters indicating that the MAnh density and distribution have a negligible effect on their molecular size and conformation (Table 4.3). Moreover, all polymers adopted random coil conformations in their respective solvents according to the Mark-Houwink parameter values (α > 0.5).[60, 61] No significant differences were observed with respect to intrinsic viscosity, which is expected for copolymers of similar molar mass, density and conformation.

Table 4.3. Features of materials in solution

	PSMA Backbones					Grafted PSMA				
	$M_{n,3d\text{-}SEC}$ [a] g mol^{-1}	R_g [a] (nm)	R_h [a] (nm)	IV [a] (dl/g)	α [a]	$M_{n,3d\text{-}SEC}$ [a] g mol^{-1}	R_g [a] (nm)	R_h [a] (nm)	IV [a] (dl/g)	α [a]
Alt-Linear	6,200 [c]	2.21 [c]	1.94 [c]	0.074 [c]	0.56 [c]	21,900 [b]	2.91 [b]	2.89 [b]	0.069 [b]	0.71 [b]
Diblock	6,400 [b]	1.88 [b]	1.87 [b]	0.065 [b]	0.88 [b]	14,700 [b]	2.74 [b]	2.61 [b]	0.077 [b]	0.73 [b]
Multiblock	5,100 [b]	1.94 [b]	1.79 [b]	0.072 [b]	0.86 [b]	11,100 [b]	2.53 [b]	2.42 [b]	0.080 [b]	0.83 [b]
Multisite	6,400 [b]	2.04 [b]	1.90 [b]	0.068 [b]	0.73 [b]	9,300 [b]	2.57 [b]	2.30 [b]	0.081 [b]	0.72 [b]
Alt-Linear	48,200 [c]	7.92 [c]	6.51 [c]	0.356 [c]	0.28 [c]	174,200 [b]	8.39 [b]	8.82 [b]	0.248 [b]	0.59 [b]
Alt-Star	44,900 [c]	7.01 [c]	5.77 [c]	0.270 [c]	0.30 [c]	180,200 [b]	8.79 [b]	8.26 [b]	0.196 [b]	0.69 [b]

[a] Obtained from triple-detection SEC (RI, Viscometer, LS) using *d*n/*d*c values measured off-line. [b] SEC in Chloroform. [c] SEC in DMF.

As expected, an increase in molecular size was observed for longer copolymers (50,000 g mol^{-1}). The 4xPSMA was smaller in molecular size compared to the linear alt-PSMA, which is attributed to its slightly lower molar mass. Moreover, it is usually observed that star polymers adopt a more compact structural conformation compared to their linear counterparts of similar molar mass.[60, 61] Herein, both alt-PSMA and 4xPSMA appeared to adopt similar hard sphere conformation in DMF ($\alpha < 0.5$), however, a difference of intrinsic viscosity was observed (0.356 dl/g for linear *vs.* 0.270 dl/g for star). This was not surprising as more compact architectures (star, comb or branched) have less impact on viscosity.[60, 61]

After functionalisation, the molecular size was found to correlate with the grafting density and the backbone length. For the materials allowing the comparison before and after functionalisation (where analysis in the same solvent was possible), slightly lower, or similar, α values were observed after grafting, due to a more compact structure. Overall, the side chain density and distribution did not impact the structures in solution as all the polymers displayed similar α values ($\alpha \approx 0.7$-0.8), corresponding to random coil conformation. For diblock, multiblock and multisite materials, an increase of IV was observed after grafting which was expected due to the increase in molecular size. A correlation between grafting density and a decrease of IV was observed, regardless of the increase of molar mass (from 9,300 g mol^{-1} for grafted multisite to 21,900 g mol^{-1} for the alternating counterpart). This indicated that the grafting density of side chains had more impact on structure density than the molar mass. The longer graft alt-PSMA and 4xPSMA copolymers showed similar molecular size and appeared to adopt a random coil conformation while being slightly more compact compared to the short backbone materials ($\alpha \approx 0.6$-0.7). Moreover, they showed a drastic increase in IV (from 0.069 to 0.248 dl/g), expected due to the difference of molar mass. The lower IV observed for the star material was expected as the increase of molecular size with respect to molar mass is slower for star materials compared to their linear counterparts. [60, 61]

4.2.8 Influence of material structure on thermal properties

TGA

The thermal stability of all PSMA materials was evaluated by thermogravimetric analysis (TGA) under N_2 gas flow in the temperature range 25-650 °C, at a heating rate of 10 °C/min. The evolution of the mass loss with temperature and the corresponding differential thermogravimetric curves (dTG) for all materials are shown in Figure 4.3 (details in appendix). Three distinct degradation steps were observed, where temperature of degradation and rate of degradation depend on the material's chemical composition and structure (*i.e*. MAnh density, *M*w, functionalisation degree). The first step (100-200 °C), predominantly observed for the copolymers with high content of MAnh (*i.e*. alt-PSMA) is due to the release of CO_2 from the decomposition of MAnh.[62, 63] The second step was attributed to the thermal degradation of the trithiocarbonate (-CS_3-) end group of CTA which usually occurs from 200-300 °C for PSty synthesised by RAFT.[64, 65] The third degradation step from 325-450 °C was observed for all the materials and is attributed to the degradation of the polymer backbone and aliphatic chains. Control analysis performed on CTA-Ester and aliphatic chains (Figure A4-38) confirmed a first mass loss for CTA-Ester from 200-270 °C (-CS_3- degradation), followed by a second degradation step from 270-350 °C (CTA alkyl chain degradation), which overlaps with the aliphatic chain degradation from 250-350 °C.

The PSMA backbones (Figure 4.3 - A and C) exhibited a maximum rate of degradation temperature (T_i) from 390-410 °C (Table A4-7). While an intermediate T_i was observed for the 4xPSMA (400 °C), the T_i for linear-PSMA and the multiblock materials were observed at a temperature 20 °C lower compared to the multisite and diblock. Moreover, a correlation between MAnh content and a decrease of the onset of degradation and the rate of degradation (dTG) was observed. This confirmed the influence of material composition, monomer distribution and type of architecture on thermal stability of PSMA materials. By comparing the two linear PSMAs (5k and 50k g mol^{-1}), similar T_i and rates of degradation were observed, indicating no significant effect of the molar mass. Interestingly, the 4xPSMA was slightly more stable (onset ≈ 340 °C *vs.* 320 °C) and exhibited slower kinetics of degradation in contrast to its linear analogue, potentially due to the increase of intermolecular interactions (cross-linking). These observations clearly showed a correlation between the macromolecular structure and thermal stability of the

polymers.

After grafting with the alkyl chains (Figure 4.3 - B and D), all the linear PSMAs degrade with very similar profiles at higher temperature and with higher rates of degradation. No major differences were observed, indicating no influence of the grafting density and distribution on thermal stability of the linear alkyl functionalised PSMA materials. The star material showed similar slower degradation kinetics after grafting, confirming the influence of the architecture (Figure 4.3 - B). Regarding the total mass loss, it was interesting to notice that all the grafted materials were fully degraded before the temperature reached 500 °C, whereas PSMA backbones produced some residues, which appears to correlate with their MAnh content (Figure 4.3 – C D). The carbonisation of PSMA has been reported before and is due to the transformation of cyclic and heterocyclic compounds to pyrolytic carbons at temperatures above 500 °C.[66] The higher amount of residues obtained for the 4xPSMA is due to the higher compactness, facilitating intermolecular interactions and carbonisation process.

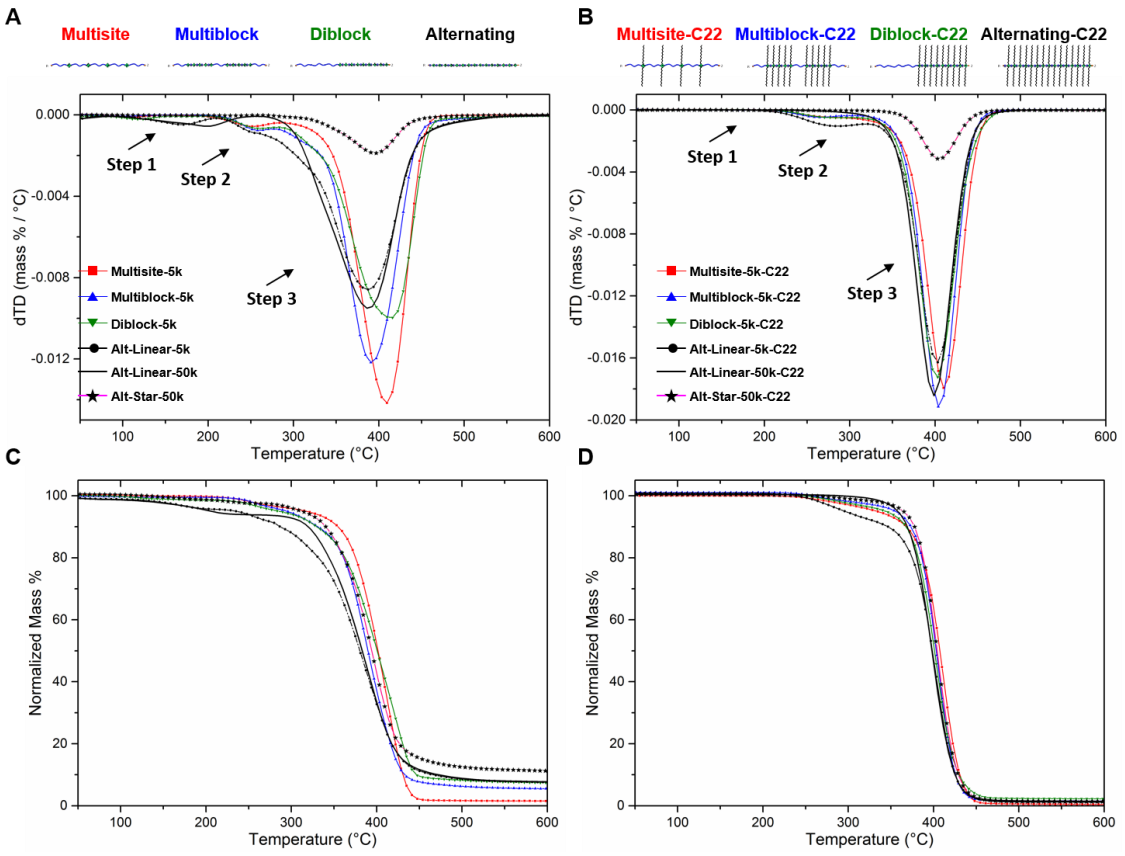

Figure 4.3. Derivative of mass loss (top) and mass loss (bottom) for PSMA materials before (left) and after (right) functionalisation measured by TGA.

DSC

Differential scanning calorimetry (DSC) was used to investigate the influence of monomer distribution and the effect of addition of crystalline side chains on a material's glass transition and/or crystallisation and melting behaviours. Experimentally, three heating and cooling cycles were performed and the values obtained at the second or third cycle were considered for comparison (Table A4-8 - Figure A4-45-Figure A4-50). This is important as the first heating cycle contains the polymer's prior thermal history and might be influenced by the release of CO_2 from the first degradation step observed for PSMA materials at low temperature (as shown by TGA analysis).

Previous studies of the thermal properties of alternating PSMA reported amorphous behaviours, with T_g values from 150 °C-202 °C depending on molar mass.[46, 47, 67] Interestingly, the alternating PSMAs synthesised in this study covered a range of molar masses between 5,000 g mol^{-1} and 50,000 g mol^{-1} and all showed similar glass transition temperatures above 200 °C (Figure 4.4). The variation of T_g values reported from one study to another is potentially due to degradation occurring in the first heating cycle modifying the copolymer composition and, therefore, the T_g values measured.

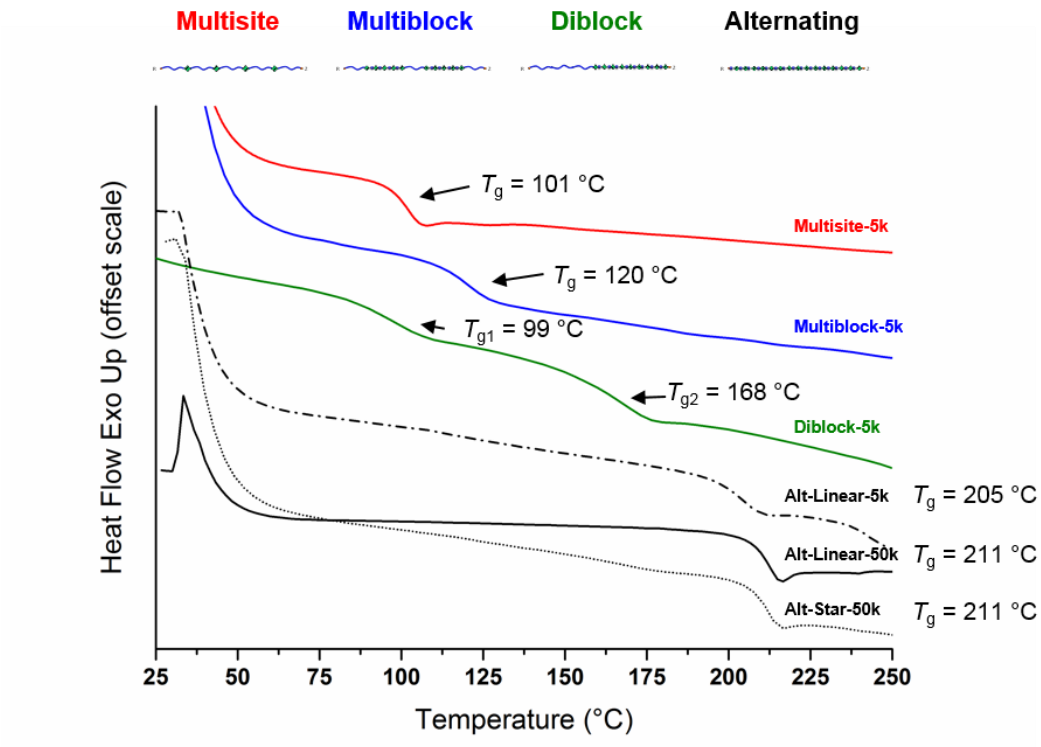

Figure 4.4. DSC heat flow graphs showing the third heating cycles for all PSMA backbones.

Previous studies on diblock and triblock (PSMA-*b*-PSty or PSMA-*b*-PSty-*b*-PSMA) showed one or two glass transition temperatures, depending on the fraction of each block.[68] For copolymers with a short PSMA block compared to PSty block, only one T_g corresponding to polystyrene was observed (100 °C) and the PSMA block was assumed miscible with PSty block.[69] Conversely, when the fraction of each block was similar, a new glass transition temperature close to pure PSMA was observed (150-200 °C).[47, 48]

In the present study, the diblock copolymer was composed of two blocks of similar length and exhibited two T_g (99 °C and 168 °C) close to the expected values for each block, showing the phase separation of these blocks. Interestingly, the T_g of the PSMA segment was lower compared to pure alternating PSMAs (168 °C *vs.* 205-211 °C), showing an influence of the PSty segment on PSMA segment mobility. The multiblock and multisite copolymers exhibited only one T_g (120 °C and 101 °C, respectively), with the latter showing a T_g very similar to polystyrene (102 °C). The multiblock showed only one T_g indicating that the SMA blocks (DP = 5) were not long enough to provide phase separation. However, the presence of short miscible PSMA segments was shown to have an influence on the T_g, as a higher T_g was observed compared to pure PSty (120 °C *vs.* 100 °C). The value obtained experimentally was in good agreement with the value calculated using the Fox equation (equation 4.1) predicting a T_g of 115 °C for a copolymer containing 75% of PSty (T_g = 100 °C) and 25% of PSMA (T_g 205 °C) in its composition.[70]

Interestingly, the comparison of all PSMA microstructures presented in this study showed a correlation between increasing MAnh content and glass transition temperatures (Figure 4.4).

The grafted materials revealed completely different behaviours as all the materials became semicrystalline, regardless of the density of alkyl side chains (Figure 4.5). All the alternating materials exhibited similar melting and crystallisation temperatures, showing no impact of molar mass or architecture (linear *vs.* star) on the thermal behaviour, which appeared to be driven by the presence of long alkyl chains only. The crystalline behaviour of copolymers with long paraffin-like side chains has already been discussed in literature.[71, 72] Moreover, the influence of copolymer microstructure on melting point was recently observed in a study on comb copolymers with long alkyl side chains.[17] The reported melting (T_m = 40-45 °C) and crystallisation (T_c = 30-35 °C) temperatures were slightly lower compared to those observed in the present study for grafted alt-PSMA (T_m

≈ 53 °C and T_c ≈ 40 °C). As observed previously, a lower melting temperature and a tailing were observed during the second heating cycle (Figure A4-45-Figure A4-50). This is due to the slow reorganisation of the crystalline phase which has not been completed by the end of the first cooling cycle.

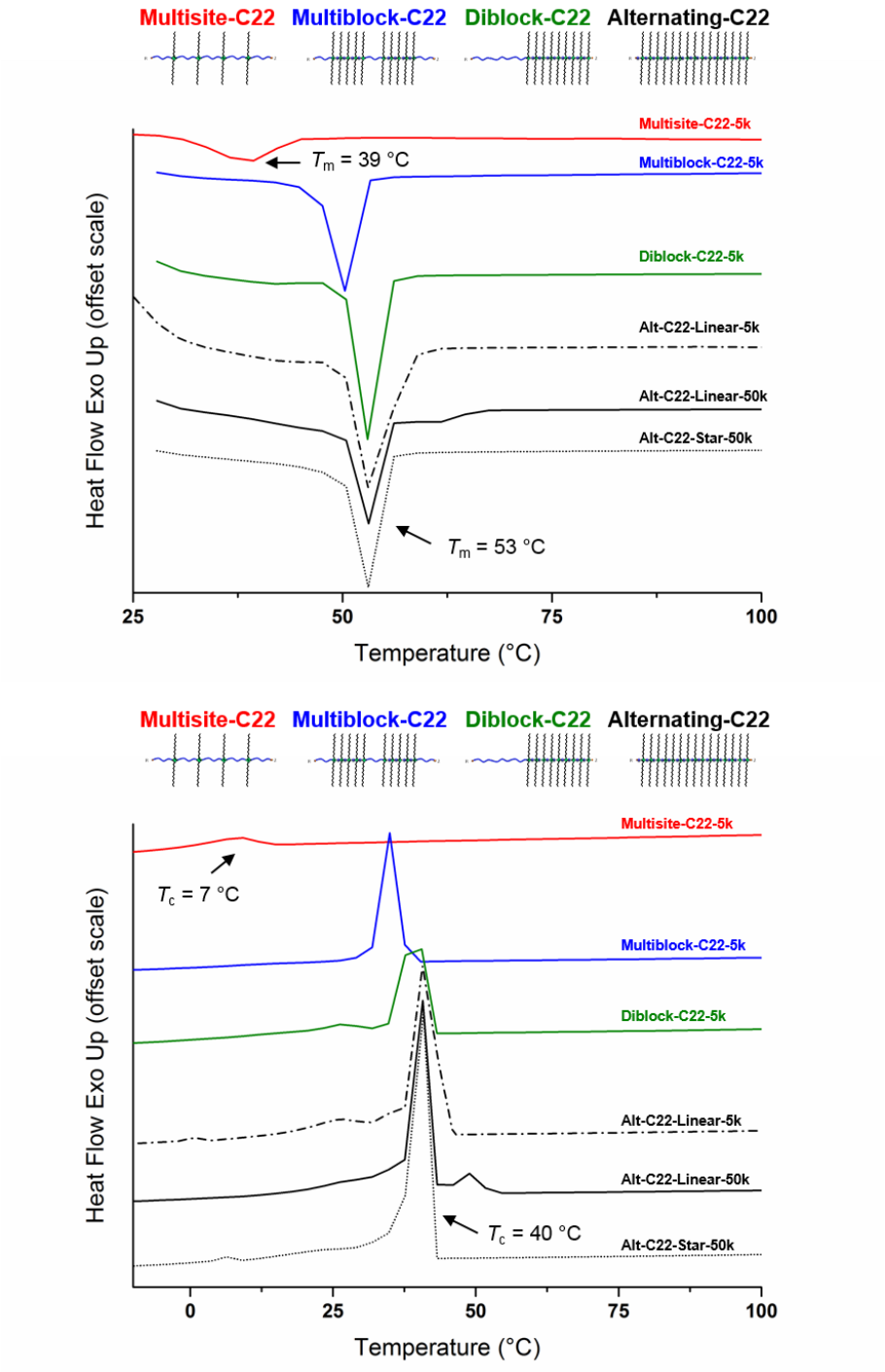

Figure 4.5. DSC heat flow graphs showing the second heating (top) and cooling (bottom) cycles for all functional materials.

While alt-PSMAs (high density of crystalline side chains) and diblock showed a sharp peak at similar melting temperature, broader peaks and lower melting temperatures were observed for multiblock and multisite materials, showing the poor reorganisation of these materials (Figure 4.5). Interestingly, all functionalised materials exhibited crystallisation temperatures between 30-40 °C, however, the crystallisation point of the multisite copolymer dropped to 7 °C. The late crystallisation and slow rearrangement of the multisite was explained by the presence of a high fraction of amorphous polystyrene and low alkyl chain density in this material. Furthermore, the space between each alkyl chain may potentially affect their intermolecular stacking, preventing high crystallisation. This observation was of great interest and demonstrates the potential of controlling the density and distribution of side chain functionalities to tune material properties.

4.3 Conclusion

In this study we describe the synthesis of a library of well-defined PSMA architectures including linear multisite, multiblock, diblock, alternating PSMA, and for the first time, an alternating 4xPSMA star. Their synthesis on gram scale was achieved by optimised RAFT polymerisation using industrial RAFT agents (CTA-Acid and CTA-Ester). Furthermore, the industrial grade CTA-Ester (80 % pure) was used without purification, demonstrating the robustness of the RAFT process and anticipating large scale production. The PSMA materials were subsequently functionalised with long aliphatic alcohols, leading to a library of graft copolymers with controlled side-group density and distribution. The influence of copolymer composition and structure, and the effect of long alkyl chain addition on copolymer behaviour in solution and the thermal properties were investigated using triple-detection SEC, TGA and DSC. The polymer behaviour in solution was shown to be dependent on copolymer molar mass and grafting density (increase of R_g, R_h and IV). The material degradation profiles were shown to be influenced by MAnh content, molar mass and polymeric architectures. While materials before grafting exhibited amorphous behaviour, with T_g values depending on MAnh content and distribution, a semi-crystalline behaviour was observed for all materials after adding long alkyl side chains. The alternating materials exhibited similar melting and crystallisation temperatures, showing no impact of molar mass or architecture (linear *vs.* star) on the thermal behaviour, which appeared to be driven by the presence of long alkyl chains only. The crystallisation temperature was shown to be highly dependent on side chain density and distribution. While alt-PSMAs (high density of crystalline side chains) and diblock showed a sharp peak at similar melting temperature, broader peaks and lower melting temperatures were observed for multiblock and multisite materials, showing the poor reorganisation of these materials. Interestingly, all functionalised materials exhibited a crystallisation temperature between 30-40 °C, however, the crystallisation point of the multisite copolymer dropped to 7 °C. This study demonstrates the importance of controlling copolymer composition and architecture for future development of material properties.

4.4 Experimental

Materials

Styrene monomer (Sty, ≥ 99 %) was obtained from Sigma-Aldrich and passed through neutral alumina prior to use to remove inhibitor. Maleic anhydride (MAnh, ≥ 99 %), 1,1'-Azobis(cyclohexane-1-carbonitrile) (V-40, $T_{1/2\text{-}10h}$ = 88 °C, 98 %), dimethyl 2,2'-azobis(2-methylpropionate) (V601, $T_{1/2\text{-}10h}$ = 66 °C, 98 %) and methane sulfonic acid (MSA, 70 wt. % in H_2O) were obtained from Sigma-Aldrich and used as received. Industrial grade CTA-Ester (≈ 80 % pure), CTA-Acid (> 95 % pure) and behenyl alcohols were generously provided by Lubrizol and used without purification.[50, 51] All solvents were obtained from either Fisher Scientific, VWR Chemical, or Sigma-Aldrich, and used as received.

Characterisation methods

NMR spectra were recorded on either a HD 400 MHz or 600 MHz Bruker Avance III systems at 25 °C using deuterated solvents obtained from Sigma-Aldrich. For quantitative ^{1}H-NMR and ^{13}C-NMR measurements, a 600 MHz Bruker Avance instrument were used (at 150 MHz) with a relaxation time of 10 s, high number of scans (>4k), and suppression of NOE (inverse gated decoupling). TMS contained in the solvent was used as internal standard and chemical shift values (δ) are reported in ppm. Chloroform-d (99.9 % D atom) and acetone-d_6 (99.9 % D atom) were obtained from Sigma-Aldrich.

DMF-SEC was carried out using an Agilent 390-LC MDS instrument equipped with differential refractive index (DRI), viscometer (VS), light scattering (LS) and dual wavelength UV detectors. The system was equipped with 2 x PLgel mixed D columns (300 x 7.5 mm) and a PLgel 5 μm guard column and autosampler. The eluent was DMF with 5 mmol NH_4BF_4. Samples were run at 1 ml min^{-1} at 50˚C. PMMA standards (Agilent EasiVials) were used for calibration. Analyte samples were filtered through a nylon membrane with 0.22 μm pore size before injection.

Chloroform-SEC was carried out using an Agilent 390-LC MDS instrument equipped with differential refractive index (DRI), viscometer (VS), light scattering (LS) and dual wavelength UV detectors. The system was equipped with 2 x PLgel mixed C columns (300 x 7.5 mm) and a PLgel 5 μm guard column and autosampler. The eluent was $CHCl_3$ with 2 wt. % of triethylamine additive. Samples were run at 1 ml min^{-1} at 30 ˚C. PMMA

and PS standards (Agilent EasiVials) were used for calibration. Analyte samples were filtered through a PVDF membrane with 0.22 μm pore size before injection.

Experimental molar mass ($M_{n,RI}$) and dispersity ($Đ_{RI}$) values of synthesised polymers were determined by conventional PS or PMMA calibration using Agilent GPC/SEC software.

Absolute molar mass ($M_{n,3d\text{-}SEC}$), intrinsic viscosity (IV), radius of gyration (R_g), hydrodynamic radius (R_h), Mark-Houwink parameter (α) and conformation data were determined by triple-detection SEC.

Refractive index increments (dn/dc) of PSMA polymers in respective eluents were determined offline using a differential refractometer. The refractive index was measured for five polymer concentrations (between 0.25 mg mL^{-1} and 5 mg mL^{-1}) and the dn/dc values were obtained from the slope of the plot of refractive index versus polymer concentration.

Table 4.4. Refractive index increments used for triple-detection SEC method.

Materials	Solvent	Temp. °C	dn/dc
Multisite PSMA	$CHCl_3$	30	0.170
Multiblock PSMA	DMF	50	0.160[a]
Multiblock PSMA	$CHCl_3$	30	0.200
Diblock PSMA	$CHCl_3$	30	0.200
Alternating PSMA	DMF	50	0.160
Multisite C22	$CHCl_3$	30	0.125
Multiblock C22	$CHCl_3$	30	0.095
Diblock C22	$CHCl_3$	30	0.085
Alternating C22	$CHCl_3$	30	0.055
PLaurylacrylate	$CHCl_3$	25	0.035[b]

[a] not measured and assumed to be similar to alternating. [b] approximate value from literature for polyethylacrylate.[73]

MALDI-ToF-MS was performed on a Bruker Daltonics Ultraflex in positive-linear mode. *trans*-2-[3-(4-*tert*-Butylphenyl)-2-methyl-2-propenylidene] malononitrile (DCTB), was used as the matrix (500 mg mL^{-1} in THF or acetone) without further purification (Sigma-Adrich). NaTFA salt was used as the ionisation agent (0.1 M in THF or acetone). Matrix, salts and polymer solution (10 mg mL^{-1} in THF or acetone) were mixed in a 1:1:1 volume ratio and then, 1 μL of the mixture was deposited onto a ground steel target plate before insertion into the ion source chamber. A linear calibration was created using insulin (Sigma-Adrich) as a reference. Insulin (0.1 mg mL^{-1} in acetonitrile/water mixture) was mixed with sinapic acid (80 mg mL^{-1} in acetonitrile/water mixture) in a 1:1 volume ratio and deposited onto MALDI target plate.

IR spectroscopy was used to evaluated the yield of esterification by following the disappearance of the MAnh ester symmetric stretch peak at 1,850 cm^{-1} and the shift of the ester asymmetric stretch peak from 1,770 cm^{-1} to 1,730 cm^{-1}. A more intense peak attributed to the alkane C-H stretch at 2,700-3,000 cm^{-1} was observed after introduction of long alkyl chains.

TGA was performed in alumina crucibles at a heating rate of 10 °C/min from 25 to 650 °C under N_2, on a Mettler Toledo TGA/DSC 1 instrument. Analysis was performed on Mettler-Toledo STARe software.

Differential Scanning Calorimetry (DSC) were recorded using a Mettler-Toledo DSC 1 Instrument using 40 μl aluminium pans under nitrogen atmosphere. Samples were heated and cooled at 10 °C/min to 40 °C/min between the range of 25 °C to 300 °C for PSMA before functionalisation. For the grafted materials, 10 °C/min heating and cooling rate was used over the range of -25 °C to 250 °C. These cycles were repeated 3 times. Samples were analysed using Mettler-Toledo STARe software. Melting and crystallisation temperatures were measured at the maximum endotherm and exotherm peaks, respectively.

Procedure for 4xCTA synthesis

The esterification of S-1-dodecyl-S'-(α,α'-dimethyl-α'-acetic acid)trithiocarbonate (CTA-Acid) (13 g, 35 mmol) with pentaerythritol (0.4 g, 3 mmol) was carried out in the presence of methane sulfonic acid (MSA) catalyst (0.180 g, 1.5 mmol, 0.1 equiv. / alcohol) under reflux of toluene using Dean-Stark apparatus under nitrogen atmosphere. After 20 hours, the toluene was evaporated and the mixture was dissolved in a minimum

amount of hexane before being purified by column chromatography (silica column SF25 40g – flow rate 40 ml/min – hexane/ethyl acetate gradient). The pure 4xCTA was recovered as orange/yellow oil (mass recovered ≈ 1 g).

Typical RAFT polymerisation (macroCTA for multiblock – PSty DP = 10)

Industrial grade CTA-Ester (1.4 g, 2.7 mmol), Sty (2.9 g, 27 mmol), V-40 (0.06 g, 0.25 mmol) and toluene (0.35 mL) were charged into a two-neck round bottom flask equipped with a magnetic stirrer bar, a condenser on one neck and a rubber septum on the other neck. The solution was degassed using nitrogen for *ca.* 15 min before being placed in a thermostated oil bath set at 100 °C. After overnight reaction (*ca.* 15 hrs) a sample was taken from the polymerisation medium for characterisation. The copolymer was characterised using ^{1}H-NMR and SEC (conv. = 96 %, $M_{n,theo}$ = 1,400 g mol^{-1}, $M_{n,RI\text{-}SEC\text{-}THF}$ = 1,200 g mol^{-1}and $Đ_{RI}$ = 1.06).

One-pot sequential chain extension (PSty$_{10}$-b-PSMA$_5$)

The reactor vessel containing the reaction mixture of macroCTA (PSty$_{10}$) synthesis was flooded with a nitrogen stream, and toluene (1.4 mL) was added for dilution. Maleic anhydride (1.4 g, 14 mmol), styrene (1.4 g, 14 mmol), and V-40 (0.05 g, 0.18 mmol) were added to the polymerisation medium *via* syringe. The reaction mixture was degassed for *ca.* 15 min and allowed to polymerise at 70 °C for the desired reaction time (*ca.* 8 hrs). A sample was taken from the polymerisation medium before and after each chain extension for characterisation. As MAnh is barely soluble in toluene, it was dissolved in a small amount of dioxane before addition. Importantly, the amount of initiator remaining after each cycle was taken into account for the following polymerisation step (equation 1.3). The copolymer was characterised using ^{1}H-NMR and SEC (conv. = 93 %, $M_{n,theo}$ = 2,400 g mol^{-1}, $M_{n,RI\text{-}SEC\text{-}THF}$ = 1,500 g mol^{-1}and $Đ_{RI}$ = 1.11).

Typical procedure for functionalisation of PSMA materials with behenyl alcohol

The pure multiblock materials (3.0 g, 0.06 mmol) were reacted with long aliphatic alcohols (C_{22}OH, 11.6 g, 35 mmol, 6 equiv. / MAnh) in the presence of methane sulfonic acid (MSA) catalyst (0.4 g, 3.5 mmol, 0.1M equiv. / alcohol). The esterification was carried out using Dean-Stark apparatus under reflux of toluene (≈ 70 wt. %). After reaction (*ca.* 20 hours), the mixture was precipitated several times in acetone from a

minimum amount of diethyl ether. The precipitate was dried in an oven and recovered as an off-yellow solid (mass recovered = 3 g). The graft copolymer was characterised using IR, quantitative ^{1}H-NMR and ^{13}C-NMR spectroscopy and SEC (yield = 95 %, $M_{n,calc}$ = 11,200 g mol^{-1}, $M_{n,3d\text{-}SEC\text{-}CHCl3}$ =10,000 g mol^{-1}and $Đ_{RI}$ = 1.17).

Determination of monomer conversion

The conversion for each block was estimated by following styrene consumption as described in previous chapters (equation 2.5). For PSMA block, the conversion of styrene and MAnh was assumed to be identical.

Calculation of $M_{n,theo}$

For the polystyrene macroCTA and PSMA blocks, the theoretical number-average molar mass ($M_{n,th}$) was calculated as described in previous chapters using equation 2.6 (M_{Sty} = 104 g mol^{-1}and M_{SMA} = 202 g mol^{-1}).

Calculation of livingness

The fraction of living chains was calculated using equation 1.2 presented in previous chapter.[74] We use fc = 1 for styrene as it mainly terminates by combination (leads to an under-estimation), however, fc = 0 was used for PSMA blocks as no information on termination are reported (leads to an over-estimation).

Fox Equation[70]:

$$\frac{1}{T_g} = \frac{x_1}{T_{g,1}} + \frac{x_2}{T_{g,2}} \qquad 4.1$$

with T_g the glass transition of the copolymer, x_1 and x_2 weight fractions of components 1 and 2, and $T_{g,1}$ and $T_{g,2}$, their respective glass transition.

4.5 References

(1) Lutz, J.-F.; Ouchi, M.; Liu, D. R.; Sawamoto, M. Sequence-Controlled Polymers. *Science* **2013**, 341 (6146), 1238149.
(2) Lutz, J.-F.; Lehn, J.-M.; Meijer, E. W.; Matyjaszewski, K. From precision polymers to complex materials and systems. *Nat. Rev. Mat.* **2016**, 1 (5), 16024.
(3) Lin, T.-P.; Chang, A. B.; Chen, H.-Y.; Liberman-Martin, A. L.; Bates, C. M.; Voegtle, M. J.; Bauer, C. A.; Grubbs, R. H. Control of Grafting Density and Distribution in Graft Polymers by Living Ring-Opening Metathesis Copolymerization. *J. Am. Chem. Soc.* **2017**, 139 (10), 3896-3903.
(4) Kerr, A.; Hartlieb, M.; Sanchis, J.; Smith, T.; Perrier, S. Complex multiblock bottle-brush architectures by RAFT polymerization. *Chem. Commun.* **2017**, 53 (87), 11901-11904
(5) Polymeropoulos, G.; Zapsas, G.; Ntetsikas, K.; Bilalis, P.; Gnanou, Y.; Hadjichristidis, N. 50th Anniversary Perspective: Polymers with Complex Architectures. *Macromolecules* **2017**, 50 (4), 1253-1290.
(6) Ren, J. M.; McKenzie, T. G.; Fu, Q.; Wong, E. H. H.; Xu, J.; An, Z.; Shanmugam, S.; Davis, T. P.; Boyer, C.; Qiao, G. G. Star Polymers. *Chem. Rev.* **2016**, 116 (12), 6743-6836.
(7) Zamfir, M.; Lutz, J.-F. Ultra-precise insertion of functional monomers in chain-growth polymerizations. *Nat. Commun.* **2012**, 3, 1138.
(8) Pfeifer, S.; Lutz, J.-F. A Facile Procedure for Controlling Monomer Sequence Distribution in Radical Chain Polymerizations. *J. Am. Chem. Soc.* **2007**, 129 (31), 9542-9543.
(9) You, Y.-z.; Hong, C.-y.; Wang, W.-p.; Wang, P.-h.; Lu, W.-q.; Pan, C.-y. A Novel Strategy To Synthesize Graft Copolymers with Controlled Branch Spacing Length and Defined Grafting Sites. *Macromolecules* **2004**, 37 (19), 7140-7145.
(10) Gallyamov, M. O.; Tartsch, B.; Khokhlov, A. R.; Sheiko, S. S.; Börner, H. G.; Matyjaszewski, K.; Möller, M. Reversible Collapse of Brushlike Macromolecules in Ethanol and Water Vapours as Revealed by Real-Time Scanning Force Microscopy. *Chem. Eur. J.* **2004**, 10 (18), 4599-4605.
(11) Denesyuk, N. A. Bottle-brush polymers as an intermediate between star and cylindrical polymers. *Phys. Rev. E* **2003**, 68 (3), 031803.
(12) Sheiko, S. S.; Prokhorova, S. A.; Beers, K. L.; Matyjaszewski, K.; Potemkin, I. I.; Khokhlov, A. R.; Möller, M. Single Molecule Rod−Globule Phase Transition for Brush Molecules at a Flat Interface. *Macromolecules* **2001**, 34 (23), 8354-8360.
(13) Paturej, J.; Sheiko, S. S.; Panyukov, S.; Rubinstein, M. Molecular structure of bottlebrush polymers in melts. *Sci. Adv.* **2016**, 2 (11), 1601478.
(14) Zhang, Q.; Ran, Q.; Zhao, H.; Shu, X.; Yang, Y.; Zhou, H.; Liu, J. pH-induced conformational changes of comb-like polycarboxylate investigated by experiment and simulation. *Colloid. Polym. Sci.* **2016**, 294 (11), 1705-1715.
(15) Daniel, W. F. M.; Burdyńska, J.; Vatankhah-Varnoosfaderani, M.; Matyjaszewski, K.; Paturej, J.; Rubinstein, M.; Dobrynin, A. V.; Sheiko, S. S. Solvent-free, supersoft and superelastic bottlebrush melts and networks. *Nat. Mater.* **2015**, 15, 183.
(16) Huang, Y.; Mai, Y.; Yang, X.; Beser, U.; Liu, J.; Zhang, F.; Yan, D.; Müllen, K.; Feng, X. Temperature-Dependent Multidimensional Self-Assembly of Polyphenylene-Based "Rod–Coil" Graft Polymers. *J. Am. Chem. Soc.* **2015**, 137 (36), 11602-11605.
(17) Srichan, S.; Kayunkid, N.; Oswald, L.; Lotz, B.; Lutz, J.-F. Synthesis and Characterization of Sequence-Controlled Semicrystalline Comb Copolymers: Influence of Primary Structure on Materials Properties. *Macromolecules* **2014**, 47 (5), 1570-1577.
(18) Watson, M. D.; Wagener, K. B. Functionalized Polyethylene via Acyclic Diene Metathesis Polymerization: Effect of Precise Placement of Functional Groups. *Macromolecules* **2000**, 33 (24), 8963-8970.
(19) Shibata, M.; Matsumoto, M.; Hirai, Y.; Takenaka, M.; Sawamoto, M.; Terashima, T. Intramolecular Folding or Intermolecular Self-Assembly of Amphiphilic Random Copolymers: On-Demand Control by Pendant Design. *Macromolecules* **2018**, 51 (10), 3738–3745.
(20) Ogura, Y.; Terashima, T.; Sawamoto, M. Amphiphilic PEG-Functionalized Gradient Copolymers via Tandem Catalysis of Living Radical Polymerization and Transesterification. *Macromolecules* **2017**, 50 (3), 822-831.
(21) Zhang, J.; Deubler, R.; Hartlieb, M.; Martin, L.; Tanaka, J.; Patyukova, E.; Topham, P. D.; Schacher, F. H.; Perrier, S. Evolution of Microphase Separation with Variations of Segments of Sequence-Controlled Multiblock Copolymers. *Macromolecules* **2017**, 50 (18), 7380-7387.

(22) Yanez-Macias, R.; Kulai, I.; Ulbrich, J.; Yildirim, T.; Sungur, P.; Hoeppener, S.; Guerrero-Santos, R.; Schubert, U. S.; Destarac, M.; Guerrero-Sanchez, C.; Harrisson, S. Thermosensitive spontaneous gradient copolymers with block- and gradient-like features. *Polym. Chem.* **2017**, 8 (34), 5023-5032.
(23) Alfrey, T.; Lavin, E. The Copolymerization of Styrene and Maleic Anhydride. *J. Am. Chem. Soc.* **1945**, 67 (11), 2044-2045.
(24) Jenkins, A. D. Alternating copolymers. *Brit. Polym. J.* **1987**, 19 (1), 91-91.
(25) Trivedi, B. C.; Culbertson, B. M., Alternating Addition Copolymerizations. In *Maleic Anhydride*, Springer US: Boston, MA, **1982**.
(26) Huang, J.; Turner, S. R. Recent advances in alternating copolymers: The synthesis, modification, and applications of precision polymers. *Polymer* **2017**, 116, 572-586.
(27) Polyscope. Polyscope promotes SMA as 'versatile' polymer modifier for amorphous thermoplastics. *Add. Polym.* **2010**, 2010 (4), 2-3.
(28) Cray Valley. SMA®. http://www.crayvalley.com/products/sma-styrene
(29) Solenis. SCRIPSET™ COPOLYMER RESINS. https://solenis.com/en/industries/specialties-wood-adhesives/innovations/scripset-copolymer-resins/
(30) Matyjaszewski, K. Atom Transfer Radical Polymerization (ATRP): Current Status and Future Perspectives. *Macromolecules* **2012**, 45 (10), 4015-4039.
(31) Anastasaki, A.; Nikolaou, V.; Nurumbetov, G.; Wilson, P.; Kempe, K.; Quinn, J. F.; Davis, T. P.; Whittaker, M. R.; Haddleton, D. M. Cu(0)-Mediated Living Radical Polymerization: A Versatile Tool for Materials Synthesis. *Chem. Rev.* **2016**, 116 (3), 835-877.
(32) Ouchi, M.; Terashima, T.; Sawamoto, M. Transition Metal-Catalyzed Living Radical Polymerization: Toward Perfection in Catalysis and Precision Polymer Synthesis. *Chem. Rev.* **2009**, 109 (11), 4963-5050.
(33) Nicolas, J.; Guillaneuf, Y.; Lefay, C.; Bertin, D.; Gigmes, D.; Charleux, B. Nitroxide-mediated polymerization. *Prog. Polym. Sci.* **2013**, 38 (1), 63-235.
(34) Moad, G.; Rizzardo, E.; Thang, S. H. Living Radical Polymerization by the RAFT Process – A Third Update. *Aust. J. Chem.* **2012**, 65 (8), 985-1076.
(35) De Brouwer, H.; Schellekens, M. A. J.; Klumperman, B.; Monteiro, M. J.; German, A. L. Controlled radical copolymerization of styrene and maleic anhydride and the synthesis of novel polyolefin-based block copolymers by reversible addition–fragmentation chain-transfer (RAFT) polymerization. *J. Polym. Sci., Part A: Polym. Chem.* **2000**, 38 (19), 3596-3603.
(36) Park, E. S.; Kim, M. N.; Lee, I. M.; Lee, H. S.; Yoon, J. S. Living Radical Copolymerization of Styrene/MaleicAnhydride. *J. Polym. Sci., Part A: Polym. Chem.* **2000**, 38 (12), 2239-2244.
(37) Chen, G.-Q.; Wu, Z.-Q.; Wu, J.-R.; Li, Z.-C.; Li, F.-M. Synthesis of Alternating Copolymers of N-Substituted Maleimides with Styrene via Atom Transfer Radical Polymerization. *Macromolecules* **1999**, 33 (2), 232-234.
(38) Koulouri, E. G.; Kallitsis, J. K.; Hadziioannou, G. Terminal Anhydride Functionalized Polystyrene by Atom Transfer Radical Polymerization Used for the Compatibilization of Nylon 6/PS Blends. *Macromolecules* **1999**, 32 (19), 6242-6248.
(39) Moriceau, G.; Gody, G.; Hartlieb, M.; Winn, J.; Kim, H.; Mastrangelo, A.; Smith, T.; Perrier, S. Functional multisite copolymer by one-pot sequential RAFT copolymerization of styrene and maleic anhydride. *Polym. Chem.* **2017**, 8 (28), 4152-4161.
(40) Xu, J.; Fu, C.; Shanmugam, S.; Hawker, C. J.; Moad, G.; Boyer, C. Synthesis of Discrete Oligomers by Sequential PET-RAFT Single-Unit Monomer Insertion. *Angew. Chem. Int. Ed.* **2017**, 56, 1-8.
(41) Zhou, C.; Qian, S.; Zhang, A.; Xu, L.; Zhu, J.; Cheng, Z.; Kang, E.-T.; Yao, F.; Fu, G. D. A well-defined amphiphilic polymer co-network from precise control of the end-functional groups of linear RAFT polymers. *RSC Adv.* **2014**, 4 (16), 8144-8156.
(42) Henry, S. M.; Convertine, A. J.; Benoit, D. S. W.; Hoffman, A. S.; Stayton, P. S. End-Functionalized Polymers and Junction-Functionalized Diblock Copolymers Via RAFT Chain Extension with Maleimido Monomers. *Bioconjugate Chem.* **2009**, 20 (6), 1122-1128.
(43) Pfeifer, S.; Lutz, J.-F. Development of a Library of N-Substituted Maleimides for the Local Functionalization of Linear Polymer Chains. *Chem. Eur. J.* **2008**, 14 (35), 10949-10957.
(44) Feng, X.-S.; Pan, C.-Y. Synthesis of Amphiphilic Miktoarm ABC Star Copolymers by RAFT Mechanism Using Maleic Anhydride as Linking Agent. *Macromolecules* **2002**, 35 (13), 4888-4893.
(45) Smith, A. A. A.; Autzen, H. E.; Laursen, T.; Wu, V.; Yen, M.; Hall, A.; Hansen, S. D.; Cheng, Y.; Xu, T. Controlling Styrene Maleic Acid Lipid Particles through RAFT. *Biomacromolecules* **2017**, 18 (11), 3706-3713.

(46) Germack, D. S.; Harrisson, S.; Brown, G. O.; Wooley, K. L. Influence of the structure of nanoscopic building blocks on the assembly of micropatterned surfaces. *J. Polym. Sci., Part A: Polym. Chem.* **2006**, 44 (17), 5218-5228.
(47) Harrisson, S.; Wooley, K. L. Shell-crosslinked nanostructures from amphiphilic AB and ABA block copolymers of styrene-alt-(maleic anhydride) and styrene: polymerization, assembly and stabilization in one pot. *Chem. Commun.* **2005**, 0 (26), 3259-3261.
(48) Zhu, M.-Q.; Wei, L.-H.; Li, M.; Jiang, L.; Du, F.-S.; Li, Z.-C.; Li, F.-M. A unique synthesis of a well-defined block copolymer having alternating segments constituted by maleic anhydride and styrene and the self-assembly aggregating behavior thereof. *Chem. Commun.* **2001**, 0 (4), 365-366.
(49) Gody, G.; Maschmeyer, T.; Zetterlund, P. B.; Perrier, S. Pushing the Limit of the RAFT Process: Multiblock Copolymers by One-Pot Rapid Multiple Chain Extensions at Full Monomer Conversion. *Macromolecules* **2014**, 47 (10), 3451-3460.
(50) Brzytwa, A. J.; Johnson, J. Scaled Production of RAFT CTA–a STAR Performer. *Polym. Prepr. (Am. Chem. Soc., Div. Polym. Chem.)* **2011**, 52 (2), 533-534.
(51) Lai, J. T.; Filla, D.; Shea, R. Functional Polymers from Novel Carboxyl-Terminated Trithiocarbonates as Highly Efficient RAFT Agents. *Macromolecules* **2002**, 35 (18), 6754-6756.
(52) Klumperman, B. Mechanistic considerations on styrene-maleic anhydride copolymerization reactions. *Polym. Chem.* **2010**, 1 (5), 558-562.
(53) Gregory, A.; Stenzel, M. H. Complex polymer architectures via RAFT polymerization: From fundamental process to extending the scope using click chemistry and nature's building blocks. *Prog. Polym. Sci.* **2012**, 37 (1), 38-105.
(54) Chaffey-Millar, H.; Stenzel, M. H.; Davis, T. P.; Coote, M. L.; Barner-Kowollik, C. Design Criteria for Star Polymer Formation Processes via Living Free Radical Polymerization. *Macromolecules* **2006**, 39 (19), 6406-6419.
(55) Yao, Z.; Zhang, J.-S.; Chen, M.-L.; Li, B.-J.; Lu, Y.-Y.; Cao, K. Preparation of well-defined block copolymer having one polystyrene segment and another poly(styrene-alt-maleic anhydride) segment with RAFT polymerization. *J. Appl. Polym. Sci.* **2011**, 121 (3), 1740-1746.
(56) Chernikova, E.; Terpugova, P.; Bui, C.; Charleux, B. Effect of comonomer composition on the controlled free-radical copolymerization of styrene and maleic anhydride by reversible addition–fragmentation chain transfer (RAFT). *Polymer* **2003**, 44 (15), 4101-4107.
(57) Wu, Y.; Ni, G.; Yang, F.; Li, C.; Dong, G. Modified Maleic Anhydride Co-polymers as Pour-Point Depressants and Their Effects on Waxy Crude Oil Rheology. *Energy Fuels* **2012**, 26 (2), 995-1001.
(58) Soni, H. P.; Kiranbala; Agrawal, K. S.; Nagar, A.; Bharambe, D. P. Designing maleic anhydride-α-olifin copolymeric combs as wax crystal growth nucleators. *Fuel Process. Technol.* **2010**, 91 (9), 997-1004.
(59) Al-Sabagh, A. M.; Noor El-Din, M. R.; Morsi, R. E.; Elsabee, M. Z. Styrene-Maleic Anhydride Copolymer Esters as Flow Improvers of Waxy Crude Oil. *J. Disp. Sci. Technol.* **2009**, 30 (3), 420-426.
(60) Agilent, *A guide to multi-detector gel permeation chromatography.* **2012**, 5990-7196EN, 1-24.
(61) Striegel, A. M. Multiple Detection in Size-Exclusion Chromatography of Macromolecules. *Anal. Chem.* **2005**, 77 (5), 104-113.
(62) Chen, P.; Huang, X.; Zhang, Q.; Xi, K.; Jia, X. Hybrid networks based on poly(styrene-co-maleic anhydride) and N-phenylaminomethyl POSS. *Polymer* **2013**, 54 (3), 1091-1097.
(63) Martínez, F.; Uribe, E.; Olea, A. F. Copolymerization of Maleic Anhydride with Styrene and α-Olefins. Molecular and Thermal Characterization. *J. Macromol. Sci., Part A: Pure Appl. Chem.* **2005**, 42 (8), 1063-1072.
(64) Postma, A.; Davis, T. P.; Evans, R. A.; Li, G.; Moad, G.; O'Shea, M. S. Synthesis of Well-Defined Polystyrene with Primary Amine End Groups through the Use of Phthalimido-Functional RAFT Agents. *Macromolecules* **2006**, 39 (16), 5293-5306.
(65) Postma, A.; Davis, T. P.; Moad, G.; O'Shea, M. S. Thermolysis of RAFT-Synthesized Polymers. A Convenient Method for Trithiocarbonate Group Elimination. *Macromolecules* **2005**, 38 (13), 5371-5374.
(66) Cascaval, C. N.; Chitanu, G.; Carpov, A. On the thermal decomposition of copolymers of maleic anhydride with styrene. *Thermochim. Acta* **1996**, 275 (2), 225-233.
(67) Qiu, G. M.; Zhu, B. K.; Xu, Y. Y.; Geckeler, K. E. Synthesis of Ultrahigh Molecular Weight Poly(styrene-alt-maleic anhydride) in Supercritical Carbon Dioxide. *Macromolecules* **2006**, 39 (9), 3231-3237.

(68) Benvenuta-Tapia, J. J.; Vivaldo-Lima, E.; Tenorio-López, J. A.; de los Ángeles Vargas-Hernández, M.; Vázquez-Torres, H. Kinetic analysis of the RAFT copolymerization of styrene and maleic anhydride by differential scanning calorimetry. *Thermochim. Acta* **2018**, 667, 93-101.
(69) Zhan, X.; He, R.; Zhang, Q.; Chen, F. Microstructure and mechanical properties of amphiphilic tetrablock copolymer elastomers via RAFT miniemulsion polymerization: influence of poly[styrene-alt-(maleic anhydride)] segments. *RSC Adv.* **2014**, 4 (93), 51201-51207.
(70) Fox, T. G. Influence of Diluent and of Copolymer Composition on the Glass Temperature of a Polymer System. *Bull. Am. Phys. Soc.* **1956**, 1, 123.
(71) Qin, S.; Matyjaszewski, K.; Xu, H.; Sheiko, S. S. Synthesis and Visualization of Densely Grafted Molecular Brushes with Crystallizable Poly(octadecyl methacrylate) Block Segments. *Macromolecules* **2003**, 36 (3), 605-612.
(72) Plate, N. A., Shibaev, V. P., Petrukhin, B. S., Zubov, Y. A., Kargin, V. A. Structure of crystalline polymers with unbranched long side chains. *J. Polym. Sci. A1* **1971**, 9 (8), 2291-2298.
(73) Hiorns, R., *Polymer Handbook* **2000**, Vol. 49.
(74) Gody, G.; Maschmeyer, T.; Zetterlund, P. B.; Perrier, S. Rapid and quantitative one-pot synthesis of sequence-controlled polymers by radical polymerization. *Nat. Commun.* **2013**, 4, 2505.

Chapter 5 Well-Defined Graft PSMA Architectures as Oil and Lubricant Additives

Abstract

The well-defined PSMA materials synthesised in the previous chapter (multisite, multiblock, diblock, alternating linear, alternating star) were esterified using long alkyl alcohols (lauryl/C12 and behenyl/C22) and investigated as rheology improvers for two mineral base oils (group II and III). The influence of grafting density and distribution, backbone length, and side chain length on pour point (PPT) was investigated. The viscosity index (VI) and thickening efficiency (TE) were also studied. All studied materials showed improvement of mineral oil properties (PPT, VI, and TE). The alternating materials (high density of side chains) functionalised with shorter alkyl chains (C12) were found to be more efficient as pour point depressants (PPDs), regardless of the oil type and the molar mass or architecture of the polymer tested. A polylaurylacrylate (PLAc) material was also synthesised and used for comparison, showing the benefit of having styrene in copolymer additive composition. The VI and TE performances were shown to be dependent on molar mass and architectures used, where the best results were obtained for high molar mass PSMA star.

5.1 Introduction

One of the major challenges of petroleum and its derivatives (crude oil, lubricating oil, fuel) is the precipitation of n-paraffin as wax at low temperature.[1] The wax formation leads to drastic changes on rheological properties and complicates oil flow at low temperatures. Wax crystallisation is responsible for many problems occurring in oil production, storage and transportation, and complicates the use of hydrocarbon fuels in cold climates (deposits and blockages).[2-7] This problem can be addressed chemically by adding polymeric additives acting as pour point depressants (PPDs) or flow improvers (FIs). Copolymers with linear or comb-like architectures have been largely investigated and proven efficient as wax inhibitors.[8, 9] Poly(ethylene-*co*-vinyl acetate) (EVA),[10-13] poly(ethylene-*co*-butene),[14-16] poly(α-olefins),[17] poly(alkylacrylates),[18, 19] poly(alkylmethacrylates),[20, 21] and copolymers of maleic anhydride with styrene, α-olefins or vinylic esters,[3, 4, 22, 23] are among the most efficient commercially available pour point depressants. Despite many investigations and extensive literature, the basic mechanism of the pour point phenomenon and how polymeric additives affect the pour point are currently not fully understood.[2, 3, 24-26] It is generally believed that the inhibition of wax crystallisation occurs *via* nucleation, co-crystallisation or adsorption of PPDs, altering the crystal morphology and growth characteristics. By destroying cohesive forces between crystals, it reduces the formation of interconnected three-dimensional wax networks leading to gelation.[19, 27] Although it is important to understand that, because of the variety of oil compositions and their multiple applications, each oil requires specific additives and therefore a universal PPD system is unlikely.[3] It is reported that the efficiency of the PPDs depends upon many factors, such as n-paraffin details (content and composition) and polymer additive features (composition, molar mass and pendant chain nature).[20, 28-31] Moreover, it has been found that greater similarity between the polymer structure and the wax constituents results in better performance. For optimal depressing results, the polymer additives must contain long aliphatic side chains and benzene rings interacting with paraffins or aromatics (asphaltenes) present in oils. Furthermore, the presence of polar groups (ester or carboxylic acids) and steric hindrance (graft or branched structure) helps to interfere with the wax crystallisation process by changing crystal size and morphology. The composition and structure of polymeric additives is thus fundamental to optimise oil derivative efficiency, durability and performance. In addition

to PPDs and flow improvers, lubricating oils also require additives such as viscosity modifiers, antiwear, antioxidants and dispersants. The development of new additives combining multifunctional property modifications is therefore of large interest to reduce the overall costs.[32]

Poly(styrene-*co*-maleic anhydride) copolymers (PSMA) with aliphatic side chains are interesting graft materials which fulfil most of the oil additive requirements and have already proven themselves as efficient PPDs/viscosity modifiers in crude oil.[4, 33-35] Their efficiencies were shown to depend on polymer structure and concentration, however, other factors were found to be crucial, such as the distance between pendant side chains, molar mass, polymer dispersity and the amorphous or crystalline nature of the additives.[4, 5, 36] Thus, controlling structural parameters of these copolymers is a major challenge in the development of efficient additives. However, most of the PSMA materials (and other graft copolymers) studied to date suffer from poor compositional and structural control due to the free radical polymerisation process typically used in industry. With the recent advances in controlled radical processes, it is now possible to access well-defined materials with novel polymeric architectures, opening the way for new materials with great potential for use as oil additives.

In this Chapter, graft PSMA materials (multisite, multiblock, diblock, alternating linear, alternating star) with short alkyl side chains (C12) were prepared and used in combination with the materials synthesised in previous chapter (PSMA-C22) to investigate the effect of structure, composition, molar mass, side chain length and type of architecture on the rheology of two mineral oils (group II and III). The pour points of oil-polymer blends were measured at different concentrations (0.2 wt. %-0.8 wt. %). The viscosity index (VI) and thickening efficiency (TE) were also investigated to determine potential performance as lubricating oil additives.

5.2 General scheme

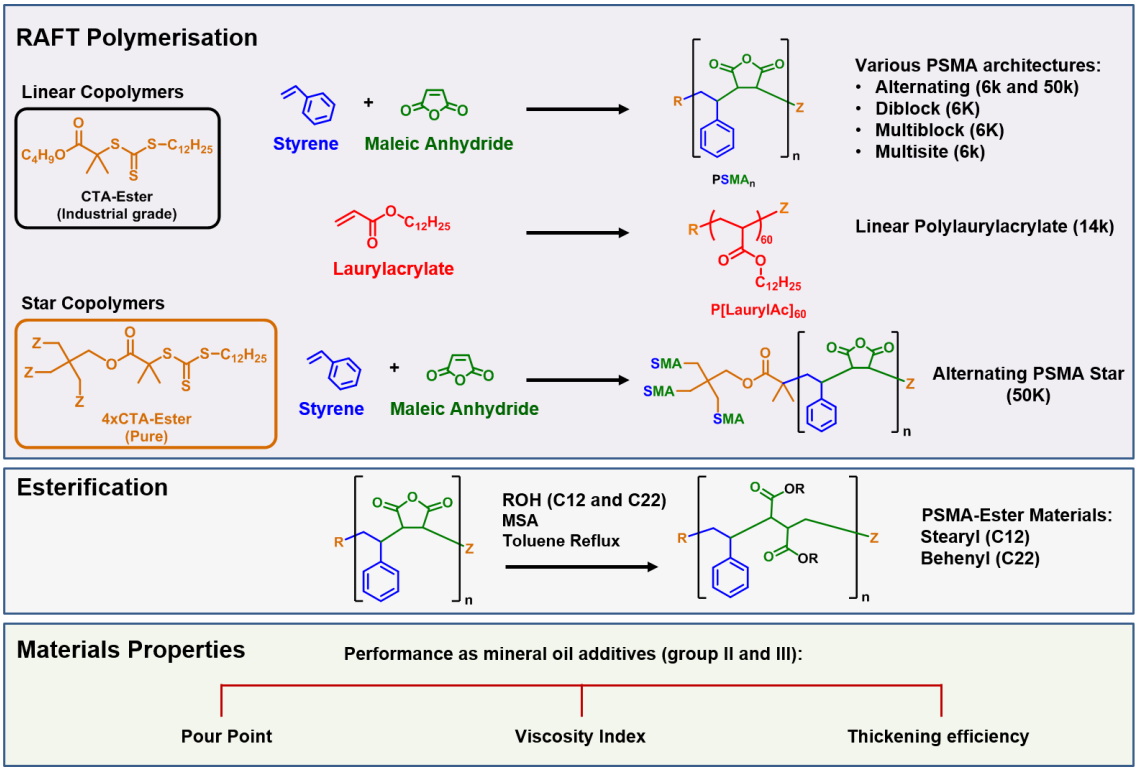

Scheme 5.1. General route for the synthesis of graft PSMA materials by RAFT and performances for oil and lubricant additives.

5.3 Results and Discussion

5.3.1 Material features

The graft PSMA materials were synthesised by optimised RAFT polymerisation and subsequent esterification as described previously in Chapter 4 (Scheme 4.1). The PSMA materials prepared in a previous chapter (PSMA-C22) were re-used here and new materials with shorter side chains (PSMA-C12) were prepared (characterisation details in Appendix). All the materials were purified by performing several precipitations to remove the excess long alkyl chains which could affect the quality of performance measurements. The features of all materials including molar mass, dispersity, yield of esterification and material behaviour in chloroform (R_g, R_h, IV, and α) are shown in Table 5.1. As discussed in a previous chapter, the comparable molar mass and narrow dispersity of the PSMA backbones (Entry 1-4) allow the study of the influence of grafting density and distribution on material properties. The increase in grafting density between materials was observed

through the number of alkyl chains inserted and the increase of molar mass after esterification. As observed previously, a small increase of molecular size (R_g and R_h) correlating with molar mass and grafting density is obtained. The increase of the side chain density was shown to give denser materials (lower IV), and all materials were seen to adopt random coil conformation in chloroform ($\alpha > 0.5$).[37, 38] When functionalised with shorter side chains, similar conformation was observed ($\alpha > 0.5$), however, lower molecular size and similar IV were observed (Entry 4 *vs.* 5). This, was attributed to the inherent decrease of molar mass associated with the use of shorter alkyl chains. Similarly, the linear material with higher molar mass exhibited lower molecular size and lower IV values when grafted with shorter side chains (Entry 6 *vs.* 7). The 4xPSMA exhibited a more compact structure compared to its linear counterpart as smaller molecular size, lower IV and lower α values were obtained (Entry 7 *vs.* 8). The linear polylaurylacrylate (PLaurylAc) synthesised to compare with the short linear PSMA exhibited similar molar mass and narrow dispersity, allowing good comparison (Entry 5 *vs.* 9). The synthesis of all these materials and their rigorous characterisation opened the way for a complete study of the influence of polymer composition, grafting density and distribution, molar mass, side chain length, and architecture on their rheological properties.

Table 5.1. Polymer Material Features

Entry	Materials	PSMA Backbones			Graft PSMAs							
		$M_{n,3d\text{-}SEC}$[a] g mol^{-1}	$Đ_{RI}$[b]	Graft	% Yield[c]	Nb graft[c]	$M_{n,3d\text{-}SEC}$[a] g mol^{-1}	$Đ_{RI}$[b]	R_g[a] (nm)	R_h[a] (nm)	IV[a] (dl/g)	α[a]
1	Multisite	6,400[d]	1.29[d]	C22	99	10	9,300[d]	1.20[d]	2.57[d]	2.30[d]	0.081[d]	0.72[d]
2	Multiblock	5,100[d]	1.20[d]	C22	95	19	11,100[d]	1.17[d]	2.53[d]	2.42[d]	0.080[d]	0.83[d]
3	Diblock	6,400[d]	1.22[e]	C22	96	25	14,700[d]	1.12[d]	2.74[d]	2.61[d]	0.077[d]	0.73[d]
4	Alt-Linear	6,200[e]	1.13[e]	C22	87	40	21,900[d]	1.16[d]	2.91[d]	2.89[d]	0.069[d]	0.71[d]
5	Alt-Linear	6,200[e]	1.13[e]	C12	97	44	19,000[d]	1.28[d]	2.87[d]	2.78[d]	0.072[d]	0.68[d]
6	Alt-Linear	48,200[e]	1.19[e]	C22	87	394	174,200[d]	1.26[d]	8.39[d]	8.82[d]	0.248[d]	0.59[d]
7	Alt-Linear	48,200[e]	1.19[e]	C12	93	419	133,000[d]	1.28[d]	8.16[d]	7.61[d]	0.209[d]	0.61[d]
8	Alt-Star	44,900[e]	1.15[e]	C12	91	364	138,900[d]	1.20[d]	7.71[d]	6.75[d]	0.139[d]	0.50[d]
9	PLaurylAc	-	-	C12	-	52	17,700[d]	1.30[d]	2.63[d]	2.84[d]	0.082[d]	0.87[d]

[a] Obtained from triple-detection SEC (RI, Viscometer, LS) using *dn*/*dc* values measured off-line. [b] Obtained using conventional SEC with RI detector. [c] Obtained from ^{13}C-NMR using peak at 64.5 ppm corresponding to the number of alkyl chains grafted and peak at 172 ppm corresponding to the number of MAnh units inserted. [d] SEC in Chloroform. [e] SEC in DMF.

5.3.2 Pour point measurements

The efficiency of all polymeric materials as pour point depressants was studied on two mineral oils (group II and III) using polymer-oil blends at different concentrations (0.2 wt. %-0.8 wt. %). The preliminary testing was conducted as a single component formulation, however, further testing on full lubricant formulation would be required to gain reliable results. Table 5.2 shows the pour point values for pure mineral oils and for the different formulations. The polylaurylacrylate and an internal reference from Lubrizol (LZPP3) were used as controls for comparison. Interestingly, the pour point of the two mineral oils was reduced for all formulations, confirming the potential of PSMA materials. Moreover, the depressant activity appeared to be highly dependent on additive composition and structure. Overall, the concentration seemed to have relatively low impact on material activity as similar results were obtained on the range of polymer concentrations.

Table 5.2. Pour point values for the different polymer-oil formulations

			Pour Point (°C)					
			Group II			Group III		
Entry	Materials	N_{graft}	0.2 wt.%	0.4 wt.%	0.8 wt.%	0.2 wt.%	0.4 wt.%	0.8 wt.%
0	Base oil	-		-15			-12	
1	Multisite-C22	10	-21	-21	-21	-27	-24	-21
2	Multiblock-C22	19	-24	-21	-21	-24	-24	-24
3	Diblock-C22	25	-24	-21	-21	-24	-24	-24
4	Alt_{28}-C22	40	-21	-27	-27	-27	-27	-27
5	Alt_{28}-C12	44	-48	-48	-51	-42	-42	-42
6	Alt_{250}-C22	394	-24	-21	-21	-27	-24	-12
7	Alt_{250}-C12	419	-48	-45	-48	-36	-39	-39
8	$4xAlt_{60}$-C12	364	-45	-48	-48	-39	-42	-42
9	$PLaurylAc_{60}$	52	-36	-36	-30	-36	-36	-27
LZPP3	PSMA	-	-45	-45	-45	-33	-36	-36

5.3.2.1 Influence of the grafting density and distribution

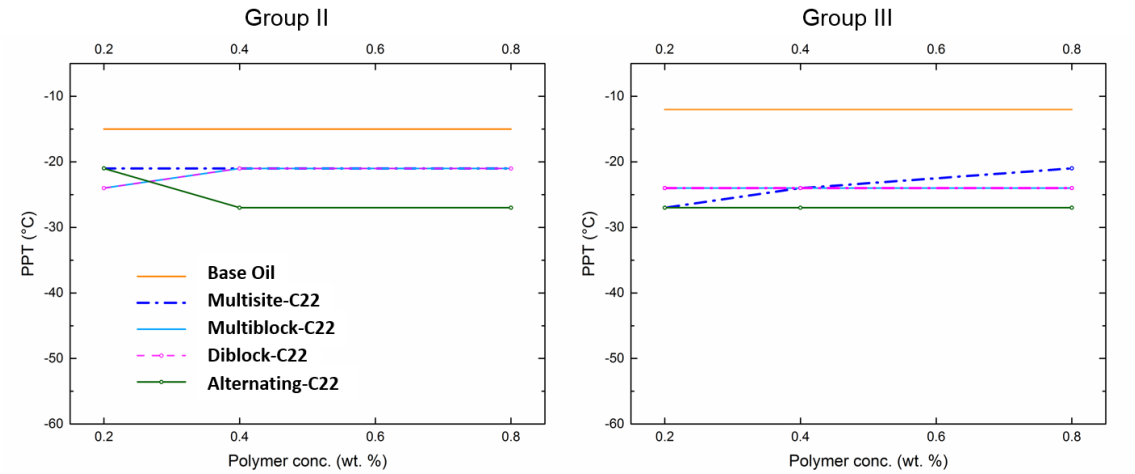

Figure 5.1. Pour point results for grafted (C22) PSMA materials of similar backbone length (5-6k g mol^{-1}) with different structure and composition measured in two different oil groups (II and III).

The PSMA materials with different structures (multisite, multiblock, diblock and alternating) functionalised with behenyl (C22) alcohol (Table 5.1 - Entry 1-4), were all shown to decrease the pour point of both oils to values between - 20 °C and - 30 °C (Figure 5.1). In oil group II, the alternating material (higher density of side chains) appeared to be slightly more efficient (ΔPPT -12 °C) compared to materials with lower side chain density (Table 5.2 –Entry 1-4). The higher number of long alkyl side chains potentially facilitates the co-crystallisation or adsorption of PPDs with paraffin chains resulting in an improved activity of alternating materials. Moreover, the increasing content of styrene in structures with lower side chain density might influence the PPD solubility resulting in lower efficiency as polystyrene is barely soluble in oil. In oil group III, similar results were obtained for all materials with a slightly better activity noticed for both alternating and multisite materials at low polymer concentration (ΔPPT -15 °C). While the grafting density and distribution seems to have less impact in oil group III, the alternating materials appeared to be efficient in both oils. The distance between pendent chains in graft copolymers was previously mentioned as a potential factor to improve PPD efficiency.[36] From our series of experiments, it appeared that the material with higher grafting density (short spacing) was slightly more efficient, confirming an influence of this criterion. Because no obvious positive contribution was observed by spacing the side chains, and because their synthesis is more straightforward (one-step), further experiments were focused on alternating PSMA materials.

5.3.2.2 Influence of the backbone length and alkyl side chain length

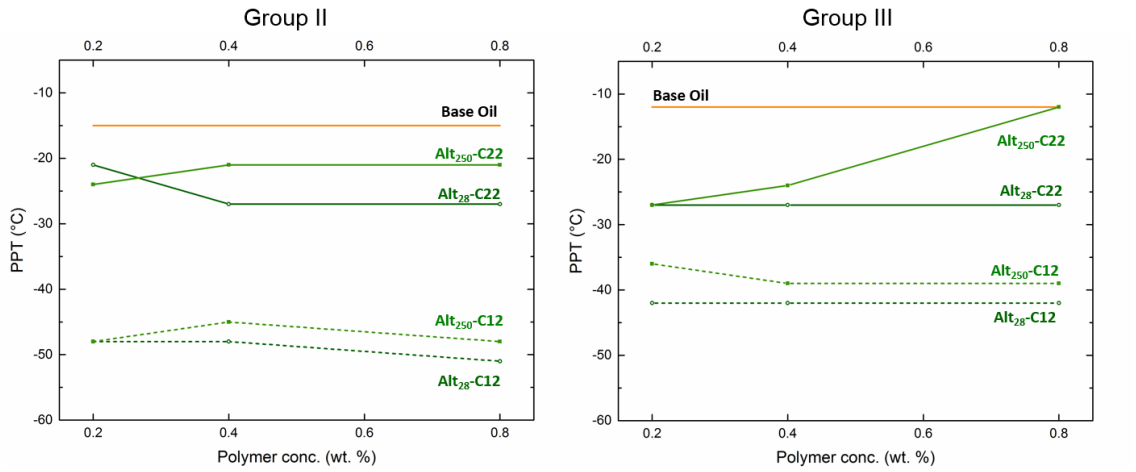

Figure 5.2. Pour point results for alternating PSMA (DP = 28 *vs.* DP = 250) of different backbone length (5k *vs.* 50k g mol^{-1}, respectively) grafted with either lauryl (C12) or behenyl (C22) side chain, measured in two different oil groups (II and III).

Alternating PSMA materials with different side chain length (C12 *vs.* C22) and larger overall molar mass (> 100k g mol^{-1}) were tested. A greater depressing activity was obtained for shorter side chains (ΔPPT -36 °C in group II and ΔPPT -30 °C in group III), however, increasing the overall molar mass seemed to have minor impact on their activity. These results were in good agreement with previous studies on lubricating oil and diesel fuels where better depressing activity was observed with shorter alkyl side chain polymers.[36, 39, 40] The lower ability of crystallisation of shorter side chains is hypothesised to reduce wax crystal formation while increasing the additive solubility and promoting the interaction with paraffin chains in solution. Interestingly, a different trend is observed in crude oil (higher paraffin content), as longer side chains (>C18) were shown to increase the depressing activity.[4, 30] These observations confirmed the dependence of depressing activity with respect to many factors, such as n-paraffin details (content and composition) and polymer additive features (composition, molar mass and pendant chain nature).

5.3.2.3 Influence of the architecture and aromatic groups

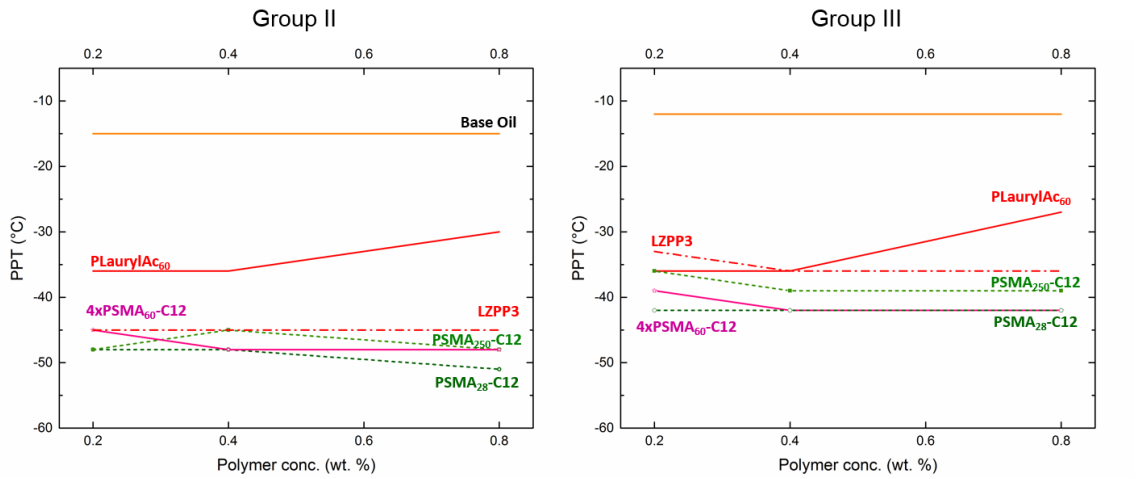

Figure 5.3. Pour point results for alternating PSMA (DP = 28 *vs.* DP = 250 *vs.* 4xDP = 60) grafted with lauryl (C12) side chain, PLaurylAc (DP = 60), and Lubrizol internal reference (LZPP3) measured in two different oil groups (II and III).

To study the influence of more compact architectures on lubricant properties, a star PSMA material was tested. Interestingly, the 4xPSMA exhibited good depressing activity but showed no major improvement compared to its linear analogue (ΔPPT -33 °C in group II and ΔPPT -30 °C in group III) (Figure 5.3). The high density of chains and the steric hindrance near to the core might reduce interaction of side chains with free paraffin chains in the core, resulting in no improvement compared to linear analogues. However, because star materials are usually more compact materials (lower IV) and exhibit better activity as viscosity modifiers (higher VI, better shear stability), the results were encouraging. In order to study the benefit of aromatic groups in the structure, a polylaurylacrylate with comparable molar mass to the linear PSMA grafted with lauryl side chains was also tested. The PLaurylAc homopolymer was shown to improve the pour point of both oils (ΔPPT -21 °C in group II and ΔPPT -24 °C in group III), however, a lower depressing activity was obtained compared to materials containing styrene in their composition. This confirms the benefit of having aromatic groups in the molecular structure of pour point depressants. This was previously reported and explained by the ability of these groups to interact (π-π stacking) with aromatic compounds present in various oils (asphaltenes).[3, 41] In fact, nucleation with these large aromatic groups can provide local defects in the structure, preventing the formation of strong interpenetrating networks. The comparison

of PSMA materials functionalised with lauryl side chains with a Lubrizol internal reference additive (LZPP3) showed relatively high efficiency of these materials as PPDs (Figure 5.3 - Table 5.2).

5.3.3 Rheology study

All the synthesised polymeric materials showed promising activity as pour point depressants, however, controlling other properties such as viscosity index and thickening efficiency is also required to optimise lubricant formulation. The viscosity index and thickening efficiency were determined for polymer–oil blends at different concentrations (0.4-0.8% equal active concentration) in group oil II and III (Table 5.3). In both oils, an increase of VI and TE correlating with the molar mass of PSMA additives was observed (Entry 1-2 *vs.* 3-4). This is usually explained by the expansion of solvated additives (increase of molecular size) occurring when temperature increases, counterbalancing the drop of oil viscosity at high temperature by thickening effects.[32]

Table 5.3. Rheology data for tested materials

Entry	Materials	Conc. %wt.	Oil Group II				Oil Group III			
			KV40 (cSt)	KV100 (cSt)	VI	TE	KV40 (cSt)	KV100 (cSt)	VI	TE
0	Oil only	100	19.80	4.12	108	-	19.23	4.25	129	-
1	Alt_{28}-C12 (19k g mol^{-1})	0.4	19.99	4.17	111	1.6	19.41	4.27	128	0.5
2		0.8	20.41	4.22	111	1.4	19.68	4.32	130	0.9
3	Alt_{250}-C12 (133k g mol^{-1})	0.4	20.51	4.26	113	3.9	19.82	4.37	133	3.0
4		0.8	21.14	4.40	119	3.7	20.37	4.5	138	3.1
5	4xAlt_{60}-C12 (138k g mol^{-1})	0.4	20.35	4.23	112	3.1	19.76	4.35	132	2.6
6		0.8	20.97	4.36	117	3.2	20.39	4.50	137	3.1
7	$PLaurylAc_{60}$ (18k g mol^{-1})k	0.4	20.08	4.15	108	0.9	19.38	4.33	135	1.9
8		0.8	20.17	4.19	111	1.0	19.62	4.30	129	0.6
LZPP3	PSMA	0.4	20.79	4.33	117	5.6	20.13	4.44	135	4.7
LZPP3		0.8	21.97	4.60	127	6.1	21.16	4.69	145	5.3

Moreover, the increase of additive concentration also increases the total volume of solvated polymer leading to better thickening effects. In this study, increasing the concentration of additives was shown to increase the VI, especially for high molar mass materials (Entry 1 *vs.* 2, 3 *vs.* 4 and 5 *vs.* 6), however, no significant effect on TE was observed on this range of concentration. Interestingly, the especially low kinematic viscosity results for short PSMA (low TE) compared to LZPP3 (Entry 1-2 vs. LZPP3), coupled with the good pour point results from Table 5.2, give an added benefit for formulations that require low viscosity grades (*e.g.* 0W-16/8). The comparison between the linear and the 4xPSMA of similar molar mass showed slightly lower VI and TE values for the star material (Entry 3-4 *vs.* 5-6). This was expected as the expansion of a star material is limited compared to its linear analogue, as shown previously from the intrinsic viscosity and Mark-Houwink parameter values in chloroform (Table 5.1). While the molar mass of polymeric additives was found to have only a minor impact on pour point depressing activity, it is now clear that controlling molar mass is essential to improve the rheological properties of the final lubricant. Moreover, in contrast with the pour point results, the presence of styrene in the additive composition did not show significant improvement, as similar VI and TE were obtained for PSMA and polylaurylacrylate of similar size (Entry 1-2 *vs.* 7-8). When compared to an internal reference from Lubrizol (LZPP3), these materials showed promising results pushing for more investigation on well-defined polymeric systems as lubricant oil additives.

5.4 Conclusion

In this chapter, well-defined graft copolymers (PSMA and polylaurylacrylate) were exploited to study the influence of additive composition, grafting density and distribution, molar mass, and side chain length on pour point, viscosity index and thickening efficiency of two mineral oils. While all the materials were shown to improve the pour point, the best pour point depressant activity was obtained for materials with higher density of side chains (alternating PSMA), with an improvement of 36 °C in group II and 30 °C in group III (PPT= -51 °C and PPT= -42 °C, respectively). The depressing activity was shown to be independent of the molar mass, however, the use of shorter aliphatic side chains (lauryl - C12) offered the best efficiency for both oils. While the molar mass of the polymeric additives did not seem to influence the pour point, high molar mass materials were shown to have more impact on the viscosity index and thickening efficiency of the two mineral oils. Moreover, the presence of styrene in the structure was shown to be highly desirable to improve the pour point, however, no effect on VI and TE was observed. According to the present results, the use of alternating PSMA materials with short side chains (C12) is recommended to improve the pour point of lubricating oil from group II and III. Moreover, varying the molar mass of the materials is suggested to control the viscosity of the final formulation. The use of compact architectures (star) seems also beneficial, however, the production of those materials is more challenging.

5.5 Experimental

5.5.1 Materials

Laurylacrylate (LaurylAc, 90 %) were obtained from Sigma-Aldrich and passed through neutral alumina prior to use to remove inhibitor. 1,1'-Azobis(cyclohexane-1-carbonitrile) (V-40, $T_{1/2\text{-}10h}$ = 88 °C, 98 %), pentaerythritol (99 %) and methane sulfonic acid (MSA, 70 wt. % in H_2O) were obtained from Sigma-Aldrich and used as received. Industrial grade CTA-Ester (≈ 80 % pure), CTA-Acid (> 95 % pure), lauryl and behenyl alcohols were generously provided by Lubrizol and used without purification.[42, 43] All solvents were obtained from either Fisher Scientific or Sigma-Aldrich and used as received. Mineral oils were provided by Lubrizol (Chevron and SK Lubricants).

5.5.2 Mineral oils compositions

Properties	Oil group II	Oil group III
Origin	Chevron	SK Lubricants
Reference	100N	100N
Density (g cm^{-3}) at 15.6°C	0.848	0.833
Viscosity at 40 °C in cSt	19.80	19.23
Viscosity at 100 °C in cSt	4.12	4.25
Viscosity Index	108	129
Pour point (°C)	-15	-12

5.5.3 Preparation of polymeric additives

5.5.3.1 PSMA materials synthesis and characterisation

All the PSMA materials were prepared by RAFT polymerisation using industrial CTA-Ester or 4xCTA-Ester following a method described in previous chapter.

5.5.3.2 PSMA materials esterification

The esterification method to prepare PSMA materials with behenyl side chains (C22) was described in a previous chapter. PSMAs with lauryl side chains (C12) were prepared following a similar method by reacting the pure PSMA copolymer (DP =250, 3.0 g, 0.06 mmol with long aliphatic alcohol ($C_{12}OH$, 16.6 g, 88 mmol, 6 equiv. / MAnh) in the presence of methane sulfonic acid (MSA) catalyst (1.1 g, 8.8 mmol, 0.1M equiv. / alcohol). The esterification was carried out using Dean-Stark apparatus under reflux of toluene (≈ 70 wt. %). After reaction (*ca.* 20 hours), the mixture was precipitated several times in cold methanol and isopropyl alcohol from a minimum amount of diethyl ether. The precipitate was dried in an oven and recovered as an off-yellow solid (mass recovered = 10 g). The graft copolymer was characterised using infrared spectroscopy (IR), quantitative ^{1}H-NMR and ^{13}C-NMR spectroscopy and SEC (yield = 93 %, $M_{n,calc}$ = 128,900 g mol^{-1}, $M_{n,3d\text{-}SEC\text{-}CHCl3}$ =133,000 g mol^{-1}and $Đ_{RI}$ = 1.28).

5.5.3.3 Polylaurylacrylate (DP =60)

The polylaurylacrylate was synthesised following a typical RAFT polymerisation procedure using industrial grade CTA-Ester without purification. Laurylacrylate (8 g, 30 mmol), CTA-Ester (0.26 g, 0.5 mmol), V601 (0.01 g, 0.045 mmol) and toluene (19.6 mL) were introduced into a vial equipped with a magnetic stirrer bar and sealed with a rubber septum. The solution was degassed using nitrogen (*ca.* 15 min) before being placed in a thermostated oil bath set at 65 °C. After reaction completion (*ca.* 20 hours), the mixture was allowed to cool down at room temperature and then purified by precipitation in cold methanol (mass recovered = 6.8 g). The copolymer was characterised using ^{1}H-NMR spectroscopy and SEC (monomer conversion = 87 %, $M_{n,theo}$ = 13,000 g mol^{-1}, $M_{n,3d\text{-}SEC\text{-}CHCl3}$ = 17,700 g mol^{-1}and $Đ_{RI}$ = 1.30).

5.5.4 Polymer materials characterisation

The monomer conversion (conv.), theoretical molar mass ($M_{n,theo}$), and esterification yield were determined using NMR and IR spectroscopy in the same conditions and following the same methodology presented in chapter 4. The average number molar mass ($M_{n,RI}$), dispersity ($Đ_{RI}$), the true molar mass ($M_{n,3d\text{-}SEC}$), intrinsic viscosity (IV), radius of gyration (R_g), hydrodynamic radius (R_h), Mark-Houwink parameter (α) and conformation data were determined by SEC (conventional or triple-detection) using similar parameters and refractive index increments values (dn/dc) as presented in chapter 4 (Table 4.4).

5.5.5 Pour point measurements

The polymer additives were mixed with mineral oils at different concentrations (0.2, 0.4, and 0.8 wt. %) and blended prior to measuring the pour point using a standard method (ASTM D5950 Automated Tilt). The instrument was run using 3 °C intervals between the range of -54 °C to +51 °C.

5.5.6 Rheology investigations (viscosity index and thickening efficiency)

The kinematic viscosity (KV) of the different formulations was measured using a capillary viscometer (Houillon viscometer VH1 – Integrated Scientific LTD) following a standard method (ASTM D7279). The viscosity/temperature relationship, or Viscosity Index (VI), was calculated using the standard method ASTM D2270 by measuring the kinematic viscosity values measured at 40 °C and 100 °C (KV40 and KV100).

The thickening efficiency (TE) is a unitless number used by oil companies to describe the benefit in viscosity at 100 °C of an oil (boost in KV100) after addition of a known amount of polymer. The TE gives an indication of the quantity of polymer required to reach a desired viscosity. The higher the TE, the lower amount of polymer is required (cost saving). Generally, polymers with higher molar mass exhibit greater thickening efficiency, however, the benefit (cost saving) is usually counterbalanced by low shear stability of these polymers, thus leading to loss in durability of the fluid.

The TE was calculated using the following equation 5.1:

$$TE = \frac{\log(KV100_{measured}/KV100_{oil})}{\%\ wt.Polymer} \times 100 \qquad 5.1$$

5.6 References

(1) Kelland, M. A., *Production chemicals for the oil and gas industry*. CRC Press, **2014**.
(2) Binks, B. P.; Fletcher, P. D. I.; Roberts, N. A.; Dunkerley, J.; Greenfield, H.; Mastrangelo, A.; Trickett, K. How polymer additives reduce the pour point of hydrocarbon solvents containing wax crystals. *PCCP* **2015**, 17 (6), 4107-4117.
(3) Wu, Y.; Ni, G.; Yang, F.; Li, C.; Dong, G. Modified Maleic Anhydride Co-polymers as Pour-Point Depressants and Their Effects on Waxy Crude Oil Rheology. *Energy Fuels* **2012**, 26 (2), 995-1001.
(4) Al-Sabagh, A. M.; Noor El-Din, M. R.; Morsi, R. E.; Elsabee, M. Z. Styrene-Maleic Anhydride Copolymer Esters as Flow Improvers of Waxy Crude Oil. *J. Disp. Sci. Technol.* **2009**, 30 (3), 420-426.
(5) Al-Sabagh, A. M.; Noor El-Din, M. R.; Morsi, R. E.; Elsabee, M. Z. Styrene-maleic anhydride copolymer esters as flow improvers of waxy crude oil. *J. Pet. Sci. Eng.* **2009**, 65 (3), 139-146.
(6) Roenningsen, H. P.; Bjoerndal, B.; Baltzer Hansen, A.; Batsberg Pedersen, W. Wax precipitation from North Sea crude oils: 1. Crystallization and dissolution temperatures, and Newtonian and non-Newtonian flow properties. *Energy Fuels* **1991**, 5 (6), 895-908.
(7) Holder, G. A.; Winkler, J. Crystal-Growth Poisoning of n-Paraffin Wax By Polymeric Additives and its Relevance to Polymer Crystallization Mechanisms. *Nature* **1965**, 207 (4998), 719.
(8) Yang, F.; Zhao, Y.; Sjöblom, J.; Li, C.; Paso, K. G. Polymeric Wax Inhibitors and Pour Point Depressants for Waxy Crude Oils: A Critical Review. *J. Disp. Sci. Technol.* **2015**, 36 (2), 213-225.
(9) Al-Sabagh, A. M.; El-Hamouly, S. H.; Khidr, T. T.; El-Ghazawy, R. A.; Higazy, S. A. Preparation the Esters of Oleic Acid-Maleic Anhydride Copolymer and Their Evaluation as Flow Improvers for Waxy Crude Oil. *J. Disp. Sci. Technol.* **2013**, 34 (11), 1585-1596.
(10) Taraneh, J. B.; Rahmatollah, G.; Hassan, A.; Alireza, D. Effect of wax inhibitors on pour point and rheological properties of Iranian waxy crude oil. *Fuel Process. Technol.* **2008**, 89 (10), 973-977.
(11) Marie, E.; Chevalier, Y.; Eydoux, F.; Germanaud, L.; Flores, P. Control of n-alkanes crystallization by ethylene–vinyl acetate copolymers. *J. Colloid Interface Sci.* **2005**, 290 (2), 406-418.
(12) Ashbaugh, H. S.; Guo, X.; Schwahn, D.; Prud'homme, R. K.; Richter, D.; Fetters, L. J. Interaction of Paraffin Wax Gels with Ethylene/Vinyl Acetate Co-polymers. *Energy Fuels* **2005**, 19 (1), 138-144.
(13) Machado, A. L. C.; Lucas, E. F.; González, G. Poly(ethylene-co-vinyl acetate) (EVA) as wax inhibitor of a Brazilian crude oil: oil viscosity, pour point and phase behavior of organic solutions. *J. Pet. Sci. Eng.* **2001**, 32 (2), 159-165.
(14) Radulescu, A.; Schwahn, D.; Stellbrink, J.; Kentzinger, E.; Heiderich, M.; Richter, D.; Fetters, L. J. Wax Crystallization from Solution in Hierarchical Morphology Templated by Random Poly(ethylene-co-butene) Self-assemblies. *Macromolecules* **2006**, 39 (18), 6142-6151.
(15) Ashbaugh, H. S.; Radulescu, A.; Prud'homme, R. K.; Schwahn, D.; Richter, D.; Fetters, L. J. Interaction of Paraffin Wax Gels with Random Crystalline/Amorphous Hydrocarbon Copolymers. *Macromolecules* **2002**, 35 (18), 7044-7053.
(16) Guo, X.; Pethica, B. A.; Huang, J. S.; Prud'homme, R. K.; Adamson, D. H.; Fetters, L. J. Crystallization of mixed paraffin from model waxy oils and the influence of micro-crystalline poly (ethylene-butene) random copolymers. *Energy Fuels* **2004**, 18 (4), 930-937.
(17) El-Gamal, I. M.; Gobiel, S. Synthesis and evaluation of poly - α - olefins for improving the flow properties of gas oil. *J. Appl. Polym. Sci.* **1996**, 61 (8), 1265-1272.
(18) Al-Sabagh, A. M.; Khidr, T. T.; Moustafa, H. Y.; Mishrif, M. R.; Al-Damasy, M. H. Synergistic effect between surfactants and polyacrylates-maleicanhydride copolymers to improve the flow properties of waxy crude oil. *J. Disp. Sci. Technol.* **2017**, 38 (7), 1055-1062.
(19) Ding, X.; Qi, G.; Yang, S. Thermodynamic analysis for the interaction of polyacrylate with wax in heptane. *Polymer* **1999**, 40 (14), 4139-4142.
(20) Song, Y.; Han, S.; Ren, T. Impact of Alkyl Methacrylate-Maleic Anhydride Copolymers as Pour Point Depressant on Crystallization Behavior of Simulated Diesel Fuel. *Pet. Sci. Technol.* **2010**, 28 (8), 860-867.
(21) Soldi, R. A.; Oliveira, A. R. S.; Barbosa, R. V.; César-Oliveira, M. A. F. Polymethacrylates: Pour point depressants in diesel oil. *Eur. Polym. J.* **2007**, 43 (8), 3671-3678.
(22) Al-Sabagh, A. M.; Sabaa, M. W.; Saad, G. R.; Khidr, T. T.; Khalil, T. M. Synthesis of polymeric additives based on itaconic acid and their evaluation as pour point depressants for lube oil in relation to rheological flow properties. *Egypt. J. Pet.* **2012**, 21 (1), 19-30.
(23) Soni, H. P.; Kiranbala; Agrawal, K. S.; Nagar, A.; Bharambe, D. P. Designing maleic anhydride-α-olifin copolymeric combs as wax crystal growth nucleators. *Fuel Process. Technol.* **2010**, 91 (9), 997-1004.

(24) Chen, W.; Zhao, Z.; Yin, C. The interaction of waxes with pour point depressants. *Fuel* **2010**, 89 (5), 1127-1132.
(25) Azevedo, L. F. A.; Teixeira, A. M. A Critical Review of the Modeling of Wax Deposition Mechanisms. *Pet. Sci. Technol.* **2003**, 21 (3-4), 393-408.
(26) Pedersen, K. S.; Rønningsen, H. P. Influence of Wax Inhibitors on Wax Appearance Temperature, Pour Point, and Viscosity of Waxy Crude Oils. *Energy Fuels* **2003**, 17 (2), 321-328.
(27) Castro, L. V.; Vazquez, F. Copolymers as Flow Improvers for Mexican Crude Oils. *Energy Fuels* **2008**, 22 (6), 4006-4011.
(28) Yao, B.; Li, C.; Zhang, X.; Yang, F.; Sun, G.; Zhao, Y. Performance improvement of the ethylene-vinyl acetate copolymer (EVA) pour point depressant by small dosage of the amino-functionalized polymethylsilsesquioxane (PAMSQ) microsphere. *Fuel* **2018**, 220, 167-176.
(29) Lemos, B. C.; Gilles, V.; Gonçalves, G. R.; de Castro, E. V. R.; Delarmelina, M.; Carneiro, J. W. M.; Greco, S. J. Synthesis, structure-activity relationship and evaluation of new non-polymeric chemical additives based on naphthoquinone derivatives as wax precipitation inhibitors and pour point depressants to petroleum. *Fuel* **2018**, 220, 200-209.
(30) Wei, B. Recent advances on mitigating wax problem using polymeric wax crystal modifier. *J. Petrol. Explor. Prod. Technol.* **2014**, 5 (4), 391-401.
(31) Tinsley, J. F.; Jahnke, J. P.; Adamson, D. H.; Guo, X.; Amin, D.; Kriegel, R.; Saini, R.; Dettman, H. D.; Prud'home, R. K. Waxy Gels with Asphaltenes 2: Use of Wax Control Polymers. *Energy Fuels* **2009**, 23 (4), 2065-2074.
(32) Ghosh, P.; Hoque, M.; Karmakar, G.; Das, M. K. Dodecyl methacrylate and vinyl acetate copolymers as viscosity modifier and pour point depressant for lubricating oil. *Int. J. Ind. Chem.* **2017**, 8 (2), 197-205.
(33) Al-Sabagh, A. M.; Khidr, T. T.; Moustafa, H. M.; Mishrif, M. R.; Al-Damasy, M. H. Investigating the synergistic effect between oil soluble surfactants and styrene–maleic anhydride copolymers to enhance the flow properties of waxy crude oil. *Pet. Sci. Technol.* **2017**, 35 (13), 1381-1388.
(34) Cao, K.; Wei, X.-x.; Li, B.-j.; Zhang, J.-s.; Yao, Z. Study of the Influence of Imidization Degree of Poly(styrene-co-octadecyl maleimide) as Waxy Crude Oil Flow Improvers. *Energy Fuels* **2013**, 27 (2), 640-645.
(35) Xu, J.; Qian, H.; Xing, S.; Li, L.; Guo, X. Synthesis of Poly(maleic acid alkylamide-co-α-olefin-co-styrene) Co-polymers and Their Effect on the Yield Stress and Morphology of Waxy Gels with Asphaltenes. *Energy Fuels* **2011**, 25 (2), 573-579.
(36) Al-Sabagh, A. M.; Khalil, T. M.; Sabaa, M. W.; Khidr, T. T.; Saad, G. R. Poly(n-Alkyl Itaconate-Co-Vinyl Acetate) as Pour Point Depressants for Lube Oil in Relation to Rheological Flow Properties. *J. Disp. Sci. Technol.* **2012**, 33 (11), 1649-1660.
(37) Agilent, *A guide to multi-detector gel permeation chromatography.* **2012**, 5990-7196EN, 1-24.
(38) Striegel, A. M. Multiple Detection in Size-Exclusion Chromatography of Macromolecules. *Anal. Chem.* **2005**, 77 (5), 104-113.
(39) Xu, G.; Xue, Y.; Zhao, Z.; Lian, X.; Lin, H.; Han, S. Influence of poly (methacrylate-co-maleic anhydride) pour point depressant with various pendants on low-temperature flowability of diesel fuel. *Fuel* **2018**, 216, 898-907.
(40) Song, Y.; Ren, T.; Fu, X.; Xu, X. Study on the relationship between the structure and activities of alkyl methacrylate–maleic anhydride polymers as cold flow improvers in diesel fuels. *Fuel Process. Technol.* **2005**, 86 (6), 641-650.
(41) Soni, H. P.; Kiranbala; Bharambe, D. P. Performance-Based Designing of Wax Crystal Growth Inhibitors. *Energy Fuels* **2008**, 22 (6), 3930-3938.
(42) Lai, J. T.; Filla, D.; Shea, R. Functional Polymers from Novel Carboxyl-Terminated Trithiocarbonates as Highly Efficient RAFT Agents. *Macromolecules* **2002**, 35 (18), 6754-6756.
(43) Brzytwa, A. J.; Johnson, J. Scaled Production of RAFT CTA–a STAR Performer. *Polym. Prepr. (Am. Chem. Soc., Div. Polym. Chem.)* **2011**, 52 (2), 533-534.

Chapter 6 Conclusion

The overall aim of this thesis was to exploit RAFT polymerisation technology to synthesise well-defined graft copolymers *via* a scalable route and study their potential for application as oil and lubricant additives.

This was achieved by adapting the RAFT process to industrial conditions (industrial grade CTA and one-pot process) and by using a comonomer system of interest for Lubrizol (polystyrene-*co*-maleic anhydride or PSMA). A library of well-defined PSMA materials grafted with long aliphatic side chains (lauryl and behenyl) was achieved using optimised RAFT process and post-polymerisation functionalisation. The influence of side chain density and distribution on material properties (thermal, solution) was confirmed and the performance of graft PSMA materials as lubricant additives demonstrated (pour point depressants and viscosity modifiers).

In chapter 2, the industrial RAFT agent (CTA-Ester) produced in metric tons by Lubrizol was investigated. The purity of the industrial grade CTA-Ester was determined and the main impurities identified. The RAFT agent performances were determined experimentally by measuring the chain transfer constant and by studying the kinetics of polymerisation for styrene and methacrylates (methyl and lauryl) monomers in solution. CTA-Ester was found efficient for the controlled polymerisation of styrene ($C_{tr}^{app} = 27$), however, poor control was obtained for methacrylate monomers ($C_{tr}^{app} < 1$). The use of different CTAs (with cyano-alkyl R group) or process optimisation (feeding) was proposed as a good alternative to achieve RAFT polymerisation of methacrylates. Considering the excellent efficiency of industrial grade CTA-Ester for styrene polymerisation, the experimental conditions for the synthesis of a DP =10 polystyrene macroCTA were optimised. To allow the chain extension strategy developed in chapter 3 to perform in the best conditions, a macroCTA with controlled molar mass, narrow dispersity and high livingness was prepared.

The main objective of chapter 3 was the synthesis of a well-defined graft PSMA material with low density of side chains compared to traditional alternating PSMA materials. A one-pot sequential monomer addition strategy using previous macroCTA and optimised RAFT conditions was developed. This allowed the preparation of a multisite copolymer composed of a polystyrene backbone (DP = 50) with maleic anhydride units inserted

locally (every 10 units in average). An average of six MAnh units were inserted along the polystyrene backbone as either one local monomeric unit or as short alternating / random blocks with an overall dispersity of 1.35. The composition and structure of the multisite materials were confirmed using several characterisation techniques such as, NMR, SEC and MALDI-ToF-MS. The MAnh moieties were subsequently functionalised with long alkyl chains (C18) yielding graft materials with low density of side chains (12 per polymer chain). By showing the possibility to make a well-defined material with such complex architectures on gram scale using industrial grade CTA-Ester, the great potential of RAFT polymerisation for industrial application was demonstrated.

The optimised RAFT polymerisation developed in chapter 2 and the one-pot sequential monomer extension strategy from chapter 3 were exploited in chapter 4 for the synthesis of various PSMA copolymers allowing the preparation of materials with controlled density and distribution of side chains (linear multisite, multiblock, diblock and alternating) and more complex architectures (alternating star). A tetrafunctional CTA-Ester (4xCTA) was specifically prepared from CTA-Acid (CTA-Ester precursor) giving access to a four arm PSMA star copolymer. To our knowledge, this was the first reported example of a 4xPSMA star prepared by RAFT. The PSMA materials were subsequently functionalised with long alkyl chains (C22), leading to a library of graft copolymers with controlled side-group density and distribution. The influence of copolymer composition and structure, and the effect of long alkyl chain addition were investigated by a variety of analytical techniques (3d-SEC, TGA and DSC) and their effect on the physical and thermal properties of materials demonstrated. For instance, a difference of crystallisation temperature of about 30 °C was observed between the low density multisite material (T_c ≈ 7 °C) and high density alternating material (T_c ≈ 40 °C) illustrating the major impact of controlling the density and distribution of the long aliphatic side chains on PSMA backbones.

Finally, in chapter 5, the well-defined PSMA materials synthesised in the previous chapters (multisite, multiblock, diblock, alternating linear, alternating star) were esterified various alkyl alcohols (lauryl/C12 and behenyl/C22) and investigated as rheology modifiers in two mineral oils (group II and III). The influence of polymer additive composition, grafting density and distribution, molar mass, and side chain length on pour point, viscosity index (VI) and thickening efficiency (TE) were investigated. All the

PSMA materials were shown to improve the pour point with an efficiency depending on material structure and composition. The most promising results with respect to pour point depressant activity were obtained for an alternating structure with lauryl side chains, showing an improvement of 36 °C in group II and 30 °C in group III (PPT= -51 °C and PPT= -42 °C, respectively). While the molar mass was shown to have little impact on pour point, the effect on the viscosity index and thickening efficiency was demonstrated. Moreover, the presence of styrene monomer in the structure was shown to be highly desirable to improve the pour point, however, no effect on VI and TE was observed. The present results suggest the use of alternating PSMA materials with short aliphatic side chains (C12) to improve the pour point of mineral oils from group II and III. Moreover, varying the molar mass of the materials is suggested to control the viscosity of the final formulation. The use of compact architectures (star) seems also beneficial, however, the production of these materials is more challenging.

In this thesis, the potential of RAFT technology for the industrial synthesis of advanced functional materials was demonstrated. The gram scale synthesis of complex PSMA architectures has allowed the preparation of materials with controlled distribution of side chain functionality and the study of their performance as oil and Lubricant additives.

The materials have shown interesting properties and promising performances for this field of application, however, many aspects remain to be explored in this particular field and beyond. In term of materials design and synthesis, the preparation of PSMA copolymers (linear and star) with high or ultra-high molar mass could be of interest for application as rheology modifiers. The investigation of various graft functionalities (*e.g.* branched olefins) could also be beneficial to improve pour point depressing activity. Further investigations varying additive concentrations, oil type, or using final formulation could also help to obtain more reliable results, however, this would require the synthesis of more materials and their functionalisation. Interestingly, with more materials it would be also possible to extend the investigation to other performance testing such as, shear stability, lubricity (friction), anti-wear properties, oxidation stability and corrosion properties.

Besides the benefits brought to the oilfield, the well-defined PSMA materials designed in this thesis could also be of interest for many other areas (*e.g.* biomedical and energy).

Appendix Chapter 1 Introduction

Appendix Chapter 2 CTA-Ester Evaluation

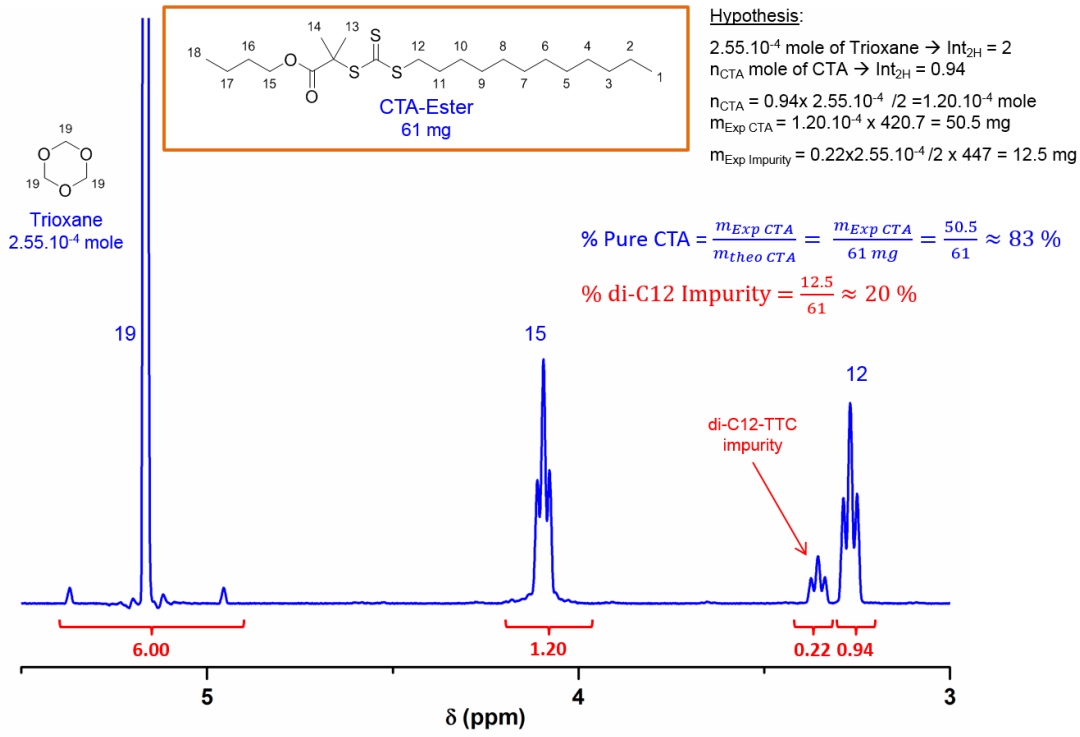

Figure A2-1 ^{1}H-NMR spectrum ($CDCl_3$) of industrial grade CTA-Ester batch used for the synthesis of all materials and purity calculation.

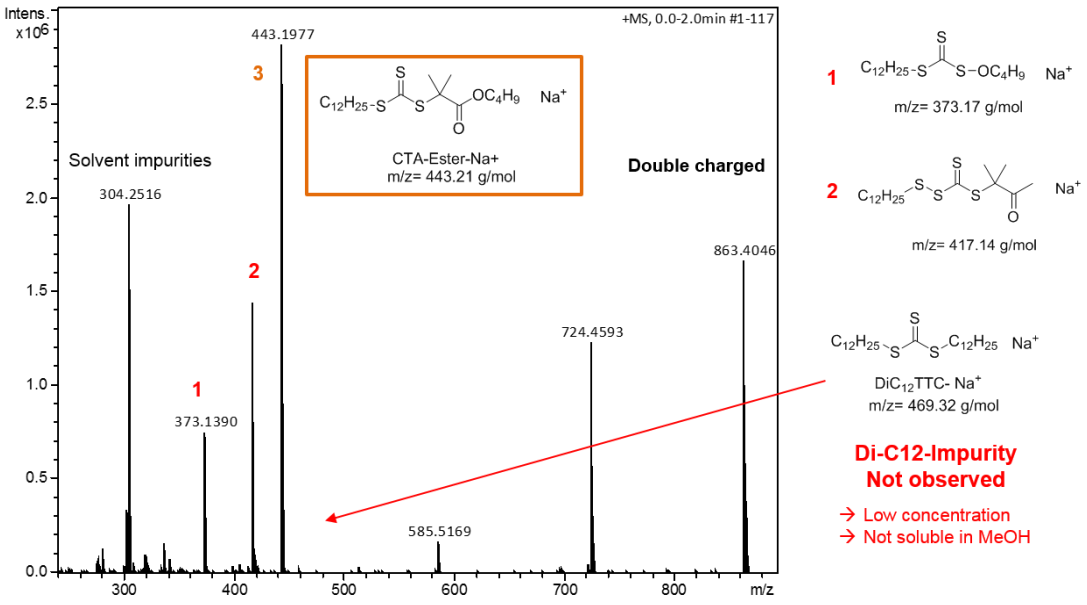

Figure A2-2 ESI-ToF-MS measurements with proposed structures for CTA-Ester mixture purified in acetonitrile.

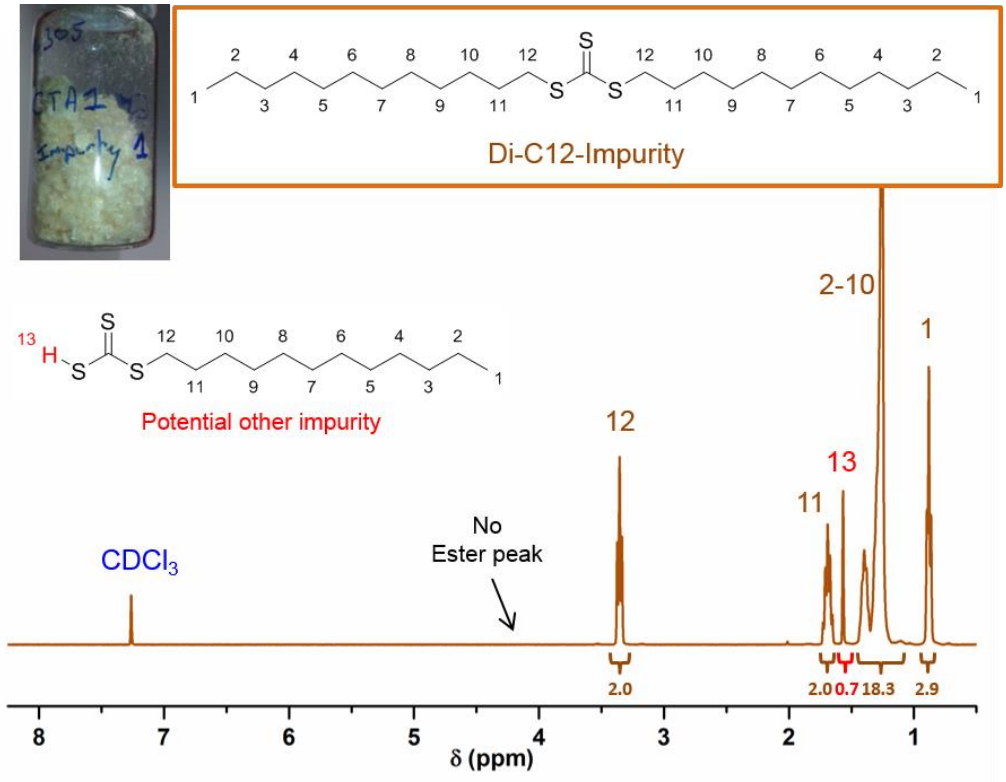

Figure A2-3 ^{1}H-NMR spectrum ($CDCl_3$) for the impurity mixture recovered after recrystallisation in acetonitrile.

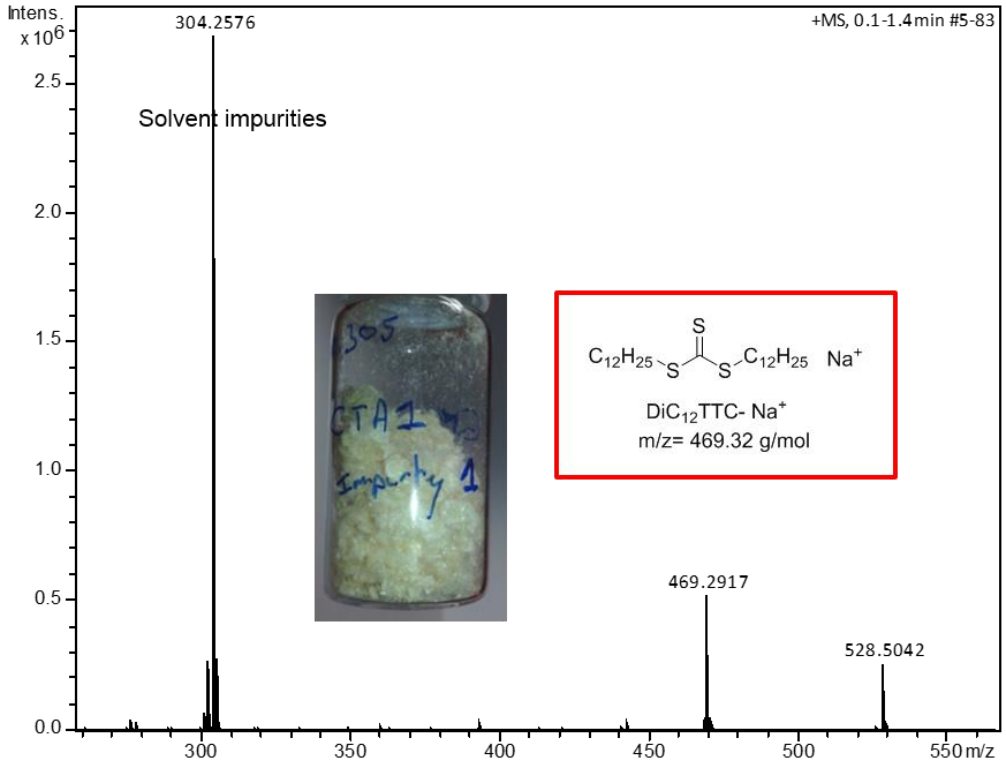

Figure A2-4 ESI-ToF-MS spectrum of the recovered impurity mixture.

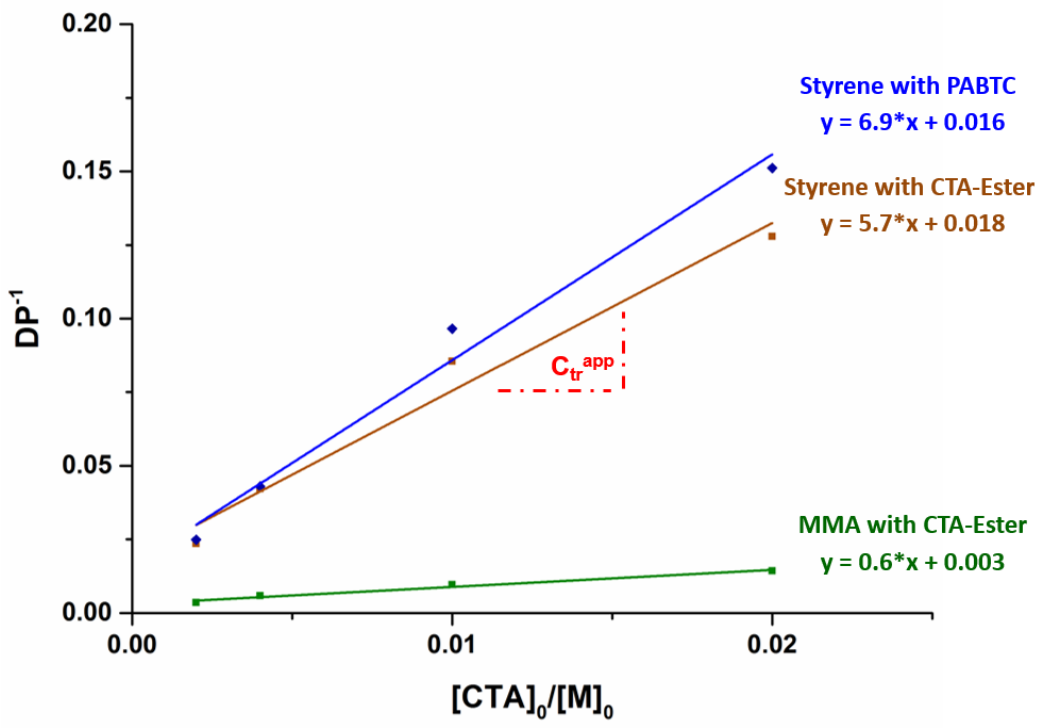

Figure A2-5 Mayo plot for styrene and MMA polymerisation using CTA-Ester (brown for styrene and green for MMA) and styrene polymerisation with PABTC (blue) at 90 °C in bulk.

Appendix Chapter 3 Multisite Synthesis

Table A3-1. Experimental conditions for each steps of multisite synthesis

Copolymers structures	Monomer	[M] (mol L^{-1})	[M] wt%	V_{tot} (mL)	[V-40] (mol L^{-1})	$[CTA]_0/[V\text{-}40]_0$	solvent	T°C	Time (hrs)
$P[Sty]_{10}$	Styrene	5.0	56	10	0.045	11	Toluene	100	15
$P[Sty_{10}\text{-}s\text{-}MAnh_{1.5}]_1$	MAnh	0.6	7	13	0.020	20	Toluene	100	5
$P[(Sty_{10}\text{-}s\text{-}MAnh_{1.5})_1\text{-}b\text{-}PSty_{10}]$	Styrene	2.7	34	19	0.021	13	Toluene	100	15
$P[Sty_{10}\text{-}s\text{-}MAnh_{1.5}]_2$	MAnh	0.3	4	25	0.010	20	Toluene	100	3
$P[(Sty_{10}\text{-}s\text{-}MAnh_{1.5})_2\text{-}b\text{-}PSty_{10}]$	Styrene	1.5	19	34	0.013	11	Toluene	100	15
$P[Sty_{10}\text{-}s\text{-}MAnh_{1.5}]_3$	MAnh	0.2	2	39	0.006	20	Toluene	100	3
$P[(Sty_{10}\text{-}s\text{-}MAnh_{1.5})_3\text{-}b\text{-}PSty_{10}]$	Styrene	1.1	13	48	0.013	8	Toluene	100	17
$P[Sty_{10}\text{-}s\text{-}MAnh_{1.5}]_4$	MAnh	0.2	2	49	0.005	20	Toluene	100	3
$P[(Sty_{10}\text{-}s\text{-}MAnh_{1.5})_4\text{-}b\text{-}PSty_{10}]$	Styrene	0.8	11	61	0.011	7	Toluene	100	15

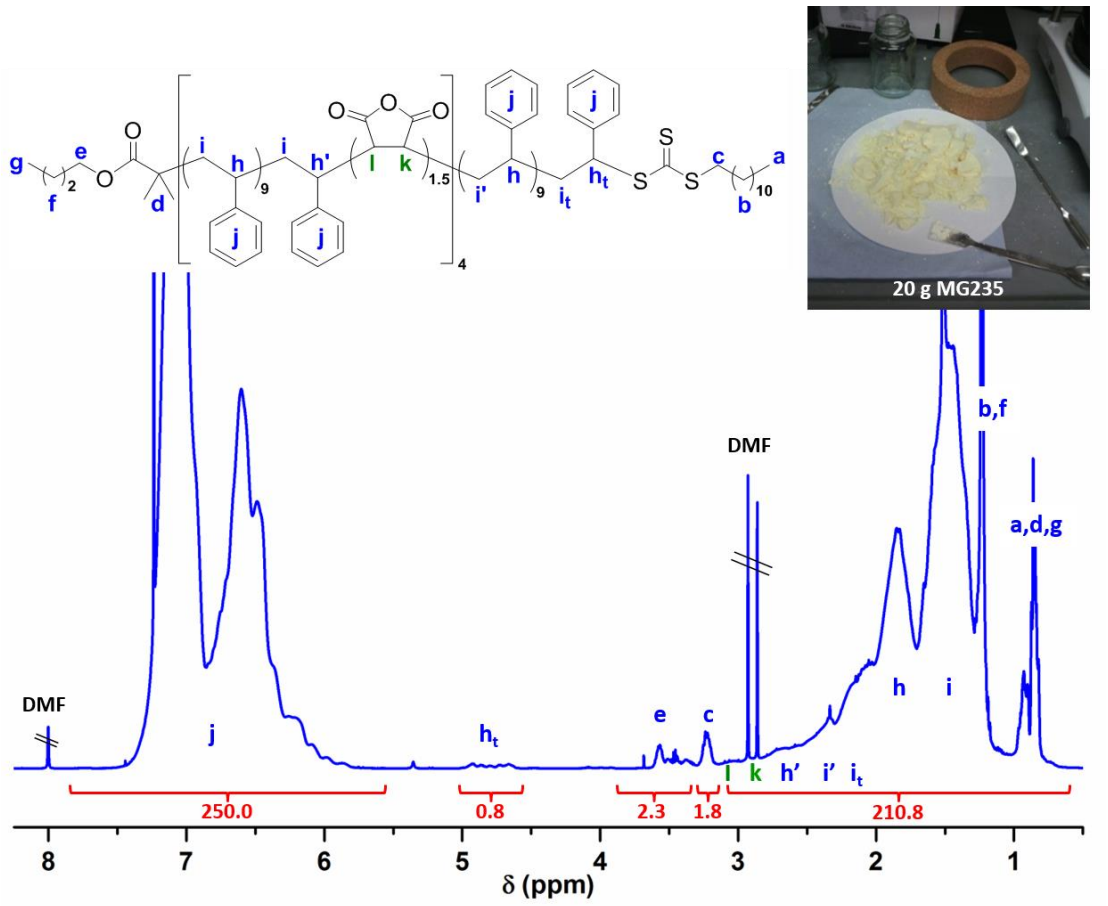

Figure A3-1 ^{1}H-NMR spectrum ($CDCl_3$) of final multisite material after purification in hexane.

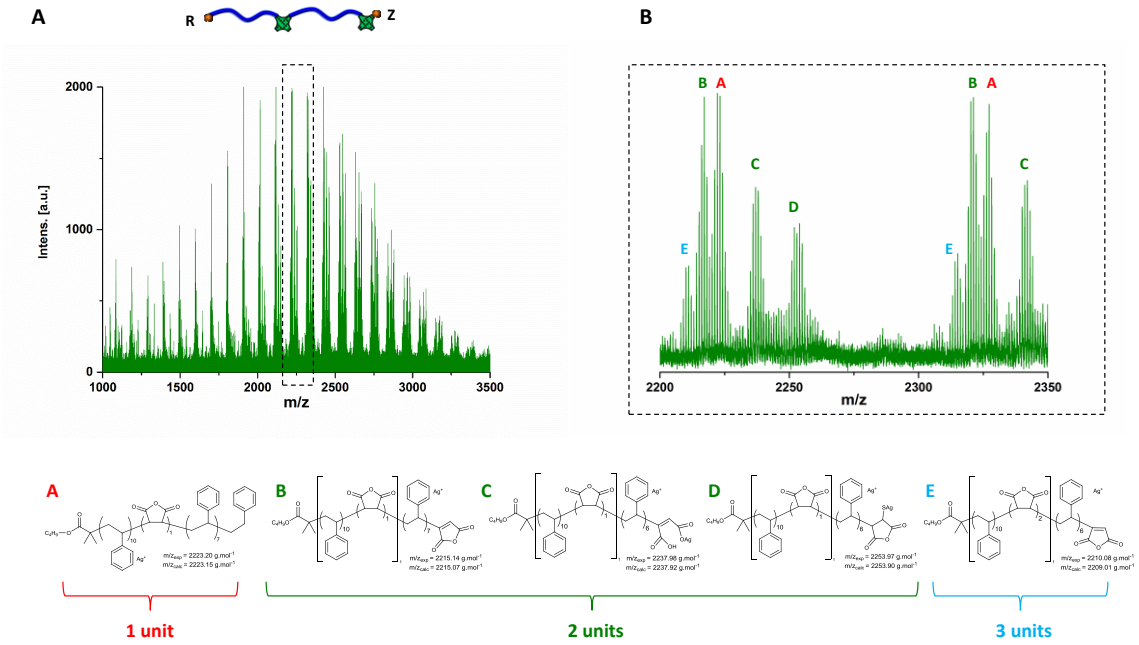

Figure A3-2. A) MALDI-ToF mass spectrum for poly[(Sty$_{10}$-*s*-MAnh$_{1.5}$)]$_2$. B) zoom corresponding to the region in the dashed square in A). Proposed structures below spectrum.

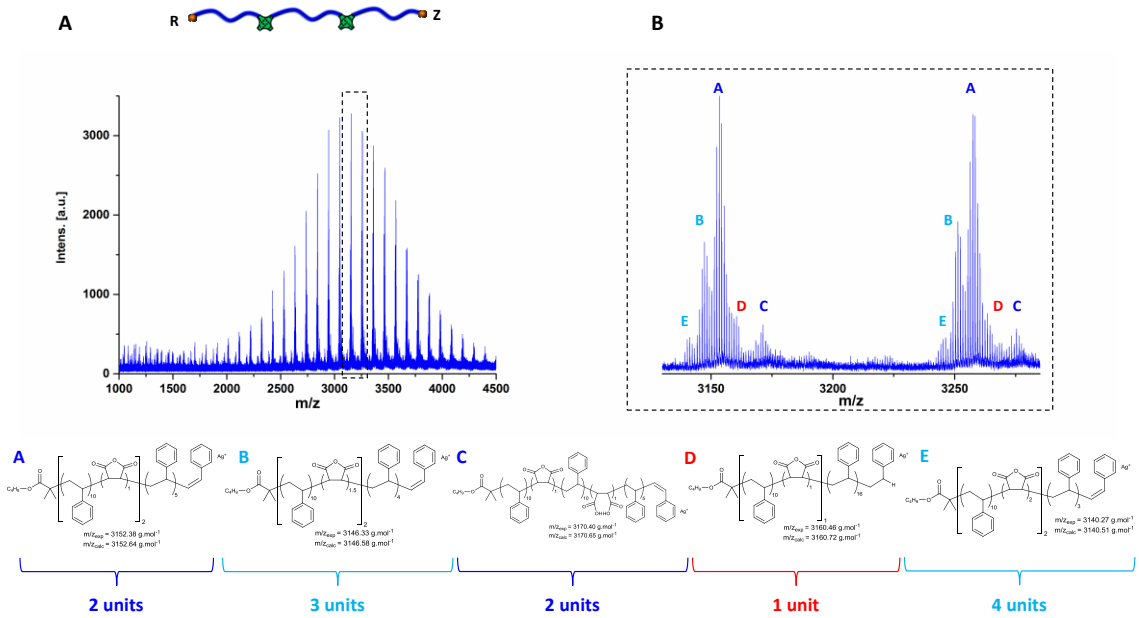

Figure A3-3. A) MALDI-ToF mass spectrum for poly[(Sty$_{10}$-*s*-MAnh$_{1.5}$)$_2$-*b*-PSty$_{10}$] B) zoom corresponding to the region in the dashed square in A).Proposed structures below spectrum.

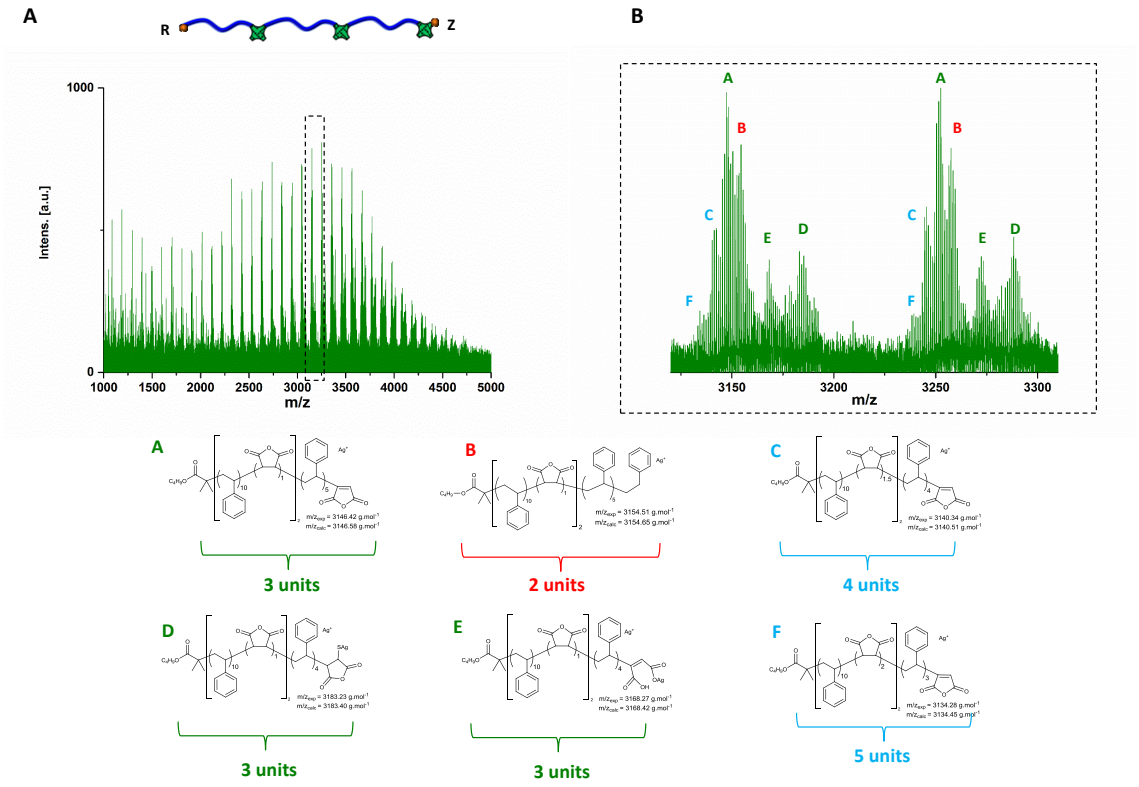

Figure A3-4. A) MALDI-ToF mass spectrum for poly[(Sty_{10}-*s*-$MAnh_{1.5}$)]$_3$ B) zoom corresponding to the region in the dashed square in A).Proposed structures below spectrum.

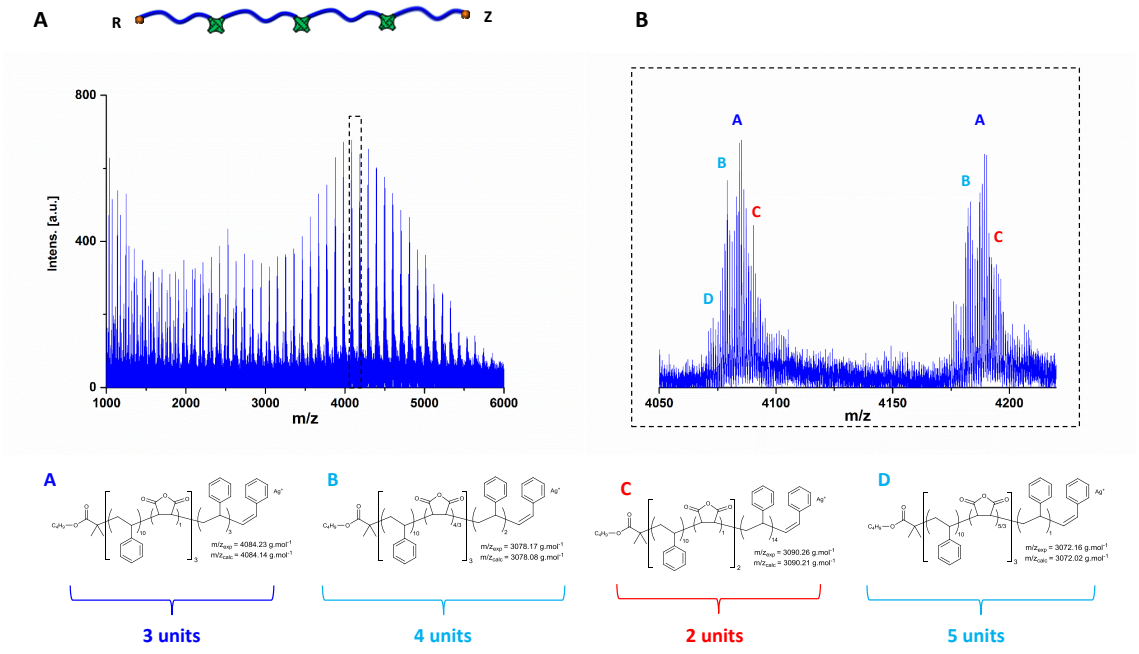

Figure A3-5. A) MALDI-ToF mass spectrum for poly[(Sty_{10}-*s*-$MAnh_{1.5}$)]$_3$-*b*-$PSty_{10}$ B) zoom corresponding to the region in the dashed square in A).Proposed structures below spectrum.

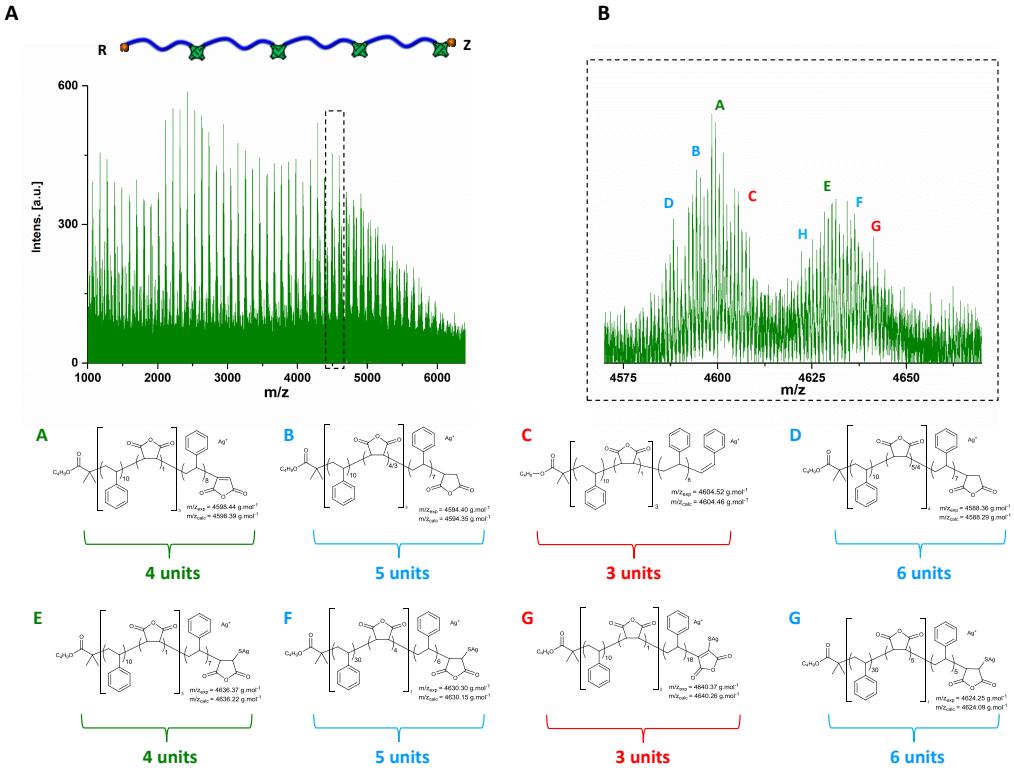

Figure A3-6. A) MALDI-ToF mass spectrum for poly[(Sty_{10}-*s*-$MAnh_{1.5}$)]$_4$ B) zoom corresponding to the region in the dashed square in A).Proposed structures below spectrum.

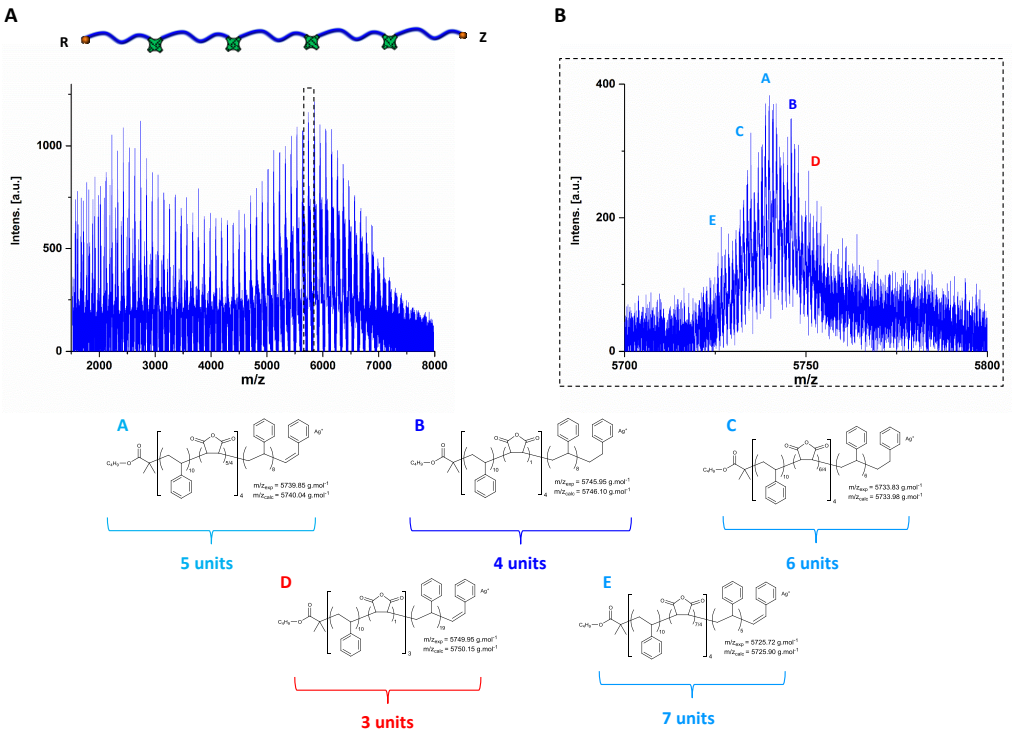

Figure A3-7. A) MALDI-ToF mass spectrum for poly[(Sty_{10}-*s*-$MAnh_{1.5}$)]$_4$-*b*-$PSty_{10}$ B) zoom corresponding to the region in the dashed square in A).Proposed structures below spectrum.

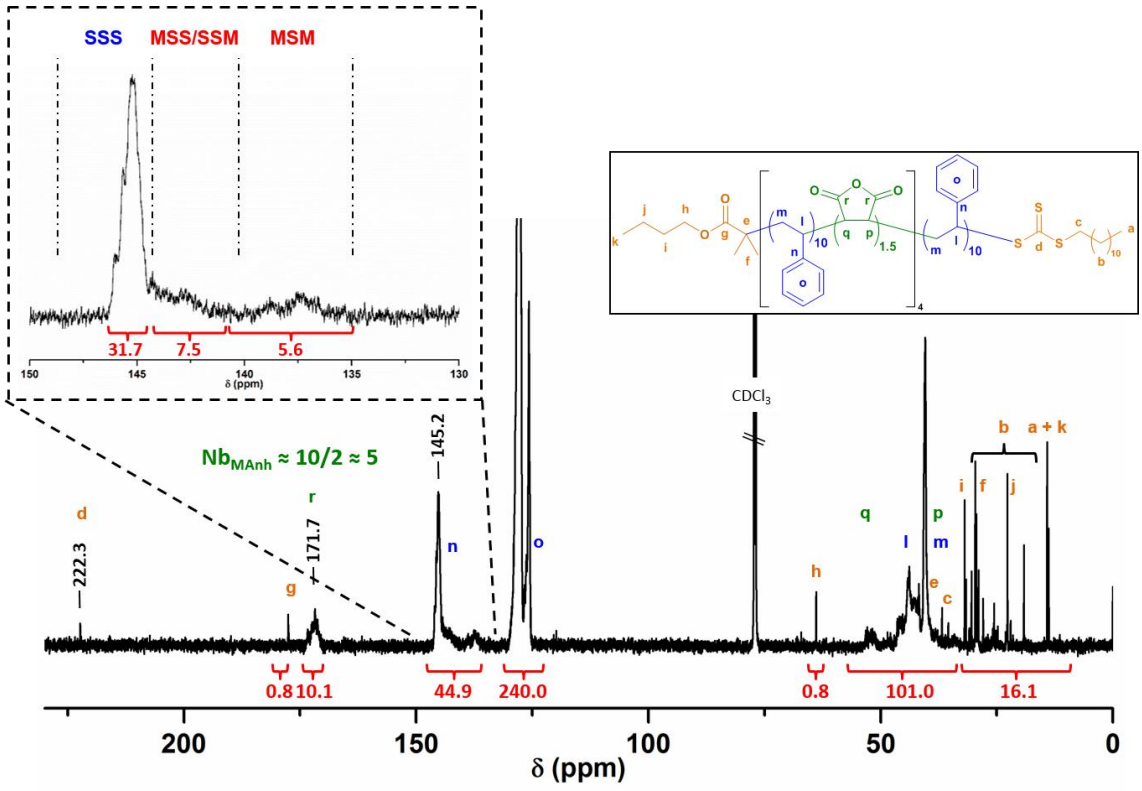

Figure A3-8. Quantitative ^{13}C-NMR (600MHz – $CDCl_3$) spectrum of pure multisite with zoomed area showing the location of the quaternary carbon from styrene depending on monomer triad.

Appendix Chapter 4 A Library of PSMA Architectures

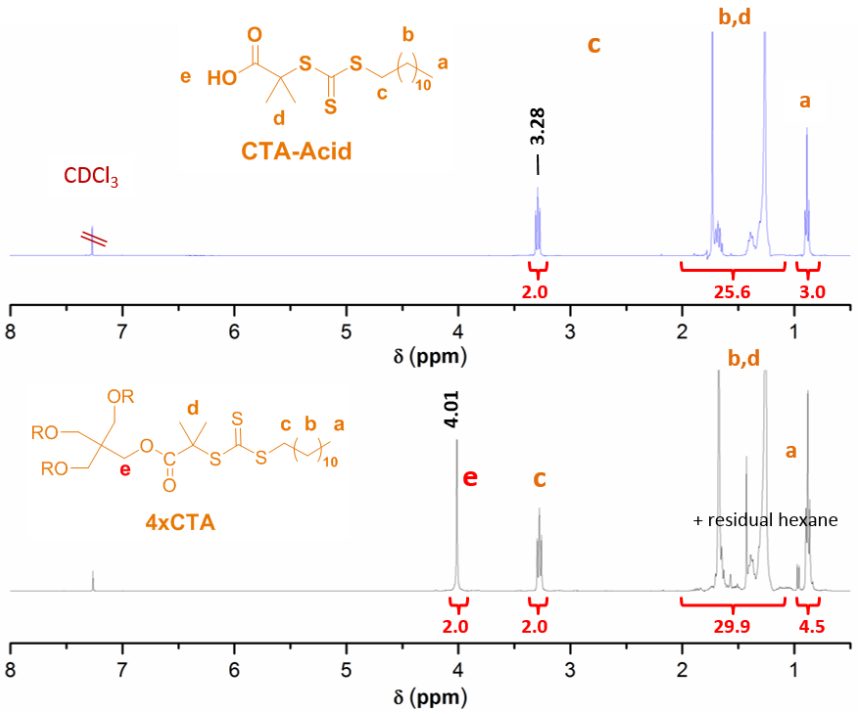

Figure A4-1. ^{1}H-NMR spectrum in deuterated chloroform for CTA-Acid (top) and 4xCTA (bottom)

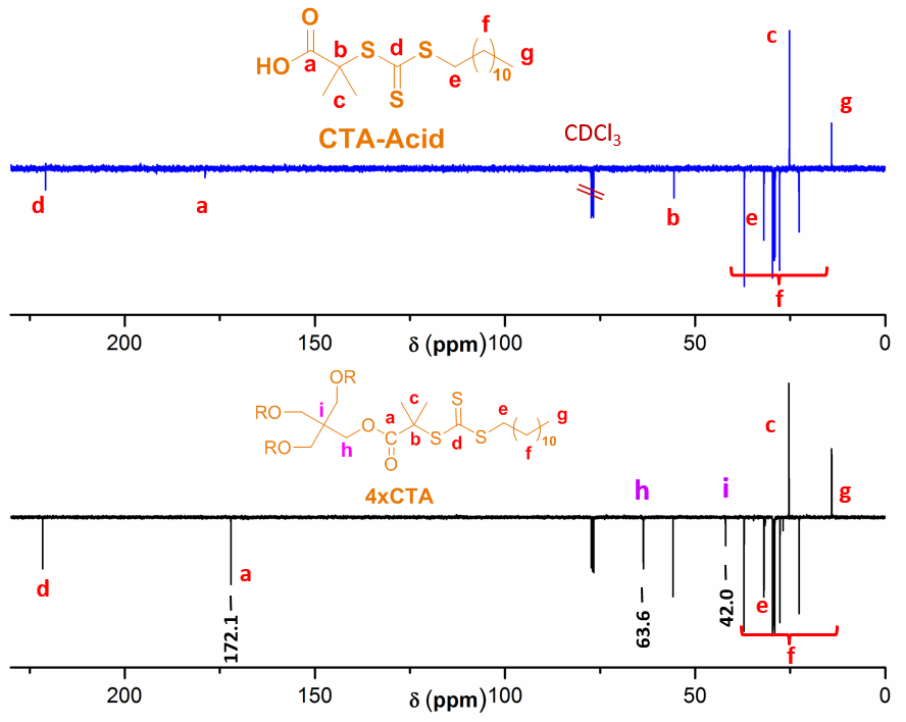

Figure A4-2. ^{13}C-NMR spectrum in deuterated chloroform for CTA-acid (top) and 4xCTA (bottom).

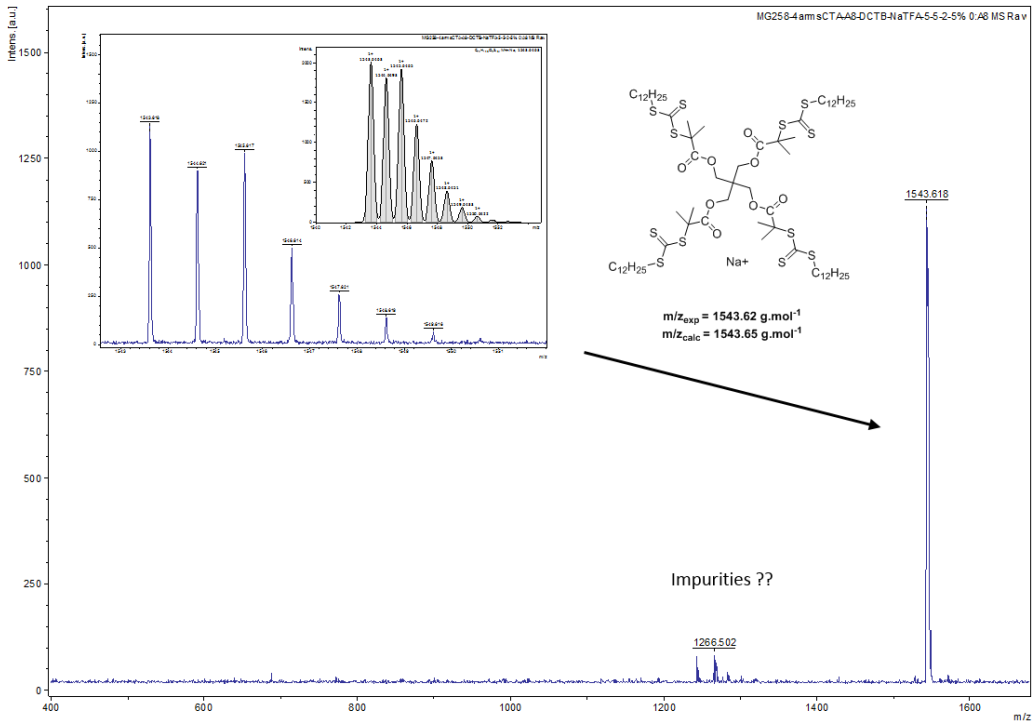

Figure A4-3. MALDI-ToF spectrum for purified 4xCTA. The spectrum was recorded using DTCB as a matrix and NaTFA as salt.

PSMA synthesis

Table A4-1. Experimental conditions for alt-PSMA copolymers synthesis in dioxane at 60°C.

Entry	Materials	Mono	$[M]_0$ (mol L^{-1})	[M] wt%	V_{tot} (mL)	$[V601]_0$ (mol L^{-1})	$[CTA]_0/[V601]_0$	Time (hrs)
Alt-PSMA 6k	P[Sty-*alt*-MAnh]$_{28}$	SMA	2*	20	50	0.001	70	24
Alt-PSMA 50k	P[Sty-*alt*-MAnh]$_{250}$	SMA	1.5*	15	20	0.002	3	12
4xPSMA 50k	4xP[Sty-*alt*-MAnh]$_{60}$	SMA	1.8*	34	28	0.001	30	26

*value for each SMA monomer (ex. 1.5M Sty + 1.5M MAnh)

Table A4-2. Feature summary for alt-PSMA copolymers

Materials	% conv.$_{sty}$ [a]	$M_{n,theo}$ [a] g mol^{-1}	$M_{n,RI\text{-}SEC}$ [b] g mol^{-1}	$Đ_{RI}$ [b]	% $L_{cumul.}$ [c]	Mass g
P[SMA]$_{28}$	92	5,600	8,100	1.13	99	19
P[SMA]$_{250}$	99	50,600	54,500	1.19	95	5
4xP[SMA]$_{60}$	95	47,600	45,200	1.15	98	8

[a] Calculated by ^{1}H NMR using eq. 2.5 and 2.6, [b] determined using SEC-DMF with PMMA standards, [c] cumulative livingness using eq.1.2.

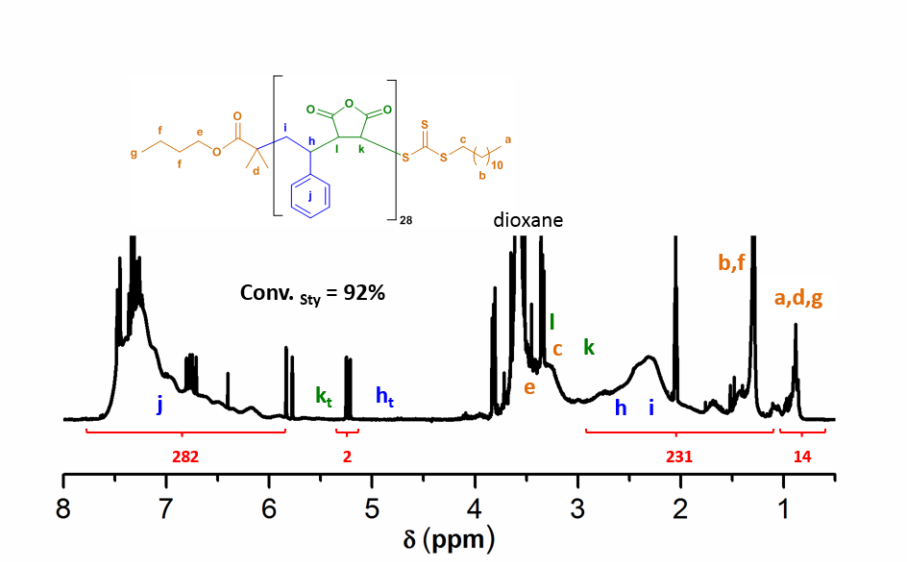

Figure A4-4. ^{1}H-NMR spectrum for alternating PSMA$_{28}$ at the end of polymerisation.

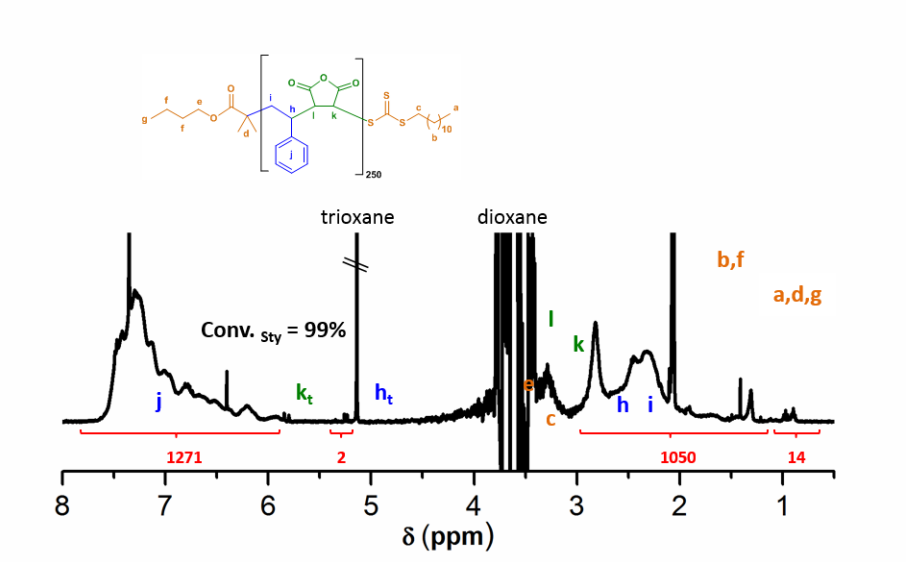

Figure A4-5. ^{1}H-NMR spectrum for alternating PSMA DP_{250} at the end of polymerisation.

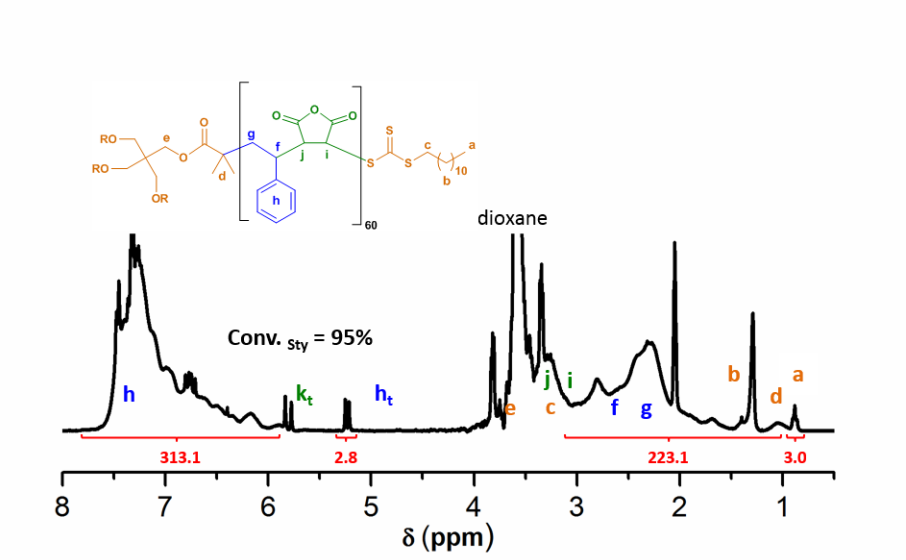

Figure A4-6. ^{1}H-NMR spectrum for 4xPSMA$_{60}$ Star after polymerization.

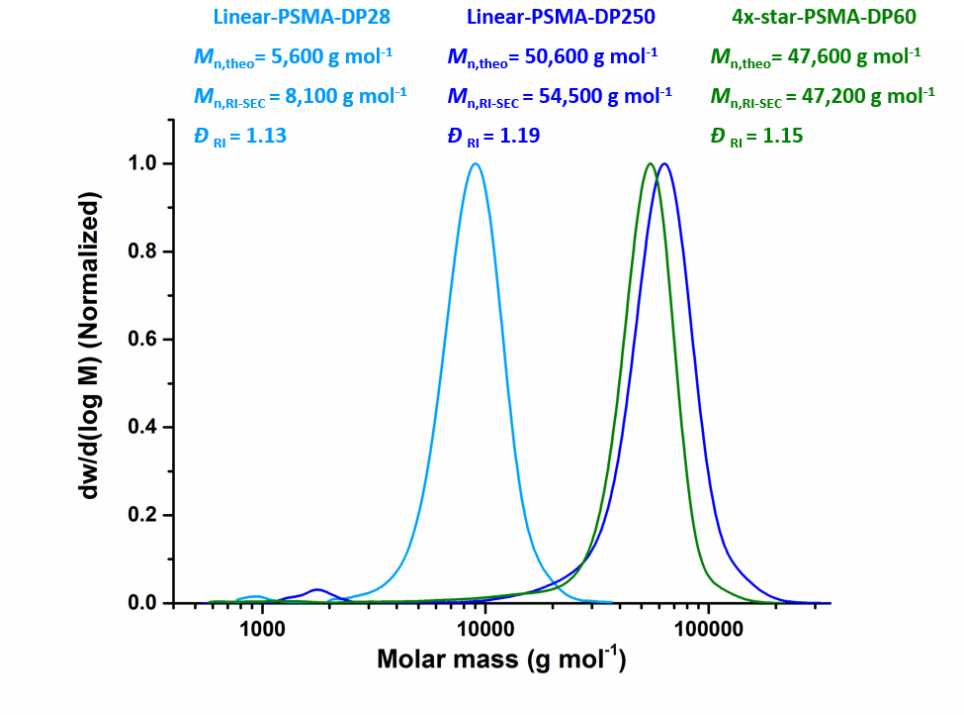

Figure A4-7. SEC molar mass distribution for alternating PSMA copolymers after purification. SEC in DMF with PMMA standards.

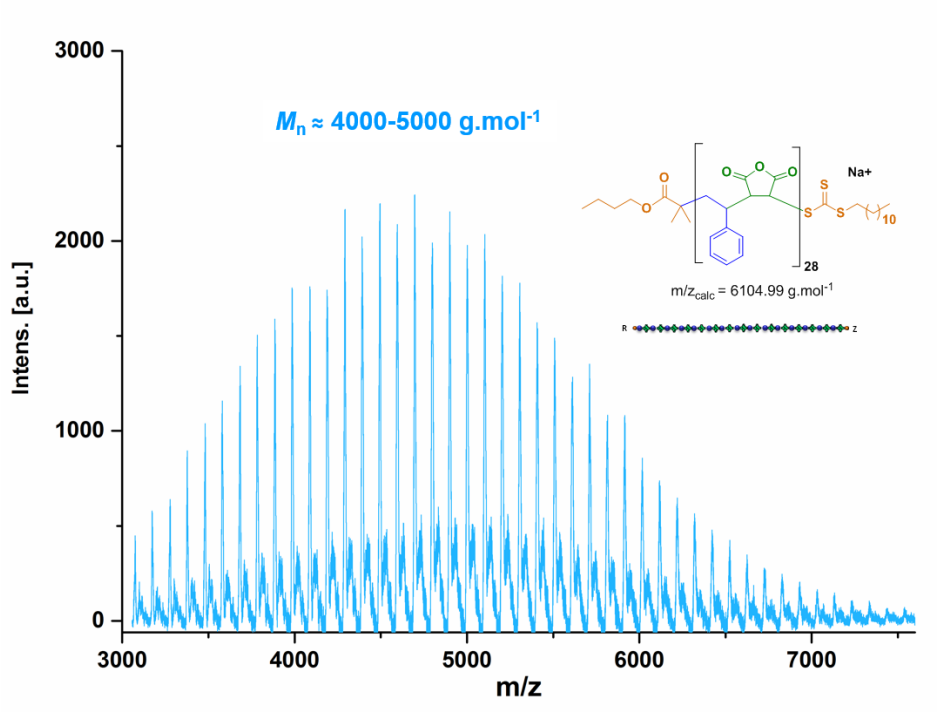

Figure A4-8. MALDI-ToF mass spectrum for pure alternating PSMA DP28. The spectrum was recorded in linear mode using DTCB as a matrix and NaTFA as salt.

Diblock synthesis

Table A4-3. Experimental conditions for each step of diblock synthesis in dioxane.

Entry	Mono	$[M]_0$ ($mol.L^{-1}$)	[M] wt%	V_{tot} (mL)	Initiator	$[Init]_0$ ($mol.L^{-1}$)	$[CTA]_0/[V\text{-}40]_0$	T°C	Time (hrs)
$PSty_{27}$	Sty	6	66	10	V40	0.040	6	100	18
$PSty_{27}$-*b*-$PSMA_{14}$	SMA	1.5*	16	21	V601	0.001	125	60	23

*value for each SMA monomer (ex. 1.5M Sty + 1.5M MAnh)

Table A4-4. Feature summary for diblock copolymer after each step.

Entry	% $conv._{sty}$ [a]	$M_{n,theo}$ [a] g mol^{-1}	$M_{n,RI\text{-}SEC}$ [b] g mol^{-1}	$Đ_{RI}$ [b]	% $L_{cumul.}$ [c]	Mass g
$PSty_{27}$	90	3000	2600	1.14	92	-
$PSty_{27}$-*b*-$PSMA_{14}$	93	5600	5300	1.22	92	10

[a] Calculated by ^{1}H NMR using eq. 2.5 and 2.6, [b] determined using SEC-THF with PS standards for MG259 and SEC-DMF with PMMA standards for MG260, [c] cumulative livingness using eq.1.2.

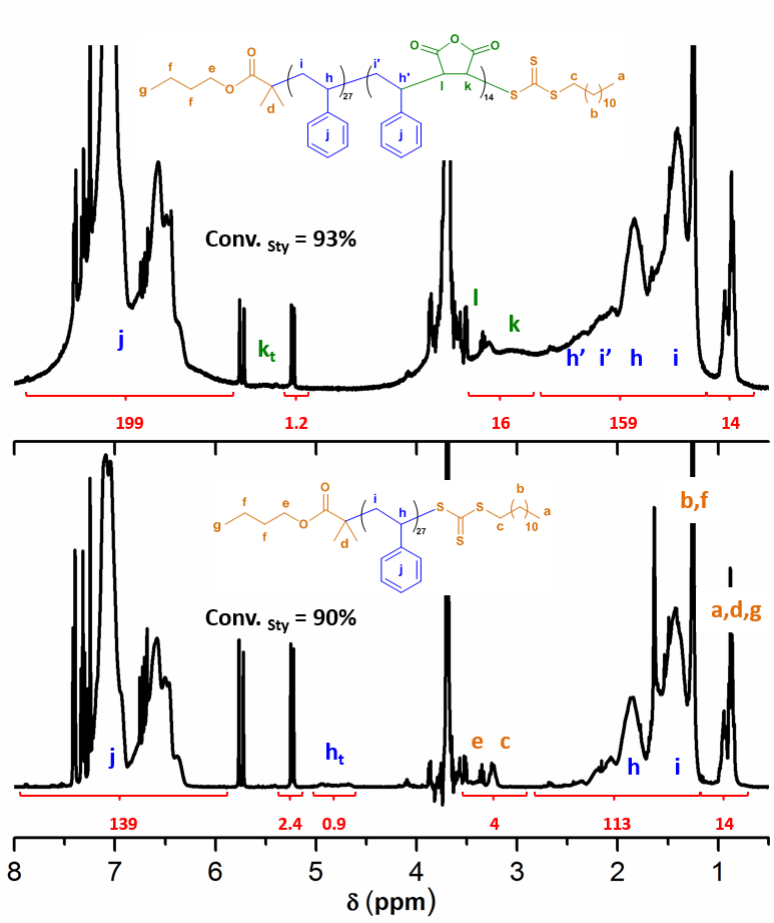

Figure A4-9. ^{1}H-NMR spectrum after each step of diblock synthesis.

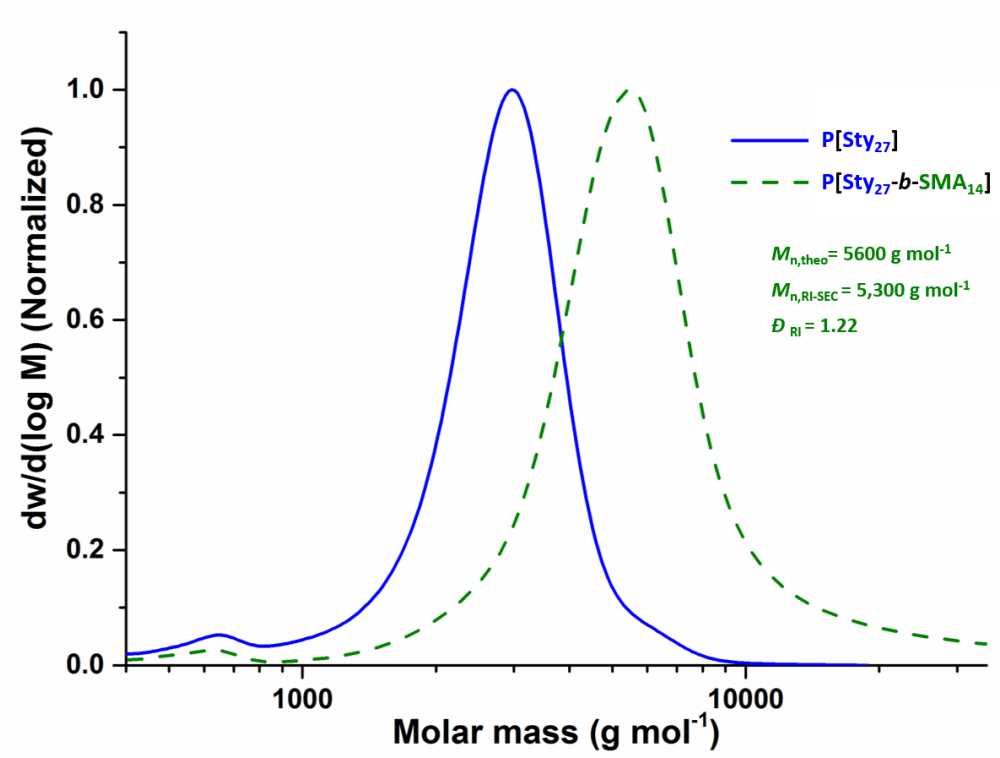

Figure A4-10. SEC molar mass distribution for diblock copolymer synthesis. Polystyrene macroCTA is shown in blue and the diblock PSMA in dashed green line. SEC in THF with polystyrene standards.

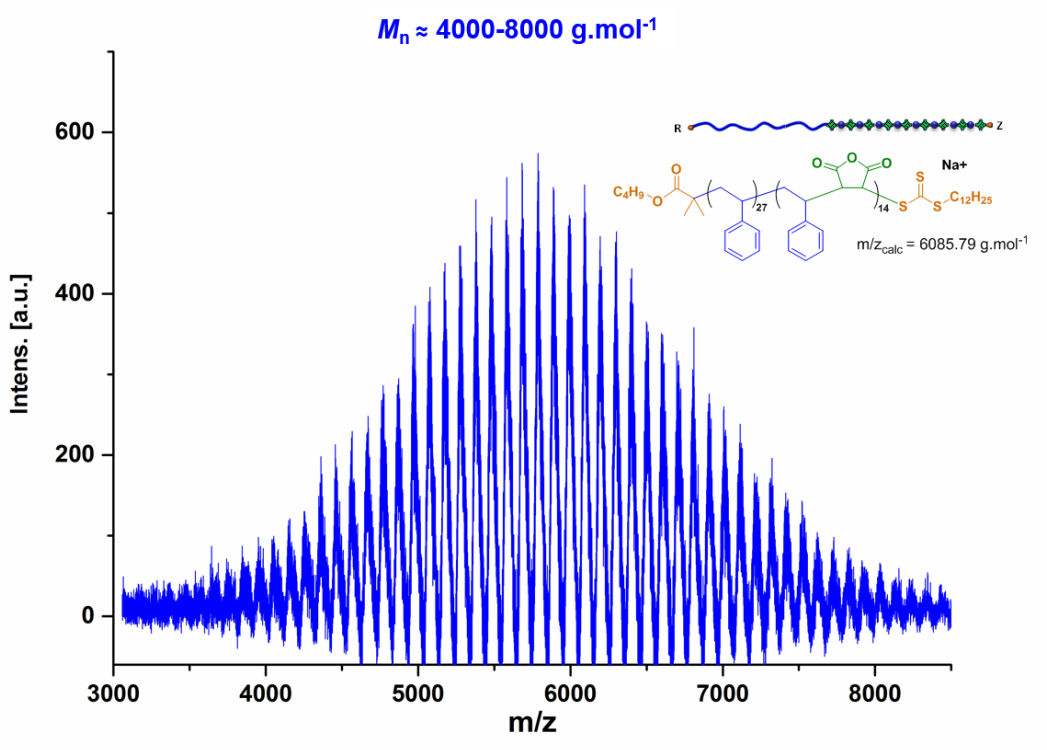

Figure A4-11. MALDI-ToF mass spectrum for pure diblock copolymers. The spectrum was recorded using DTCB as a matrix and NaTFA as salt.

Multiblock synthesis

Table A4-5. Experimental conditions for each step of multiblock synthesis in toluene.

Entry	Mono	$[M]_0$ ($mol.L^{-1}$)	[M] wt%	V_{tot} (mL)	$[V\text{-}40]_0$ ($mol.L^{-1}$)	$[CTA]_0/[V\text{-}40]_0$	T°C	Time (hrs)
$P[Sty]_{10}$	Sty	5.5	62	5	0.050	11	100	15
$P[Sty_{10}\text{-}b\text{-}(SMA)_5]$	SMA	1.5*	18	9	0.021	15	70	8
$P[Sty_{10}\text{-}b\text{-}(SMA)_5\text{-}b\text{-}PSty_{10}]$	Sty	1.9	23	14	0.017	11	100	15
$P[Sty_{10}\text{-}b\text{-}(SMA)_5]_2$	SMA	0.5*	6	28	0.008	12	70	18
$P[Sty_{10}\text{-}b\text{-}(SMA)_5]_2\text{-}b\text{-}PSty_{10}$	Sty	0.9	10	31	0.008	11	100	15

*value for each SMA monomer (ex. 1.5M Sty + 1.5M MAnh)

Table A4-6. Feature summary for multiblock copolymer after each step

Entry	% $conv._{sty}$ [a]	$M_{n,theo}$ [a] g mol^{-1}	$M_{n,RI\text{-}SEC}$ [b] g mol^{-1}	$Đ_{RI}$ [b]	% $L_{cumul.}$ [c]
$P[Sty]_{10}$	96	1400	1200	1.06	96
$P[Sty_{10}\text{-}b\text{-}(SMA)_5]$	93	2400	1500	1.11	95
$P[Sty_{10}\text{-}b\text{-}(SMA)_5\text{-}b\text{-}PSty_{10}]$	93	3300	2600	1.19	91
$P[Sty_{10}\text{-}b\text{-}(SMA)_5]_2$	82	4200	3200	1.20	91
$P[Sty_{10}\text{-}b\text{-}(SMA)_5]_2\text{-}b\text{-}PSty_{10}$	88	5100	3800	1.25	87

[a] Calculated by ^1H NMR using eq. 2.5 and 2.6,[b] determined using SEC-THF with polystyrene standards,[c] cumulative livingness using eq. 1.2. MAnh conversion was not measurable by ^1H NMR due to peak overlap with styrene.

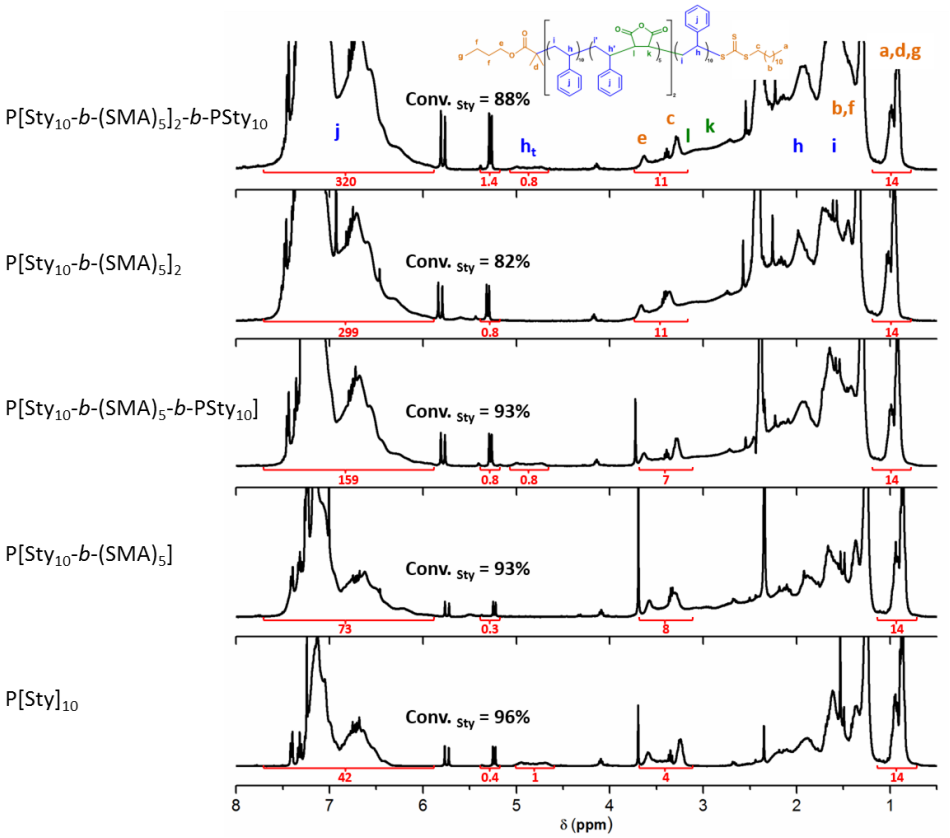

Figure A4-12. ^{1}H-NMR spectrum after each step of multiblock synthesis.

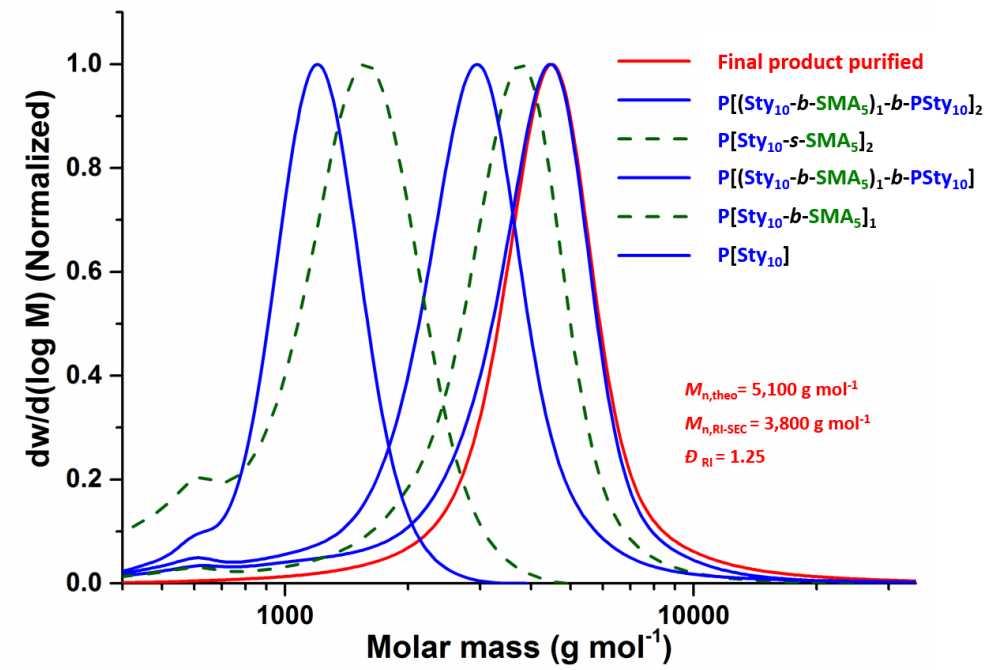

Figure A4-13. SEC molar mass distribution for multiblock copolymer synthesis. Polystyrene block are shown in blue and PSMA block in dashed green line. The final product after purification is shown in red. SEC in THF with polystyrene standards.

Characterisation of graft PSMA

IR

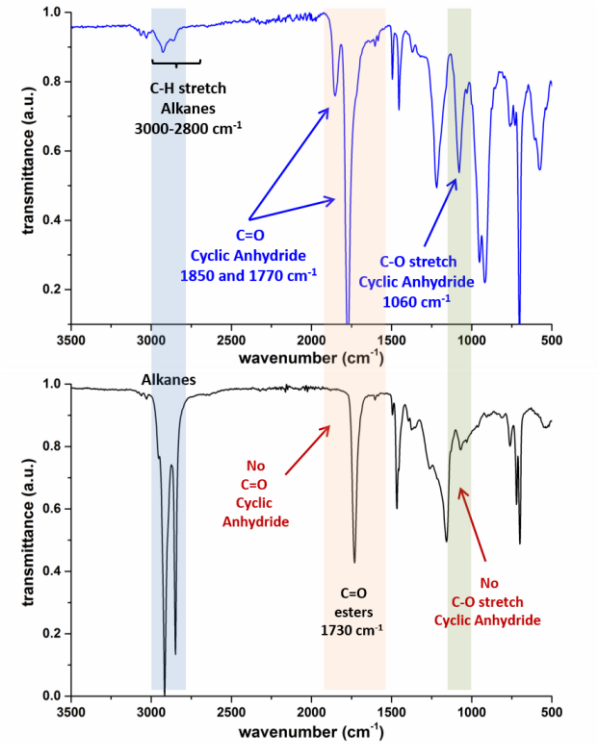

Figure A4-14. IR spectra for $PSMA_{28}$ copolymer before (top) and after esterification (bottom).

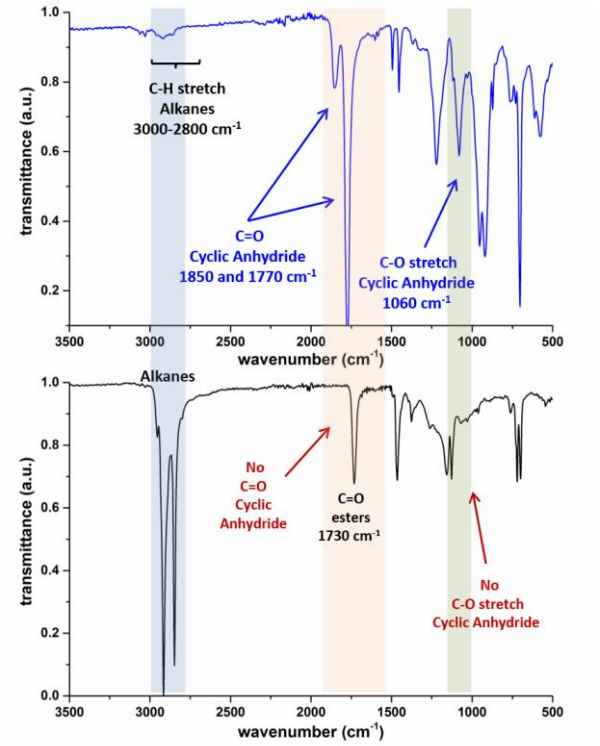

Figure A4-15. IR spectra for $PSMA_{250}$ copolymer before (top) and after esterification (bottom).

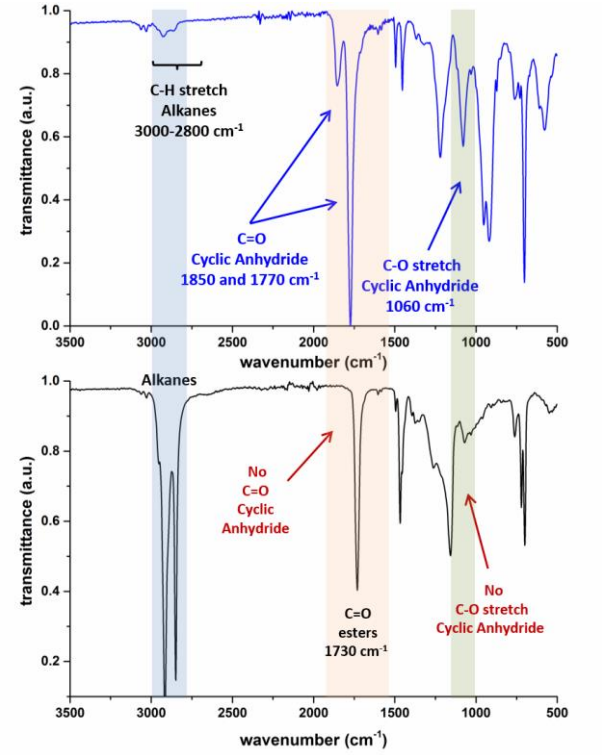

Figure A4-16. IR spectra for 4xPSMA$_{60}$ copolymer before (top) and after esterification (bottom).

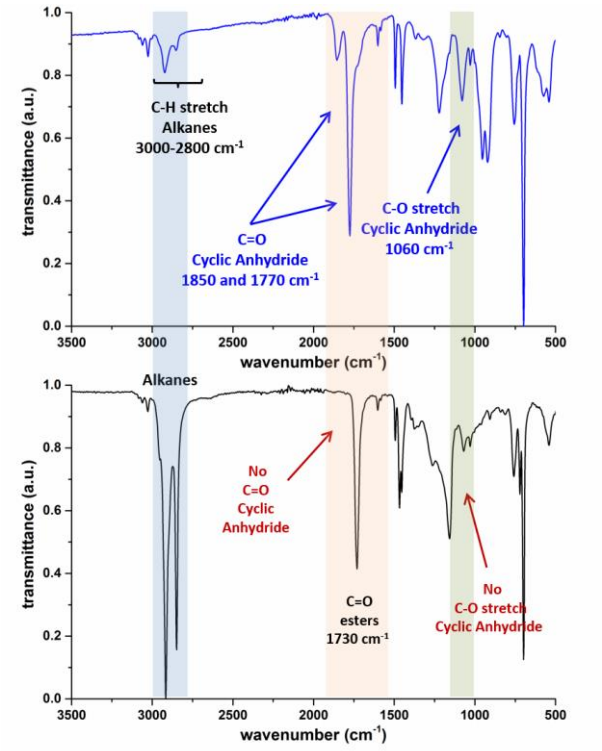

Figure A4-17. IR spectra for diblock copolymer before (top) and after esterification (bottom).

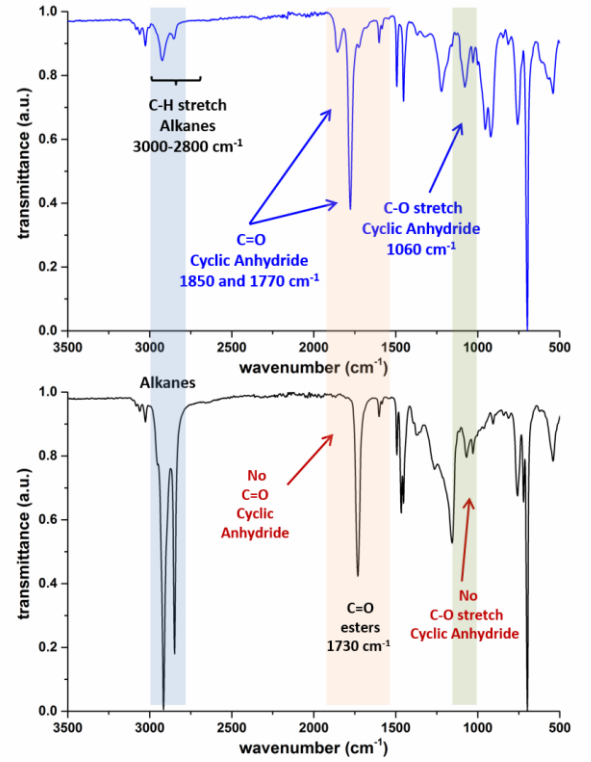

Figure A 4-18. IR spectra for multiblock copolymer before (at the top) and after esterification (bottom).

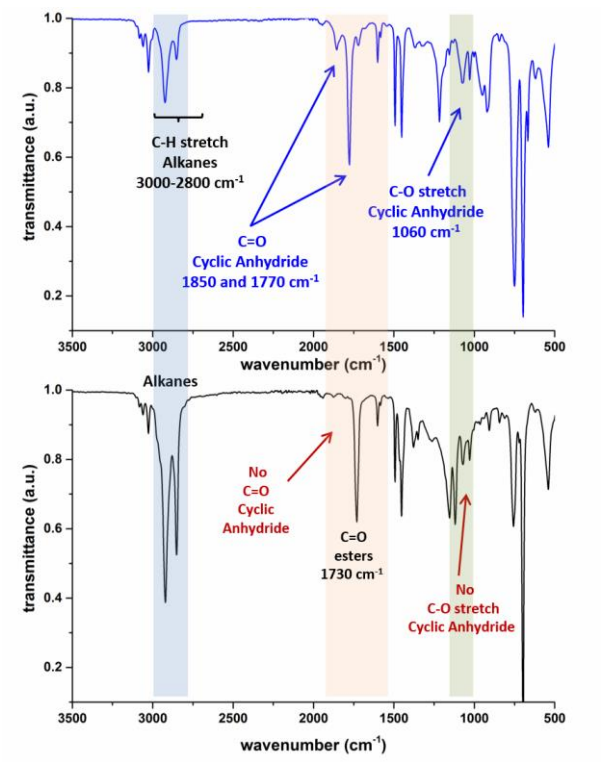

Figure A 4-19. IR spectra for multisite copolymer before (at the top) and after esterification (bottom).

NMR

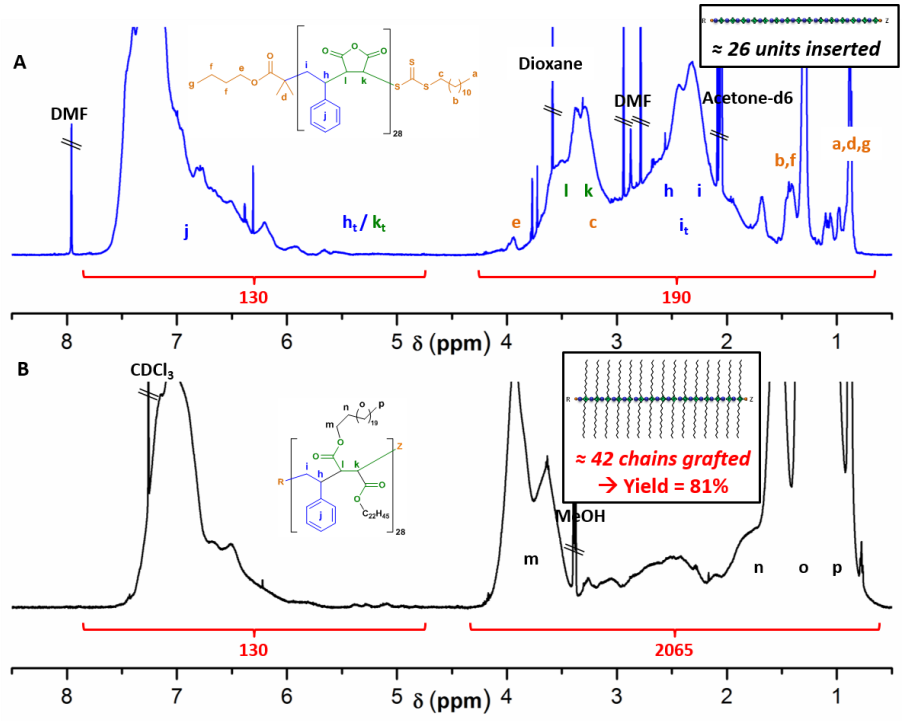

Figure A4-20. Quantitative ^{1}H NMR spectra ($CDCl_3$) for alternating $PSMA_{28}$ before (A) and after (B) esterification. Esterification yield obtained by comparing integration between 0.5-4ppm before and after esterification.

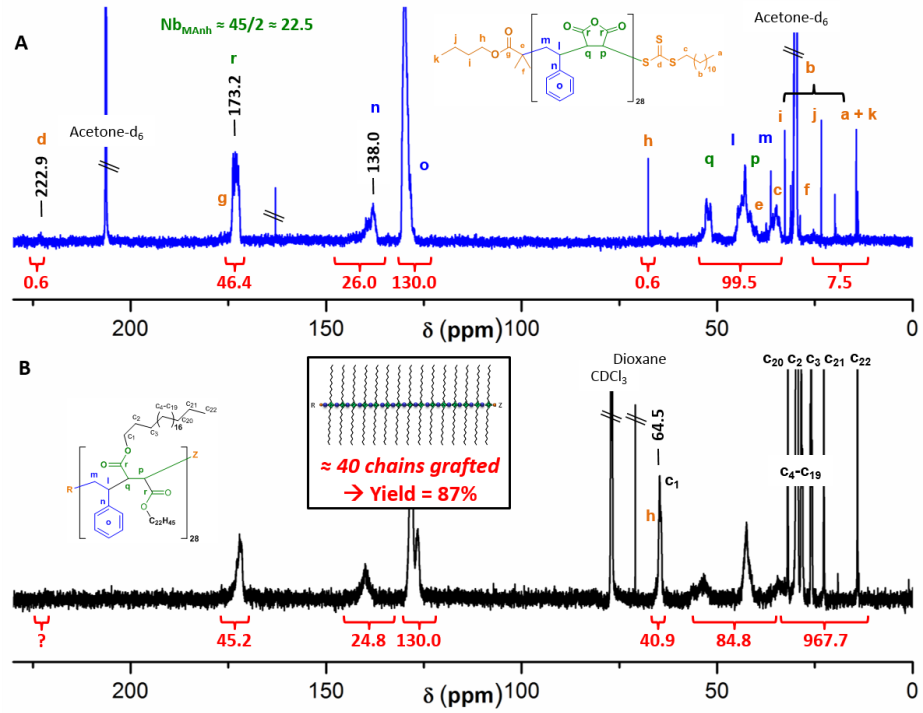

Figure A4-21. Quantitative ^{13}C NMR spectra ($CDCl_3$) for alternating $PSMA_{28}$ before (A) and after (B) esterification. Esterification yield obtained by comparing number of MAnh (spectrum A at 172 ppm) and number of alkyl chains (spectrum B at 64ppm).

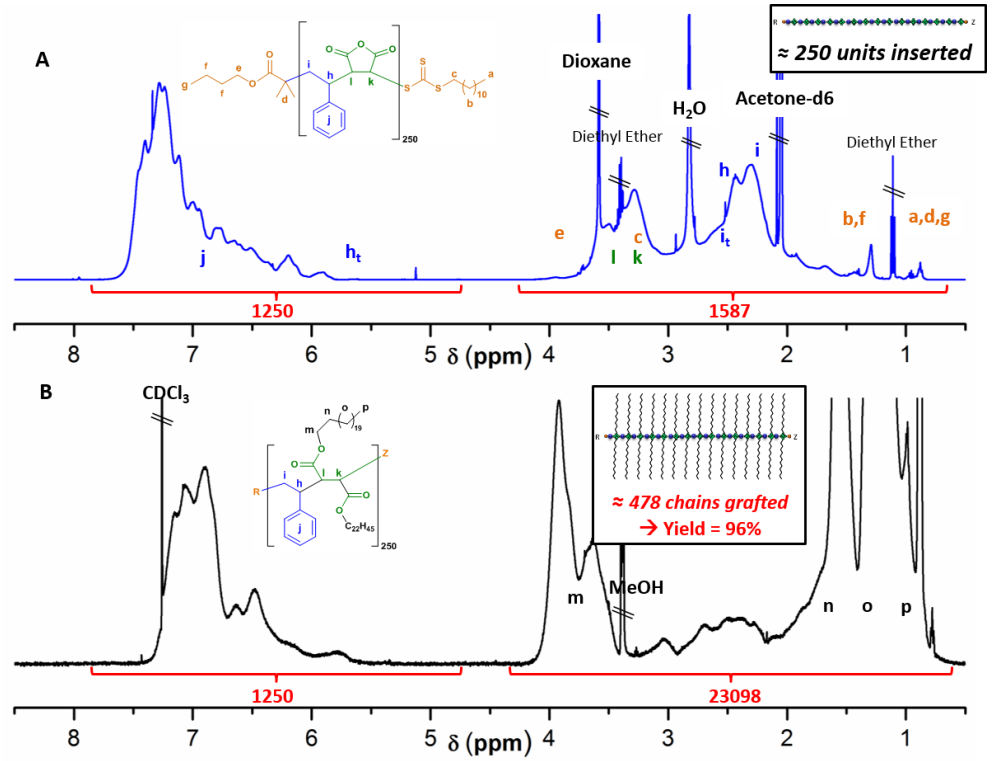

Figure A4-22. Quantitative ^{1}H NMR spectra ($CDCl_3$) for alternating $PSMA_{250}$ before (A) and after (B) esterification. Esterification yield obtained by comparing integration between 0.5-4ppm before and after esterification.

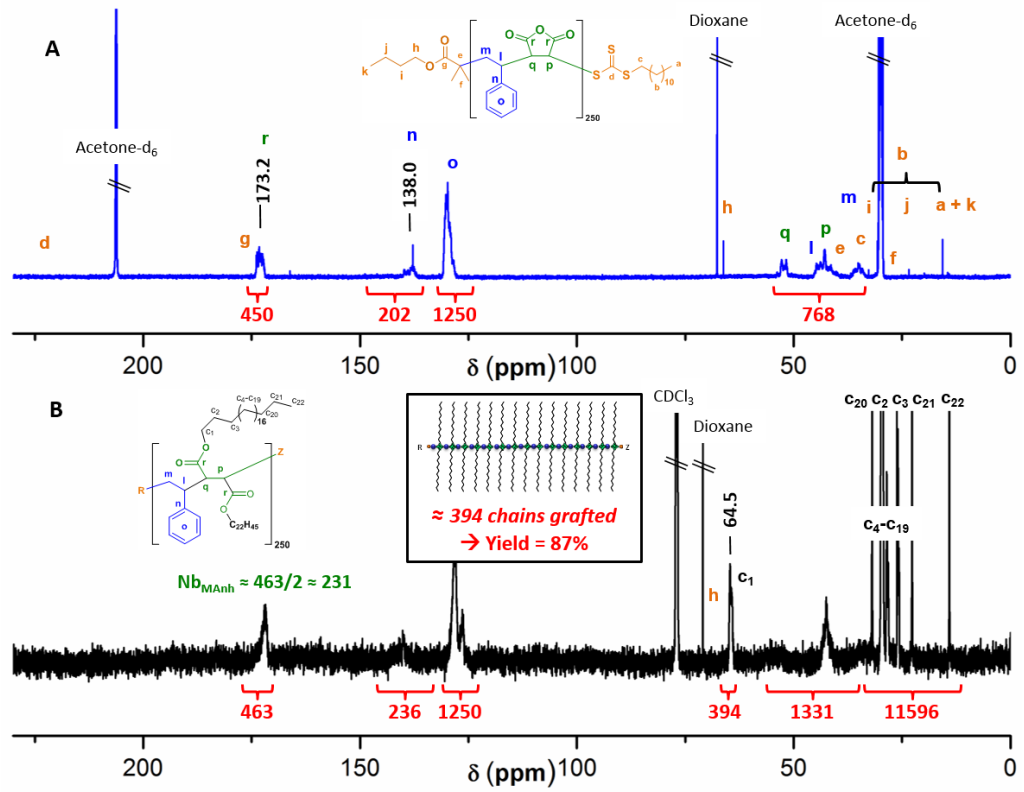

Figure A4-23. Quantitative ^{13}C NMR spectra ($CDCl_3$) for alternating $PSMA_{250}$ before (A) and after (B) esterification. Esterification yield obtained by comparing number of MAnh (spectrum A at 172 ppm) and number of alkyl chains (spectrum B at 64ppm).

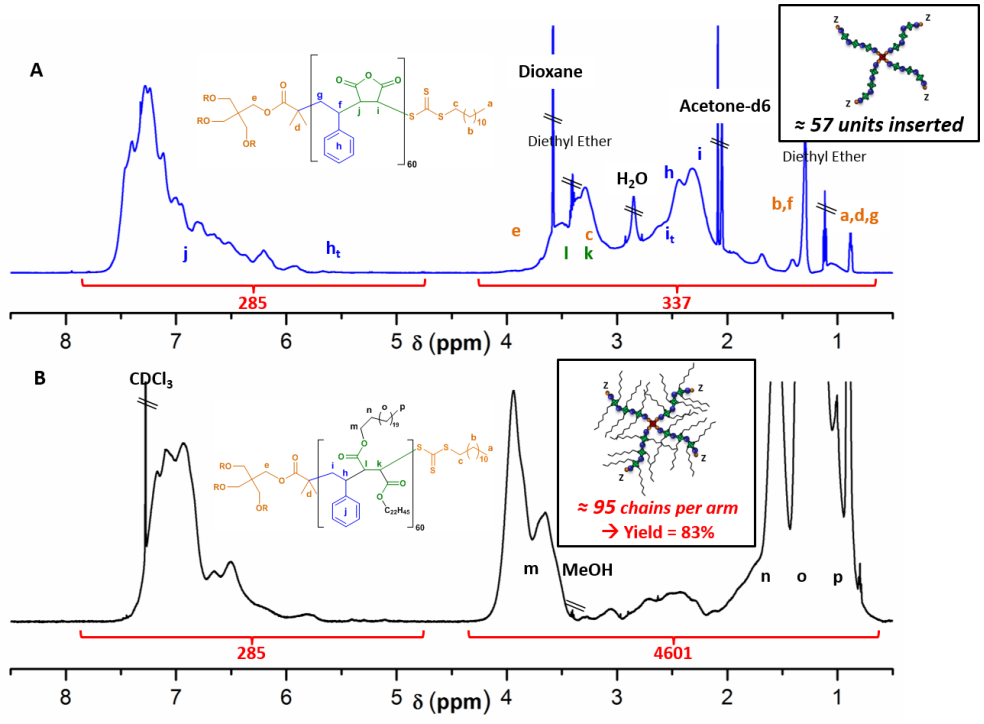

Figure A4-24. Quantitative ^{1}H-NMR spectra for alternating 4xPSMA$_{60}$ before (A) and after (B) esterification. Esterification yield obtained by comparing integration between 0.5-4ppm before and after esterification.

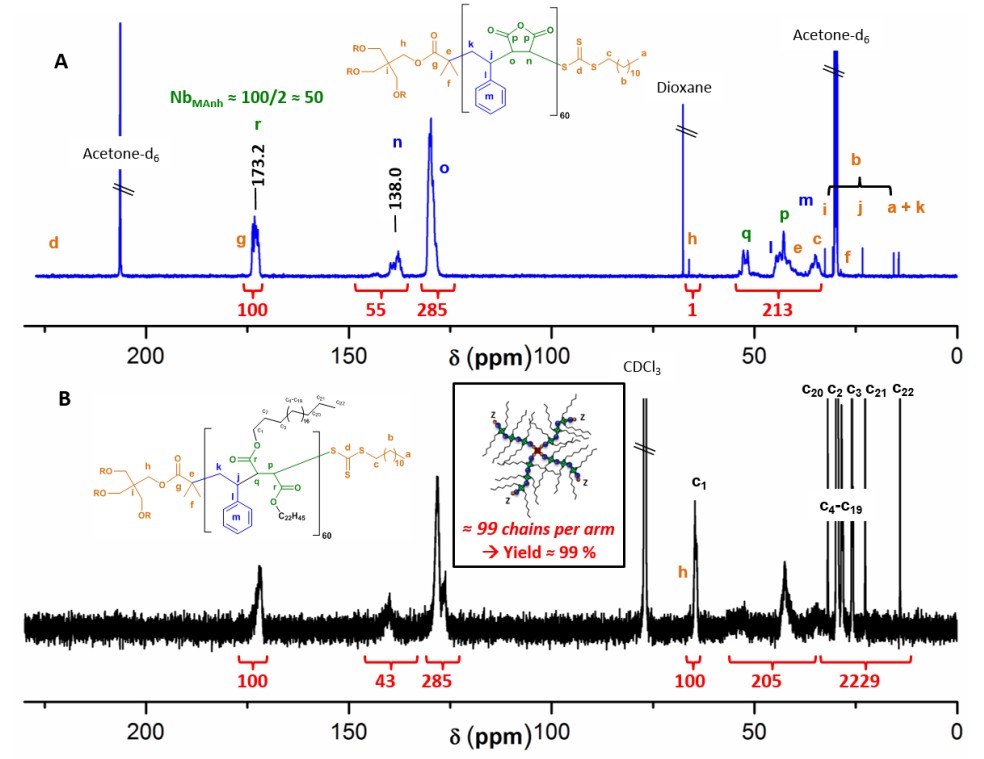

Figure A4-25. Quantitative ^{13}C NMR spectra for alternating 4xPSMA$_{60}$ before (A) and after (B) esterification. Esterification yield obtained by comparing number of MAnh (spectrum A at 172 ppm) and number of alkyl chains (spectrum B at 64 ppm).

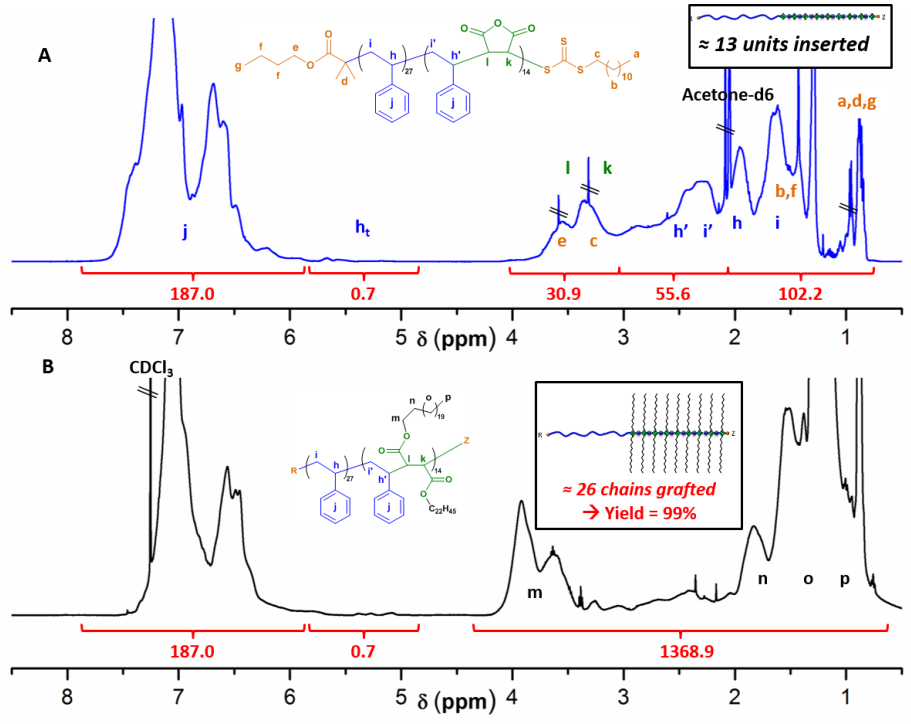

Figure A4-26. Quantitative ^{1}H NMR spectra ($CDCl_3$) for diblock copolymer before (A) and after (B) esterification. Esterification yield obtained by comparing integration between 0.5-4ppm before and after esterification.

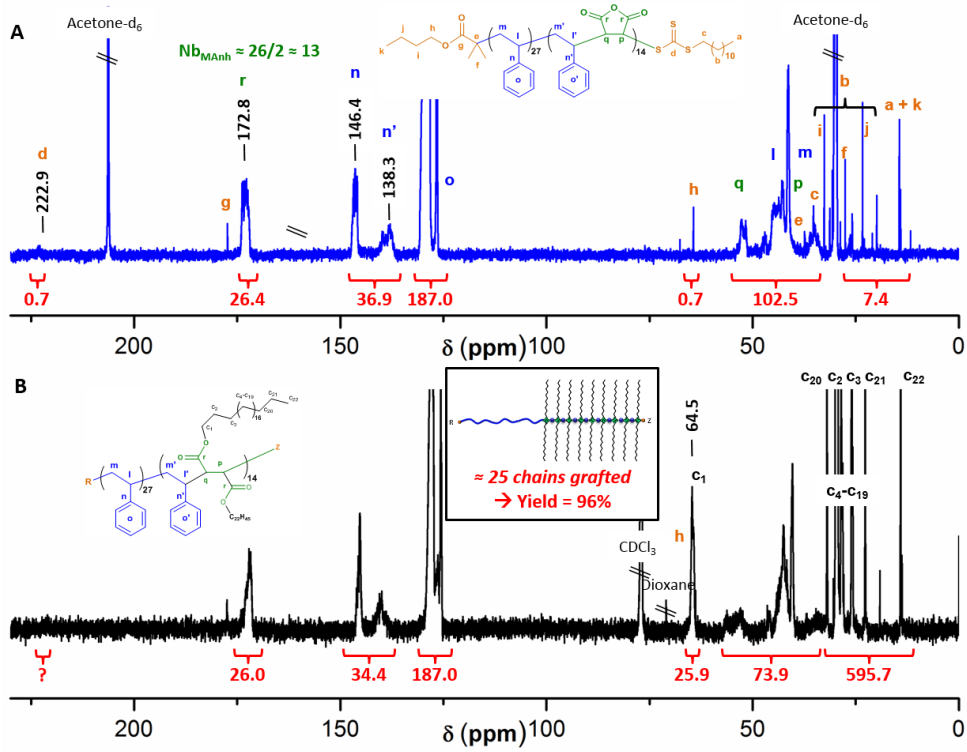

Figure A4-27. Quantitative ^{13}C NMR spectra ($CDCl_3$) for diblock copolymer before (A) and after (B) esterification. Esterification yield obtained by comparing number of MAnh (spectrum A at 172 ppm) and number of alkyl chains (spectrum B at 64 ppm).

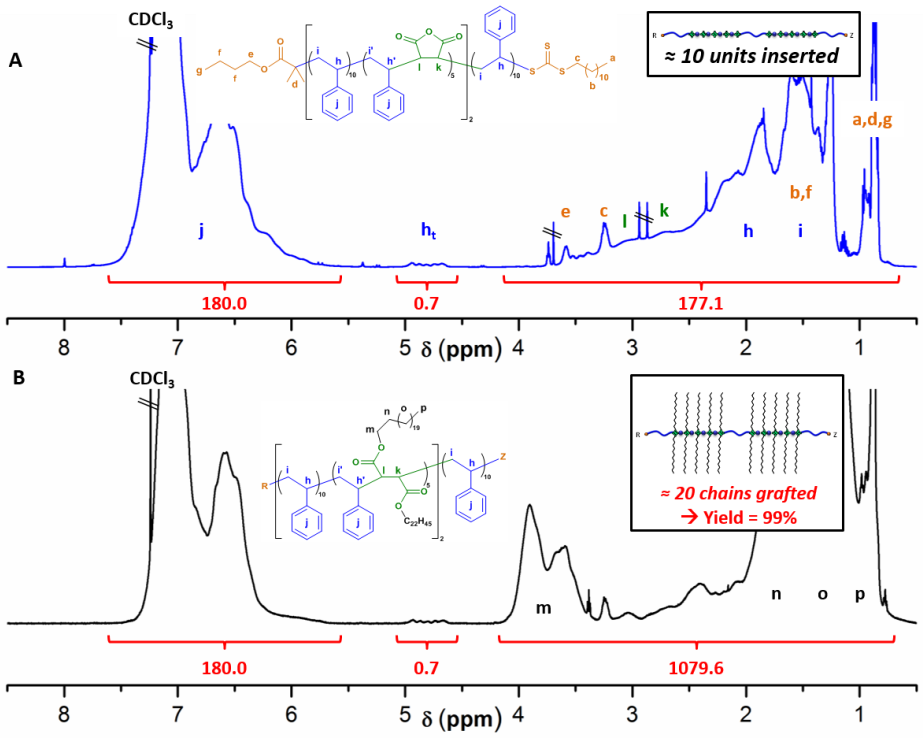

Figure A4-28. Quantitative ^{1}H-NMR spectra ($CDCl_3$) for multiblock copolymer before (A) and after (B) esterification. Esterification yield obtained by comparing integration between 0.5-4ppm before and after esterification.

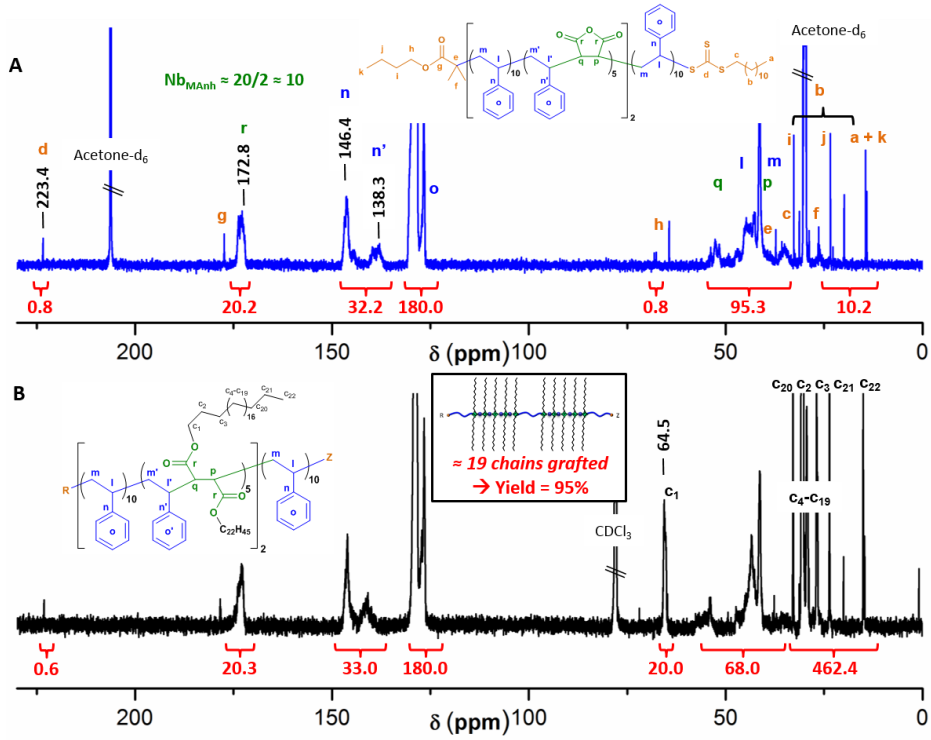

Figure A4-29. Quantitative 13C-NMR spectra (CDCl3) for multiblock copolymer before (A) and after (B) esterification. Esterification yield obtained by comparing number of MAnh (spectrum A at 172 ppm) and number of alkyl chains (spectrum B at 64 ppm)

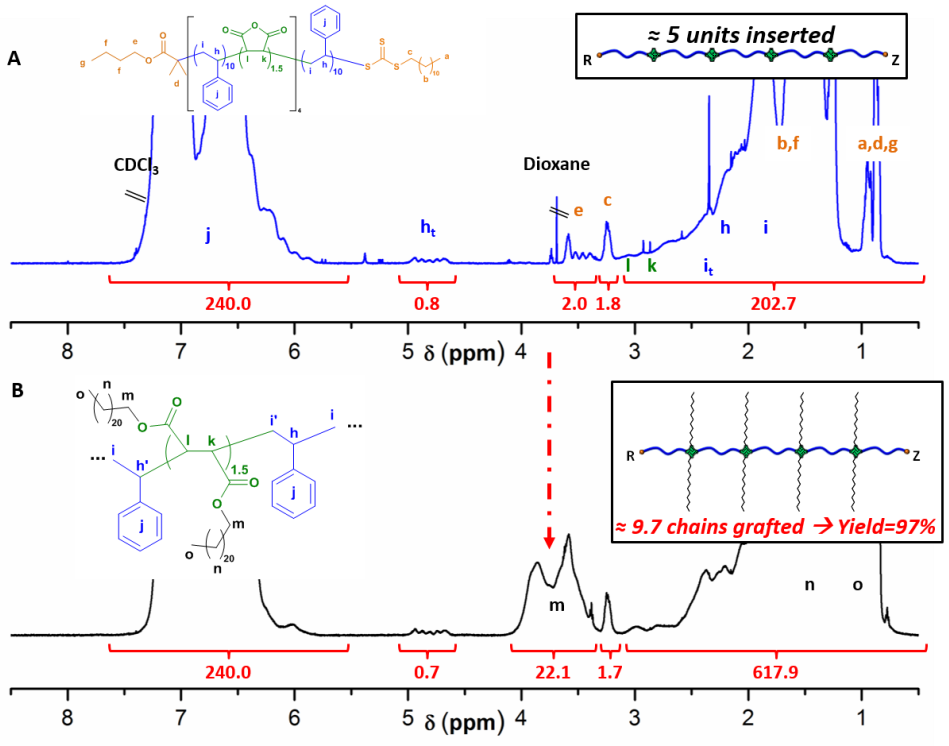

Figure A4-30. Quantitative ^{1}H-NMR spectra ($CDCl_3$) for multisite copolymer before (A) and after (B) esterification. Esterification yield obtained by comparing integration between 0.5-4ppm before and after esterification.

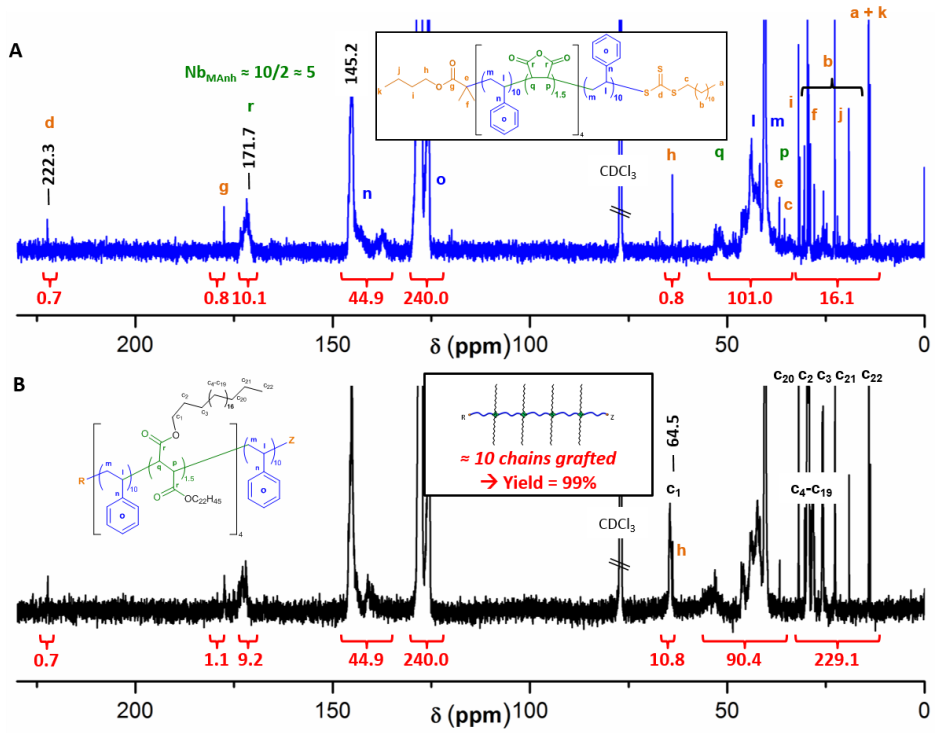

Figure A4-31. Quantitative ^{13}C-NMR spectra ($CDCl_3$) for multisite copolymer before (A) and after (B) esterification. Esterification yield obtained by comparing number of MAnh (spectrum A at 172 ppm) and number of alkyl chains (spectrum B at 64 ppm)

SEC

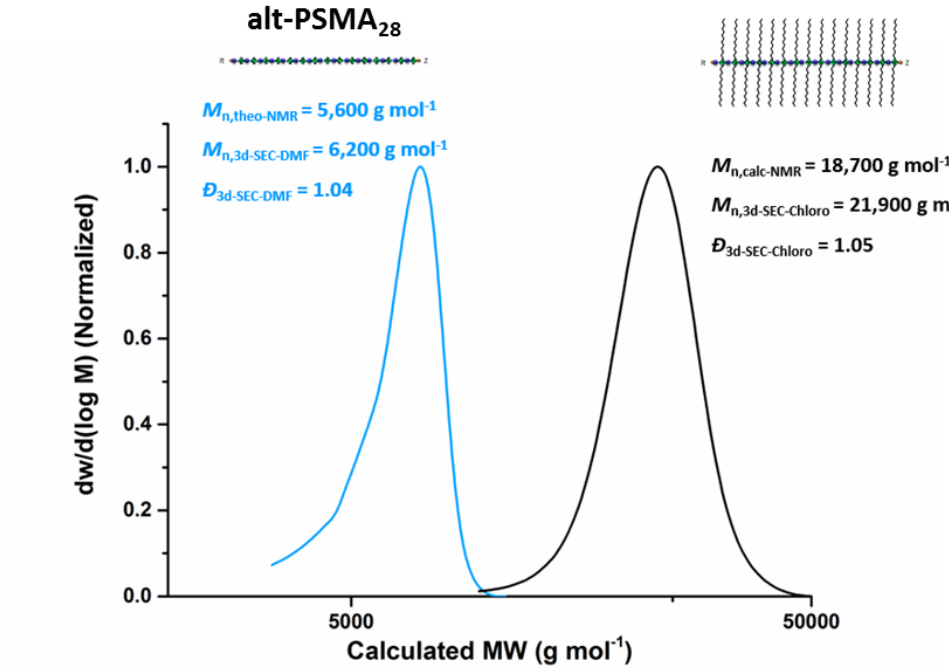

Figure A4-32. SEC molar mass distribution for alternating $PSMA_{28}$ before (blue) and after (Black) esterification. SEC using triple-detection in DMF (blue) and chloroform (black).

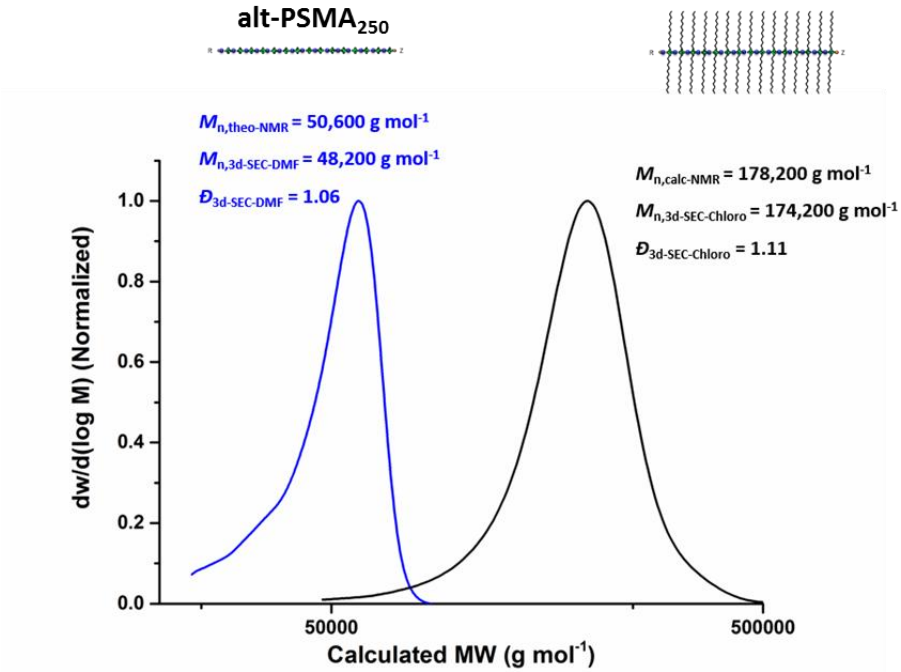

Figure A4-33. SEC molar mass distribution for alternating $PSMA_{250}$ before (blue) and after (Black) esterification. SEC using triple-detection in DMF (blue) and chloroform (black).

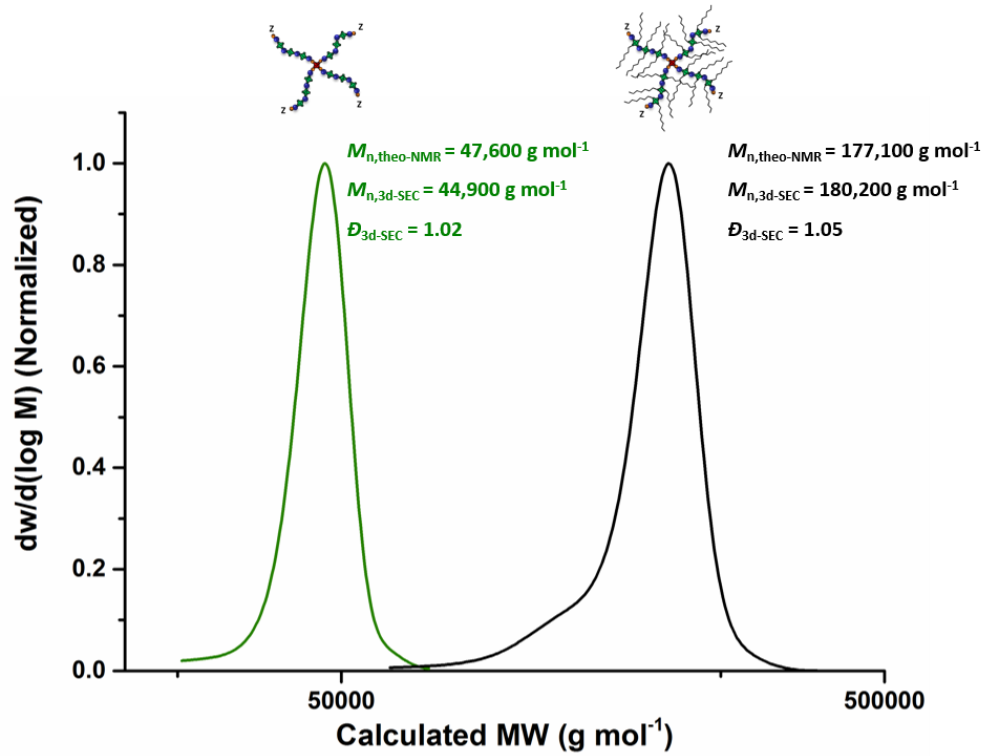

Figure A4-34. SEC molar mass distribution for alternating 4xPSMA$_{60}$ before (green) and after (Black) esterification. SEC using triple-detection in DMF (green) and chloroform (black).

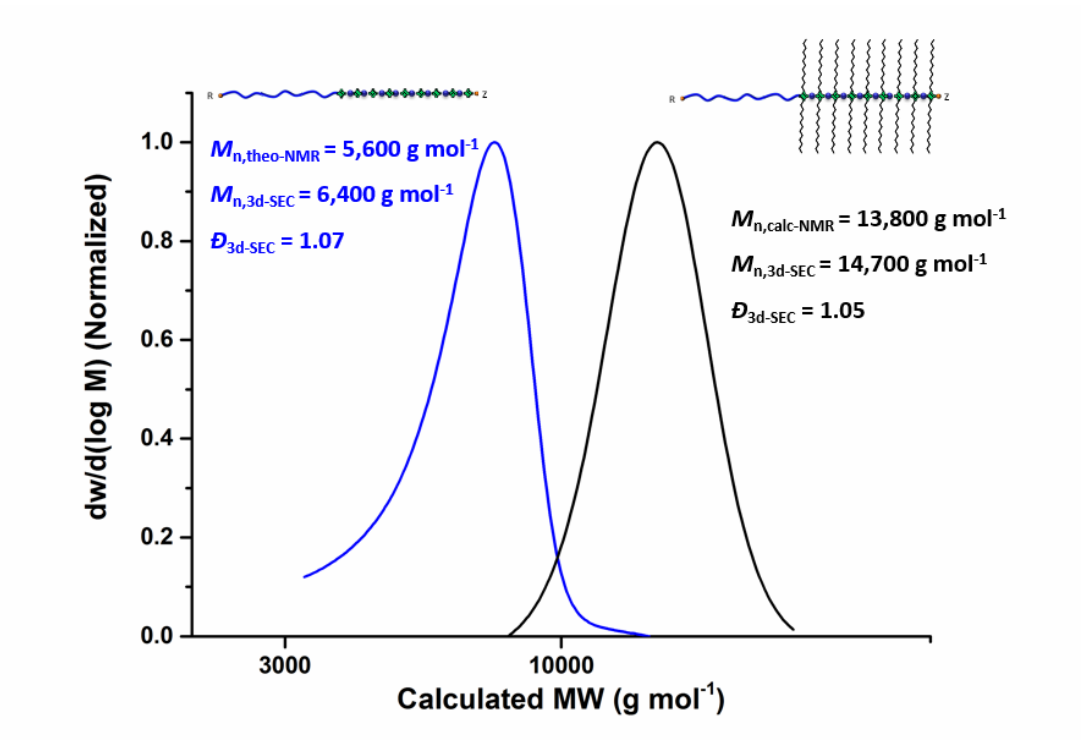

Figure A4-35. SEC molar mass distribution of diblock copolymer before (blue) and after (Black) esterification obtained using triple-detection SEC in chloroform.

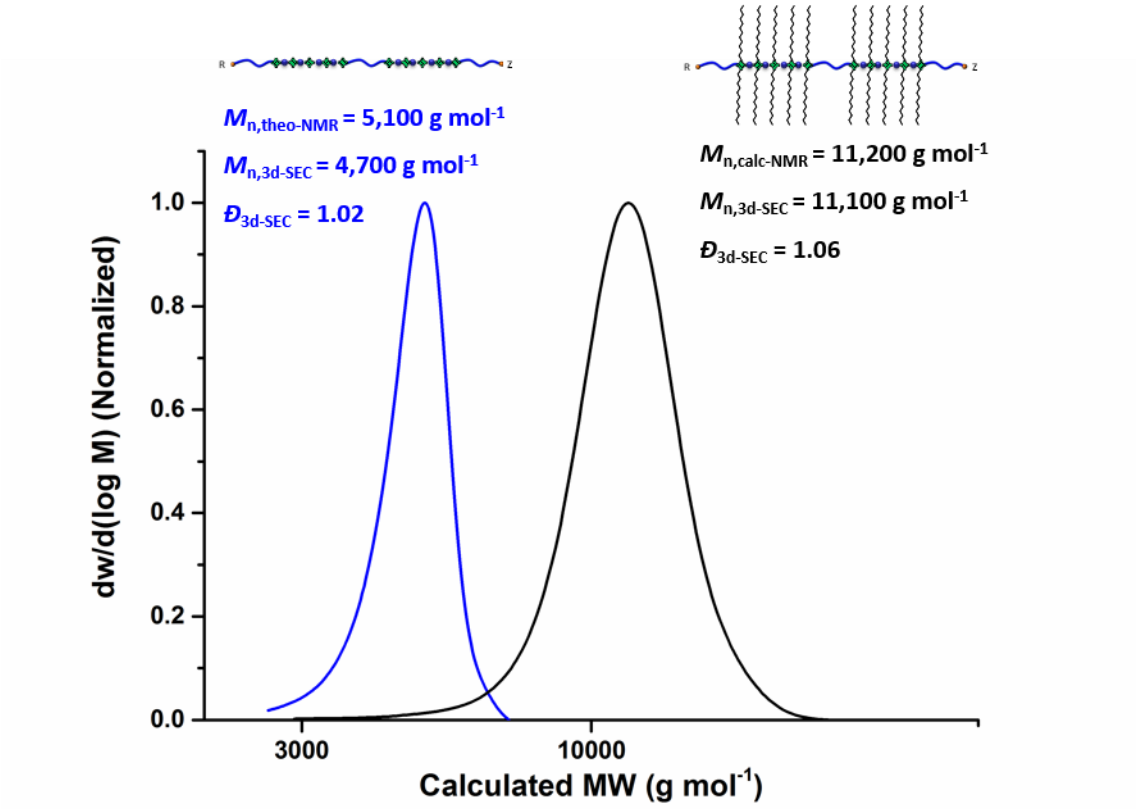

Figure A4-36. SEC molar mass distribution of multiblock copolymer before (blue) and after (Black) esterification obtained using triple-detection SEC in chloroform.

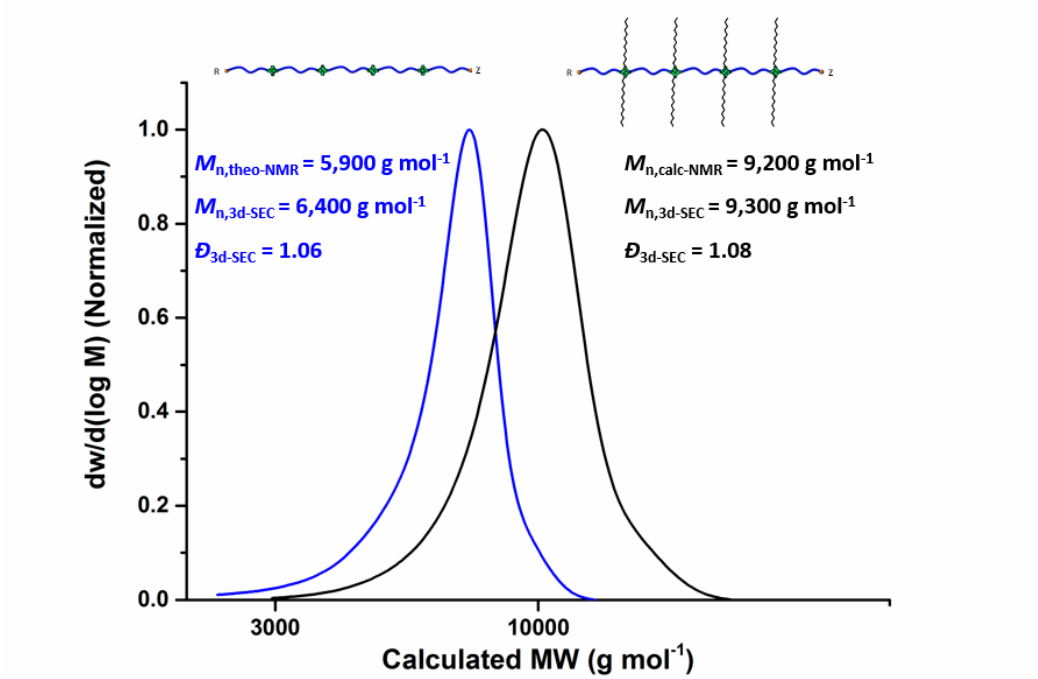

Figure A4-37. SEC molar mass distribution of multisite copolymer before (blue) and after (Black) esterification obtained using triple-detection SEC in chloroform.

TGA

Table A4-7. Summary of TGA results

Entry	$M_{n,NMR}$ (g/mol)	Structures	Onset (10% wt. loss) (°C)	Step I		Step II		Step III		Total %wt loss
				%wt loss	T_i (°C)	%wt loss	T_i (°C)	%wt loss	T_i (°C)	
Multisite	**5,900**		350	-	-	4	250	95	410	99
Multisite-Ester	**9,200**	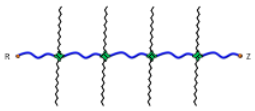	370	-	-	3	260	97	410	99
Multiblock	**5,100**		330	-	-	4	260	91	390	95
Multiblock-Ester	**11,200**	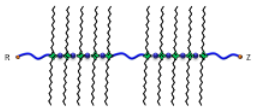	370	-	-	2	260	97	400	99
Diblock	**5,600**		330	2	120	4	260	88	410	94
Diblock-Ester	**13,800**	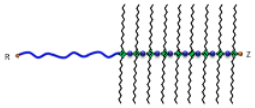	370	-	-	3	260	96	400	98
alt-PSMA$_{6k}$	**5,600**	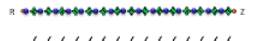	290	3	170	5	250	82	390	91
alt-PSMA$_{6k}$-Ester	**18,700**	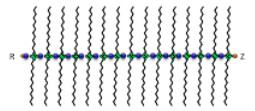	340	-	-	8	280	91	400	99
alt-PSMA$_{50k}$	**50,600**		320	6	200	-	-	86	390	92
alt-PSMA$_{50k}$-Ester	**179,800**	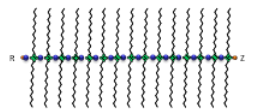	370	-	-	-	-	99	400	99
4xPSMA$_{50k}$	**47,600**	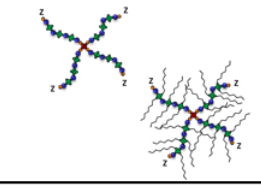	340	2	150	5	230	83	400	90
4xPSMA$_{50k}$-Ester	**177,100**		370	-	-	-	-	99	400	99

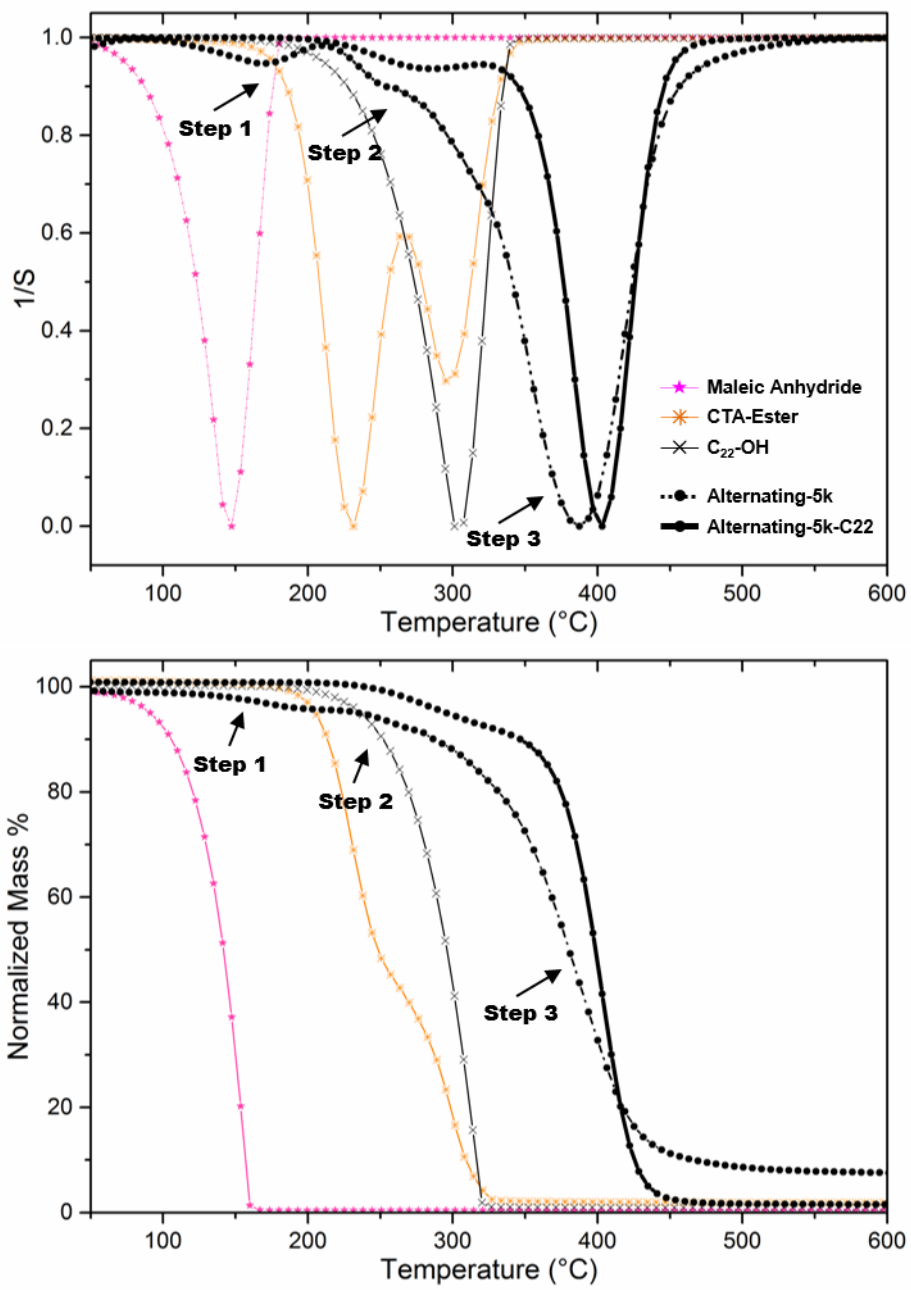

Figure A4-38. Normalized mass loss (bottom) and first derivative of mass loss (top) for controls (MAnh, side chains, CTA) and alternating PSMA copolymers. TGA in nitrogen with a heating rate of 10 °C/min and temperature range from 25 to 650 °C).

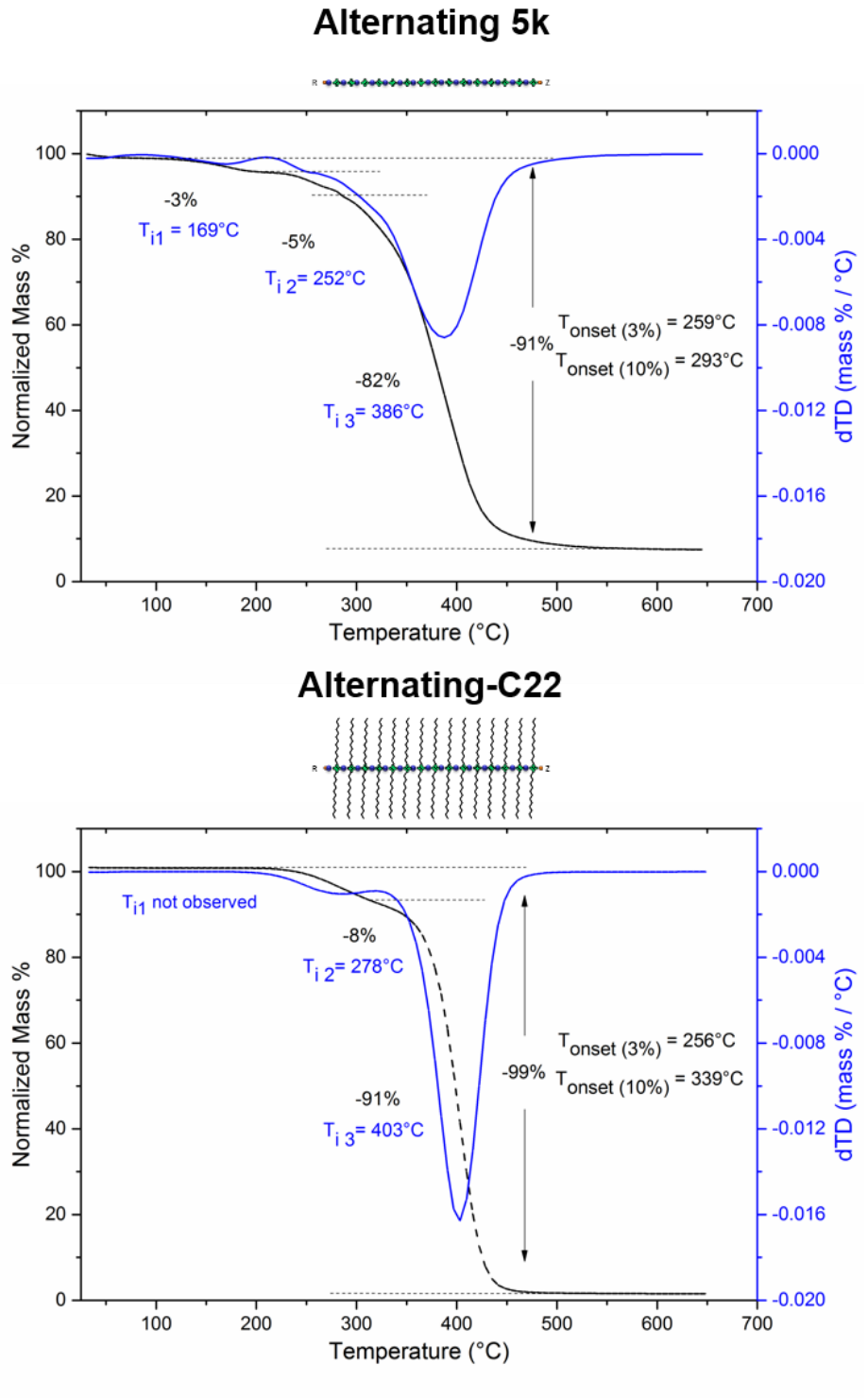

Figure A4-39. Normalized mass loss (black) and first derivative of mass loss (blue) are presented for alternating $PSMA_{28}$ copolymer (top) and after esterification with alkyl chain (bottom). TGA in nitrogen with a heating rate of 10 °C/min and temperature range from 25 to 650 °C).

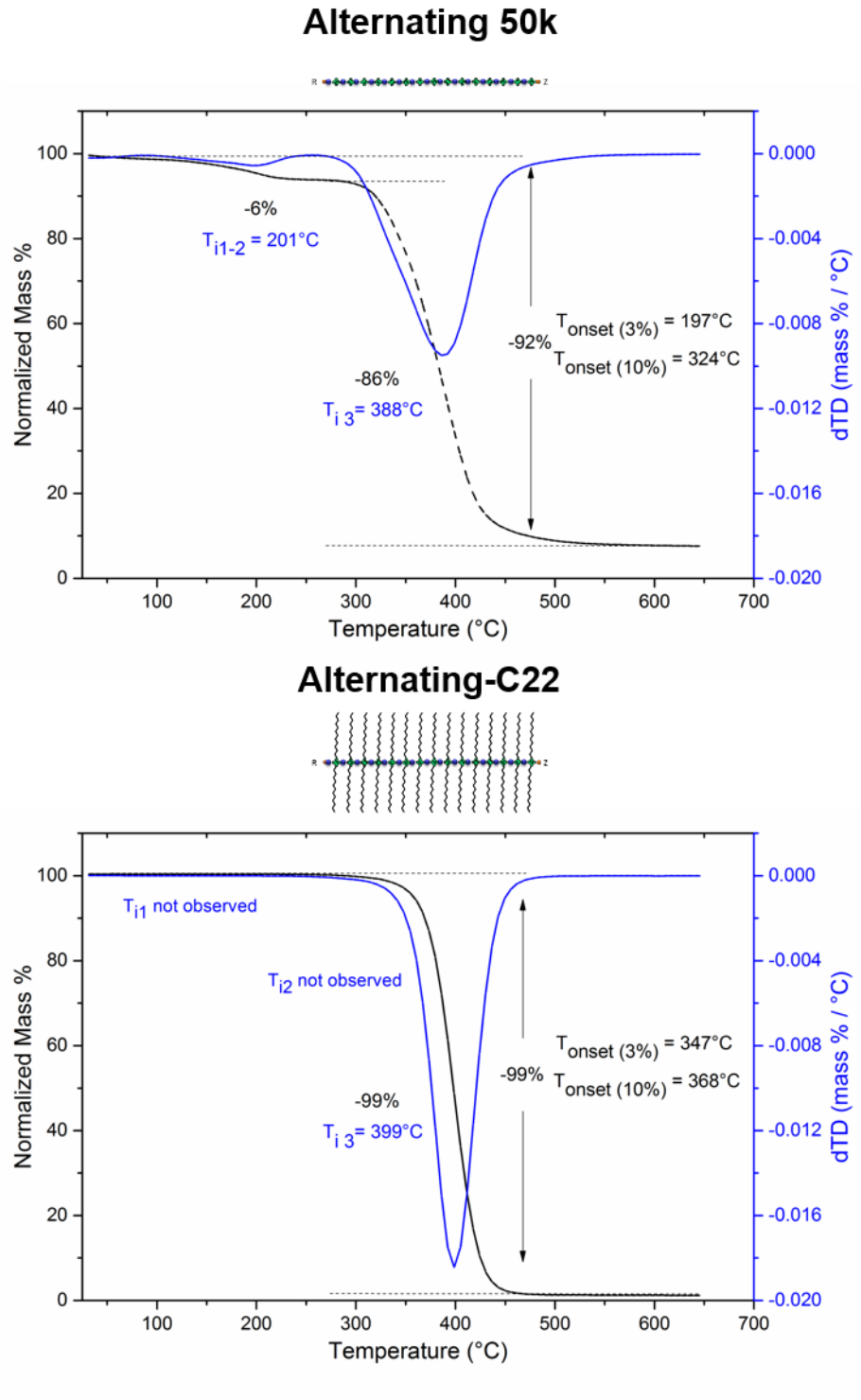

Figure A4-40. Normalized mass loss (black) and first derivative of mass loss (blue) are presented for alternating $PSMA_{250}$ copolymer (top) and after esterification with alkyl chain (bottom). TGA in nitrogen with a heating rate of 10 °C/min and temperature range from 25 to 650 °C).

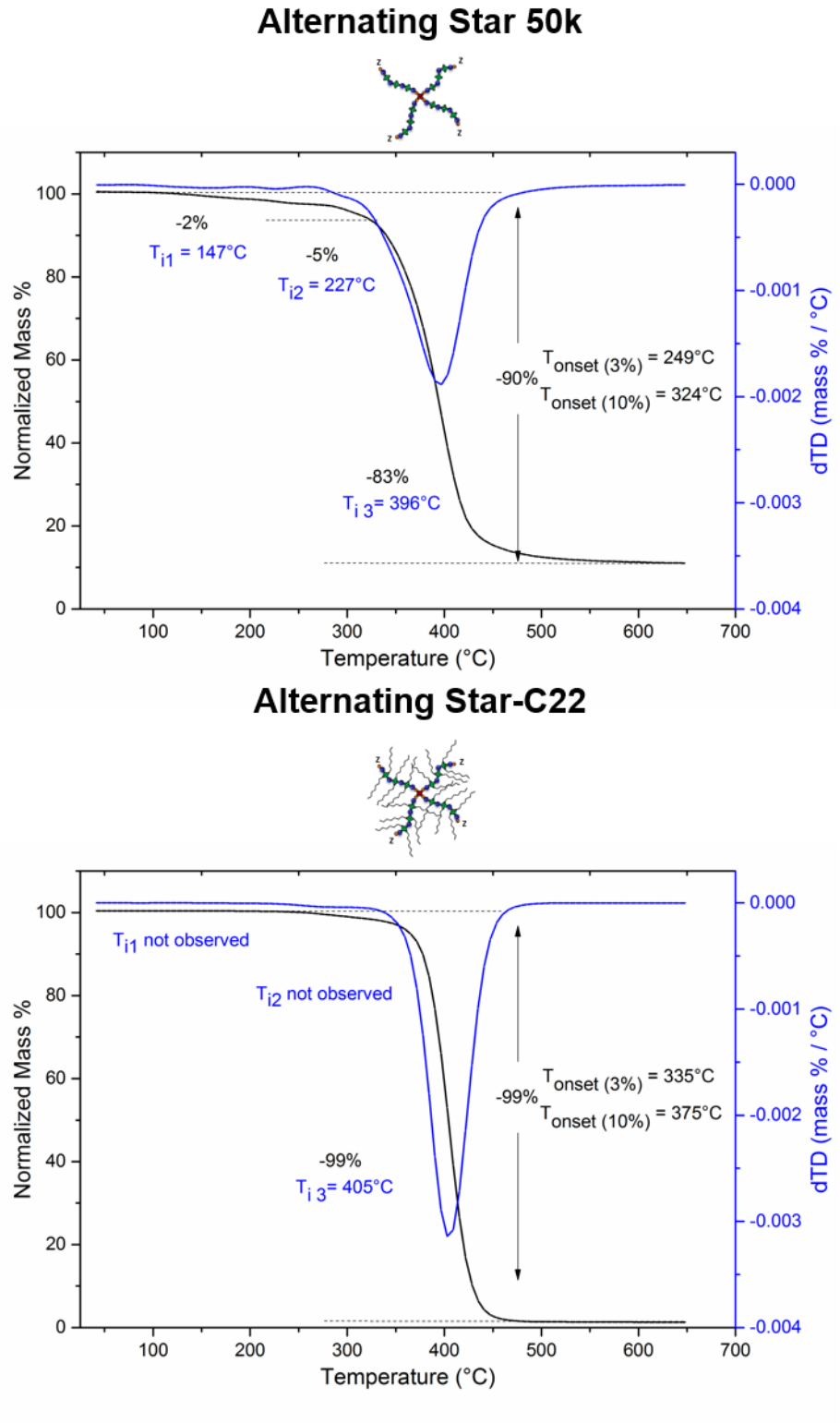

Figure A4-41. Normalized mass loss (black) and first derivative of mass loss (blue) are presented for alternating star 4xPSMA$_{60}$ copolymer (top) and after esterification with alkyl chain (bottom). TGA in nitrogen with a heating rate of 10 °C/min and temperature range from 25 to 650 °C).

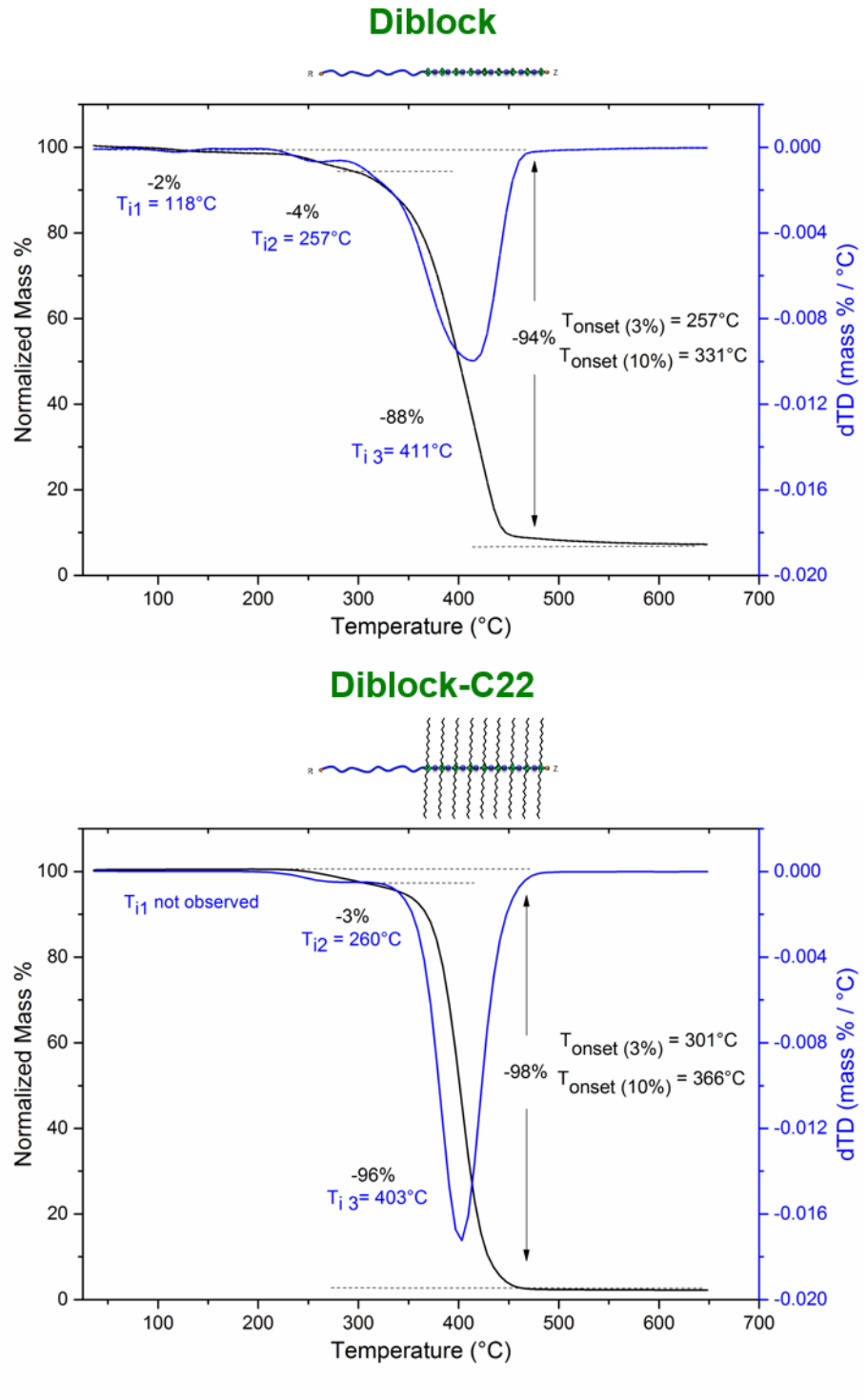

Figure A4-42. Normalized mass loss (black) and first derivative of mass loss (blue) are presented for diblock copolymer before (top) and after esterification with alkyl chain (bottom). TGA in nitrogen with a heating rate of 10 °C/min and temperature range from 25 to 650 °C).

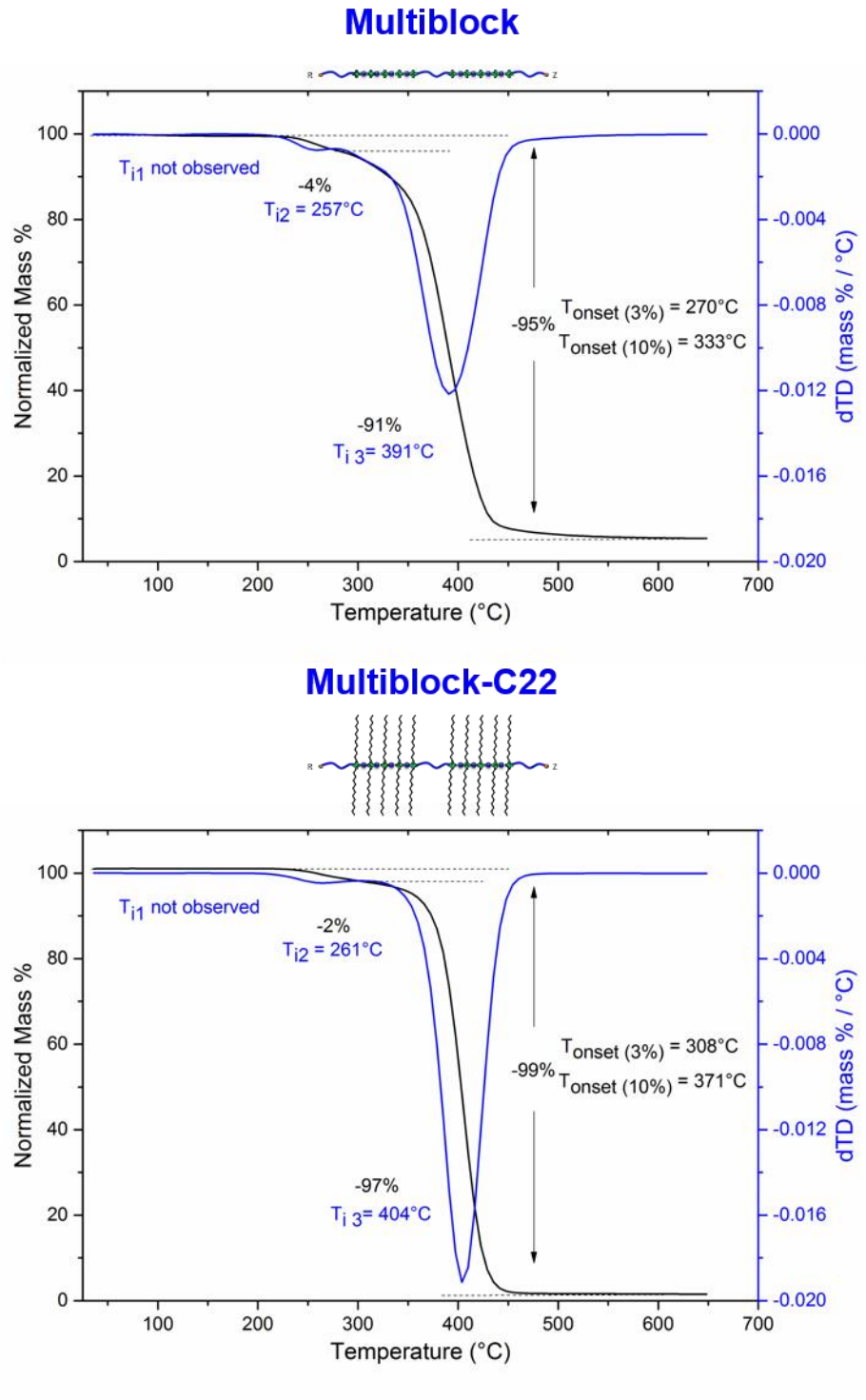

Figure A4-43. Normalized mass loss (black) and first derivative of mass loss (blue) are presented for multiblock copolymer before (top) and after esterification with alkyl chain (bottom). TGA in nitrogen with a heating rate of 10 °C/min and temperature range from 25 to 650 °C).

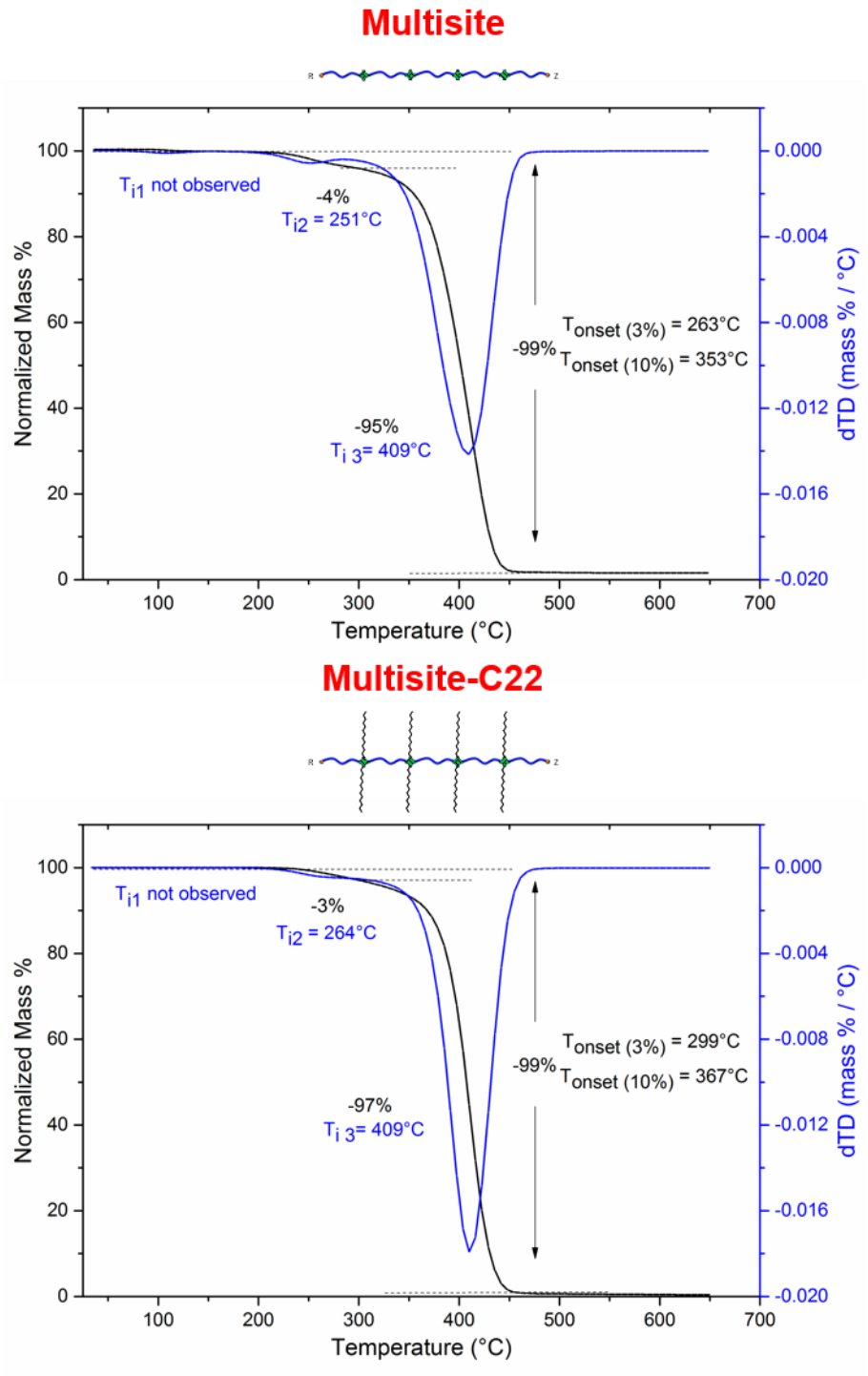

Figure A4-44. Normalized mass loss (black) and first derivative of mass loss (blue) are presented for multisite copolymer before (top) and after esterification with alkyl chain (bottom). TGA in nitrogen with a heating rate of 10 °C/min and temperature range from 25 to 650 °C).

DSC

Table A4-8. Summary of DSC results

Entry	$M_{n,NMR}$ (g/mol)	Structures	Structure	T_g (°C)			T_m (°C)			T_c (°C)	
				Heat cycle 1	Heat cycle 2	Heat cycle 3	Heat cycle 1	Heat cycle 2	Heat cycle 3	Cool cycle 1	Cool cycle 2
Multisite	**5,900**		amorphous	95	98	101	-	-	-	-	-
Multisite-Ester	**9,200**	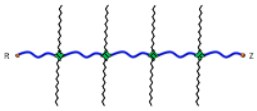	semi-crystalline	-	-	-	53	39	39	7	7
Multiblock	**5,100**		amorphous	122	121	120	-	-	-	-	-
Multiblock-Ester	**11,200**	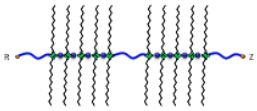	semi-crystalline	-	-	-	59	50	50	35	35
Diblock	**5,600**		amorphous	-	92 165	99 168	-	-	-	-	-
Diblock-Ester	**13,800**	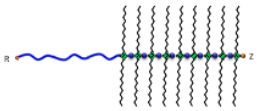	semi-crystalline	-	-	-	62	53	53	39	39
alt-PSMA$_{6k}$	**5,600**		amorphous	-	207	205	-	-	-	-	-
alt-PSMA$_{6k}$-Ester	**18,700**	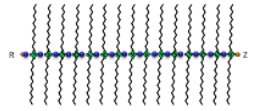	semi-crystalline	-	-	-	62	56	56	40	40
alt-PSMA$_{50k}$	**50,600**		amorphous	-	209	211	-	-	-	-	-
alt-PSMA$_{50k}$-Ester	**179,800**	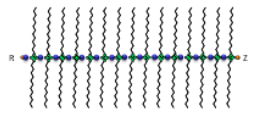	semi-crystalline	-	-	-	63	53	53	40	40
4xPSMA$_{50k}$	**47,600**	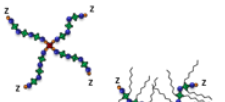	amorphous	-	208	211	-	-	-	-	-
4xPSMA$_{50k}$-Ester	**177,100**	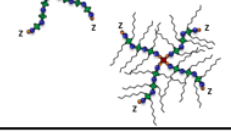	semi-crystalline	-	-	-	62	53	53	40	40

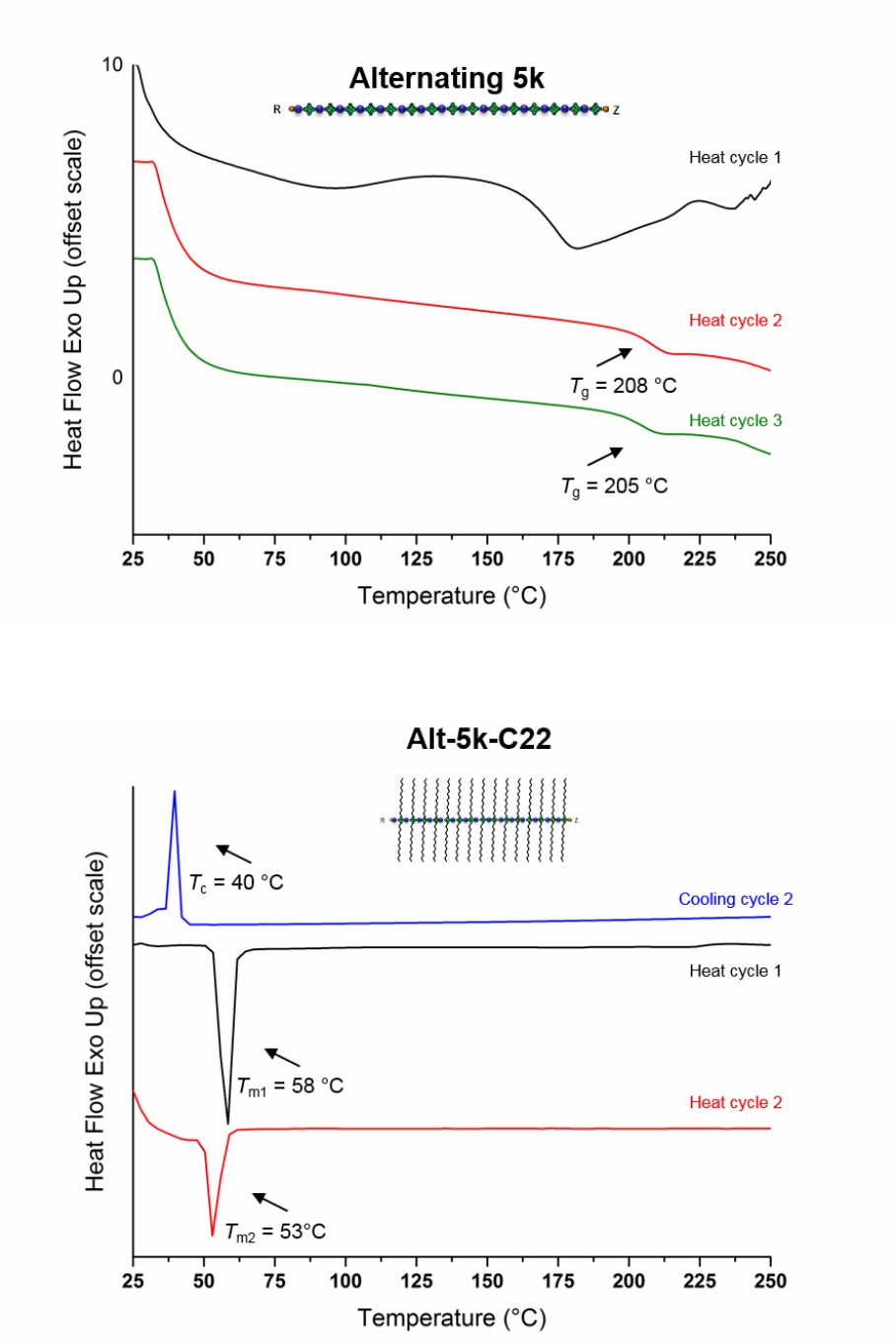

Figure A4-45. DSC curves measured for alternating $PSMA_{28}$ copolymer before (top) and after esterification with alkyl chain (bottom). DSC in nitrogen with a heating rate of 30 °C/min and temperature range from 25 to 300 °C before esterification and heating rate of 10 °C/min and temperature range from 25 to 250 °C after.

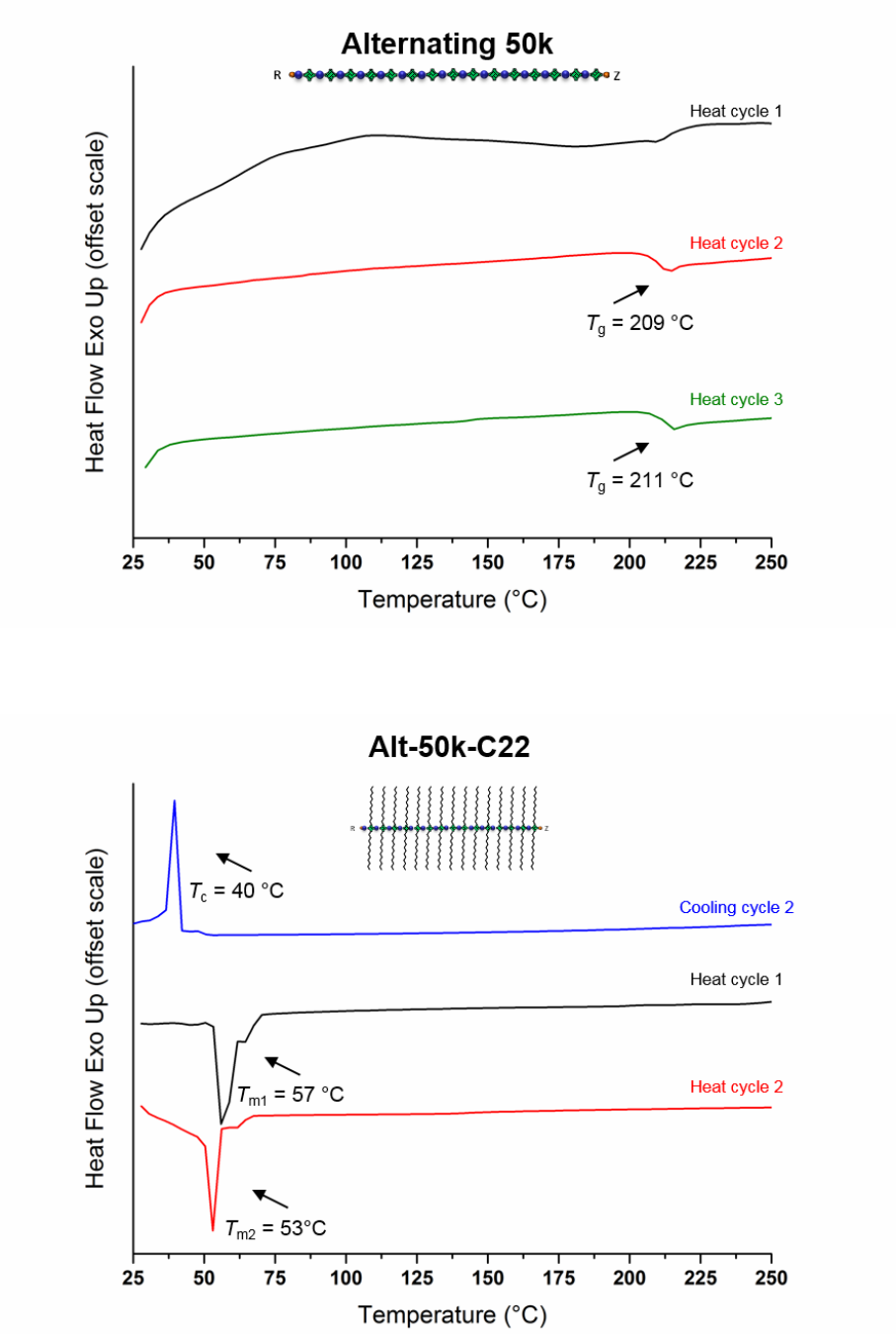

Figure A4-46. DSC curves measured for alternating $PSMA_{250}$ copolymer before (top) and after esterification with alkyl chain (bottom). DSC in nitrogen with a heating rate of 30 °C/min and temperature range from 25 to 300 °C before esterification and heating rate of 10 °C/min and temperature range from 25 to 250 °C after.

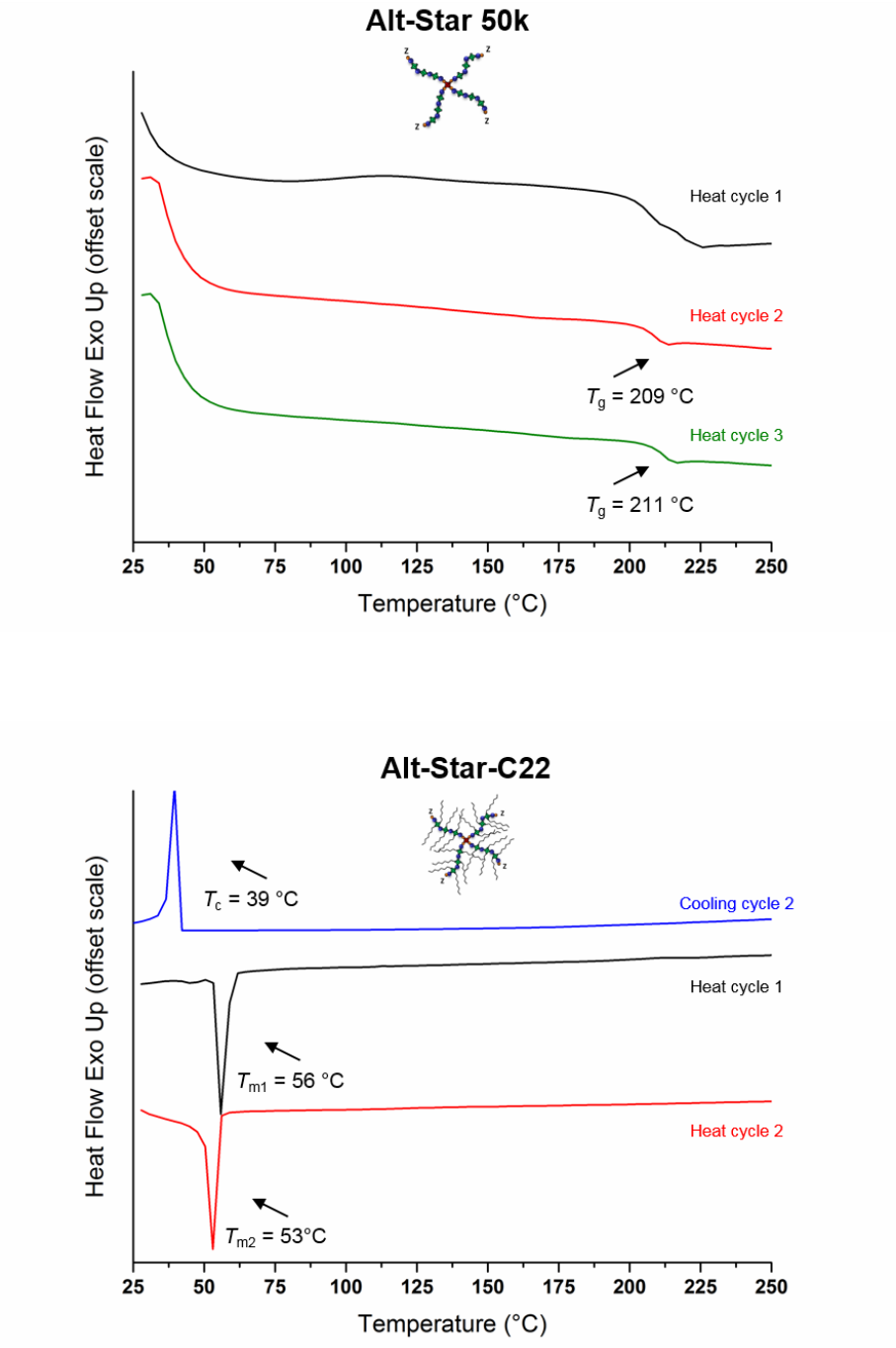

Figure A4-47. DSC curves measured for alternating star 4xPSMA$_{60}$ copolymer before (top) and after esterification with alkyl chain (bottom). DSC in nitrogen with a heating rate of 30 °C/min and temperature range from 25 to 300 °C before esterification and heating rate of 10 °C/min and temperature range from 25 to 250 °C after.

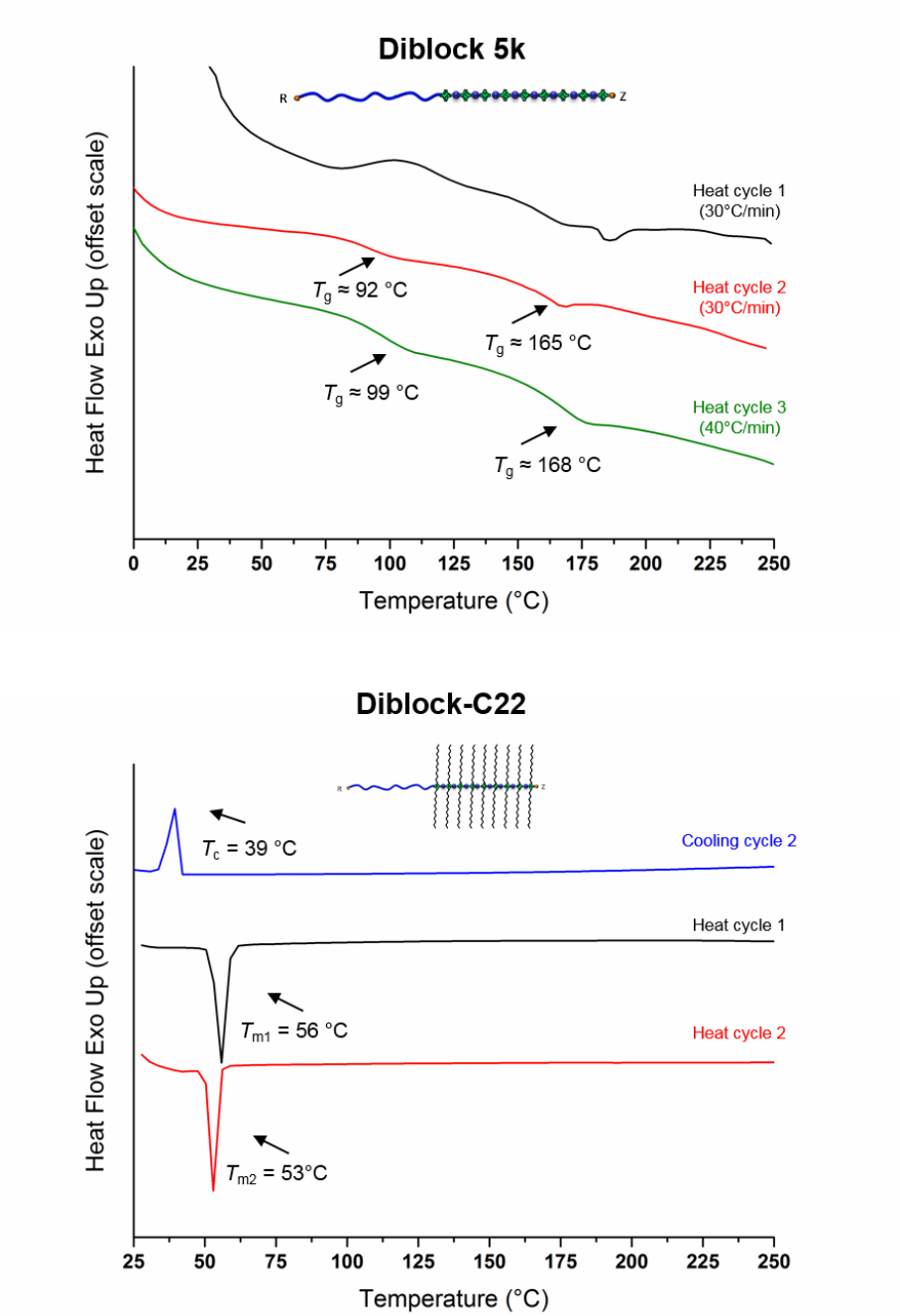

Figure A4-48. DSC curves measured for diblock copolymer before (top) and after esterification with alkyl chain (bottom). DSC in nitrogen with a heating rate of 30 °C/min and temperature range from 25 to 300 °C before esterification and heating rate of 10 °C/min and temperature range from 25 to 250 °C after.

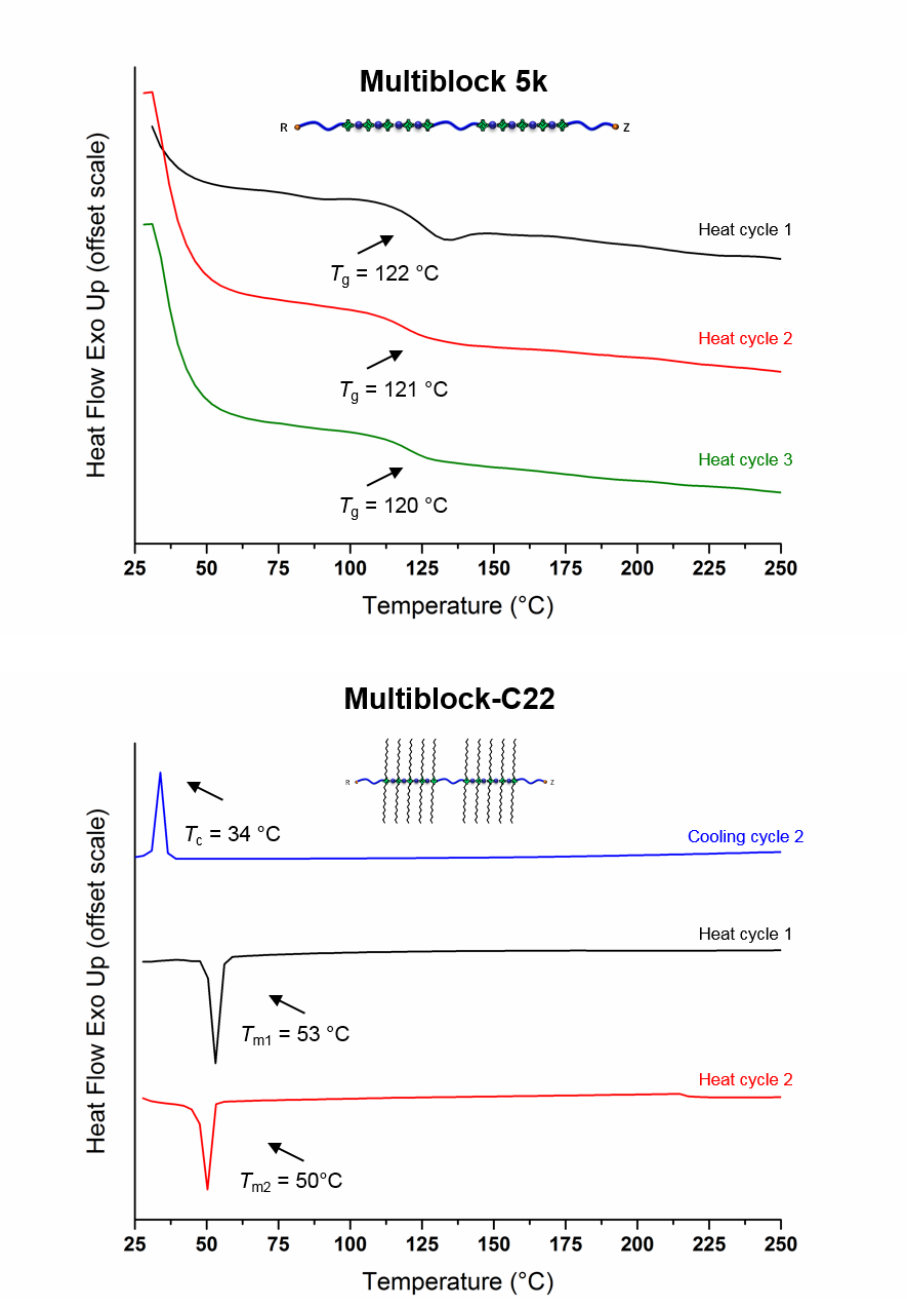

Figure A4-49. DSC curves measured for multiblock copolymer before (top) and after esterification with alkyl chain (bottom). DSC in nitrogen with a heating rate of 20 °C/min and temperature range from 25 to 300 °C before esterification and heating rate of 10 °C/min and temperature range from 25 to 250 °C after.

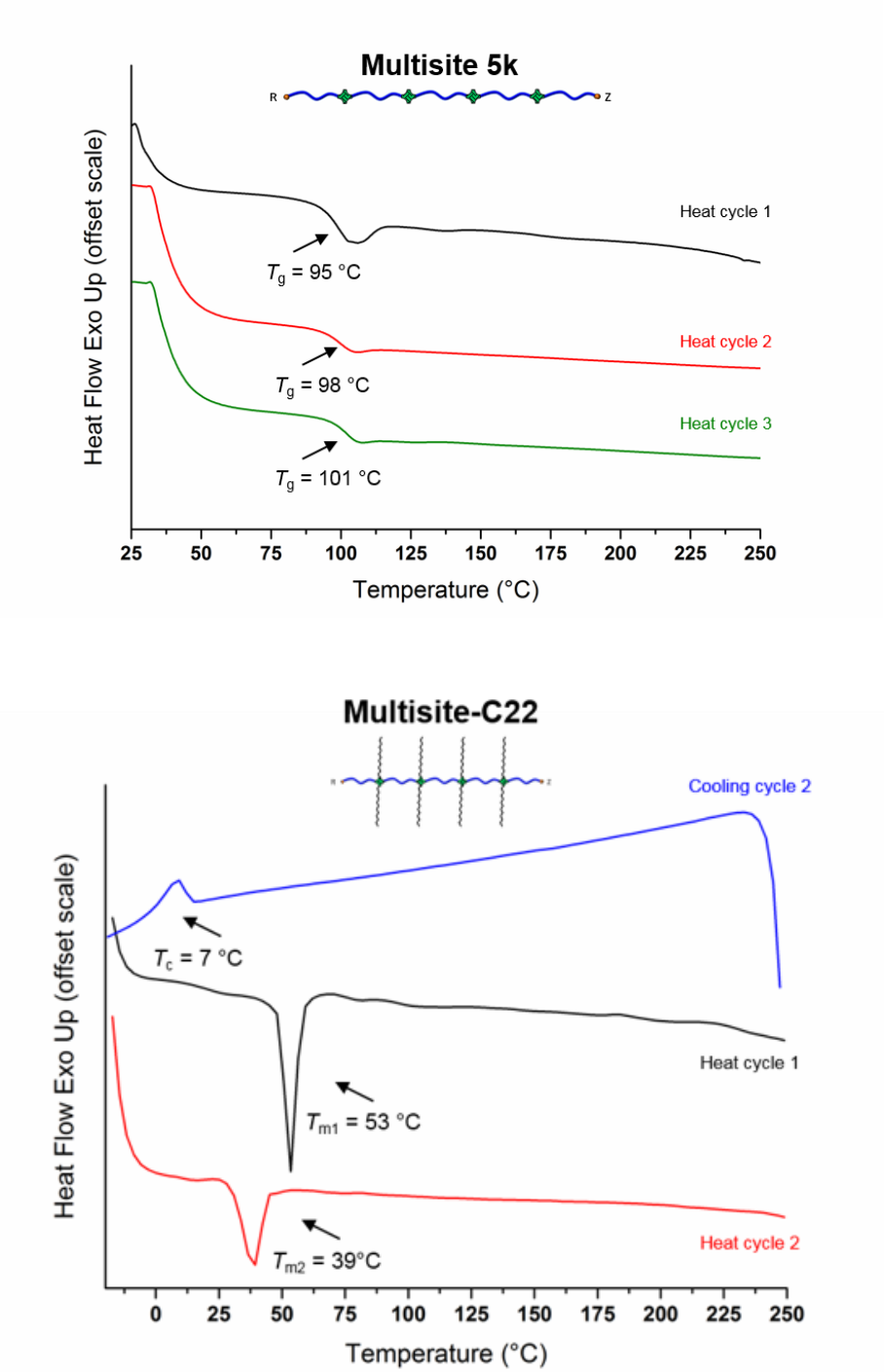

Figure A4-50. DSC curves measured for multisite copolymer before (top) and after esterification with alkyl chain (bottom). DSC in nitrogen with a heating rate of 20 °C/min and temperature range from 25 to 300 °C before esterification and heating rate of 10 °C/min and temperature range from -20 to 250 °C after.

Appendix Chapter 5 PSMA as Oil and Lubricant Additives

The details concerning materials with behenyl side chains (C22) are available in previous chapter. The esterification data concerning the lauryl functionalised materials (PSMA-C12 and polylaurylacrylate) are available in following supporting information.

Short PSMA with C12

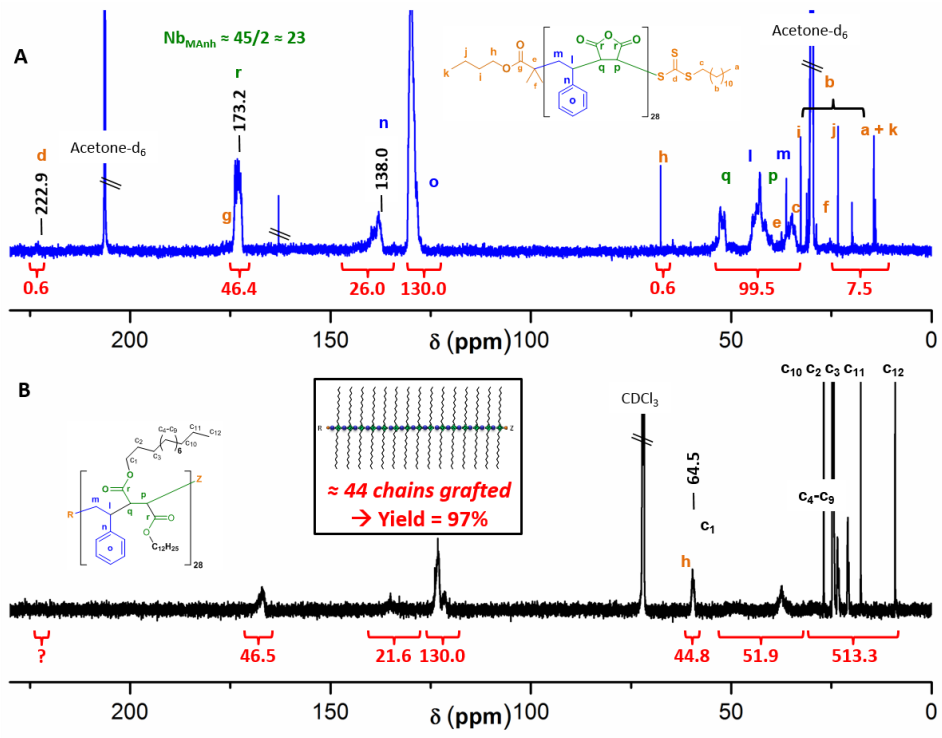

Figure A5-1. Quantitative ^{13}C NMR spectra ($CDCl_3$) for pure alternating $PSMA_{28}$ before (A) and after (B) esterification. Esterification yield obtained by comparing number of MAnh (spectrum A at 173 ppm) and number of alkyl chains (spectrum B at 64ppm).

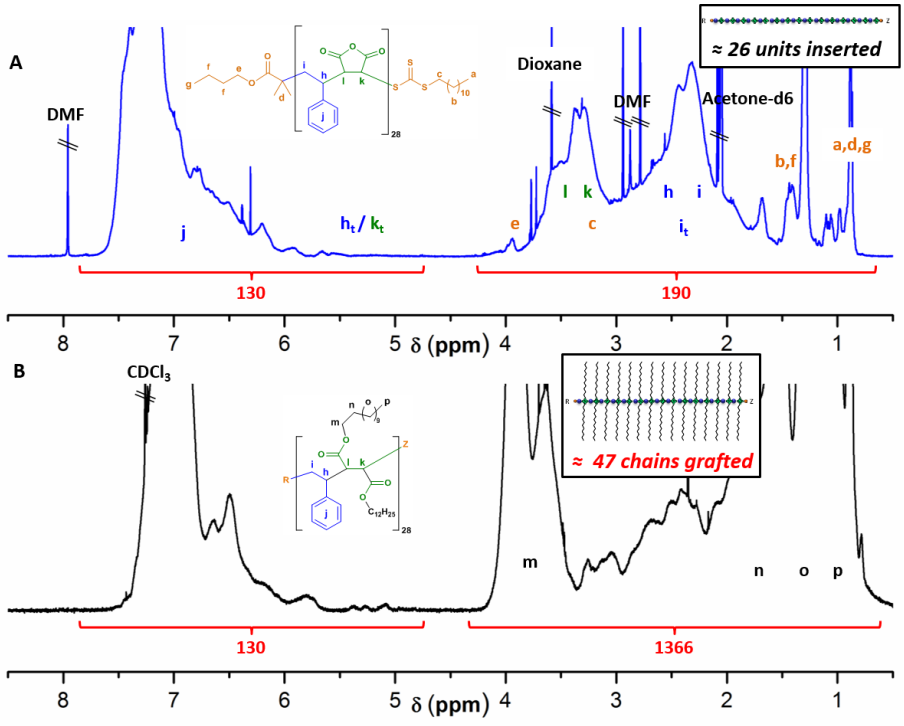

Figure A5-2. Quantitative ^{1}H NMR spectra ($CDCl_3$) for pure alternating $PSMA_{28}$ before (A) and after (B) esterification.

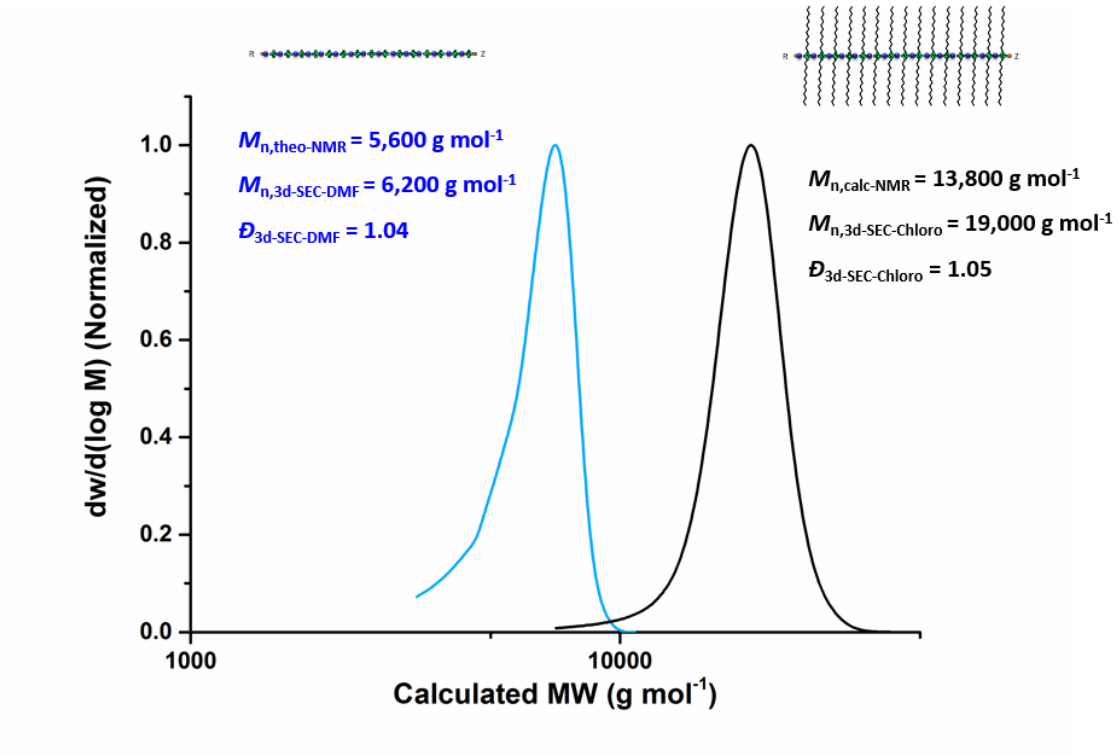

Figure A5-3. Molar mass distribution for alternating $PSMA_{28}$ before (blue) and after (Black) esterification. SEC using triple-detection in DMF (blue) and chloroform (black).

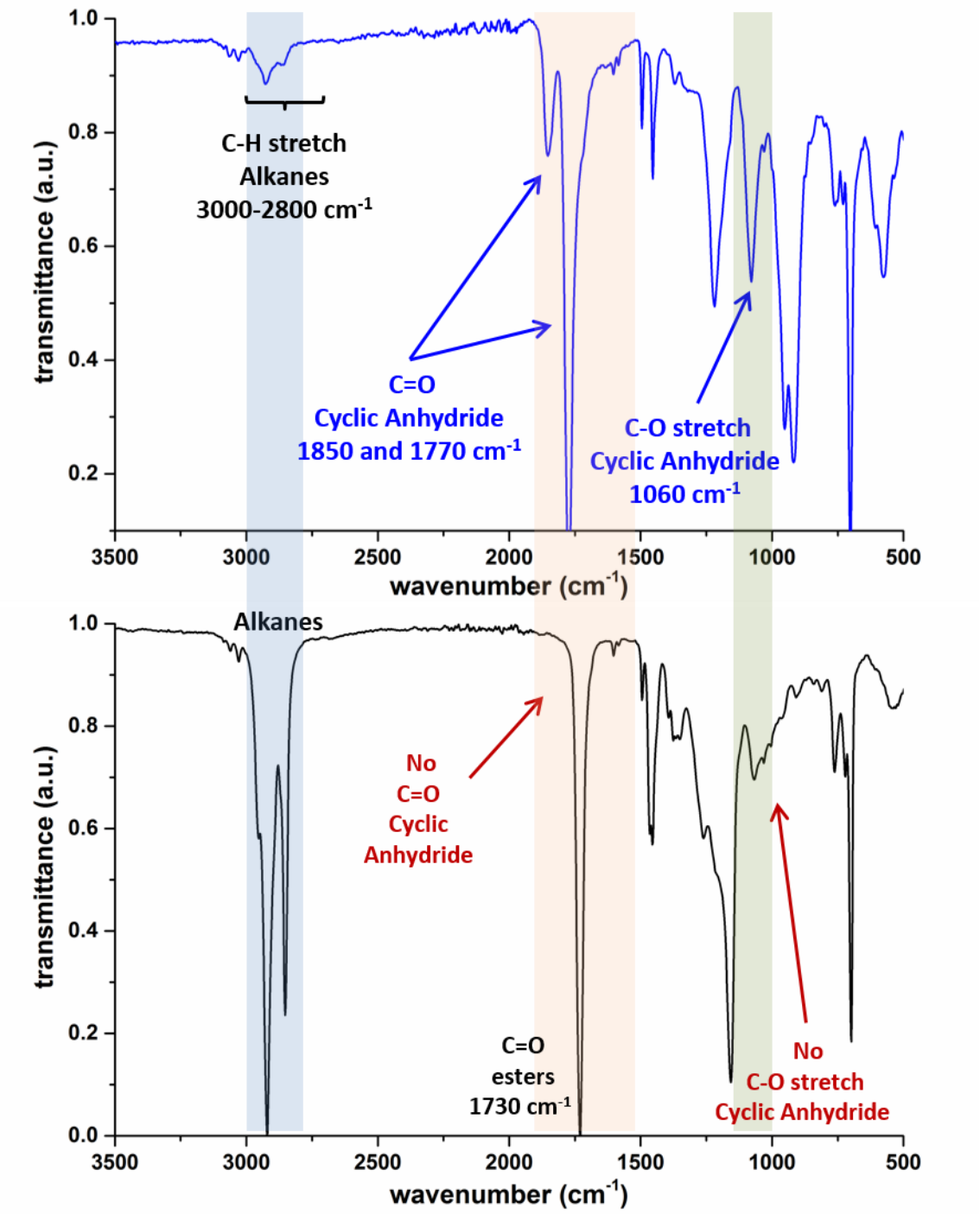

Figure A5-4. IR spectra for $PSMA_{28}$ copolymer before (top) and after esterification (bottom) with lauryl alcohol (C12).

Long Alternating with C12

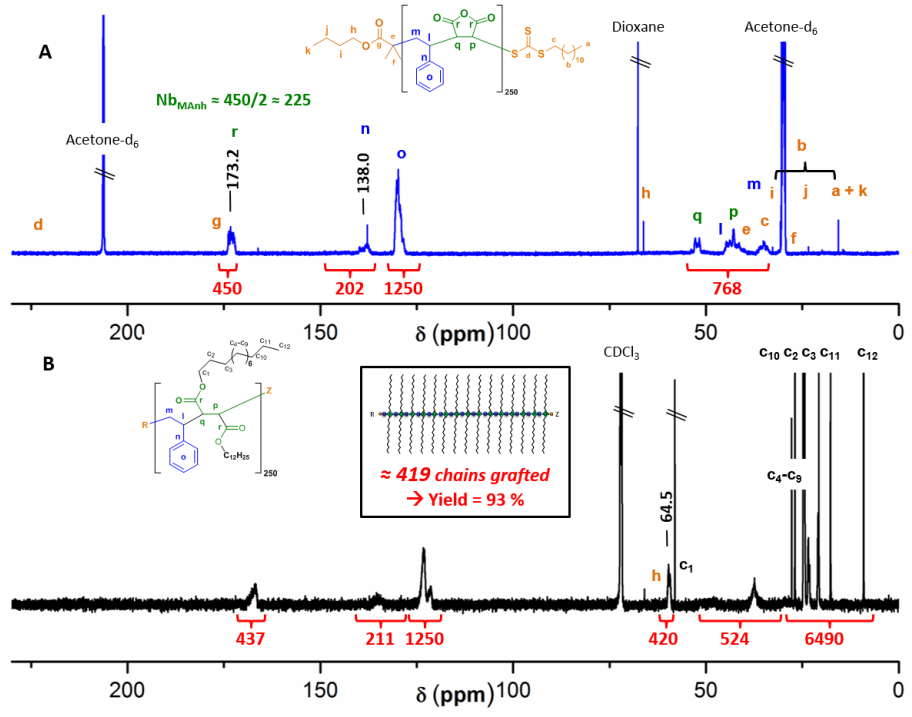

Figure A5-5.Quantitative ^{13}C NMR spectra ($CDCl_3$) for alternating $PSMA_{250}$ before (A) and after (B) esterification. Esterification yield obtained by comparing number of MAnh (spectrum A at 173 ppm) and number of alkyl chains (spectrum B at 64ppm).

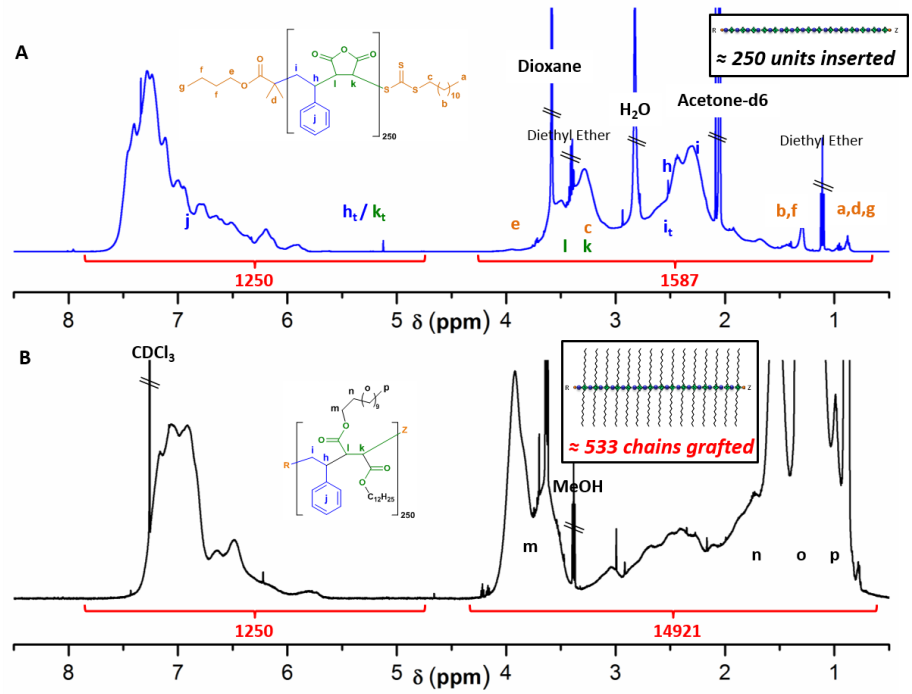

Figure A5-6. Quantitative ^{1}H NMR spectra ($CDCl_3$) for alternating $PSMA_{250}$ before (A) and after (B) esterification.

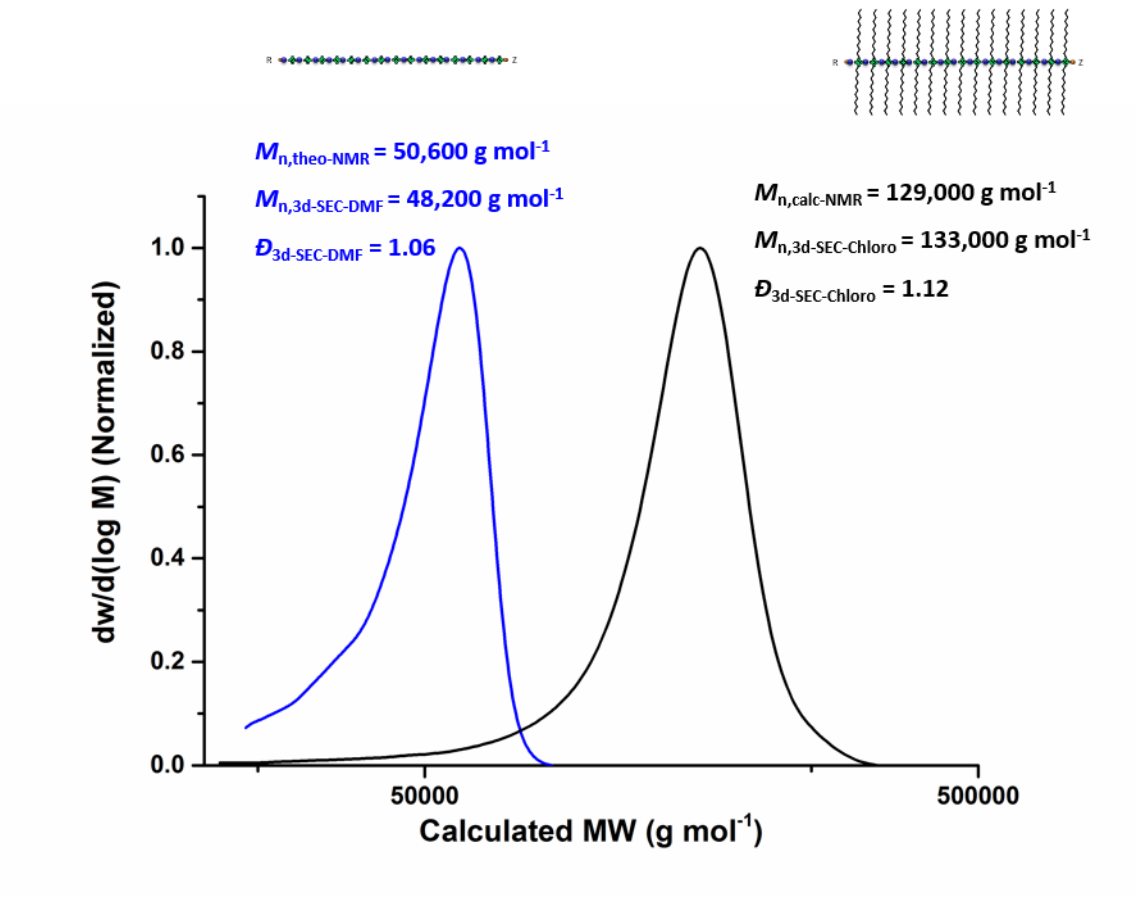

Figure A5-7. Molar mass distribution for alternating $PSMA_{250}$ before (blue) and after (Black) esterification. SEC using triple-detection in DMF (blue) and chloroform (black).

Star PSMA with C12

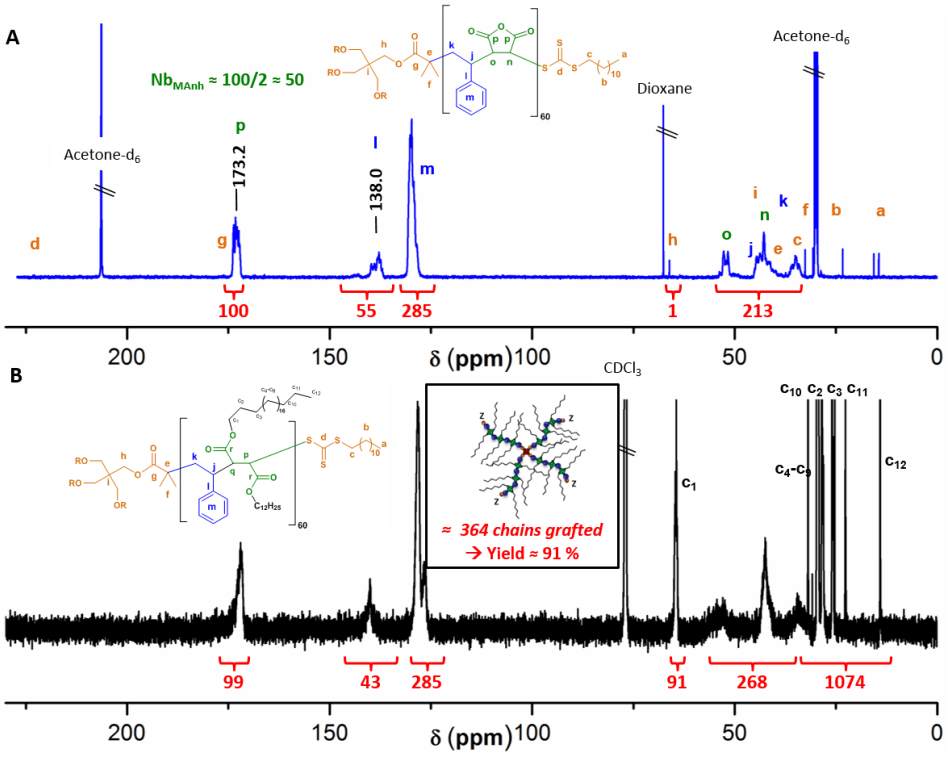

Figure A5-8. Quantitative ^{13}C NMR spectra ($CDCl_3$) for alternating star 4xPSMA$_{60}$ before (A) and after (B) esterification. Esterification yield obtained by comparing number of MAnh (spectrum A at 173 ppm) and number of alkyl chains (spectrum B at 64ppm).

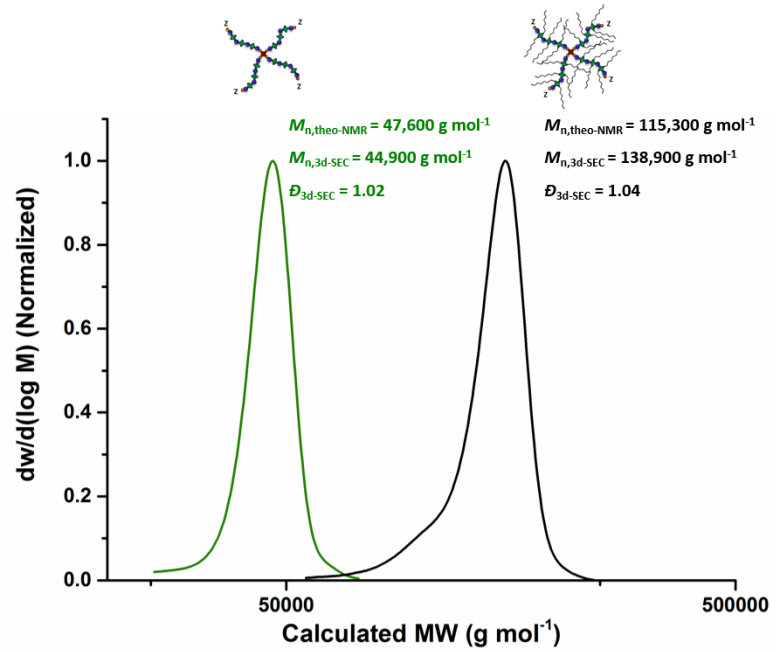

Figure A5-9. Molar mass distribution for alternating 4xPSMA$_{60}$ before (green) and after (Black) esterification. SEC using triple-detection in DMF (green) and chloroform (black).

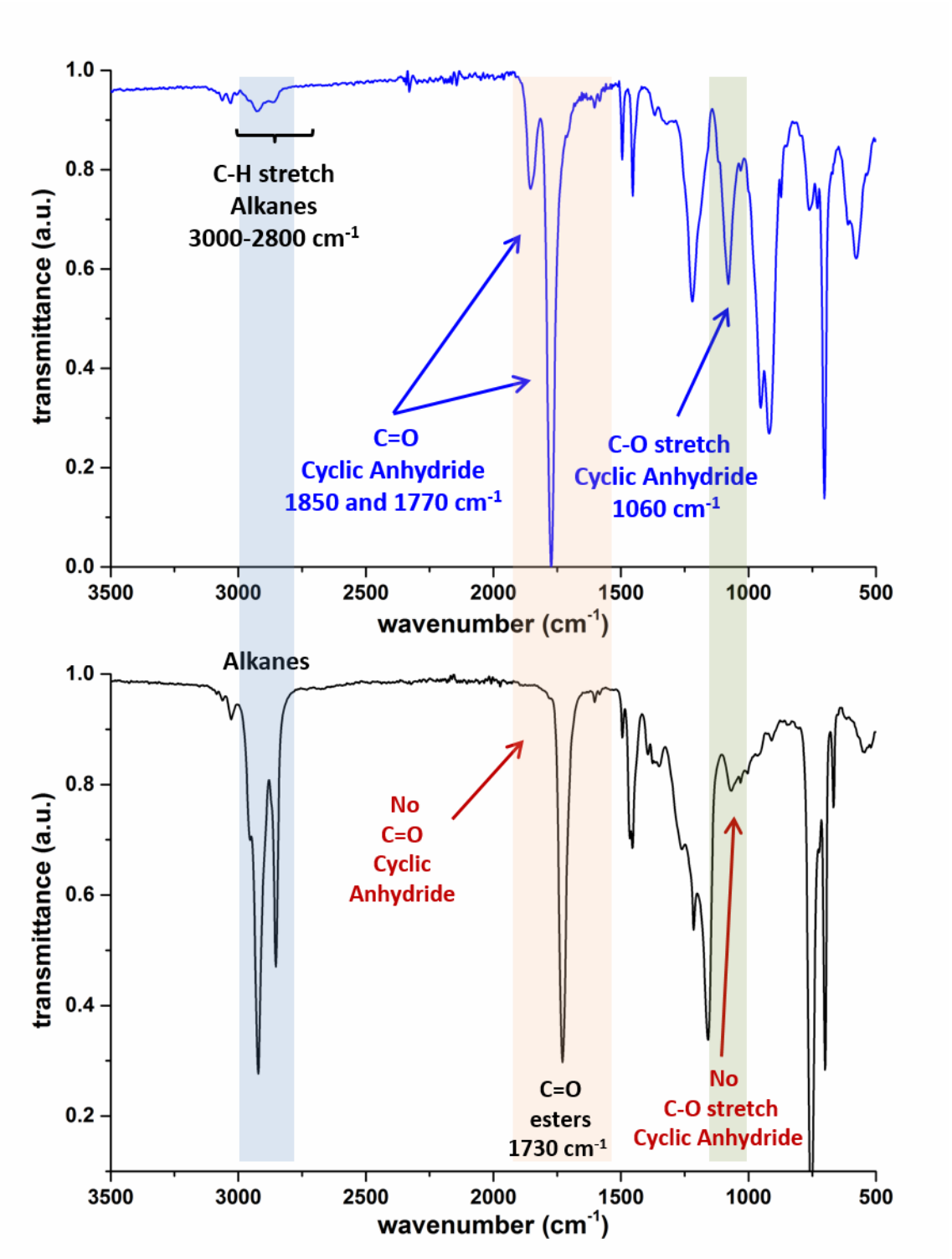

Figure A5-10. IR spectra for 4xPSMA$_{60}$ copolymer before (top) and after esterification (bottom) with lauryl alcohol (C12).

Polylaurylacrylate

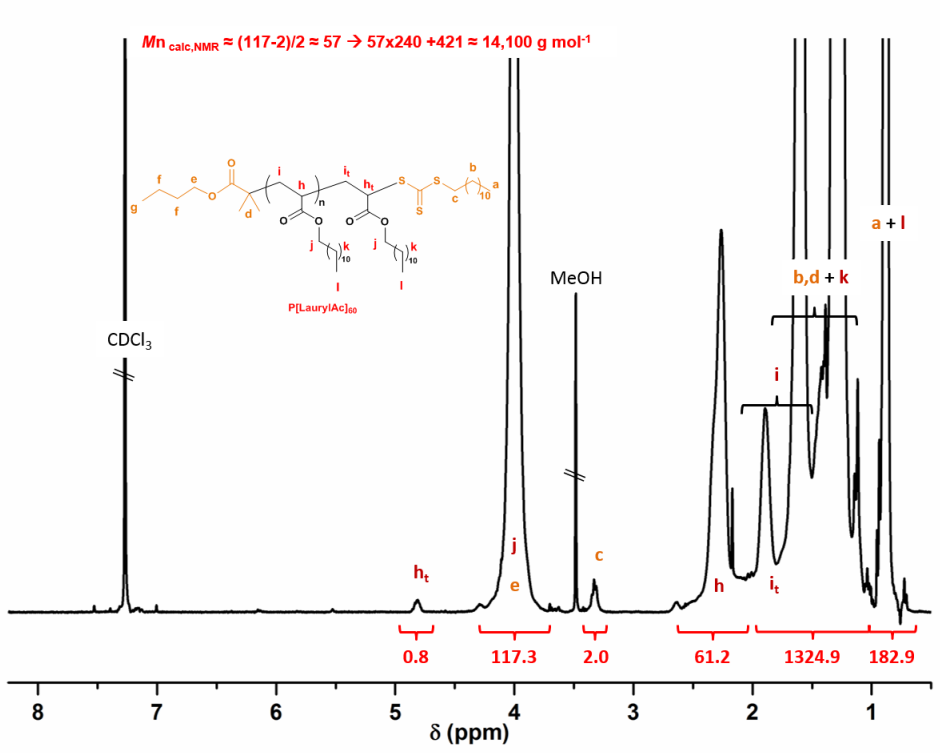

Figure A5-11. ^{1}H-NMR spectrum ($CDCl_3$) for pure PLaurylAc$_{60}$.

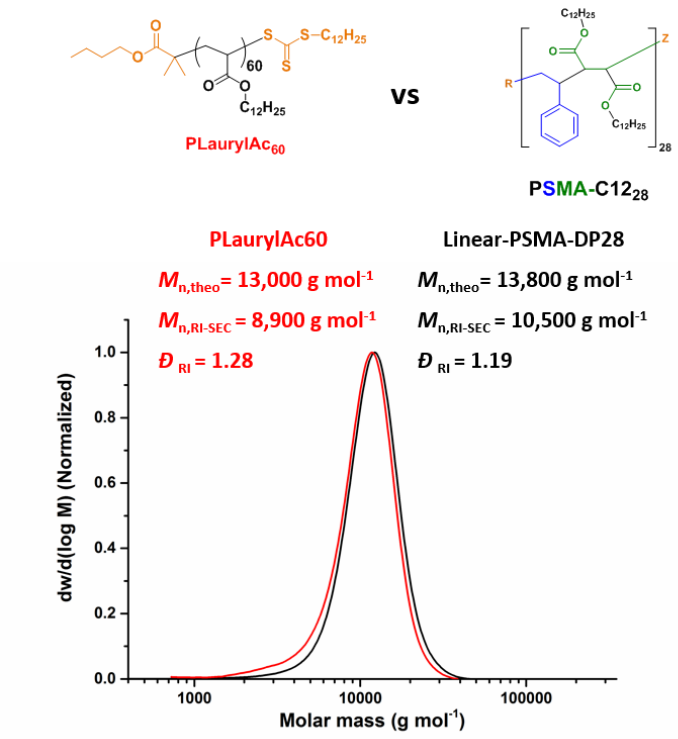

Figure A5-12. Molar mass distribution for PLaurylAc$_{60}$ (red) and PSMA$_{28}$-C12 (black). SEC in chloroform using polystyrene calibration.